Università degli Studi di Ferrara

DOTTORATO DI RICERCA IN
FISICA

XXI° CICLO

COORDINATORE Prof. Filippo Frontera

Photon Propagation as a Probe for Fundamental Physics

Settore Scientifico Disciplinare FIS/05

Dottorando	**Tutore**
Dott. Matteo Galaverni	Prof. Nazzareno Mandolesi

_____   _____
(firma)   *(firma)*

Co-Tutori
Dott. Fabio Finelli
Prof. Günter Sigl

Anni 2006/2008

Contents

Introduction

Shortcomings of the Standard Model of particle physics have been established in the literature both on the theoretical side (large number of free parameters, fine tuning, lack of unification of interactions, ...) and on the experimental /observational side (neutrino oscillations, smallness of strong CP violation in QCD, evidence of dark matter and dark energy, ...). Astrophysical and cosmological observations provide the main compelling evidences for new physics beyond the Standard Model. This fact led to the proposal of several modifications and extensions of the Standard Model, which can already be constrained by using current experiments and observations.

In this thesis we will focus mainly on light propagation in order to constrain particle physics models beyond the Standard Model.

The spectrum and the anisotropy pattern, in intensity and polarization, of the Cosmic Microwave Background (CMB) is one of the main pillars of modern cosmology. The black body spectrum and the anisotropy pattern are so well observed and understood that little room is left for non-standard interactions. We consider in detail how the coupling between photons and pseudoscalars, in particular axions [1, 2] (particle introduced to solve the strong CP-problem of QCD and which are also good candidates for dark matter), can be constrained looking at linear and circular polarization of CMB [3]. We modify the public Einstein-Boltzmann code CAMB [4] by introducing a rotation of the linear polarization plane. We show how the widely used approximation of describing the rotation of linear polarization with a constant angle [5] (as used also by WMAP team [6]) may be a very

crude approximation for most of the dynamical pseudoscalar field models. We also estimate the effect of the photon coupling with ultralight pseudo Nambu-Goldstone bosons as dark energy candidates [7]; effects on polarization seem too small for current CMB missions (e.g. WMAP or PLANCK), but they may be detected by the next generation of CMB experiments.

Many extensions involving non-renormalizable terms in effective field theory predict modifications that grow with energy, therefore stronger constraints are obtained looking at photons of very high energies. In particular theories trying to unify quantum mechanics with general relativity and many supersymmetry models predict that Lorentz symmetry has to be modified at energies of the order of the Planck scale (10^{28} eV). If standard dispersion relations of elementary particles are modified, then the propagation and therefore also the energy spectrum of ultrahigh-energy cosmic rays (UHECRs) can be considerably changed. It was already known that violation of Lorentz invariance could inhibit some reactions and change the energy thresholds for others [8], but today it is already possible to establish real constraints using the data from UHECR detectors, in particular upper limits on the flux of photons obtained by the Pierre Auger Observatory [9]. We study in particular how it is possible to constrain Lorentz invariance violation in the QED sector for photons [10] and electrons [11] improving current constraints by several orders of magnitude.

This thesis is divided in two parts, the first one concerns photon coupling with pseudoscalar particles and its effects on CMB polarization

- in the first chapter we present an introduction to CMB polarization;

- the second chapter is a general overview of particle physics models involving pseudoscalar fields;

- in chapter 3 we discuss the constraints that CMB polarization imposes on photon-pseudoscalar coupling.

In the second part of the thesis, developed thanks to the support of the International Doctorate on Astroparticle Physics (IDAPP) program of the MiUR

[12], we consider ultrahigh energy photons as a probe for possible Lorentz invariance violation terms in the dispersion relation of photons, electrons and positrons:

- chapter 4 is a short introduction to ultrahigh energy cosmic rays;

- in chapter 5 we present some Lorentz invariance violating terms and summarize the current upper limits;

- in the last chapter we show how it is possible to constrain $\mathcal{O}(p/M_{\mathrm{pl}})$ and $\mathcal{O}(p/M_{\mathrm{pl}})^2$ modifications of the dispersion relation in the QED sector by using the current upper limits on the flux of ultrahigh energy photons.

In appendix we present a brief review concerning systematics of cosmic microwave background polarization [13].

Chapter 1

Cosmic microwave background polarization

1.1 Introduction

Polarization of Cosmic Microwave Background (CMB) was predicted soon after its discovery [14]: Thompson scattering of unpolarized photons on electrons at last scattering surface generates linear polarization if the incident intensities varies with direction (anisotropies). Thompson cross-section depends on polarization [15]:

$$\frac{d\sigma}{d\Omega} \propto \left| \hat{\varepsilon} \cdot \hat{\varepsilon}' \right|^2 , \qquad (1.1)$$

where $\hat{\varepsilon}'$ is the polarization direction of incident radiation, and $\hat{\varepsilon}$ of outgoing radiation. The incident light sets up oscillations of the target electron of the electric field, so the scattered radiation intensity peaks in the direction perpendicular to the incident polarization (see Fig. 1.1).

If incoming radiation field on the electron were isotropic, then radiation would remain unpolarized. Conversely if the incident radiation field possesses a quadrupolar variation in intensity the result is a linear polarization of the scattered radiation [16].

Polarization measurements are quite challenging: since the level of po-

5
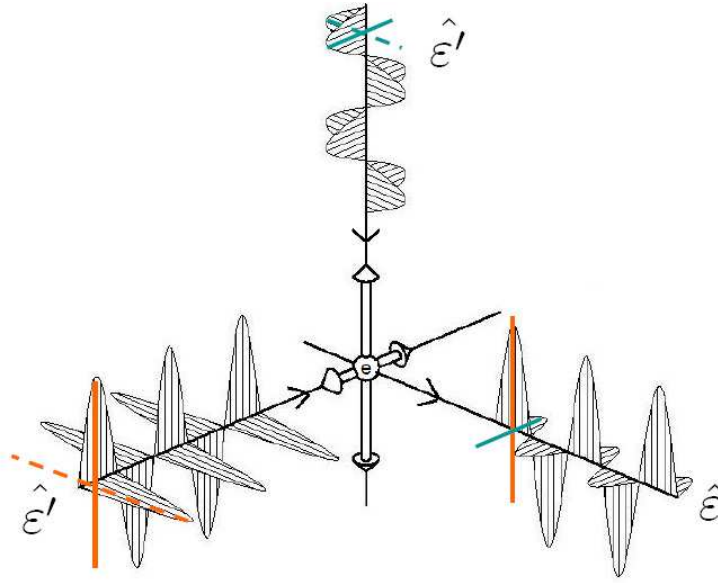
Figure 1.1: Idealization of Thomson scattering process at last scattering. Unpolarized incident radiation ($\hat{\varepsilon}'$), represented here as superposition of two opposite polarized waves, sets up oscillations of the target electron (e). Incoming radiation polarized parallel to the outgoing direction cannot scatter (dashed line), while the perpendicular components (continuous line) can. Since the incoming radiation on the last scattering electron is not isotropic the outgoing wave ($\hat{\varepsilon}$) is linearly polarized.

larization is expected to be 1-10% of the amplitude of the temperature anisotropies depending on the angular scale (see Fig. 1.2). The first detection was announced in 2002 by the DASI (Degree Angular Scale Interferometer) team [17], in 2006 WMAP (Wilkinson Microwave Anisotropy Probe) [18] released the first full sky maps. Actually there are several experiments confirming DASI detection (especially at small angular scales): AMiBA (Array for Microwave Background Anisotropy), BOOMERanG (Balloon Observations Of Millimetric Extragalactic Radiation and Geophysics), CAPMAP (Cosmic Anisotropy Polarization MAPper), QuaD (Quest (Q and U Extra-Galactic Sub-mm Telescope) at DASI), ..., and next spring also the Planck satellite is
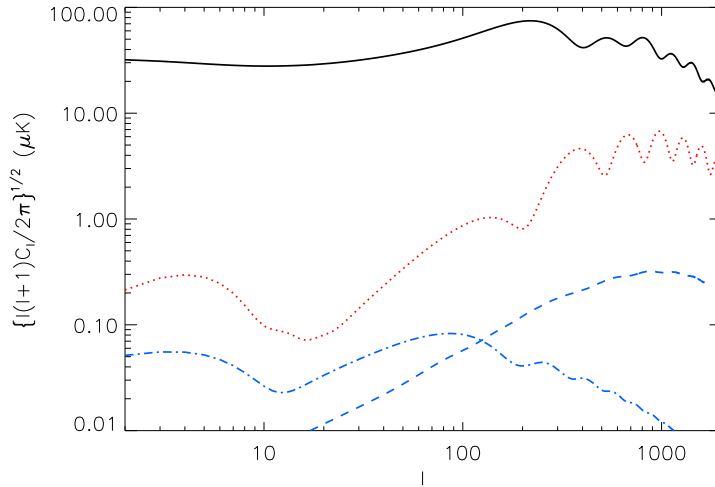
Figure 1.2: Plots of angular power spectra for TT (black continuous line) and EE (red dotted line); for BB we show a model with a tensor to scalar ratio $r = 0.1$ (blue dot-dashed line) and the lensing signal (blue dashed line). The cosmological parameters of the flat ΛCDM model used here are: $\Omega_b h^2 = 0.022$, $\Omega_c h^2 = 0.123$, $\tau = 0.09$, $n_s = 1$, $A_s = 2.3 \times 10^{-9}$, $H_0 = 100 \, h \, \mathrm{km \, s^{-1} \, Mpc^{-1}} = 72 \, \mathrm{km \, s^{-1} \, Mpc^{-1}}$.

planned to be launched. This increasing number of observations confirming theoretical predictions reduces therefore the room for non-standard interactions.

1.2   Stokes parameters

The complex electric field vector for a plane wave propagating along $\hat{\boldsymbol{z}}$ direction at a point (x, y) in some transverse plane $z = z_0$ is:

$$\begin{aligned} \boldsymbol{E} &= (E_x(t), E_y(t)) \\ &= \left[\hat{\boldsymbol{e}}_{\boldsymbol{x}} \varepsilon_x(t) e^{i\varphi_x(t)} + \hat{\boldsymbol{e}}_{\boldsymbol{y}} \varepsilon_y(t) e^{i\varphi_y(t)} \right] e^{-ikt}, \end{aligned} \tag{1.2}$$

where the physical quantity is the real part of $\boldsymbol{E}$. For a spatially flat Friedmann-Robertson-Walker metric ($ds^2 = a^2(\eta)\left[-d\eta^2 + d\boldsymbol{x}^2\right]$) the relation between the electromagnetic tensor and the physical fields is:

$$
F_{\mu\nu} = a(\eta)\begin{pmatrix} 0 & -E_x & -E_y & -E_z \\ E_x & 0 & B_z & -B_y \\ E_y & -B_z & 0 & B_x \\ E_z & B_y & -B_x & 0 \end{pmatrix}. \tag{1.3}
$$

In general we consider quasi-monochromatic waves: the amplitudes ($\varepsilon_x(t)$ and $\varepsilon_y(t)$) and the phases ($\varphi_x(t)$ and $\varphi_y(t)$) are slowly varying functions of time respect to the inverse frequency of the wave.

According to [19, 20] we introduce the *covariance* or *equal time coherence matrix*:

$$
\begin{aligned}
\boldsymbol{J} &= a^2\begin{pmatrix} \langle E_x^*(t)E_x(t)\rangle & \langle E_x^*(t)E_y(t)\rangle \\ \langle E_y^*(t)E_x(t)\rangle & \langle E_y^*(t)E_y(t)\rangle \end{pmatrix} \\
&= \frac{1}{2}\begin{pmatrix} I+Q & U-iV \\ U+iV & I-Q \end{pmatrix},
\end{aligned} \tag{1.4}
$$

where $\langle\cdots\rangle$ denotes the *ensemble average*, the average over all possible realizations of a given quasi-monochromatic wave. Each element of the coherence matrix is related to a particular combination of the Stokes parameters I, Q, U and V:

$$
\begin{aligned}
I &\equiv \frac{1}{a^2}\left(\langle E_x^*(t)E_x(t)\rangle + \langle E_y^*(t)E_y(t)\rangle\right), \tag{1.5} \\
Q &\equiv \frac{1}{a^2}\left(\langle E_x^*(t)E_x(t)\rangle - \langle E_y^*(t)E_y(t)\rangle\right), \tag{1.6} \\
U &\equiv \frac{1}{a^2}\left(\langle E_x^*(t)E_y(t)\rangle + \langle E_y^*(t)E_x(t)\rangle\right) \\
&= \frac{2}{a^2}\langle \varepsilon_x\varepsilon_y\cos(\varphi_x - \varphi_y)\rangle, \tag{1.7} \\
V &\equiv -\frac{i}{a^2}\left(\langle E_x^*(t)E_y(t)\rangle - \langle E_y^*(t)E_x(t)\rangle\right) \\
&= \frac{2}{a^2}\langle \varepsilon_x\varepsilon_y\sin(\varphi_x - \varphi_y)\rangle. \tag{1.8}
\end{aligned}
$$

For a pure monochromatic wave ensemble averages can be omitted and the wave is completely polarized:

$$4 \det \boldsymbol{J} = I^2 - Q^2 - U^2 - V^2 = 0 \,. \tag{1.9}$$

The parameter I gives the total intensity of the radiation, Q and U describe linear polarization and V circular polarization. Linear polarization can also be characterized through a vector of modulus:

$$P_L \equiv \sqrt{Q^2 + U^2} \,, \tag{1.10}$$

and an angle θ, defined as:

$$\theta \equiv \frac{1}{2} \arctan \frac{U}{Q} \,. \tag{1.11}$$

Sometimes it is also useful define the degrees of linear and circular polarization:

$$\Pi_L \equiv \frac{P_L}{I} \quad \text{and} \quad \Pi_C \equiv \frac{|V|}{I} \,. \tag{1.12}$$

Given the intensity of the polarized part $P^2 = Q^2 + U^2 + V^2 = P_L^2 + V^2$ and the total intensity I, the intensity of the non polarized part is:

$$I_{NP} \equiv \sqrt{I^2 - P^2} \,, \tag{1.13}$$

$$\Pi_{NP} \equiv \sqrt{1 - \Pi_L^2 - \Pi_V^2} = \frac{2\sqrt{\det \boldsymbol{J}}}{\text{tr}\boldsymbol{J}} \,. \tag{1.14}$$

It is important to underline that I and V are physical observables, since they are independent on the particular orientation of the reference frame in the plane perpendicular to the direction of propagation $\hat{\boldsymbol{n}}$, while Q and U depend on the orientation of this basis [21]. After a rotation of the reference frame of an angle θ $(R(\theta))$ they transform according to:

$$\begin{aligned} Q &\xrightarrow{R(\theta)} Q\cos(2\theta) + U\sin(2\theta) \,, \\ U &\xrightarrow{R(\theta)} -Q\sin(2\theta) + U\cos(2\theta) \,. \end{aligned} \tag{1.15}$$

Also linear polarization, like total intensity and circular polarization, can be described through quantities independent on the orientation of the reference

frame in the plane perpendicular to the direction of propagation of the wave. In the context of CMB anisotropies, the linear polarization vector field is usually described in terms of a gradient-like component (*E mode*) and of a curl-like component (*B mode*).

If incoming radiation field on the electron were isotropic, then radiation would remain unpolarized. Conversely if the incident radiation field possesses a quadrupolar variation in intensity the result is a linear polarization of the scattered radiation [16]. Expanding the incident intensity in spherical harmonics:

$$I'(\hat{\boldsymbol{n}}) = \sum_{lm} a_{I',lm} Y_{lm}(\boldsymbol{n}) \,, \tag{1.16}$$

and integrating over all incoming intensities, we obtain the following expression for the outgoing Stokes parameters [21]:

$$I = \frac{3\sigma_T}{16\pi} \left(\frac{8}{3}\sqrt{\pi} a_{I',00} + \frac{4}{3}\sqrt{\frac{\pi}{5}} a_{I',20} \right) \,, \tag{1.17}$$

$$Q = \frac{3\sigma_T}{4\pi} \sqrt{\frac{2\pi}{15}} \Re a_{I',22} \,, \tag{1.18}$$

$$U = -\frac{3\sigma_T}{4\pi} \sqrt{\frac{2\pi}{15}} \Im a_{I',22} \,, \tag{1.19}$$

$$\tag{1.20}$$

where σ_T is the total Thompson cross section.

In a similar way it is possible to describe the electric vector field in the $x-y$ plane through a superposition of left and right circular polarized waves defining:

$$\hat{\boldsymbol{e}}_+ \equiv \frac{\hat{\boldsymbol{e}}_{\boldsymbol{x}} + i\hat{\boldsymbol{e}}_{\boldsymbol{y}}}{\sqrt{2}} \qquad \text{and} \qquad \hat{\boldsymbol{e}}_- \equiv \frac{\hat{\boldsymbol{e}}_{\boldsymbol{x}} - i\hat{\boldsymbol{e}}_{\boldsymbol{y}}}{\sqrt{2}} \,. \tag{1.21}$$

In this new basis:

$$\begin{aligned} \boldsymbol{J} &= a^2 \begin{pmatrix} \langle E_+^*(t)E_+(t) \rangle & \langle E_+^*(t)E_-(t) \rangle \\ \langle E_-^*(t)E_+(t) \rangle & \langle E_-^*(t)E_-(t) \rangle \end{pmatrix} \\ &= \frac{1}{2} \begin{pmatrix} I+V & Q-iU \\ Q+iU & I-V \end{pmatrix} \,, \end{aligned} \tag{1.22}$$

and

$$I \equiv \frac{1}{a^2} \left(\left\langle E_+^*(t) E_+(t) \right\rangle + \left\langle E_-^*(t) E_-(t) \right\rangle \right) , \tag{1.23}$$

$$Q \equiv \frac{1}{a^2} \left(\left\langle E_+^*(t) E_-(t) \right\rangle + \left\langle E_-^*(t) E_+(t) \right\rangle \right)$$

$$= \frac{2}{a^2} \left\langle \varepsilon_+ \varepsilon_- \cos(\varphi_+ - \varphi_-) \right\rangle , \tag{1.24}$$

$$U \equiv -\frac{i}{a^2} \left(\left\langle E_+^*(t) E_-(t) \right\rangle - \left\langle E_-^*(t) E_+(t) \right\rangle \right)$$

$$= \frac{2}{a^2} \left\langle \varepsilon_+ \varepsilon_- \sin(\varphi_+ - \varphi_-) \right\rangle , \tag{1.25}$$

$$V \equiv \frac{1}{a^2} \left(\left\langle E_+^*(t) E_+(t) \right\rangle - \left\langle E_-^*(t) E_-(t) \right\rangle \right) . \tag{1.26}$$

The elements of the coherence matrix in the Fourier space are:

$$\tilde{J}_{ij} = a^2 \left\langle \tilde{E}_i^*(k, \eta) \tilde{E}_j^*(k, \eta) \right\rangle , \tag{1.27}$$

where $i, j = \{+, -\}$. Stokes parameters and the degrees of polarization are defined starting from the elements of $\tilde{J}$ as in real space.

The relation between the vector potential and the electric field for a wave propagating in a charge-free region is:

$$\boldsymbol{E} = -\frac{\partial \boldsymbol{A}}{\partial t} = -\frac{\boldsymbol{A}'}{a} , \tag{1.28}$$

According to definition given in the previous section the Stokes Parameters in terms of the vector potential are:

$$I = \frac{1}{a^4} \left(\left\langle A_+'^* A_+' \right\rangle + \left\langle A_-'^* A_-' \right\rangle \right) , \tag{1.29}$$

$$Q = \frac{1}{a^4} \left(\left\langle A_+'^* A_-' \right\rangle + \left\langle A_-'^* A_+' \right\rangle \right)$$

$$= \frac{2}{a^4} \Re \left(\left\langle A_+'^* A_-' \right\rangle \right) , \tag{1.30}$$

$$U = -\frac{i}{a^4} \left(\left\langle A_+'^* A_-' \right\rangle - \left\langle A_-'^* A_+' \right\rangle \right)$$

$$= \frac{2}{a^4} \Im \left(\left\langle A_+'^* A_-' \right\rangle \right) , \tag{1.31}$$

$$V = \frac{1}{a^4} \left(\left\langle A_+'^* A_+' \right\rangle - \left\langle A_-'^* A_-' \right\rangle \right) . \tag{1.32}$$

1.3   Rotational invariant description of Stokes parameters

Considering the polarization of CMB I and V depend only on the particular region of the celestial sphere observed, while Q and U depend also on the orientation of the reference frame in the plane perpendicular to the observation direction $\hat{\boldsymbol{n}} = \hat{\boldsymbol{n}}(\theta, \varphi)$. So I and V can be directly expanded in spherical harmonics:

$$I(\hat{\boldsymbol{n}}) = \sum_{lm} a_{I,lm} Y_{lm}(\hat{\boldsymbol{n}}), \tag{1.33}$$

$$V(\hat{\boldsymbol{n}}) = \sum_{lm} a_{V,lm} Y_{lm}(\hat{\boldsymbol{n}}). \tag{1.34}$$

In order to obtain a rotational invariant description of linear polarization (independent from the orientation of the basis in the plane perpendicular to $\hat{\boldsymbol{n}}$) it is useful to introduce two new quantity: E and B [22, 23].

A function $_s f(\hat{\boldsymbol{n}})$ defined on the sphere is said to have spin s if under a rotation of an angle θ of the reference frame changes according to:

$$_s f(\hat{\boldsymbol{n}}) \xrightarrow{R(\theta)} e^{-is\theta} {}_s f(\hat{\boldsymbol{n}}). \tag{1.35}$$

Starting from a function $_s f(\hat{\boldsymbol{n}})$ of spin s it is possible to obtain a function of spin:

- $s+1$ using the spin raising operator $\eth$:

$$\eth\, {}_s f(\hat{\boldsymbol{n}}) \xrightarrow{R(\theta)} e^{-i(s+1)\theta} \eth\, {}_s f(\hat{\boldsymbol{n}}),$$

- $s-1$ using the spin lowering operator $\bar{\eth}$:

$$\bar{\eth}\, {}_s f(\hat{\boldsymbol{n}}) \xrightarrow{R(\theta)} e^{-i(s-1)\theta} \bar{\eth}\, {}_s f(\hat{\boldsymbol{n}}).$$

When this operators act on tensor spherical harmonics the following relation are useful:

$$\eth\, {}_{\pm s} Y_{lm} = \sqrt{(l-s)(l+s+1)}\, {}_{\pm(s+1)} Y_{lm},$$
$$\bar{\eth}\, {}_{\pm s} Y_{lm} = \sqrt{(l+s)(l-s+1)}\, {}_{\pm(s-1)} Y_{lm}.$$

From Eq. (1.15) we see that $Q \pm iU$ is a spin-2 variable:

$$(Q \pm iU)(\hat{\boldsymbol{n}}) \xrightarrow{R(\theta)} e^{\mp 2i\theta}(Q \pm iU)(\hat{\boldsymbol{n}}) \,,$$

so it can be expanded on spin-2 spherical harmonics:

$$(Q \pm iU)(\hat{\boldsymbol{n}}) \;=\; \sum_{lm} a_{\pm 2,lm} \,_{\pm 2}Y_{lm}(\hat{\boldsymbol{n}}) \,.$$

Two spin-0 quantity are derived from $(Q \pm iU)(\hat{\boldsymbol{n}})$ using spin raising and lowering operators:

$$\bar{\eth}^{\,2}(Q + iU)(\hat{\boldsymbol{n}}) \;=\; \sum_{lm} a_{2,lm}\sqrt{\frac{(l+2)!}{(l-2)!}}Y_{lm}(\hat{\boldsymbol{n}}) \,,$$

$$\eth^{\,2}(Q - iU)(\hat{\boldsymbol{n}}) \;=\; \sum_{lm} a_{-2,lm}\sqrt{\frac{(l+2)!}{(l-2)!}}Y_{lm}(\hat{\boldsymbol{n}}) \,.$$

Defining:

$$a_{E,lm} \;\equiv\; -\sqrt{\frac{(l+2)!}{(l-2)!}}\frac{a_{2,lm} + a_{-2,lm}}{2} \,,$$

$$a_{B,lm} \;\equiv\; -i\sqrt{\frac{(l+2)!}{(l-2)!}}\frac{a_{2,lm} - a_{-2,lm}}{2} \,,$$

we obtain:

$$\begin{aligned}
E(\hat{\boldsymbol{n}}) &= \sum_{lm} a_{E,lm}Y_{lm}(\boldsymbol{n}) \\
&= -\frac{1}{2}\left[\bar{\eth}^{\,2}\left(Q + iU\right)(\hat{\boldsymbol{n}}) + \eth^{\,2}\left(Q - iU\right)(\hat{\boldsymbol{n}})\right] , \quad (1.36) \\
B(\hat{\boldsymbol{n}}) &= \sum_{lm} a_{B,lm}Y_{lm}(\boldsymbol{n}) \\
&= -\frac{i}{2}\left[\bar{\eth}^{\,2}\left(Q + iU\right)(\hat{\boldsymbol{n}}) - \eth^{\,2}\left(Q - iU\right)(\hat{\boldsymbol{n}})\right] , \quad (1.37)
\end{aligned}$$

where the explicit expressions for raising and lowering operators in this particular case are:

$$\bar{\eth}^{\,2}(Q + iU)(\hat{n}) \;=\; \left(-\frac{\partial}{\partial\mu} + \frac{m}{1-\mu^2}\right)^2 \left[(1-\mu^2)(Q+iU)(\hat{n})\right] , (1.38)$$

$$\eth^{\,2}(Q - iU)(\hat{n}) \;=\; \left(-\frac{\partial}{\partial\mu} - \frac{m}{1-\mu^2}\right)^2 \left[(1-\mu^2)(Q-iU)(\hat{n})\right] , (1.39)$$

with $\mu \equiv \cos\theta$.

1.4   Polarization properties under parity

Stokes parameters have definite behavior under parity transformation:

$$
\begin{aligned}
I &\xrightarrow{P} I \,, \\
Q &\xrightarrow{P} Q \,, \\
U &\xrightarrow{P} -U \,, \\
V &\xrightarrow{P} -V \,.
\end{aligned}
$$

Raising and lowering operators (1.38,1.39) change under parity transformations according to:

$$
\begin{aligned}
\bar{\eth}^2 \, (Q + iU) &\xrightarrow{P} \eth^2 \, (Q - iU) \,, \\
\eth^2 \, (Q - iU) &\xrightarrow{P} \bar{\eth}^2 \, (Q + iU) \,,
\end{aligned}
$$

so, E and B, defined in equations (1.36,1.37), change according to:

$$
\begin{aligned}
E &\xrightarrow{P} E \,, \\
B &\xrightarrow{P} -B \,.
\end{aligned}
$$

The transformations properties of the coefficients $a_{X,lm}$ ($X \in \{I, E, B, V\}$) of the expansion of X in spherical harmonics can be easily obtained using the parity properties of spherical harmonics $Y_{lm}(\boldsymbol{n}) \xrightarrow{P} (-1)^l Y_{lm}(\boldsymbol{n})$:

$$
\begin{aligned}
a_{I,lm} &\xrightarrow{P} (-1)^l \, a_{I,lm} \,, \\
a_{E,lm} &\xrightarrow{P} (-1)^l \, a_{E,lm} \,, \\
a_{B,lm} &\xrightarrow{P} (-1)^{l+1} \, a_{B,lm} \,, \\
a_{V,lm} &\xrightarrow{P} (-1)^{l+1} \, a_{V,lm} \,.
\end{aligned}
$$

Defined the power spectrum as:

$$
C_l^{XY} \equiv \frac{1}{2l+1} \sum_m \left\langle \left(a_{X,lm}\right)^* a_{Y,lm} \right\rangle \,, \tag{1.40}
$$

where $X, Y \in \{I, E, B, V\}$, from the previous relations we obtain the following properties for power spectra under parity transformations:

$$C_l^{II} \xrightarrow{P} C_l^{II}$$
$$C_l^{IE} \xrightarrow{P} C_l^{IE} \qquad C_l^{EE} \xrightarrow{P} C_l^{EE}$$
$$C_l^{IB} \xrightarrow{P} -C_l^{IB} \qquad C_l^{EB} \xrightarrow{P} -C_l^{EB} \qquad C_l^{BB} \xrightarrow{P} C_l^{BB}$$
$$C_l^{IV} \xrightarrow{P} -C_l^{IV} \qquad C_l^{EV} \xrightarrow{P} -C_l^{EV} \qquad C_l^{BV} \xrightarrow{P} C_l^{BV} \qquad C_l^{VV} \xrightarrow{P} C_l^{VV}$$

In absence of parity-violating interactions, the ensemble of fluctuations is statistically parity symmetric and therefore the parity odd correlators (C_l^{IB}, C_l^{IB}, C_l^{IV} and C_l^{EV}) have to vanish.

A considerable effort had been devoted to the study of parity violating interactions of the photons of CMBR through the observational constraints on C_l^{IB} and C_l^{EB} [5]. Actually also the correlators C_l^{IV} and C_l^{EV} contains information about parity violating interactions; they can be used to discriminate between different parity violating interactions. Faraday Conversion (FC), for instance, converts linear into circular polarization [24] and so generates $C_l^{EV} \neq 0$, while Faraday Rotation, which simply rotates the plane of linear polarization, does not.

1.5 Boltzmann equation

In the synchronous gauge metric perturbations are described by [25]:

$$ds^2 = a(\eta) \left[-d\eta^2 + (\delta_{i,j} + h_{ij}) \, dx^i dx^j \right] , \qquad (1.41)$$

g_{00} and g_{0i} are by definition unperturbed. Metric perturbations can be decomposed in a trace part $h \equiv h_{ii}$ and a traceless part (consisting of three pieces). $h_{ij} = h\delta_{ij}/3 + h_{ij}^{\parallel} + h_{ij}^{\perp} + h_{ij}^{T}$:

$$\epsilon_{ijk}\partial_j\partial_l h_{lk}^{\parallel} = 0 , \quad \partial_i\partial_j h_{ij}^{\perp} = 0 , \quad \partial_i h_{ij}^{T} = 0 . \qquad (1.42)$$

Perturbations are expanded in Fourier modes characterized by the wavevector $\mathbf{k}$. Introduced the two fields $h(\mathbf{k}, \eta)$ and $\tilde{\eta}(\mathbf{k}, \eta)$ the scalar mode of h_{ij} can

be written as Fourier integrals:

$$h_{ij}(\mathbf{k},\eta) = \int d^3k\, e^{i\mathbf{k}\cdot\mathbf{x}}\left[\hat{\mathbf{k}}_i\hat{\mathbf{k}}_j h(\mathbf{k},\eta) + \left(\hat{\mathbf{k}}_i\hat{\mathbf{k}}_j - \delta_{ij}/3\right)6\tilde{\eta}(\mathbf{k},\eta)\right]. \qquad (1.43)$$

Note the difference between $\tilde{\eta}$ describing the Fourier transform of metric perturbations and the cosmic time η.

The Boltzmann equations for the evolution of the temperature and polarization scalar perturbations, in the synchronous gauge, are [26, 22]:

$$\Delta'_T + ik\mu\Delta_T = -\frac{h'}{6} - \frac{(h'+6\tilde{\eta}')}{3}P_2(\mu)$$
$$+\kappa'\left[-\Delta_T + \Delta_{T0} + iv_b\mu - \frac{1}{2}P_2(\mu)\Pi\right], \qquad (1.44)$$
$$\Delta'_{Q\pm iU}(k,\eta) + ik\mu\Delta_{Q\pm iU}(k,\eta) =$$
$$\kappa'\left[-\Delta_{Q\pm iU} + \frac{1}{2}\left(1 - P_2(\mu)\right)\Pi\right], \qquad (1.45)$$
$$\Pi = \Delta_{T,2} + \Delta_{Q\pm iU,0} + \Delta_{Q\pm iU,2}. \qquad (1.46)$$

where μ is the cosine of the angle between the CMB photon direction and the Fourier wave vector, κ' is the differential optical depth ($\kappa' \equiv n_e\sigma_T a/a_0$, n_e is the number density of free electrons, σ_T is the Thomson cross section) $P_2(\mu)$ is the Legendre polynomial of l−th order ($P_2(\mu) = (3\mu^2 - 1)/3$), and the multipole moments of temperature and polarization are:

$$\Delta_T(k,\mu) = \sum_l (-i)^l (2l+1)\Delta_{T,l}P_l(\mu), \qquad (1.47)$$

$$\Delta_{Q\pm iU}(k,\mu) = \sum_l (-i)^l (2l+1)\Delta_{Q\pm iU,l}P_l(\mu). \qquad (1.48)$$

If the orientation of linear polarization changes of an angle θ the Stokes parameters changes according Eq. (1.15). Assuming that the rotation angle varies with conformal time ($\theta = \theta(\eta)$), the derivative of Q and U respect to time is:

$$Q'(\eta) = 2\theta'\left[-Q\sin(2\theta) + U\cos(2\theta)\right] = 2\theta'U, \qquad (1.49)$$
$$U'(\eta) = -2\theta'\left[Q\cos(2\theta) + U\sin(2\theta)\right] = -2\theta'Q. \qquad (1.50)$$

So, for the evolution of linear polarization perturbation:

$$\Delta_Q' \quad \propto \quad 2\theta' \Delta_U \,, \tag{1.51}$$

$$\Delta_U' \quad \propto \quad -2\theta' \Delta_Q \,. \tag{1.52}$$

therefore:

$$\Delta_{Q\pm iU}' \propto \mp i2\theta' \Delta_{Q\pm iU} \,. \tag{1.53}$$

The effect of a physical mechanism rotating the linear polarization plane was included for the first time in Boltzmann equations in order to study Faraday rotation of CMB radiation [27, 28, 29, 30] . The Boltzmann equation for spin-2 functions $Q \pm iU$ is:

$$\Delta_{Q\pm iU}'(k,\eta) + ik\mu \Delta_{Q\pm iU}(k,\eta) =$$
$$\kappa' \left[-\Delta_{Q\pm iU} + \frac{1}{2} \left(1 - P_2(\mu) \right) \Pi \right]$$
$$\mp i2\theta'(\eta) \Delta_{Q\pm iU}(k,\eta) \,. \tag{1.54}$$

Note that Eq. (1.54) corrects some typos in Eq. (1) of Ref. [31].

As we already discussed in section 1.3 that the quantity $\Delta_{Q\pm iU}$ is related to the rotation invariant polarization fields Δ_E and Δ_B through the spin raising ($\eth$) and lowering ($\bar{\eth}$) operators [32]:

$$\Delta_E \quad \equiv \quad -\frac{1}{2} \left(\bar{\eth}^2 \Delta_{Q+iU} + \eth^2 \Delta_{Q-iU} \right) \,, \tag{1.55}$$

$$\Delta_B \quad \equiv \quad -\frac{i}{2} \left(\bar{\eth}^2 \Delta_{Q+iU} - \eth^2 \Delta_{Q-iU} \right) \,. \tag{1.56}$$

If linear polarization is isotropically rotated of an angle $\theta = \theta(\eta)$, then:

$$\begin{aligned}
\Delta_{E_2} &= -\frac{1}{2} \left[\bar{\eth}^2 \left(e^{-2i\theta} \Delta_{Q_1+iU_1} \right) + \eth^2 \left(e^{2i\theta} \Delta_{Q_1-iU_1} \right) \right] \\
&= -\frac{1}{2} \cos(2\theta) \left(\bar{\eth}^2 \Delta_{Q_1+iU_1} + \eth^2 \Delta_{Q_1-iU_1} \right) \\
&\quad + \frac{i}{2} \sin(2\theta) \left(\bar{\eth}^2 \Delta_{Q_1+iU_1} - \eth^2 \Delta_{Q_1-iU_1} \right) \\
&= \Delta_{E_1} \cos(2\theta) - \Delta_{B_1} \sin(2\theta) \,,
\end{aligned} \tag{1.57}$$

and:

$$
\begin{aligned}
\Delta_{B_2} &= -\frac{i}{2}\left[\bar{\eth}^{\,2}\left(e^{-2i\theta}\Delta_{Q_1+iU_1}\right) - \eth^{\,2}\left(e^{2i\theta}\Delta_{Q_1-iU_1}\right)\right] \\
&= -\frac{i}{2}\cos(2\theta)\left(\bar{\eth}^{\,2}\Delta_{Q_1+iU_1} - \eth^{\,2}\Delta_{Q_1-iU_1}\right) \\
&\quad -\frac{1}{2}\sin(2\theta)\left(\bar{\eth}^{\,2}\Delta_{Q_1+iU_1} + \eth^{\,2}\Delta_{Q_1-iU_1}\right) \\
&= \Delta_{B_1}\cos(2\theta) + \Delta_{E_1}\sin(2\theta)\,. \qquad\qquad\qquad (1.58)
\end{aligned}
$$

Note that this is true only for isotropic angles of rotations, otherwise:

$$
\bar{\eth}^{\,2}\left(e^{-2i\theta}\Delta_{Q_1+iU_1}\right) \neq e^{-2i\theta}\bar{\eth}^{\,2}\Delta_{Q_1+iU_1}\,,
$$

(e.g. this is not true for Faraday rotation (see section 1.6)). Therefore, combining the two results:

$$
\Delta_{E_2} + i\Delta_{B_2} = \Delta_{E_1}\left[\cos(2\theta) + i\sin(2\theta)\right] + \Delta_{B_1}\left[-\sin(2\theta) + i\cos(2\theta)\right].(1.59)
$$

If $\Delta_{B_1} = 0$:

$$
\Delta_{E_2} + i\Delta_{B_2} = \Delta_{E_1}e^{i2\theta}\,, \qquad\qquad\qquad (1.60)
$$

where:

$$
\theta(\eta) = \int_0^\eta d\eta_*\,\theta'(\eta_*)\,. \qquad\qquad\qquad (1.61)
$$

Following the line of sight strategy for scalar perturbations we obtain, in agreement with Ref. [31]:

$$
\begin{aligned}
\Delta_T(k,\eta) &= \int_0^{\eta_0} d\eta\, g(\eta) S_T(k,\eta) j_\ell(k\eta_0 - k\eta)\,, \qquad\qquad (1.62) \\
\Delta_E(k,\eta) &= \int_0^{\eta_0} d\eta\, g(\eta) S_P^{(0)}(k,\eta)\frac{j_\ell(k\eta_0 - k\eta)}{(k\eta_0 - k\eta)^2}\cos\left[2\theta(\eta)\right]\,, \quad (1.63) \\
\Delta_B(k,\eta) &= \int_0^{\eta_0} d\eta\, g(\eta) S_P^{(0)}(k,\eta)\frac{j_\ell(k\eta_0 - k\eta)}{(k\eta_0 - k\eta)^2}\sin\left[2\theta(\eta)\right]\,. \quad (1.64)
\end{aligned}
$$

where $g(\eta)$ is the visibility function, $S_T(k,\eta)$ is the source term for temperature anisotropies, $S_P^{(0)}(k,\eta)$ is the source term for polarization, and j_ℓ is the spherical Bessel function of order ℓ. The polarization C_ℓ auto- and

cross-spectra are given by:

$$C_\ell^{EE} = (4\pi)^2 \frac{9\,(\ell+2)!}{16\,(\ell-2)!} \int k^2 dk \, [\Delta_E(k,\eta_0)]^2 \,, \tag{1.65}$$

$$C_\ell^{BB} = (4\pi)^2 \frac{9\,(\ell+2)!}{16\,(\ell-2)!} \int k^2 dk \, [\Delta_B(k,\eta_0)]^2 \,, \tag{1.66}$$

$$C_\ell^{EB} = (4\pi)^2 \frac{9\,(\ell+2)!}{16\,(\ell-2)!} \int k^2 dk \, \Delta_E(k,\eta_0)\Delta_B(k,\eta_0) \,, \tag{1.67}$$

$$C_\ell^{TE} = (4\pi)^2 \sqrt{\frac{9\,(\ell+2)!}{16\,(\ell-2)!}} \int k^2 dk \, \Delta_T(k,\eta_0)\Delta_E(k,\eta_0) \,, \tag{1.68}$$

$$C_\ell^{TB} = (4\pi)^2 \sqrt{\frac{9\,(\ell+2)!}{16\,(\ell-2)!}} \int k^2 dk \, \Delta_T(k,\eta_0)\Delta_B(k,\eta_0) \,. \tag{1.69}$$

In the approximation in which $\theta = \bar\theta$, with $\bar\theta$ constant in time, Eqs. (1.63) and (1.64) simplify in

$$\Delta_E^{obs} = \Delta_E(\theta=0)\cos(2\bar\theta) \,, \tag{1.70}$$

$$\Delta_B^{obs} = \Delta_E(\theta=0)\sin(2\bar\theta) \,, \tag{1.71}$$

and the power spectra are given by [5, 33]:

$$C_\ell^{EE,obs} = C_\ell^{EE}\cos^2(2\bar\theta) \,, \tag{1.72}$$

$$C_\ell^{BB,obs} = C_\ell^{EE}\sin^2(2\bar\theta) \,, \tag{1.73}$$

$$C_\ell^{EB,obs} = \frac{1}{2}C_\ell^{EE}\sin(4\bar\theta) \,, \tag{1.74}$$

$$C_\ell^{TE,obs} = C_\ell^{TE}\cos(2\bar\theta) \,, \tag{1.75}$$

$$C_\ell^{TB,obs} = C_\ell^{TE}\sin(2\bar\theta) \,. \tag{1.76}$$

The expression for $\bar\theta$ to insert in Eqs. (1.71-1.76) is:

$$\bar\theta = \frac{g_\phi}{2}\left[\phi(\eta_0) - \phi(\eta_{\rm rec})\right] \,. \tag{1.77}$$

Several limits on the constant rotation angle $\bar\theta$ have been already obtained using current observation of CMBP (see Tab. 1.1).

This time independent rotation angle approximation is an operative approximation, clearly inconsistent since for $\theta = $ const the term proportional

Data set	$\bar{\theta}\ (2\sigma)$ [deg]
WMAP3 and Boomerang (B03) [33]	$-13.7 < \bar{\theta} < 1.9$
WMAP3 [34]	$-8.5 < \bar{\theta} < 3.5$
WMAP5 [6]	$-5.9 < \bar{\theta} < 2.4$
QUaD [35]	$-1.2 < \bar{\theta} < 3.9$

Table 1.1: Constraints on linear polarization rotation $\bar{\theta}$ in the constant angle approximation.

to θ' in the Boltzmann equation (1.54) vanishes and therefore there is no rotation of the linear polarization plane. See section 3.6 for a comparison of this approximation with a full Boltzmann description of the birefringence effect for a dynamical pseudoscalar field.

If $\theta = \bar{\theta}$ the degree of linear polarization is conserved from recombination to nowadays. Conversely in the general case of a time dependent rotation angle $\theta = \theta(\eta)$ liner polarization is no more conserved and other phenomena like depolarization, generation of circular polarization, ... can be allowed.

1.6   Faraday rotation and conversion

A possible mechanism responsible for linear polarization plane rotation is photon propagation through a plasma in presence of a magnetic field **B** (generalized Faraday rotation). Properties of the wave will depend on the direction of propagation relative to the direction of the magnetic field [36].

First we consider an electromagnetic wave propagating along the magnetic field direction (see Fig.1.3a), in this case normal modes are circular polarized waves. A linearly polarized wave can be composed of two orthogonal circularly polarized modes shifted in phase. The circular modes will resonate with either electrons or positrons gyrating around the magnetic fields. The latter will again emit circular polarized wave, producing a phase shift in the circular modes. Recombining the circular polarized modes after leaving the
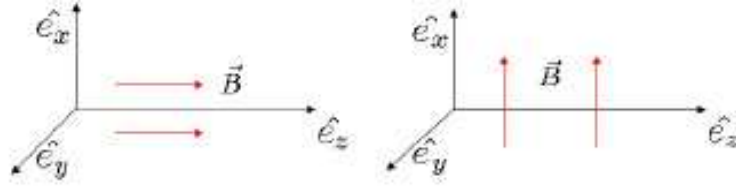
Figure 1.3: Faraday rotation (magnetic field component along the line of sight) and Faraday conversion (magnetic field component perpendicular to the line of sight).

plasma results in a rotated linear polarization of an angle (*Faraday rotation*):

$$
\begin{aligned}
\Delta\theta_{FR} &= \frac{e^3\lambda^2}{2\pi m_{\mathrm{e}}^2 c^4}\int dl\, n_{\mathrm{e}}(l)B\mu \\[2mm]
&\simeq 8\times 10^{-2}\,\mathrm{rad}\,(1+z)^{-2}\left(\frac{\lambda_0}{1\,\mathrm{cm}}\right)^2 \\[2mm]
&\quad \int \frac{dl}{1\,\mathrm{kpc}}\left(\frac{n_{\mathrm{e}}}{0.1\,\mathrm{cm}^{-3}}\right)\left(\frac{B}{10\,\mu\mathrm{G}}\right)\mu\,,
\end{aligned}
\tag{1.78}
$$

where μ is the cosine of the angle between the line of sight direction and the magnetic field $\mathbf{B}$, n_{e} is the number density of electrons, $\lambda = \lambda_0(1+z)^{-1}$ is the wavelength of radiation with wavelength today given by λ_0.

Perpendicular to the magnetic field normal modes are linearly polarized (see Fig.1.3b). The resonating electrons or positrons will themselves act as antennas and emit a somewhat delayed wave, leading to a resulting phase-shift between vertical and horizontal modes. This lead to a cyclic transformation of linear polarization U into V (*Faraday conversion*):

$$
\begin{aligned}
\Delta\theta_{FC} &= \frac{e^4\lambda^3}{\pi^2 m_{\mathrm{e}}^3 c^5}\left(\frac{\beta-1}{\beta-2}\right)\int dl\, n_{\mathrm{r}}(l)\gamma_{\min}B^2(1-\mu^2) \\[2mm]
&\simeq 3\times 10^{-7}\,\mathrm{rad}\,(1+z)^{-3}\left(\frac{\lambda_0}{1\,\mathrm{cm}}\right)^3\left(\frac{\beta-1}{\beta-2}\right)_{\beta=2.5} \\[2mm]
&\quad \int \frac{dl}{1\,\mathrm{kpc}}\left(\frac{n_{\mathrm{r}}}{0.1\,\mathrm{cm}^{-3}}\right)\left(\frac{\gamma_{\min}}{300}\right)\left(\frac{B}{10\,\mu\mathrm{G}}\right)^2(1-\mu^2)\,,
\end{aligned}
\tag{1.79}
$$

where n_{r} is the number density of relativistic particles and β defines the power-law distribution of the particles, in terms of the Lorentz factor γ, such

that:

$$N(\gamma) = N_0\gamma^{-\beta} \quad \text{for} \quad \gamma_{\min} < \gamma < \gamma_{\max}\,. \tag{1.80}$$

Normal modes in a plasma are generally elliptically polarized, however conversion is mainly produced by magnetic fields components perpendicular to the line of sight, while Faraday rotation is produced by magnetic field components along the line of sight [37].

The effect of Faraday conversion on CMBP and the possible generation of a certain degree of circular polarization were discussed in Ref. [24]. Usually CMBP experiments are not sensitive to circular polarization, because it cannot be generated through Thomson scattering (see section 1.2). However first upper limits on circular polarization were already presented in 1983 by P. Lubin, P. Melese and G. Smoot [38], see also Ref. [39] for an update on possible systematics. Today, as far as we know, measurement of the four Stokes parameters, T, Q, U, and V can be performed only by few interferometric experiments (e.g. AMiBA [40]).

Chapter 2

Pseudoscalar fields - an introduction

2.1 Introduction

We briefly present here the main theoretical motivations, experimental/observational constraints, and cosmological implications for axions and others ultralight pseudoscalar particles beyond the standard model. The existence of low mass particles is related to symmetries by the Nambu-Goldstone theorem:

whenever a global continuous symmetry of the action is not respected by the ground state, there appear massless particles, one for each broken generator of the symmetry group.

Here we are interested mainly in theories where continuous symmetries are just approximate, the potential is divided in a symmetric part $V_0(\phi)$ and a breaking term $V_1(\phi)$. If the breaking term is small the new particle can have small mass (pseudo Nambu-Goldstone bosons).

2.2   Axions

This section is mainly based on Refs. [1, 2, 41], more details can be found in Refs. [42, 43, 44, 45, 46, 47, 48, 49] and references therein. See Ref. [50] for an original pedagogical review.

2.2.1   Theoretical motivations

Non-Abelian gauge theories have a rich vacuum state structure; degenerate vacuum configurations are classified by the topological winding number n associated with them:

$$n = \frac{ig^3}{24\pi^2} \int dx^3 \, \text{Tr} \, \epsilon_{ijk} A^i(\mathbf{x}) A^j(\mathbf{x}) A^k(\mathbf{x}) \,, \tag{2.1}$$

where g is the gauge coupling, A^i is the gauge field (temporal gauge $A^0 = 0$). The correct vacuum state of the theory is a superposition of different states:

$$|\Theta\rangle = \sum_n \exp\left(-in\Theta\right) |n\rangle \,, \tag{2.2}$$

Θ is an arbitrary parameter of the theory which must be measured; we refer to $|\Theta\rangle$ as the Θ-vacuum.

The effects of the Θ-vacuum can be recast into a single additional non-perturbative term in the QCD Lagrangian:

$$\begin{aligned} \mathcal{L}_{\text{QCD}} &= \mathcal{L}_{\text{PERT}} + \bar{\Theta} \frac{g^2}{32\pi^2} G^{a\mu\nu} \tilde{G}^a_{\ \mu\nu} \,, \tag{2.3} \\ \bar{\theta} &\equiv \Theta + \text{Arg} \, \det\mathcal{M} \,, \tag{2.4} \end{aligned}$$

where $G^{a\mu\nu}$ is the gluon field strength tensor, $\tilde{G}^a_{\ \mu\nu}$ is its dual, $\mathcal{M}$ is the quark mass matrix ($\det\mathcal{M}$ would vanish if one of the quark were exactly massless). Under the combined action of charge conjugation (C) and parity transformation (P) the new term changes sign violating the CP invariance of QCD ($G^{a\mu\nu} \tilde{G}^a_{\ \mu\nu} \propto \mathbf{E}_{color} \cdot \mathbf{B}_{color}$ the scalar product of a polar with an axial vector is CP-odd). This new term leads to a neutron dipole moment of the order:

$$|d_n| \simeq |\bar{\Theta}| \, 10^{-16} \, \text{e cm} \,. \tag{2.5}$$

The present experimental bound to the electric dipole moment of the neutron [51]

$$|d_n| < 2.9 \times 10^{-26} \, \text{e cm} \tag{2.6}$$

indicates $\bar{\Theta} < 10^{-10}$. The sum of two very different quantities Θ and Arg det$\mathcal{M}$ must be surprisingly small; this value is small even compared with the phase $\delta = 3.3 \times 10^{-3}$ which appears in the Cabibbo-Kobayashi-Maskawa matrix and which explains the observed effects in the $K^0 - \bar{K}^0$ system. This is called the strong CP-problem of QCD.

In 1977 R. Peccei and H. Quinn [52] suggested a solution to this problem introducing a new global chiral symmetry $U(1)_{\text{PQ}}$ which is broken at scale f_a by the vacuum expectation value of a complex scalar field

$$\Phi = f_a e^{i\frac{\phi}{f_a}} \, , \tag{2.7}$$

$\bar{\Theta}$ becomes a dynamical variable which is driven to zero by the action of its classical potential.

The following year Weinberg [53] and Wilczek [54] pointed out, almost simultaneously, that because $U(1)_{\text{PQ}}$ is a spontaneously broken global symmetry, there must be a Nambu-Goldstone boson (the axion) associated with it.

$\bar{\Theta}$ is now replaced by ϕ/f_a, including a kinetic term for the axion Eq. (2.3) now becomes:

$$\mathcal{L}_{\text{QCD}} = \mathcal{L}_{\text{PERT}} + \frac{1}{2}\nabla_\mu\phi\nabla^\mu\phi + \frac{g^2}{32\pi^2}\frac{\phi}{f_a}G^{a\mu\nu}\tilde{G}^a_{\ \mu\nu} \, . \tag{2.8}$$

This lagrangian is the minimal ingredient for any axion model.

Even if axions were constructed to be massless they acquire an effective mass by their interaction with gluons. This coupling induces a transition to $q\bar{q}$ states and thus to neutral pions, so axions mix with pions an pick up a small mass:

$$m \simeq \frac{f_\pi m_\pi}{f_a}\frac{z^{1/2}}{1+z} \sim 0.6 \, \text{eV}\frac{10^{16} \, \text{eV}}{f_a} \, , \tag{2.9}$$

where $f_\pi \simeq 92$ MeV is the pion decay constant, $m_\pi = 135$ MeV is the pion mass, and $z \equiv m_u/m_d \simeq 0.56$ is the up/down quark mass ratio. Because

of the mixing with π^0, axions share not only their mass, but also their couplings to photons and nucleons with a strength reduced by about f_π/f_a. The effective lagrangian for the interaction of the axion with ordinary matter (nucleons, electrons and photons) is:

$$\mathcal{L}_{\text{INT}} = i\frac{g_{\phi N}}{2m_N}\partial_\mu\phi\left(\bar{N}\gamma^\mu\gamma_5 N\right) + i\frac{g_{\phi e}}{2m_e}\partial_\mu\phi\left(\bar{e}\gamma^\mu\gamma_5 e\right) - \frac{g_{\phi\gamma}}{4}\phi F_{\mu\nu}\tilde{F}^{\mu\nu}, \quad (2.10)$$

with:

$$g_{\phi N} = C_N\frac{m_N}{f_a}, \quad g_{\phi e} = C_e\frac{m_e}{f_a}, \quad g_{\phi\gamma} = \xi\frac{3}{4}\frac{\alpha_{\text{EM}}}{2\pi f_a}, \quad (2.11)$$

where C_N, C_e, ξ are model dependent constants. Note that all coupling constants are proportional to $1/f_a$, or equivalently, to m: the smaller the axion mass, or the larger the PQ breaking scale, the more weakly the axion couples (see Fig. 2.1).
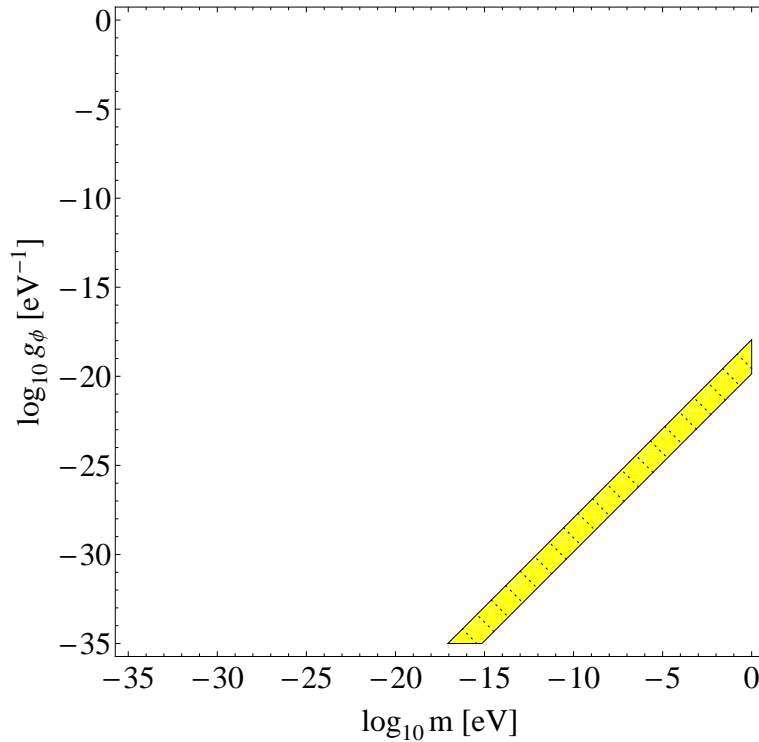

Figure 2.1: Predicted $g_{\phi\gamma}$ for KSVZ and DFSZ invisible axion models.

In the first axion models (*standard model axions*), proposed at the end of the seventies, the breaking scale was of the same order of the weak scale ($f_a \sim f_{\text{weak}} \simeq 250$ GeV), now this models are ruled out both by experiments and observations. Taking $f_a \gg f_{\text{weak}}$ the axion mass becomes very small and its interactions very weak (*invisible axion models*): two widely discussed models of this kind are the hadronic or KSVZ model (Kim; Shifman, Vainshtein, and Zakharov) [55, 56] and the DFSZ model (Dine, Fischler, Srednicki; Zhitnitskii) [57, 58]. The main difference between these two models is that in DFSZ axions couple to charged leptons in addition to nucleons and photons. In these models $f_a \gg f_{\text{weak}}$, so one may attempt to identify f_a with the grand unification scale $f_{\text{GUT}} \simeq 10^{16}$ GeV, however the cosmological bounds disfavor this under particular assumptions for $\bar{\Theta}$ initial value (see section 2.2.3).

2.2.2 Experimental and astrophysical constraints

Coupling with photons plays a key role for most of the axion searches. The most promising approaches uses the axion-two-photon vertex indeed, allowing axions and photons to convert into each others in the presence of an external magnetic or electric field (see Fig. 2.2).
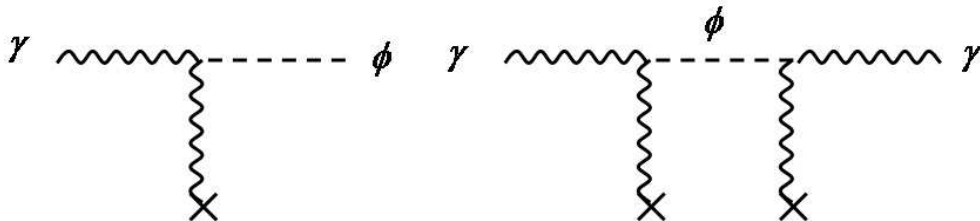

Figure 2.2: Most of the axion searches make use of the Primakoff effect, by which axions convert into photons in presence of an external electromagnetic field. *(Left)* Dichroism in polarization experiments; *(right)* birefringence in polarization experiments, light shining through walls experiments.

Currently the best laboratory limit comes from **photon regeneration experiments**, in particular from experiments based on astrophysical sources

of axions. Axion produced by the Sun core by the Primakoff effect are converted back into photons in a strong magnetic field. Eventually these photons, which have the same energy spectrum as the incoming axions, could be collected by a X-ray detector placed at the end of the magnetic field area. The CAST (Cern Axion Solar Telescope) experiment obtained the constraint [59]:

$$g_{\phi\gamma} < 8.8 \times \times 10^{-20} \, \text{eV}^{-1} \quad \text{for} \quad m < 0.02 \, \text{eV} \,, \tag{2.12}$$

using a decommissioned LHC dipole magnet ($B \sim 9.0$ T and $L \sim 9.26$ m). It is possible to constrain $g_{\phi\gamma}$ only in a specific mass range because axion and photon fields must remain in phase over the length of the magnetic field; coherence can be restored for higher axion masses by filling the magnetic cavity with a buffer gas, such that the photons inside the magnet pipe acquire an effective mass.

Another different approach to detect solar axions uses the intense Coulomb field of nuclei in a crystal lattice, instead of an external magnetic field, to convert axions into photons by the Primakoff effect (Bragg diffraction) [60, 61]. It was shown in Ref. [62] that the annual modulation observed by the DAMA experiments can be interpreted in terms of a KeV-mass axion like particles with $g_{\phi e} \sim 2 \times 10^{-11}$. However couplings of these orders between pseudoscalar particles and electrons are excluded by globular cluster limits on stellar energy losses and by limits on solar neutrino flux (SNO) [63].

Galactic halo cold dark matter axions can be detected by their resonant conversion into a quasi-monochromatic microwave signal in an electromagnetic cavity permeated by a strong static magnetic field (microwave cavity experiments). Due to the very low mass of dark matter axions the expected signal is minuscule and therefore the sensitivity of the experiment crucially depend on the quality of the microwave receiver. Today experiments such as ADMX (Axion Dark Matter Experiment) are taking data and providing very good upper limits for $g_{\phi\gamma}$ in the mass range between 10^{-4} eV and 10^{-6} eV [64].

An alternative to regenerating the lost photons is to detect directly the

photon-axion conversion looking at changes in photon polarization propagation through magnetic fields [65] (**photon polarization experiments**). The two effects which modify polarization are:

- *Dichroism.* The component of the electric field parallel to the magnetic field ($E_\parallel$), but not the perpendicular component ($E_\perp$), will be depleted by the production of axions and thus there will be in general a small rotation of the polarization vector of linearly polarized light (see left side of Fig. 2.2).

- *Birefringence.* This rotation occurs because there is a mixing of virtual axions in the $E_\parallel$ state, but not in the $E_\perp$ component (see right side of Fig. 2.2). Hence initially linearly polarized light will become elliptically polarized.

Note that a non-vanishing signal for dichroism is expected anyhow in standard QED, arising from photon-photon scattering induced by an electron loop. Using the well-known Euler-Heisenberg effective lagrangian [66, 67], the linear polarization angle rotates of [65]

$$\theta_{\text{QED}} = \frac{\alpha_{\text{EM}}^2}{30\pi} \frac{L\omega B^2}{m_e^4} \,, \tag{2.13}$$

if light propagates in a region of length L with magnetic field B.

In 2006 PVLAS collaboration reported a signature of magnetically induced vacuum dichroism, which could have been interpreted as evidence for light pseudoscalar field with mass $m \sim 10^{-3}$ eV and photon coupling of order $g_{\phi\gamma} \sim 10^{-15}$ eV^{-1} [68]. This result was in disagreement with more restrictive limits on $g_{\phi\gamma}$ (e.g. CAST constraint) and one year later was retracted also by the PVLAS collaboration. They conclude that the effects where instrumental artifacts, with no evidence for new physics [69]. Anyhow this claim has inspired a lot of fruitful experimental and theoretical activity.

Stellar energy loss limits. Low mass weakly interacting particles are produced in hot astrophysical plasmas, and can thus transport energy out of stars. The coupling strength of the particles with normal matter and
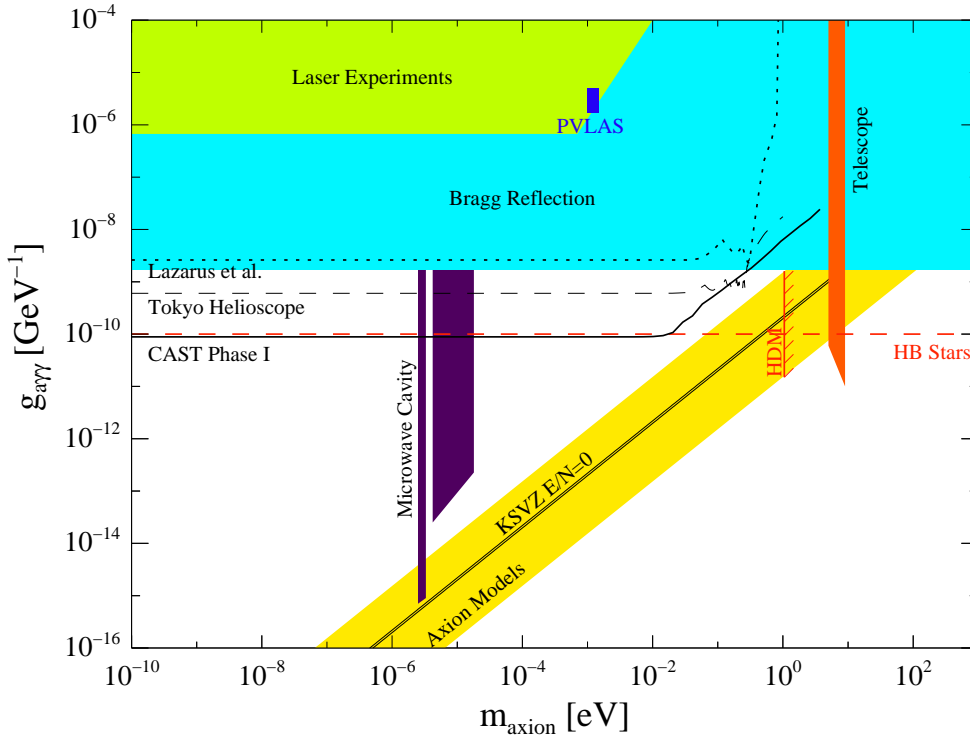
Figure 2.3: Exclusion plots in the m versus $g_{\phi\gamma}$ parameter space. Figure taken from [49].

radiation is bounded by the constraint that stellar evolution lifetimes or energy-loss rates not conflict with observations. A restrictive limit on the axion-photon coupling constant comes from globular cluster stars[1], the main effect is accelerated consumption of helium; a reasonably conservative limit is [2, 44]:

$$g_{\phi\gamma} < \times 10^{-19}\,\mathrm{eV}^{-1}\,. \tag{2.14}$$

In models where axion couples directly to electrons (e.g. DFSZ) processes of the form $\gamma\,e^- \rightarrow e^-\,\phi$ and $\gamma\,Ze \rightarrow Ze\,e^-\,\phi$ are more efficient than the Primakoff effect, so it is possible to obtain quite strong constraints [41]:

$$g_{\phi e} < 1.3 \times 10^{-13}\,. \tag{2.15}$$

---

[1]A *globular cluster* is a gravitationally bound system of a homogeneous population of low-mass stars allowing for a detailed test for stellar-evolution theory.

2.2.3 Cosmology

The invisible axion with a large decay constant ($f_a \simeq 10^{21}$ eV) was found to be a good candidate for cold dark matter component of the universe.
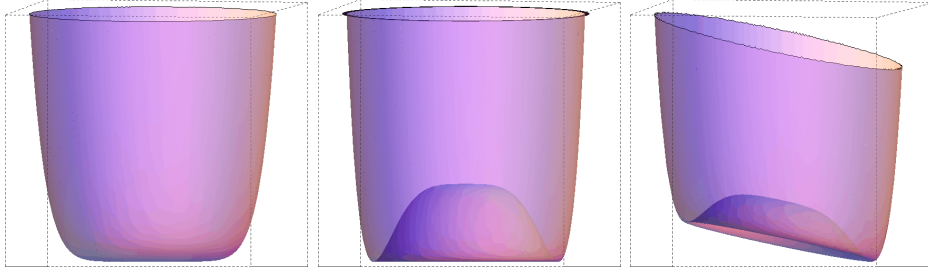

Figure 2.4: Potential for the field Φ: *(a) $T > f_a$, (b) $f_a > T > \Lambda_{\mathrm{QCD}}$, (c) $\Lambda_{\mathrm{QCD}} > T$.*

At temperatures higher than f_a the complex scalar field associated with the Peccei-Quinn symmetry has its minimum at $\Phi = 0$ (see Fig.2.4a). At $T \sim f_a$ the symmetry is broken and Φ is driven by the potential (see Fig.2.4b):

$$V(\Phi) = \lambda \left(|\Phi|^2 - \frac{f_a^2}{2} \right)^2 . \tag{2.16}$$

It has an absolute minimum at $|\Phi| = f_a/\sqrt{2}$; the ground state is characterized by a non-vanishing vacuum expectation value $\langle \Phi \rangle = f_a/\sqrt{2} e^{i\Theta}$, where Θ is an arbitrary phase. Φ can be written in terms of two real fields ρ and ϕ which represent the radial and the angular excitations:

$$\Phi = \frac{f_a + \rho}{\sqrt{2}} e^{i\frac{\phi}{f_a}} . \tag{2.17}$$

The potential $V(\Phi)$ provides a large mass for ρ, a field which will be of no further interest for low-energy considerations. The massless degree of freedom is the *axion* $\Theta = \phi/f_a$.

At temperatures much larger than the QCD scale ($\Lambda_{\mathrm{QCD}} \simeq 200$ MeV) the axion is massless; however at temperatures $T \sim \Lambda_{\mathrm{QCD}}$ it develops a mass due to its mixing with π^0 and η mesons (non perturbative QCD effects

associated with instantons). The temperature dependence of the axion mass is approximatively given by [1, 70]:

$$m(T) = \begin{cases} m(T=0) \sim \frac{f_\pi m_\pi}{f_a} \text{ for } T \ll \Lambda_{\text{QCD}} \\ \frac{m(T=0)}{10} \left(\frac{\Lambda_{\text{QCD}}}{T} \right)^{3.7} \text{ for } T \sim \Lambda_{\text{QCD}} \\ m(T=0) \sim 0 \text{ for } T \gg \Lambda_{\text{QCD}} \end{cases} \qquad (2.18)$$

The axion potential is now of the form (see Fig.2.5):

$$V(\phi) = m^2 f_a^2 \left(1 - \cos \frac{\phi}{f_a} \right) . \qquad (2.19)$$
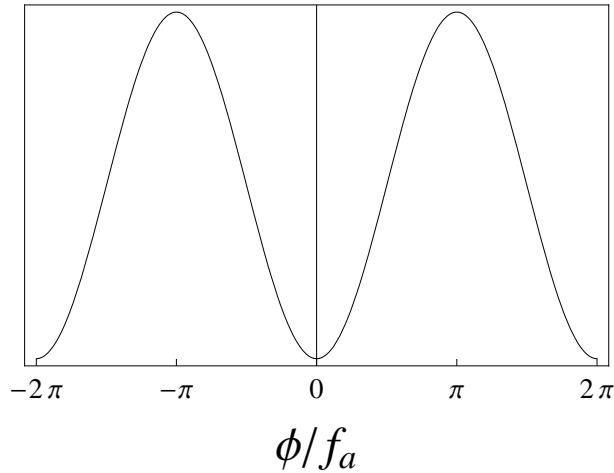
Figure 2.5: The potential $V(\phi)$ for $T \ll \Lambda_{\text{QCD}}$.

Axions can be produced in the early universe; relic axions arise due to three different processes:

- thermal relics, through the usual freeze-out processes (hot dark matter candidates);

- non thermal relics, through the decay of axionic strings (cold dark matter candidates);

- non thermal relics, through coherent production due to initial misalignment of the axion field $\Theta_i \neq 0$ (cold dark matter candidates) [71, 72, 73].

Here we are interested in particular to misalignment axion production. Today Θ is fixed at the CP-conserving value ($\Theta = 0$), but at earlier times the initial value of Θ must be chosen by a stochastic process. When temperature falls below f_a the axion field settles somewhere in the minimum of its mexican hat potential, afterward when hat tilts at QCD phase transition the field begins to oscillate (see Fig.2.4c). These cosmic oscillations of the axion field correspond to a zero-momentum condensate of axions, they contribute to CDM because of their intrinsically small velocities. Near the minimum the axion potential of Eq. (2.19) is:

$$V(\phi) \simeq \frac{1}{2}m^2\phi^2 \,, \tag{2.20}$$

and the equation of motion is:

$$\ddot{\Theta} + 3H\dot{\Theta} + m^2\Theta = 0 \,. \tag{2.21}$$

At higher temperatures $T \gg \Lambda_{\text{QCD}}$ mass vanishes and the solution simply is $\Theta = \Theta_i = \text{const}$. When the axion becomes greater than the expansion rate ($m \gtrsim 3H$) it begins to oscillate with frequency m (see Fig.2.6).
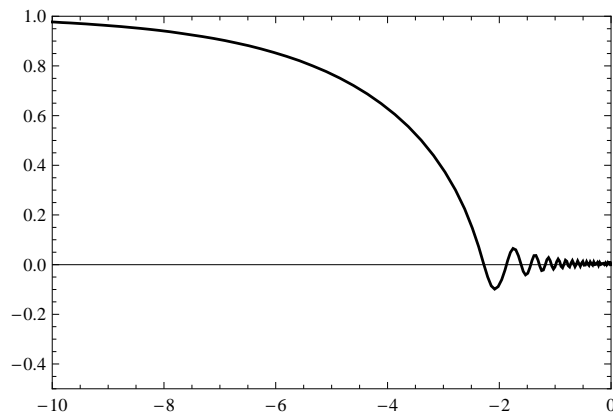

Figure 2.6: Evolution of the axion field Θ, in arbitrary units, near QCD scale where the axion acquire mass and start to oscillate around its minimum.

The critical density associated with the misalignment production of axions strongly depends on the initial misalignment angle associated with the

axion field Θ_i through the following relation [1, 2]:

$$\Omega_{\mathrm{mis}}h^2 \sim 0.23 \times 10^{\pm 0.6} \left(\frac{f_a}{10^{12}\,\mathrm{GeV}}\right)^{1.175} \Theta_i^2 F\left(\Theta_i\right), \qquad (2.22)$$

h encodes the actual value of the Hubble parameter ($H_0 = 100h\,\mathrm{km\,s^{-1}\,Mpc^{-1}}$) and $F(\Theta_i)$ accounts for anharmonic effects if $\Theta_i \gg 1$. The demand $\Omega_{\mathrm{mis}} \leq \Omega_{DM}$ provides an upper bound on $f_a^{1.175}\Theta_i^2$ (assuming $F\left(\Theta_i\right) \simeq 1$) [71, 72, 73]:

$$f_a\Theta_i^{1.7} \leq 2 \times 10^{11 \div 12}\,\mathrm{GeV}. \qquad (2.23)$$

This condition becomes also an upper bound for f_a under the assumption that inflation occurred before the breaking of PQ-symmetry ($f_a \leq f_{INF}$) [1]: in this scenario different regions have different values for Θ_i, so averaging over all observable universe the value of Θ_i in equation can replaced by its *rms* value ($\pi/\sqrt{3}$) and the limit $f_a \leq 10^{11 \div 12}\,\mathrm{GeV}$ is obtained. As can be seen from Fig. 2, CAST disfavors values of $g_\phi \sim 10^{-11 \div -12}\,\mathrm{GeV^{-1}}$ with a mass up to 0.02eV. Note however that our calculation cannot be applied directly to this case since we assume ϕ homogeneous in our universe, whereas it is not if the PQ symmetry breaking occurs after inflation: although taking into account space inhomogeneities were a second order effect in cosmological perturbation theory, cosmological birefringence might be larger than the one computed in this chapter.

Our calculations apply without modifications to the case in which inflation occurs after PQ-symmetry breaking: the initial misalignment angle Θ_i is homogeneous throughout our universe and can be much smaller than $\pi/\sqrt{3}$. Such possibility allow the scale of PQ-symmetry breaking f_a to be much higher than $10^{11 \div 12}\,\mathrm{GeV}$ and is motivated by anthropic considerations [74, 75, 76, 77]. These smaller values of g_ϕ can be constrained by present data in CMB polarization in a much better way than CAST, in particular for small masses.

The impact of pseudoscalar interaction with CMBP photons is therefore complementary to its impact on the initial conditions for dark matter inhomogeinities. If the PQ-symmetry breaking would have occurred before or

during inflation, initial conditions for dark matter perturbations are essentially adiabatic and the rotation of CMBP gives a constraint on g_ϕ. If the PQ-symmetry breaking would have occurred after inflation, the rotation of linear polarization does not produce a stringent constraint, but axion dark matter start with isocurvature initial conditions leading to constraints on f_a (see [78] for an updated study of this topic).

2.3   Ultralight pseudo Nambu-Goldstone bosons

Many different models for pseudoscalar axion-like particles were proposed in the past: Familons [79], Majorons [80], Stückelberg axions [81], . . . ; here we briefly focus on accelerons [7] ultralight pseudo Nambu-Goldstone bosons able to explain the current dark energy density. For more details on Ultralight pseudo Nambu-Goldstone bosons acting as dark energy see [82, 83, 84, 85], and, in general, for particle physics motivated quintessence models see Refs. [86, 87, 88] and references therein. L. Amendola and R. Barbieri in Ref. [89] studied the possibility that a field with mass between 10^{-33} eV and 10^{-23} eV can contribute simultaneously to dark matter and dark energy.

Nowadays a growing number of observations indicate that the expansion of the universe is accelerating. However it is still unclear what drives this acceleration: while a cosmological constant Λ is the simplest explanation, its value seems completely at odd with the naive estimate of vacuum energy due to quantum effects. If gravity is described by Einstein's general relativity the acceleration must be due to a dark energy component that represents roughly 70% of the total universe energy density.

The simplest physical model for an appropriate dark energy component is a simple slowly-rolling scalar field (quintessence). In an expanding universe a spatially homogeneous scalar field obeys:

$$\ddot{\phi} + 3H\dot{\phi} - \frac{dV}{d\phi} = 0 \,, \tag{2.24}$$

with temporal derivative respect to cosmic time, or:

$$\phi'' + 2\mathcal{H}\phi' - a^2 \frac{dV}{d\phi} = 0 \,, \tag{2.25}$$

respect to conformal time ($\mathcal{H} \equiv a'/a$).

In order to have a slowly-rolling field today:

$$m \sim \left. \sqrt{\frac{d^2 V}{d\phi^2}} \right|_0 \sim H_0 \simeq 6.4h \times 10^{-33} \text{ eV} \,. \tag{2.26}$$

This is an incredibly small number for particle physics, one possible solution is that the mass of the quintessence field is protected by an underlying symmetry. Moreover scalars of such a low mass give rise to long-range forces if they couple to ordinary matter; current limits imply that there must be a suppression of these quintessence couplings through the imposition of an approximate global symmetry.

One of the most well motivated quintessence models from particle physics perspective was proposed by J.A. Friemann et al. in Ref. [7], and by M. Fukugita and T. Yanagida in Ref. [91]. It is based on pseudo Nambu-Goldstone bosons which arises in models with a an approximate global symmetry of the form:

$$\phi \rightarrow \phi + \text{const} \,, \tag{2.27}$$

The pseudoscalar field is described by the lagrangian density:

$$\mathcal{L} = -\frac{1}{2} \nabla_\mu \phi \nabla^\mu \phi - M^4 \left(1 + \cos \frac{\phi}{f} \right) \,. \tag{2.28}$$

Neglecting spatial fluctuations of the field the equation of motion is:

$$\ddot{\phi} + 3H\dot{\phi} - \frac{M^4}{f} \sin \frac{\phi}{f} = 0 \,, \tag{2.29}$$

near the potential minimum ($\phi/f = \pi$) the previous equation becomes:

$$\ddot{\phi} + 3H\dot{\phi} + m^2 \phi = 0 \,, \tag{2.30}$$

where $m = M^2/f$. Note that ϕ contributes to dark energy density only if $m \lesssim 3H$. In order to fit current observation the quintessence model must behave

today approximately as cosmological constant [92]. In the far future the expansion rate of the universe becomes smaller than the axion mass ($3H \lesssim m$), ϕ starts to oscillate and the universe becomes cold axion dominated.

The evolution of ϕ is determined solving the following system of equations:

$$\begin{cases} \ddot{\phi} + 3H\dot{\phi} - \frac{M^4}{f}\sin\frac{\phi}{f} = 0 \,, \\ H^2 = \frac{8\pi}{3M_{\text{pl}}^2}\left(\rho_{\text{RAD}} + \rho_{\text{MAT}} + \rho_\phi\right) \,. \end{cases} \tag{2.31}$$

We solve numerically this system in the new variable $x \equiv= \log t/t_i$, from a fixed point in radiation dominated era (t_i) to nowadays (t_0):

$$\begin{cases} \frac{d\Theta}{dx^2} + \left(\frac{3}{a}\frac{da}{dx} - 1\right)\frac{d\Theta}{dx} - e^{2x}\frac{M^4 t_i^2}{f^2}\sin\Theta = 0 \,, \\ \frac{da}{dx} = t_i H_i a e^x \left[\Omega_{\text{MAT},1}\left(\frac{a_i}{a}\right)^3 + \Omega_{\text{RAD},1}\left(\frac{a_i}{a}\right)^4 \right. \\ \qquad \left. + \frac{8\pi}{6}\frac{f^2}{H_i^2 t_i^2 M_{\text{pl}}^2}e^{-2x}\left(\frac{d\Theta}{dx}\right)^2 + \frac{8\pi}{3}\frac{M^4}{H_i^2 M_{\text{pl}}^2}\left(1 + \cos\Theta\right)\right]^{1/2} \,. \end{cases} \tag{2.32}$$

where $\Theta = \phi/f$. See section 3.5 for some plots of the evolution of ϕ.

These cosmological pseudo Nambu-Goldstone bosons suitable to act as dark energy candidates are potentially detectable through CMB cosmological birefringence[5, 93]. No detailed investigation have been carried for the model proposed by J. A. Frieman *et al.* [7] and this is the topic of section 3.5.

Chapter 3

Pseudoscalar fields - coupling with photons

3.1 Introduction

In this chapter we study in detail the interaction of a pseudoscalar field with photons. This coupling modifies the polarization of an electromagnetic wave propagating along intervening magnetic fields, or through a slowly varying background field ϕ [94]. Here we are interested in the second case (see Fig. 3.1), which does not require the presence of a magnetic field (note that in the first case the polarization is also modified in absence of axions, e.g. by Faraday rotation, see section 1.6 for more details). We consider the time dependent pseudoscalar condensate acting as dark matter or dark energy and study the impact of its time derivative on the polarization of the photons. As a consequence of its coupling with a pseudoscalar field, the plane of linear polarization of light is rotated (*cosmological birefringence*) [95, 96].

In the case of Cosmic Microwave Background (CMB) photons, we pay attention to the rotation along the path between the last scattering surface (LSS) and the observer, modifying the polarization pattern generated by Thomson scattering at LSS [5]. This rotation induced by the pseudoscalar interaction modifies the gradient and curl of the polarization pattern, creating
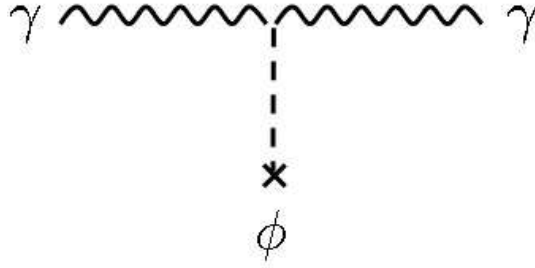
Figure 3.1: Photon propagation in a cosmological axion field background.

B modes from E modes. The parity violating nature of the interaction generates non-zero parity-odd correlators (TB and EB) which would be otherwise vanishing for the standard Gaussian cosmological case [16, 23]. In particular the TB power spectrum may be very useful to constrain the coupling constant g_ϕ between photons and pseudoscalars, since it is larger than the auto and cross power spectra in polarization; in general, these non-standard correlators are already constrained by present data sets [6, 33, 34] (see also Tab. 1.1).

We study two representative examples for the dynamics of a pseudo-Goldstone field behaving as dark matter (cosine-type and exponential potential) and one where the pseudoscalar field explains the current dark energy density. The case of a field growing linearly in time has been studied in [99]. We compare the polarization power spectra obtained describing the rotation of linear polarization with a time dependent angle with the ones obtained considering a constant rotation angle.

3.2 Equations of motion

The lagrangian density $\mathcal{L}$ for the photons and the pseudoscalar field ϕ is [100] (following the notation of [101]):

$$\mathcal{L} = -\frac{1}{4}F_{\mu\nu}F^{\mu\nu} - \frac{1}{2}\nabla_\mu\phi\nabla^\mu\phi - V(\phi) - \frac{g_\phi}{4}\phi F_{\mu\nu}\tilde{F}^{\mu\nu}\,. \qquad (3.1)$$

where g_ϕ is the coupling constant, $F^{\mu\nu}$ the electromagnetic tensor, $\tilde{F}^{\mu\nu}$ its dual ($\tilde{F}^{\mu\nu} \equiv \frac{1}{2}\epsilon^{\mu\nu\rho\sigma}F_{\rho\sigma}$), and ϕ the pseudoscalar field. The Euler-Lagrange equation for the scalar field is:

$$\nabla_\mu\frac{\partial\mathcal{L}}{\partial\left(\nabla_\mu\phi\right)} = \frac{\partial\mathcal{L}}{\partial\phi}\,, \qquad (3.2)$$

so:

$$\Box\phi \equiv \nabla_\mu\nabla^\mu\phi = \frac{dV}{d\phi} + \frac{g_\phi}{4}F_{\mu\nu}\tilde{F}^{\mu\nu}\,, \qquad (3.3)$$

Similarly for the vector potential:

$$\nabla_\mu\frac{\partial\mathcal{L}}{\partial\left(\nabla_\mu A_\nu\right)} = \frac{\partial\mathcal{L}}{\partial A_\nu}\,, \qquad (3.4)$$

so:

$$\nabla_\mu F^{\mu\nu} = -g_\phi(\nabla_\mu\phi)\tilde{F}^{\mu\nu}\,, \qquad (3.5)$$

Also the Bianchi identity is verified:

$$\nabla_\mu\tilde{F}^{\mu\nu} = 0\,. \qquad (3.6)$$

Using the definition of the electromagnetic tensor $F^{\mu\nu} \equiv \nabla^\mu A^\nu - \nabla^\nu A^\mu$ Eq. (3.5) becomes:

$$\Box A_\nu - \nabla_\nu\left(\nabla_\mu A^\mu\right) - R^\mu{}_\nu A_\mu = -\frac{g_\phi}{2}(\nabla_\mu\phi)\epsilon^\mu{}_\nu{}^{\rho\sigma}F_{\rho\sigma}\,, \qquad (3.7)$$

where $\epsilon^\mu{}_\nu{}^{\rho\sigma}$ is the complete antisymmetric tensor, it contains the determinant of the metric g and $[\cdots]$ guarantees anti-symmetry in the four indexes [103]:

$$\epsilon_{\alpha\beta\gamma\delta} = \sqrt{-g}\,[\alpha\beta\gamma\delta]\,, \qquad (3.8)$$

$$\epsilon^{\alpha\beta\gamma\delta} = -\left(\sqrt{-g}\right)^{-1}[\alpha\beta\gamma\delta]\,. \qquad (3.9)$$

In order to evaluate the d'Alembert operator of the vector potential we explicitly write:

$$
\begin{aligned}
\Box A_i &= g^{\mu\nu}\nabla_\mu\nabla_\nu A_i \\
&= g^{\mu\nu}\nabla_\mu\left(\partial_\nu A_i - \Gamma^\sigma_{\nu i}A_\sigma\right) \\
&= g^{\mu\nu}\left[\nabla_\mu\left(\partial_\nu A_i\right) - \nabla_\mu\left(\Gamma^\sigma_{\nu i}A_\sigma\right)\right] \\
&= g^{\mu\nu}\left[\partial_\mu\partial_\nu A_i - \Gamma^\rho_{\mu\nu}\partial_\rho A_i - \Gamma^\rho_{\mu i}\partial_\nu A_\rho - \partial_\mu\left(\Gamma^\sigma_{\nu i}A_\sigma\right)\right. \\
&\quad \left. +\Gamma^\rho_{\mu\nu}\Gamma^\sigma_{\rho i}A_\sigma + \Gamma^\rho_{\mu i}\Gamma^\sigma_{\nu\rho}A_\sigma\right] .
\end{aligned} \tag{3.10}
$$

For a spatially flat Friedmann-Robertson-Walker universe the metric is:

$$
ds^2 = -dt^2 + a^2(t)d\boldsymbol{x}^2 = a^2(\eta)\left[-d\eta^2 + d\boldsymbol{x}^2\right] , \tag{3.11}
$$

where t is the cosmic time, η is conformal time and $\boldsymbol{x}$ denotes the space coordinates; working in conformal time its useful to define:

$$
g_{\mu\nu} = \begin{pmatrix} -a^2 & 0 & 0 & 0 \\ 0 & a^2 & 0 & 0 \\ 0 & 0 & a^2 & 0 \\ 0 & 0 & 0 & a^2 \end{pmatrix} \quad \text{and} \quad g^{\mu\nu} = \begin{pmatrix} -a^{-2} & 0 & 0 & 0 \\ 0 & a^{-2} & 0 & 0 \\ 0 & 0 & a^{-2} & 0 \\ 0 & 0 & 0 & a^{-2} \end{pmatrix} ,
$$

so $\sqrt{-g} = a^4$. The connection coefficients are defined as:

$$
\Gamma^\lambda_{\mu\nu} \equiv \frac{1}{2}g^{\lambda\rho}\left(\frac{\partial g_{\rho\mu}}{\partial x^\nu} + \frac{\partial g_{\rho\nu}}{\partial x^\mu} - \frac{\partial g_{\mu\nu}}{\partial x^\rho}\right) , \tag{3.12}
$$

the non-vanishing ones are:

$$
\Gamma^\eta_{\eta\eta} = \Gamma^\eta_{xx} = \Gamma^\eta_{yy} = \Gamma^\eta_{zz} = \frac{a'}{a} , \tag{3.13}
$$

$$
\Gamma^i_{\eta j} = \Gamma^i_{j\eta} = \frac{a'}{a}\delta^i_j . \tag{3.14}
$$

The Ricci tensor is:

$$
\begin{aligned}
R_{\mu\kappa} &\equiv R^\lambda_{\mu\lambda\kappa} \\
&= \frac{\partial\Gamma^\lambda_{\mu\kappa}}{\partial x^\lambda} - \frac{\partial\Gamma^\lambda_{\mu\lambda}}{\partial x^\kappa} + \Gamma^\sigma_{\mu\kappa}\Gamma^\lambda_{\lambda\sigma} - \Gamma^\sigma_{\mu\lambda}\Gamma^\lambda_{\kappa\sigma} ,
\end{aligned} \tag{3.15}
$$

the non-vanishing components are:

$$R_{\eta\eta} = -3\frac{a''a - a'^2}{a^2}, \tag{3.16}$$

$$R_{xx} = R_{yy} = R_{zz} = \frac{a''a - a'^2}{a^2}. \tag{3.17}$$

Following the conventions of Ref. [103] the relation between the electromagnetic tensor and the physical fields E and B is:

$$F_{\mu\nu} = a \begin{pmatrix} 0 & -E_x & -E_y & -E_z \\ E_x & 0 & B_z & -B_y \\ E_y & -B_z & 0 & B_x \\ E_z & B_y & -B_x & 0 \end{pmatrix}, \tag{3.18}$$

$$F^{\mu\nu} = \frac{1}{a^3} \begin{pmatrix} 0 & E_x & E_y & E_z \\ -E_x & 0 & B_z & -B_y \\ -E_y & -B_z & 0 & B_x \\ -E_z & B_y & -B_x & 0 \end{pmatrix}, \tag{3.19}$$

while for its dual:

$$\tilde{F}_{\mu\nu} = a \begin{pmatrix} 0 & B_x & B_y & B_z \\ -B_x & 0 & E_z & -E_y \\ -B_y & -E_z & 0 & E_x \\ -B_z & E_y & -E_x & 0 \end{pmatrix}, \tag{3.20}$$

$$\tilde{F}^{\mu\nu} = \frac{1}{a^3} \begin{pmatrix} 0 & -B_x & -B_y & -B_z \\ B_x & 0 & E_z & -E_y \\ B_y & -E_z & 0 & E_x \\ B_z & E_y & -E_x & 0 \end{pmatrix}. \tag{3.21}$$

The invariants of the electromagnetic tensor are:

$$F_{\mu\nu}F^{\mu\nu} = \frac{2}{a^2}\left(\mathbf{B}^2 - \mathbf{E}^2\right), \tag{3.22}$$

$$F_{\mu\nu}\tilde{F}^{\mu\nu} = \frac{4}{a^2}\left(\mathbf{E} \cdot \mathbf{B}\right). \tag{3.23}$$

Therefore Eq. (3.3) for the pseudoscalar field can be written as:

$$\frac{\partial^2 \phi}{\partial \eta^2} + 2\mathcal{H}\frac{\partial \phi}{\partial \eta} - \nabla^2 \phi + a^2\frac{dV}{d\phi} = g_\phi \mathbf{E} \cdot \mathbf{B}. \tag{3.24}$$

Expressing Eq. (3.5) and the Bianchi identity (Eq. (3.6)) in terms of $\mathbf{E}$ and $\mathbf{B}$ we obtain the modified Maxwell equations:

$$\nabla \cdot \mathbf{E} = -g_\phi \left(\nabla \phi \right) \cdot \mathbf{B} \,, \tag{3.25}$$

$$\frac{\partial}{\partial \eta} \left(a\mathbf{E} \right) - \nabla \times \left(a\mathbf{B} \right) = -g_\phi \left[\frac{\partial \phi}{\partial \eta} a\mathbf{B} + \left(\nabla \phi \right) \times a\mathbf{E} \right] \,, \tag{3.26}$$

$$\nabla \cdot \mathbf{B} = 0 \,, \tag{3.27}$$

$$\frac{\partial}{\partial \eta} \left(a\mathbf{B} \right) + \nabla \times \left(a\mathbf{E} \right) = 0 \,. \tag{3.28}$$

We consider in particular a plane wave propagating along $\hat{\boldsymbol{n}}$ in Coulomb (radiation) gauge ($\nabla \cdot \boldsymbol{A} = 0$, $A_0 = 0$). In the quantum-mechanical description the photon field can be expressed as [21, 104]:

$$\hat{A}_i = \int \frac{d^3 \mathbf{k}}{(2\pi)^3} \left[\hat{a}_s(k) \tilde{A}(k, \eta) \epsilon_{si}(k) e^{i\mathbf{k} \cdot \mathbf{x}} + \hat{a}_s^\dagger(k) \tilde{A}^*(k, \eta) \epsilon_{si}^*(k) e^{-i\mathbf{k} \cdot \mathbf{x}} \right] \,, \tag{3.29}$$

where $\epsilon_{si}(k)$ are the photon polarization 4-vectors, s labels the photon polarization, the creation and annihilation operators $\hat{a}_s(k)$ and $\hat{a}_s^\dagger(k)$ satisfy the canonical commutation rules.

Assuming the direction of propagation aligned with the z axis, neglecting the spatial variation of the pseudoscalar field $\phi = \phi(\eta)$, and writing polarization in terms of left and right circular polarized waves ($s \in \{+, -\}$), the two relevant components of Eq. (3.7) for the electromagnetic vector potential are:

$$\tilde{A}_\pm''(k, \eta) + \left[k^2 \pm g_\phi \phi' k \right] \tilde{A}_\pm(k, \eta) = 0 \,. \tag{3.30}$$

3.2.1   Energy-momentum tensor

Following the conventions of Ref. [103, 105] we define the energy momentum tensor:

$$T_{\mu\nu} \;=\; -2 \frac{\delta \mathcal{L}}{\delta g^{\mu\nu}} + g_{\mu\nu} \mathcal{L} \,, \tag{3.31}$$

$$T^{\mu\nu} \;=\; 2 \frac{\delta \mathcal{L}}{\delta g_{\mu\nu}} + g^{\mu\nu} \mathcal{L} \,, \tag{3.32}$$

since $\delta g^{\mu\nu} = -g^{\mu\rho} g^{\mu\sigma} \delta g_{\rho\sigma}$ (e.g. see [106]).

For the *scalar field* described by the Lagrangian:

$$\mathcal{L}_\phi = -\frac{1}{2}\phi_{,\mu}\phi^{,\mu} - V(\phi) \,, \tag{3.33}$$

we obtain:

$$T_{\phi\,\mu\nu} = \phi_{,\mu}\phi_{,\nu} + g_{\mu\nu}\mathcal{L} \,, \tag{3.34}$$

so:

$$T_\phi{}^0{}_0 = -\frac{(\phi')^2}{2a^2} - V \equiv -\rho_\phi \,, \tag{3.35}$$

$$T_\phi{}^i{}_i = \frac{(\phi')^2}{2a^2} - V \equiv p_\phi \,. \tag{3.36}$$

For the *electromagnetism* Lagrangian:

$$\mathcal{L}_{\rm EM} = -\frac{1}{4}F_{\mu\nu}F^{\mu\nu} \,, \tag{3.37}$$

we obtain:

$$T_{\rm EM\mu\nu} = F_{\mu\alpha}F_\nu{}^\alpha - \frac{1}{4}g_{\mu\nu}F_{\alpha\beta}F^{\alpha\beta} \,, \tag{3.38}$$

so:

$$T_{\rm EM}{}^0{}_0 = -\frac{\mathbf{E}^2}{a^2} - \frac{1}{2a^2}\left(\mathbf{B}^2 - \mathbf{E}^2\right) = -\frac{\mathbf{E}^2 + \mathbf{B}^2}{2a^2} = -\rho_{\rm EM} \,. \tag{3.39}$$

For the Lagrangian defined in Eq. (3.1) and including the *coupling between pseudoscalars and photons* we have the following energy-momentum tensor:

$$
\begin{aligned}
T_{\rm PS\mu\nu} = {} & F_{\mu\alpha}F_\nu{}^\alpha - \frac{1}{4}g_{\mu\nu}F_{\alpha\beta}F^{\alpha\beta} + \phi_{,\mu}\phi_{,\nu} - \frac{1}{2}g_{\mu\nu}\phi_{,\alpha}\phi^{,\alpha} - g_{\mu\nu}V(\phi) \\
& -\frac{g_\phi}{2}\phi F^{\alpha\beta}\tilde{F}_{\alpha\beta}g_{\mu\nu} \,.
\end{aligned}
\tag{3.40}
$$

3.2.2   Chern-Simons Lagrangian

The Lagrangian density describing interaction between pseudoscalars and photons in Eq. (3.1) is:

$$\mathcal{L}_{\rm PS} = -\frac{g_\phi}{4}\phi F_{\mu\nu}\tilde{F}^{\mu\nu} \,. \tag{3.41}$$

It can be written also in a different form [95], using the definition of the electromagnetic tensor and integrating by parts:

$$
\begin{aligned}
\mathcal{L}_{\text{PS}} &= -\frac{g_\phi}{2} \phi \tilde{F}^{\mu\nu} \nabla_\mu A_\nu \\
&= \frac{g_\phi}{2} \left[A_\nu \nabla_\mu \left(\phi \tilde{F}^{\mu\nu} \right) - \nabla_\mu \left(\phi \tilde{F}^{\mu\nu} A_\nu \right) \right] .
\end{aligned}
\tag{3.42}
$$

According to Eq. (3.6) $\nabla_\mu \tilde{F}^{\mu\nu} = 0$, so, within a divergence:

$$
\bar{\mathcal{L}}_{\text{PS}} = \frac{g_\phi}{2} \left(\nabla_\mu \phi \right) A_\nu \tilde{F}^{\mu\nu} .
\tag{3.43}
$$

Note how only the gradient of ϕ enters the field equations, and not ϕ itself. This last equation is not manifestly invariant under gauge transformations $A_\mu \to A_\mu + \partial_\mu \lambda$, note however that $\mathcal{L}_{\text{PS}}$ is changed by an irrelevant divergence by gauge transformations.

The Chern-Simons Lagrangian (e.g. see Ref. [102]) is:

$$
\mathcal{L}_{\text{CS}} = -\frac{g_\phi}{4} p_\mu A_\nu \tilde{F}^{\mu\nu} ,
\tag{3.44}
$$

where the vector p_μ can be a constant vector field which violates Lorentz invariance by defining a preferred reference frame which violates Lorentz invariance, otherwise it is possible to define $p_\mu = -2\nabla_\mu \phi$, where ϕ is a dynamical scalar field. In this case the gauge and Lorentz invariance are preserved, and:

$$
\mathcal{L}_{\text{CS}} = -\frac{g_\phi}{2} \left(\nabla_\mu \phi \right) A_\nu \tilde{F}^{\mu\nu} = \bar{\mathcal{L}}_{\text{PS}} .
\tag{3.45}
$$

3.3   Cosine-type potential

In this section we assume that dark matter is given by massive axions. The pseudoscalar field ϕ is g governed by the potential (see chapter 10 of Ref. [1] and section 2.2.3):

$$
V(\phi) = m^2 \frac{f_a^2}{N^2} \left(1 - \cos \frac{\phi N}{f_a} \right) ,
\tag{3.46}
$$

where N is the color anomaly of the Peccei-Quinn symmetry. Here we are interested in the regime where the axion field oscillates near the minimum

of the potential (for simplicity we shall consider $N = 1$ in the following): $\phi/f_a \ll 1$ and the potential can be approximated with $V(\phi) \simeq m^2\phi^2/2$. In this case $\phi(t)$ satisfies the equation:

$$\ddot{\phi} + 3H\dot{\phi} + m^2\phi = 0\,. \qquad (3.47)$$

When $m > 3H$ the scalar field begins to oscillate, and the solution in a matter dominated universe ($\dot{a}/a = 2/3t$) is [71]:

$$
\begin{aligned}
\phi(t) &= t^{-1/2}\left[c_1 J_{1/2}(mt) + c_2 J_{-1/2}(mt)\right] \\
&\stackrel{mt\gg 1}{\simeq} \frac{\phi_0}{mt}\sin(mt)\,,
\end{aligned}
\qquad (3.48)
$$

where the time-independent coefficients of the Bessel functions c_1, c_2 depend on the initial conditions.

The averaged energy and pressure densities associated with the field are:

$$\overline{\rho_\phi} = \frac{\overline{\dot{\phi}^2}}{2} + \frac{1}{2}m^2\overline{\phi}^2 \stackrel{mt\gg 1}{\simeq} \frac{\phi_0^2}{2t^2}\left[1 + \mathcal{O}\left(\frac{1}{mt}\right)^2\right]\,, \qquad (3.49)$$

$$\overline{P_\phi} = \frac{\overline{\dot{\phi}^2}}{2} - \frac{1}{2}m^2\overline{\phi}^2 \stackrel{mt\gg 1}{\simeq} \frac{\phi_0^2}{2t^2} \times \mathcal{O}\left(\frac{1}{mt}\right)^2\,, \qquad (3.50)$$

where $^-$ denotes the average over an oscillation period of the axion condensate. Note that we are implicitly assuming that the pseudoscalar field is homogeneous. In the context of axion physics, this means that in our observable universe we have just one value for the misalignment angle, which means that the PQ symmetry has occurred before or during inflation.

We fix the constant ϕ_0 comparing ρ_ϕ with the energy density in a matter dominated universe:

$$\rho_M = \frac{3H^2 M_{\rm pl}^2}{8\pi} = \frac{M_{\rm pl}^2}{6\pi t^2} \quad\Longrightarrow\quad \phi_0 = \frac{M_{\rm pl}}{\sqrt{3\pi}}\,, \qquad (3.51)$$

$$\phi(t) \simeq \frac{M_{\rm pl}}{\sqrt{3\pi}mt}\sin(mt)\,, \qquad (3.52)$$

where $M_{\rm pl} \simeq 1.22 \times 10^{19}$ GeV is the Planck mass.

Using the relation between cosmic and conformal time in a universe of matter:

$$t = \frac{\eta_0}{3} \left(\frac{\eta}{\eta_0}\right)^3 , \tag{3.53}$$

we find the following approximation for $\phi(\eta)$:

$$\phi(\eta) \simeq \sqrt{\frac{3}{\pi}} \frac{M_{\text{pl}}}{m\eta_0 \left(\frac{\eta}{\eta_0}\right)^3} \sin\left[m\frac{\eta_0}{3} \left(\frac{\eta}{\eta_0}\right)^3\right] , \tag{3.54}$$

and

$$\phi'(\eta) \simeq \sqrt{\frac{3}{\pi}} \frac{M_{\text{pl}}}{\eta} \left\{ \cos\left[m\frac{\eta_0}{3} \left(\frac{\eta}{\eta_0}\right)^3\right] \right.$$
$$\left. - \frac{3\eta_0^2}{m\eta^3} \sin\left[m\frac{\eta_0}{3} \left(\frac{\eta}{\eta_0}\right)^3\right] \right\} . \tag{3.55}$$

If m is not too small the value of $\mathcal{H} \equiv a'/a$ obtained with the scalar field density in the Friedmann equation coincides with that of a matter dominated universe $\mathcal{H} = 2/\eta$ once the average through oscillations is performed [107] (see Fig. 3.2). The derivative can be replaced in Eq. (3.30) for the evolution of the electromagnetic vector:

$$\tilde{A}_{\pm}''(k,\eta) + k^2 \left[1 \pm \Delta(\eta; g_\phi, m, k, \eta_0)\right] \tilde{A}_{\pm}(k,\eta) = 0 , \tag{3.56}$$

defined the function:

$$\Delta(\eta; g_\phi, m, k, \eta_0) \equiv \sqrt{\frac{3}{\pi}} \frac{g_\phi M_{\text{pl}}}{k\eta} \left\{ \cos\left[m\frac{\eta_0}{3} \left(\frac{\eta}{\eta_0}\right)^3\right] \right.$$
$$\left. - \frac{3\eta_0^2}{m\eta^3} \sin\left[m\frac{\eta_0}{3} \left(\frac{\eta}{\eta_0}\right)^3\right] \right\} . \tag{3.57}$$

This term, induced by axion-photon coupling, oscillates with frequency proportional to the mass of the axion and its amplitude decreases with time.

In the next two subsections we study analytically and numerically Eq. (3.56) for different values of the parameters m and g_ϕ; we exclude the region where the mass of the pseudoscalar field is so small that the field starts to oscillate after equivalence ($m < 3H_{\text{eq}}$), and the region corresponding to a PQ symmetry broken at energies higher than Planck scale ($f_a > M_{\text{pl}}$): see Fig. 3.3.
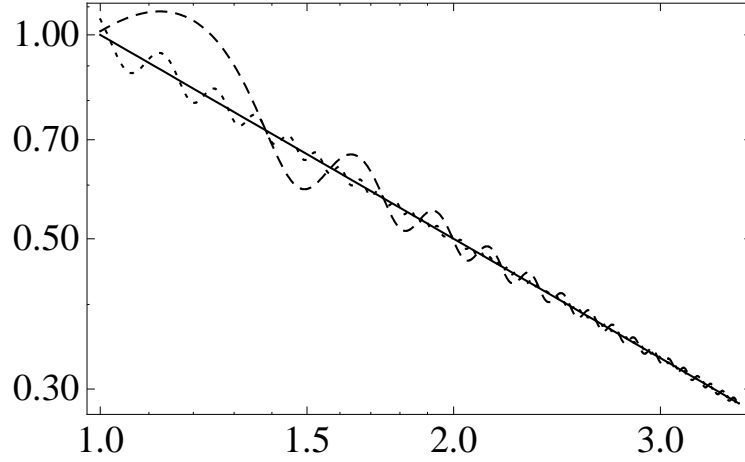
Figure 3.2: Evolution of $\mathcal{H}/\mathcal{H}_{\text{rec}}$ in function of conformal time for $m = 10^{-28}$eV (dashed line), $m = 5 \times 10^{-27}$eV (dotted line) and for a matter dominated universe (continuous line), from recombination (η_{rec}) to $3.5\eta_{\text{rec}}$. Present time corresponds to $\eta_0 = \eta_{\text{rec}}\sqrt{1 + z_{\text{rec}}} \simeq 33.18\eta_{\text{rec}}$.

3.3.1   Adiabatic solution

Adiabatic solutions of Eq. (3.56) are:

$$\tilde{A}_s = \frac{1}{\sqrt{2\omega_s}}e^{\pm i \int \omega_s d\eta} , \qquad (3.58)$$

where $\omega_s(\eta) = k\sqrt{1 \pm \frac{g_\phi \phi'(\eta)}{k}} = k\sqrt{1 \pm \Delta(\eta)}$ and $s = \pm$.
The first and second derivative respect to conformal time are:

$$\tilde{A}'_s = \tilde{A}_s \left(-i\omega_s - \frac{\omega'_s}{2\omega_s} \right) , \qquad (3.59)$$

$$\tilde{A}''_s = \tilde{A}_s \left(-\omega_s^2 + \frac{3\omega_s'^2}{4\omega_s^2} - \frac{\omega''_s}{2\omega_s} \right) . \qquad (3.60)$$
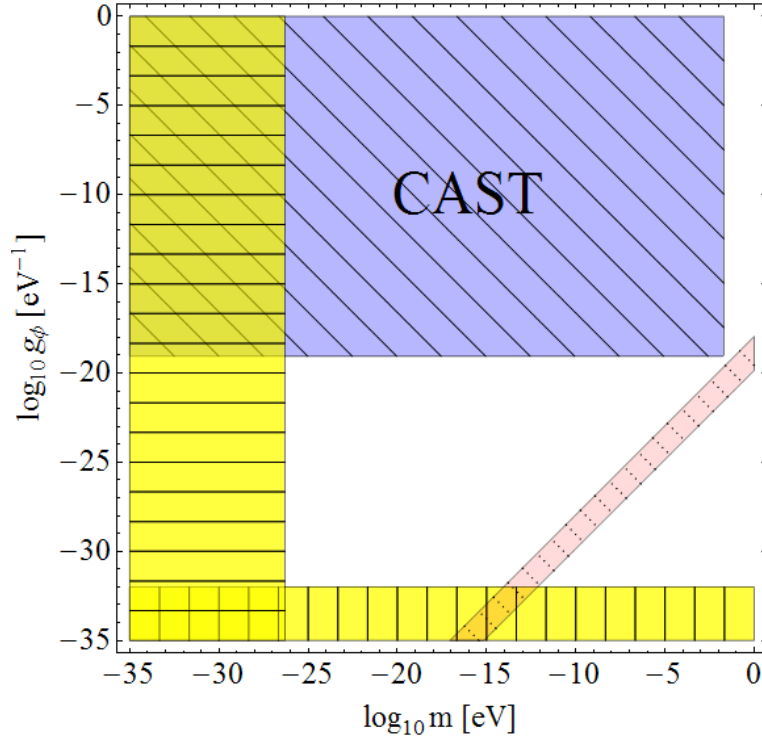
Figure 3.3: Plane $(\log_{10} m \, [\text{eV}], \log_{10} g_\phi \, [\text{eV}^{-1}])$: region excluded by CAST [59] (blue with oblique lines), region where the mass of the pseudoscalar field is too small $(m < 3H_{\text{eq}})$ (yellow with horizontal lines), region where PQ symmetry is broken at energies higher than Planck scale $(f_a > M_{\text{pl}})$ (yellow with vertical lines), and (m, g_ϕ) values expected in main QCD axion models (red with dots).

The adiabatic solution (3.58) is a good approximation for the vector potential when the terms $\frac{3\omega_s'^2}{4\omega_s^2}$ and $\frac{\omega_s''}{2\omega_s}$ are small compared to ω_s^2:

$$\frac{3\omega_s'^2}{4\omega_s^4} = \frac{3\Delta'^2}{16k^2 \left(1 \pm \Delta\right)^3} \ll 1 \,, \tag{3.61}$$

$$\frac{\omega_s''}{2\omega_s^3} = \frac{\pm 2(1 \pm \Delta)\Delta'' - \Delta'^2}{8k^2 \left(1 \pm \Delta\right)^3} \ll 1 \,. \tag{3.62}$$

If both condition are satisfied and $\Delta \ll 1$:

$$\begin{aligned}
\tilde{A}_{\pm} &\simeq \frac{1}{\sqrt{2k\left(1 \pm \Delta/4\right)}} \exp\left[\pm ik\left(\eta \pm \frac{1}{2}\int \Delta d\eta\right)\right] \\
&= \frac{1}{\sqrt{2k\left(1 \pm \pi g_\phi \phi' k\right)}} \exp\left[\pm i\left(k\eta \pm 2\pi g\phi\right)\right] \,.
\end{aligned} \tag{3.63}$$

In the adiabatic regime the coupling between photons and axions produces a frequency independent shift between the two polarized waves, which corresponds to a rotation of the plane of linear polarization:

$$\theta_{\text{adiabatic}} = \frac{g_\phi}{2}\left[\phi(\eta_0) - \phi(\eta_{\text{rec}})\right] \,. \tag{3.64}$$

This result agrees with the one obtained in Ref. [94], which therefore holds in the adiabatic regime. More important than this, $\theta_{\text{adiabatic}} = \bar{\theta}$, i.e. Eq. (3.64) agree with the rotation angle which is approximated by Eq. (1.77) in the Boltzmann section 1.5. This agreement is not a coincidence and shows the usefulness of studying the gauge potential as done in this section: the estimate based on the adiabatic approximation of the rotation angle due to cosmological birefringence can be also obtained by studying the gauge potential A_s.

Typically $\phi(\eta_{\text{rec}}) \gg \phi(\eta_0)$; from last scattering to now $\bar{\rho} \simeq m^2\bar{\phi}^2$ so, in a matter dominated universe:

$$\bar{\phi}(\eta) \simeq \sqrt{\frac{3}{8\pi}}\frac{M_{\text{pl}}\mathcal{H}(\eta)}{m} \simeq \sqrt{\frac{3}{2\pi}}\frac{M_{\text{pl}}}{m\eta_0}\left(\frac{\eta_0}{\eta}\right)^3 \,. \tag{3.65}$$

An estimate of the angle $\theta_{\text{adiabatic}}$ is:

$$\theta_{\text{adiabatic}} \simeq g_\phi \sqrt{\frac{3}{8\pi}}\frac{M_{\text{pl}}}{m\eta_0}\left[\left(1 + z_{\text{rec}}\right)^{3/2} - 1\right] \,. \tag{3.66}$$

Note the dependence of $\theta_{\text{adiabatic}}$ on the coupling constant and on the mass of the pseudoscalar field: for fixed g_ϕ the effect is larger for smaller masses.

The amplitude of the electromagnetic field changes according to:

$$\left|\tilde{\boldsymbol{E}}\right|^2 = \frac{\left|\tilde{\boldsymbol{A}}'\right|^2}{a^2} \simeq \frac{\omega_s}{2a^2}, \tag{3.67}$$

so the degree of circular polarization evolves according:

$$
\begin{aligned}
\tilde{\Pi}_C &= \frac{\left|\tilde{A}'_+\right|^2 - \left|\tilde{A}'_-\right|^2}{\left|\tilde{A}'_+\right|^2 + \left|\tilde{A}'_-\right|^2} \\
&= \frac{\sqrt{1+\Delta} - \sqrt{1-\Delta}}{\sqrt{1+\Delta} + \sqrt{1-\Delta}} \simeq \frac{\Delta}{2} = \frac{g_\phi \phi'}{2k}.
\end{aligned} \tag{3.68}
$$

Note that according to [97, 98] it is better to define the Stokes parameters starting from the number of photons. In this case:

$$\tilde{I}_2 = \frac{1}{2a^4}\left(\langle\tilde{A}'^*_+\tilde{A}'_+\rangle + k^2\langle\tilde{A}^*_+\tilde{A}_+\rangle + \langle\tilde{A}'^*_-\tilde{A}'_-\rangle + k^2\langle\tilde{A}^*_-\tilde{A}_-\rangle\right), \tag{3.69}$$

$$\tilde{Q}_2 = \frac{1}{2a^4}\left(\langle\tilde{A}'^*_+\tilde{A}'_-\rangle + k^2\langle\tilde{A}^*_+\tilde{A}_-\rangle + \langle\tilde{A}'^*_-\tilde{A}'_+\rangle + k^2\langle\tilde{A}^*_-\tilde{A}_+\rangle\right), \tag{3.70}$$

$$\tilde{U}_2 = -\frac{i}{2a^4}\left(\langle\tilde{A}'^*_+\tilde{A}'_-\rangle + k^2\langle\tilde{A}^*_+\tilde{A}_-\rangle - \langle\tilde{A}'^*_-\tilde{A}'_+\rangle - k^2\langle\tilde{A}^*_-\tilde{A}_+\rangle\right), \tag{3.71}$$

$$\tilde{V}_2 = \frac{1}{2a^4}\left(\langle\tilde{A}'^*_+\tilde{A}'_+\rangle + k^2\langle\tilde{A}^*_+\tilde{A}_+\rangle - \langle\tilde{A}'^*_-\tilde{A}'_-\rangle - k^2\langle\tilde{A}^*_-\tilde{A}_-\rangle\right). \tag{3.72}$$

In the adiabatic approximation we can use the relation:

$$\tilde{A}_s = -\left(i\omega_s + \frac{\omega'_s}{2\omega_s}\right)^{-1}\tilde{A}'_s, \tag{3.73}$$

therefore the equations for the Stokes parameters become:

$$\tilde{I}_2 = \frac{1}{2a^4}\left\{\left[1 + \frac{k^2}{\omega_+^2 + \left(\frac{\omega_+'}{2\omega_+}\right)^2}\right]\langle\tilde{A}_+^{\prime*}\tilde{A}_+'\rangle + \left[1 + \frac{k^2}{\omega_-^2 + \left(\frac{\omega_-'}{2\omega_-}\right)^2}\right]\langle\tilde{A}_-^{\prime*}\tilde{A}_-'\rangle\right\},$$

$$\tilde{Q}_2 = \frac{1}{2a^4}\left\{\left[1 + \frac{k^2}{\left(-i\omega_+ + \frac{\omega_+'}{2\omega_+}\right)\left(i\omega_- + \frac{\omega_-'}{2\omega_-}\right)}\right]\langle\tilde{A}_+^{\prime*}\tilde{A}_-'\rangle\right.$$
$$\left. + \left[1 + \frac{k^2}{\left(-i\omega_- + \frac{\omega_-'}{2\omega_-}\right)\left(i\omega_+ + \frac{\omega_+'}{2\omega_+}\right)}\right]\langle\tilde{A}_-^{\prime*}\tilde{A}_+'\rangle\right\},$$

$$\tilde{U}_2 = -\frac{i}{2a^4}\left\{\left[1 + \frac{k^2}{\left(-i\omega_+ + \frac{\omega_+'}{2\omega_+}\right)\left(i\omega_- + \frac{\omega_-'}{2\omega_-}\right)}\right]\langle\tilde{A}_+^{\prime*}\tilde{A}_-'\rangle\right.$$
$$\left. - \left[1 + \frac{k^2}{\left(-i\omega_- + \frac{\omega_-'}{2\omega_-}\right)\left(i\omega_+ + \frac{\omega_+'}{2\omega_+}\right)}\right]\langle\tilde{A}_-^{\prime*}\tilde{A}_+'\rangle\right\},$$

$$\tilde{V}_2 = \frac{1}{2a^4}\left\{\left[1 + \frac{k^2}{\omega_+^2 + \left(\frac{\omega_+'}{2\omega_+}\right)^2}\right]\langle\tilde{A}_+^{\prime*}\tilde{A}_+'\rangle - \left[1 + \frac{k^2}{\omega_-^2 + \left(\frac{\omega_-'}{2\omega_-}\right)^2}\right]\langle\tilde{A}_-^{\prime*}\tilde{A}_-'\rangle\right\}.$$

Note that these expressions coincide with the standard definition of Stokes parameters given in section 1.2 (Eqs. (1.29-1.32)) when $\omega_\pm^2 = k^2$.

Always in the adiabatic approximation the degree of circular polarization evolves according to:

$$
\begin{aligned}
\tilde{\Pi}_{C2} &= \frac{\tilde{V}_2}{\tilde{I}_2} \\
&\simeq \frac{1 - \sqrt{1+\Delta}\sqrt{1-\Delta}}{1 + \sqrt{1+\Delta}\sqrt{1-\Delta}} \times \frac{\sqrt{1+\Delta} - \sqrt{1-\Delta}}{\sqrt{1+\Delta} + \sqrt{1-\Delta}} \\
&\simeq \left(\frac{\Delta}{2}\right)^3 = \left(\frac{g_\phi\phi'}{2k}\right)^3.
\end{aligned}
\tag{3.74}
$$

So if we include the term $k^2\left(\left|\tilde{A}_+\right|^2 - \left|\tilde{A}_-\right|^2\right)$ in the definition of V the degree of circular polarization would be proportional to $\mathcal{O}(k^{-3})$. On the contrary, the linear polarization rotation angle θ does not change whether we use the definition of Stokes parameters given in Eqs. (1.29-1.32) or the new one (Eqs. (3.69-3.72)).

3.3.2   CMBP constraints on the (m, g_ϕ) plane

In a flat universe dominated by dust $(w = 0)$ plus a component with $w = -1$ (cosmological constant) the evolution of the scale factor in terms of cosmic time is [108]:

$$a(t) = \left(\frac{\Omega_{\mathrm{MAT}}}{1 - \Omega_{\mathrm{MAT}}} \right)^{\frac{1}{3}} \sinh \left[\frac{3}{2} \sqrt{1 - \Omega_{\mathrm{MAT}}} H_0 t \right]^{\frac{2}{3}} , \qquad (3.75)$$

where Ω_{MAT} is the density parameter for matter nowadays. The Hubble parameter is:

$$H = H_0 \sqrt{1 - \Omega_{\mathrm{MAT}}} \coth \left(\frac{3}{2} \sqrt{1 - \Omega_{\mathrm{MAT}}} H_0 t \right) , \qquad (3.76)$$

and:

$$t_0 = \frac{2}{3 \sqrt{1 - \Omega_{\mathrm{MAT}}} H_0} \mathrm{arcsinh} \sqrt{\frac{1 - \Omega_{\mathrm{MAT}}}{\Omega_{\mathrm{MAT}}}} . \qquad (3.77)$$

The pseudoscalar field evolves according to:

$$\phi(t) \stackrel{mt \gg 1}{\simeq} \frac{\phi_0}{\left[\sinh \left(\frac{3}{2} \sqrt{1 - \Omega_{\mathrm{MAT}}} H_0 t \right) \right]}$$

$$\times \sin \left[mt \sqrt{1 - (1 - \Omega_{\mathrm{MAT}}) \left(\frac{3 H_0}{2m} \right)^2} \right] . \qquad (3.78)$$

The energy density is:

$$\rho_\phi = \frac{\overline{\dot{\phi}^2}}{2} + \frac{1}{2} m^2 \overline{\phi}^2$$

$$\stackrel{mt \gg 1}{\simeq} \frac{m^2 \phi_0^2}{2 \left[\sinh \left(\frac{3}{2} \sqrt{1 - \Omega_{\mathrm{MAT}}} H_0 t \right) \right]^2} \propto a^{-3} . \qquad (3.79)$$

Assuming that the axion-like particles contribute to the cold dark matter density $\rho_{\phi, 0} = \Omega_{\mathrm{MAT}} \rho_{\mathrm{CR}, 0}$:

$$\frac{m^2 \phi_0^2}{2 \left[\sinh \left(\frac{3}{2} \sqrt{1 - \Omega_{\mathrm{MAT}}} H_0 t_0 \right) \right]^2} = \Omega_{\mathrm{MAT}} \frac{3 H_0^2 M_{\mathrm{pl}}^2}{8 \pi} , \qquad (3.80)$$

and using:

$$a(t_0) = 1 \implies \left[\sinh \left(\frac{3}{2} \sqrt{1 - \Omega_C} H_0 t_0 \right) \right]^2 = \frac{1 - \Omega_{\mathrm{MAT}}}{\Omega_{\mathrm{MAT}}} ,$$

we can estimate ϕ_0:

$$\phi_0 = \sqrt{\frac{3(1 - \Omega_{\mathrm{MAT}})}{\pi}} \frac{H_0 M_{\mathrm{pl}}}{2m} \, . \tag{3.81}$$

Therefore the evolution of the pseudoscalar field as a function of cosmic time is:

$$
\begin{aligned}
\phi(t) &= \sqrt{\frac{3(1 - \Omega_{\mathrm{MAT}})}{\pi}} \frac{H_0 M_{\mathrm{pl}}}{2m \sinh\left(\frac{3}{2}\sqrt{1 - \Omega_{\mathrm{MAT}}} H_0 t\right)} \\
&\quad \times \sin\left[mt\sqrt{1 - (1 - \Omega_{\mathrm{MAT}})\left(\frac{3H_0}{2m}\right)^2}\right] \\
&= \sqrt{\frac{3\Omega_{\mathrm{MAT}}}{\pi}} \frac{H_0 M_{\mathrm{pl}}}{2m a^{3/2}(t)} \\
&\quad \times \sin\left[mt\sqrt{1 - (1 - \Omega_{\mathrm{MAT}})\left(\frac{3H_0}{2m}\right)^2}\right] \, .
\end{aligned}
\tag{3.82}
$$

Note how this equations reduces to Eq. (3.52) in a matter dominated universe: $\Omega_{\mathrm{MAT}} = 1$, $H_0/(2a^{3/2}) = 1/(3t)$. The linear polarization plane, from last scattering surface, rotates according to:

$$\theta(t) = \frac{g_\phi}{2}\left[\phi(t) - \phi(t_{\mathrm{rec}})\right] \, . \tag{3.83}$$

The Boltzmann equation contains the derivative of the rotation angle respect to of conformal time (cfr. Eq. (1.54)), so we need the relation between cosmic and conformal time. For a particular model with $\Omega_{\mathrm{MAT}} = 0.3$ it is possible to fit numerically the relation between cosmic and conformal time from last scattering to nowadays:

$$t \simeq \frac{\eta_0}{3.45}\left(\frac{\eta}{\eta_0}\right)^{3.09} \, . \tag{3.84}$$

Replacing this expression in Eq. (3.82) we obtain the evolution of the pseudoscalar field as a function of conformal time $\phi = \phi(\eta)$.

The linear polarization angle is not constant in time, but it oscillates with varying amplitude. If the field represents a fraction Ω_{MAT} of the universe
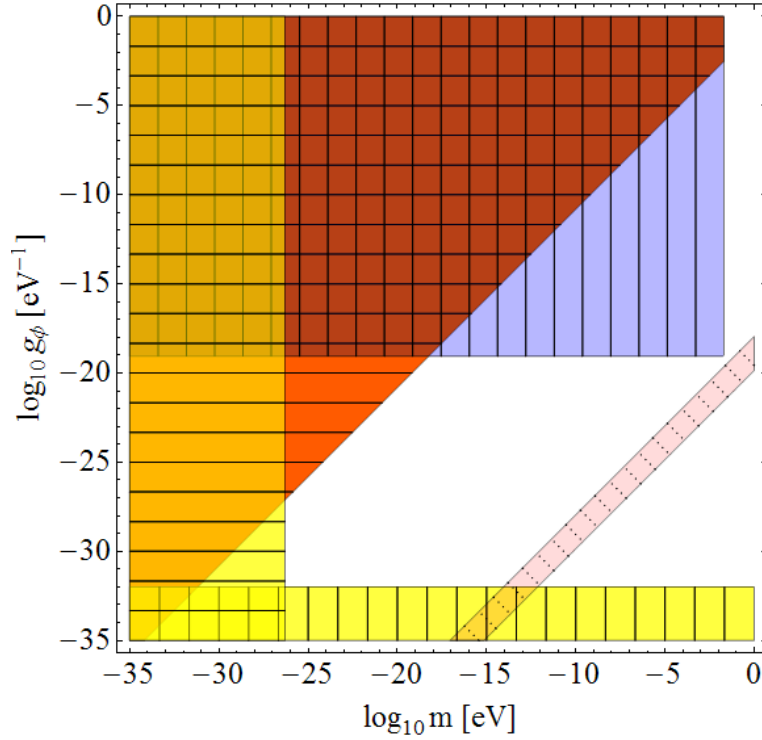
Figure 3.4: Plane $(\log_{10} m \,[\text{eV}], \log_{10} g_\phi \,[\text{eV}^{-1}])$: region excluded by CAST [59] (blue with vertical lines), region where $|\theta_A(\Omega_{\text{MAT}} = 0.3, m, g_\phi)| > 10$ deg (red region with horizontal lines), region where the mass of the pseudoscalar field is too small in order to explain dark matter $(m < 3H_{\text{eq}})$ (yellow with horizontal lines), and region where PQ symmetry is broken at energies higher than Planck scale $(f_a > M_{\text{pl}})$ (yellow with vertical lines) and values expected in main QCD axion models (red with dots).

energy density, then the amplitude of these oscillations is:

$$
\begin{aligned}
\theta_A(\Omega_{\mathrm{MAT}}, m, g_\phi) &= \frac{1}{4}\sqrt{\frac{3\Omega_{\mathrm{MAT}}}{\pi}}\frac{g_\phi M_{\mathrm{pl}} H_0}{m}\left(\frac{1}{a_0^{3/2}} - \frac{1}{a_{\mathrm{rec}}^{3/2}}\right) \\
&\simeq \frac{1}{4}\sqrt{\frac{3\Omega_{\mathrm{MAT}}}{\pi}}\frac{g_\phi M_{\mathrm{pl}} H_0}{m} z_{\mathrm{rec}}^{3/2} .
\end{aligned}
\tag{3.85}
$$

Fixed Ω_{MAT}, it is possible to constraint a certain region of the (m, g_ϕ)-plane requiring $\theta_A(\Omega_{\mathrm{MAT}}, m, g_\phi)$ to be smaller of a certain angle, typically of the order of few degrees (see Tab. 1.1). The excluded region considering current limits on CMB birefringence is shown in Fig. 3.4.

Fixed a particular value for the pseudoscalar field mass and for its coupling with photons we can also estimate how the polarization angular power spectra are modified by a rotation of the linear polarization plane. We modified the source term for linear polarization in the public Boltzmann code CAMB [4] following Eqs. (1.63) and (1.64). The linear polarization rotation angle is given by Eq. (3.83) and the evolution of the pseudoscalar field by Eq. (3.82). The new power spectra are compared with the standard unrotated ones in Fig. 3.6 fixed $m = 10^{-22}$ eV and $g_\phi = 5 \times 10^{-21}$ eV^{-1}, and in Fig 3.7 fixed $m = 10^{-22}$ eV and $g_\phi = 10^{-20}$ eV^{-1}.

3.4 Exponential potential

We consider in this section a pseudoscalar field with an exponential potential:

$$
V(\phi) = V_0 \exp(-\lambda\kappa\phi) ,
\tag{3.86}
$$

with $\kappa^2 \equiv 8\pi G$. It is known [109] that such potential with $\lambda^2 > 3(1 + w_{\mathrm{F}})$ leads to a component which tracks the dominant background fluid with equation of state $p_\phi = w_\phi\rho_\phi$. In order to satisfy the nucleosynthesis bound we choose $\lambda = 4.5$. During the matter dominated era the scalar field behaves
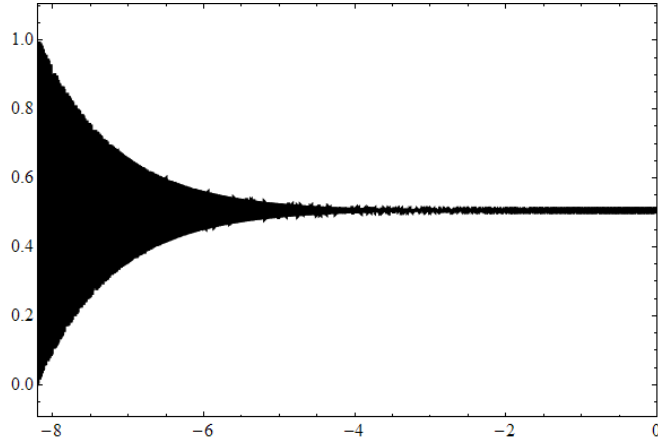
Figure 3.5: Evolution of the linear polarization rotation angle $\theta(\eta)$ for the oscillating behavior for $m = 10^{-22}$ eV and $g_\phi = 10^{-20}$ eV^{-1}, in terms of the natural logarithm of the scale factor (from $\log a = -8.2$ to nowadays $\log a_0 = 0$) in a ΛCDM model with $\Omega_{\mathrm{MAT}} = 0.3$.

as:

$$\rho_\phi = \frac{\dot{\phi}^2}{2} + V_0 \exp\left(-\lambda\kappa\phi\right) = f\,\rho_{\mathrm{MAT}} \equiv f\frac{\rho_{\mathrm{MAT},0}}{a^3}, \qquad (3.87)$$

$$P_\phi = \frac{\dot{\phi}^2}{2} - V_0 \exp\left(-\lambda\kappa\phi\right), \qquad (3.88)$$

where $\rho_{\mathrm{MAT}} = \rho_{\mathrm{DM}} + \rho_{\mathrm{baryons}} + \rho_\phi$.

For $\lambda = 4.5$ the contribution of the pseudoscalar field to universe energy density is shown in Fig. 3.8. The value of Ω_ϕ changes with time, but it is almost constant ($\Omega_\phi \simeq \Omega_{\phi,0} = 0.148$) from recombination ($\log a_{\mathrm{rec}} \simeq -7$) to nowadays.

The derivative of the pseudoscalar field respect to conformal time is proportional to $a^{-1/2}$ and the evolution of the scale factor in the matter dominated phase is $a(\eta) = (\eta/\eta_0)^2$ so:

$$\phi' = \sqrt{f\,\rho_{\mathrm{MAT},0}}\frac{\eta_0}{\eta}\,. \qquad (3.89)$$

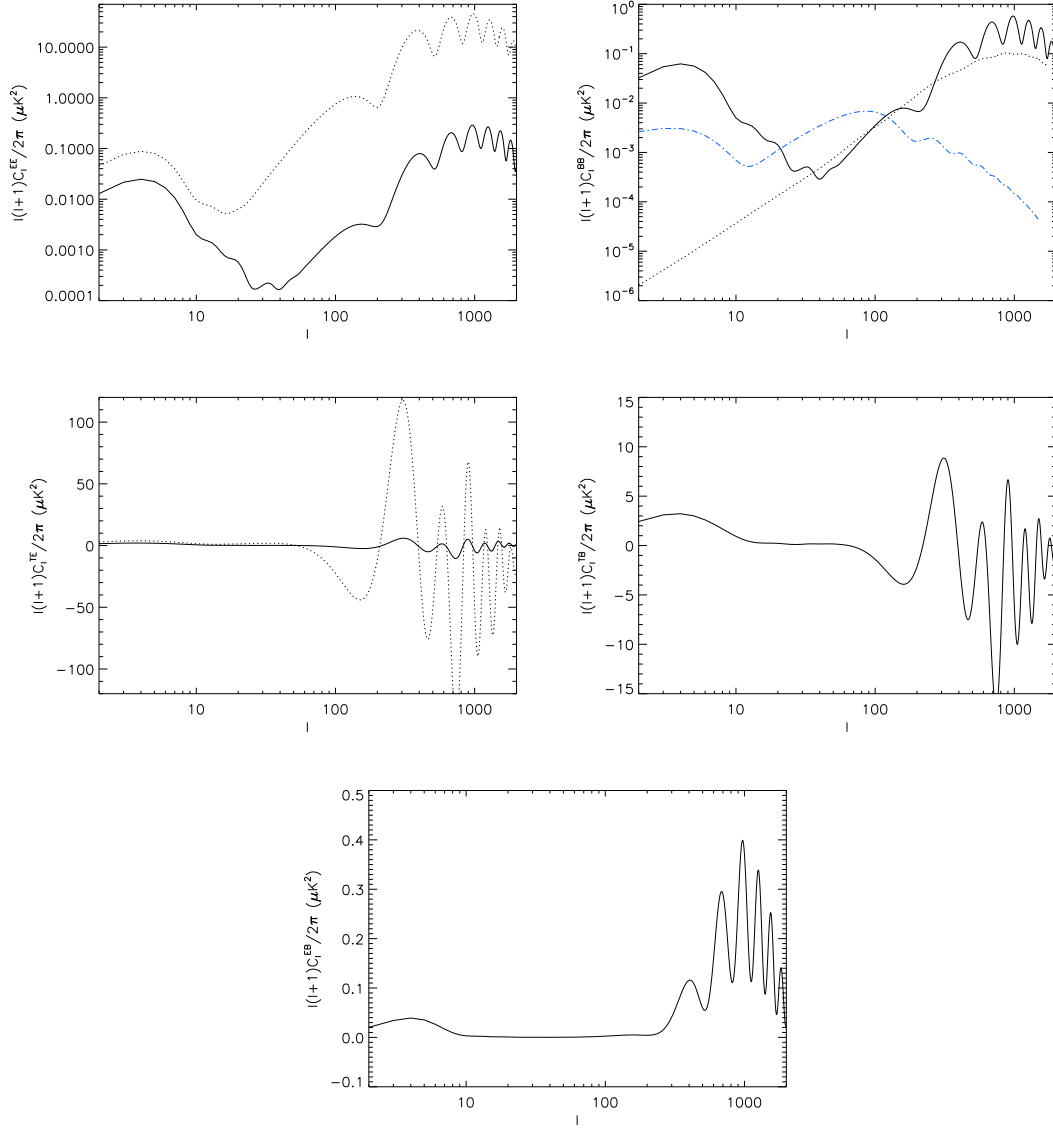Substituting this relation in Eq. (3.30) we obtain the following expression for

Figure 3.6: Cosine-type potential case. EE (a), BB (b), TE (c), TB (d), and EB (e) angular power spectra for $m = 10^{-22}$ eV and $g_\phi = 5 \times 10^{-21}$ eV^{-1} (black solid line), the black dotted line is the standard case in which there is no coupling between photons and pseudoscalars ($\theta = 0$). For the BB power spectrum (b) we plot for comparison also the polarization signal induced by gravitational lensing (black dotted line), and primordial BB signal if $r = 0.1$ (blue dot-dashed line). The cosmological parameters of the flat ΛCDM model used here are $\Omega_b\,h^2 = 0.022$, $\Omega_c\,h^2 = 0.123$, $\tau = 0.09$, $n_s = 1$, $A_s = 2.3 \times 10^{-9}$, $H_0 = 100\,h\,\mathrm{km\,s^{-1}\,Mpc^{-1}} = 72\,\mathrm{km\,s^{-1}\,Mpc^{-1}}$.
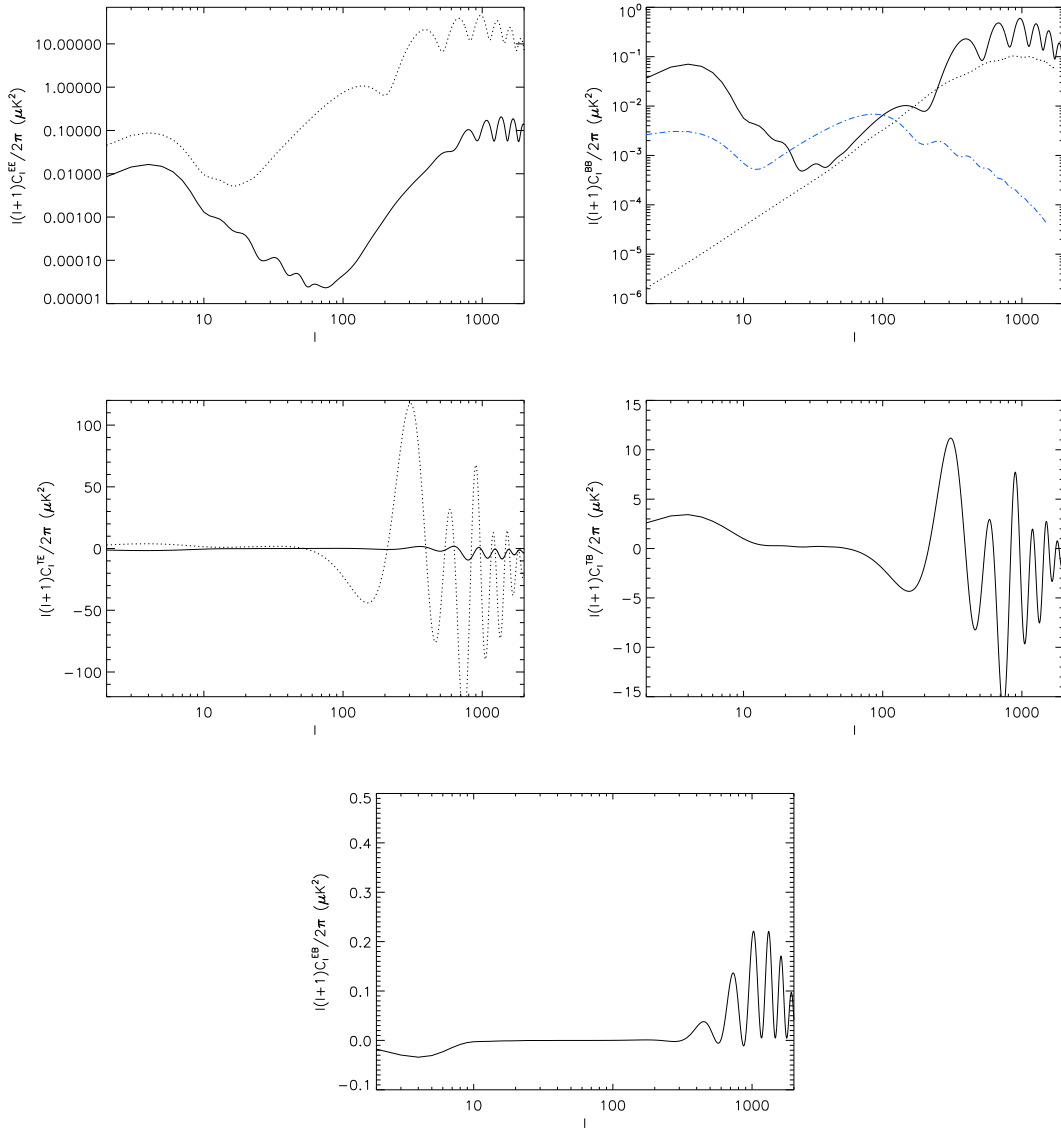
Figure 3.7: Cosine-type potential case. EE (a), BB (b), TE (c), TB (d), and EB (e) angular power spectra for $m = 10^{-22}$ eV and $g_\phi = 10^{-20}\,\mathrm{eV}^{-1}$ (black solid line), the black dotted line is the standard case in which there is no coupling between photons and pseudoscalars ($\theta = 0$). For the BB power spectrum (b) we plot for comparison also the polarization signal induced by gravitational lensing (black dotted line), and primordial BB signal if $r = 0.1$ (blue dot-dashed line). The cosmological parameters of the flat ΛCDM model used here are $\Omega_b\, h^2 = 0.022$, $\Omega_c\, h^2 = 0.123$, $\tau = 0.09$, $n_s = 1$, $A_s = 2.3 \times 10^{-9}$, $H_0 = 100\, h\,\mathrm{km\, s}^{-1}\,\mathrm{Mpc}^{-1} = 72\,\mathrm{km\, s}^{-1}\,\mathrm{Mpc}^{-1}$.
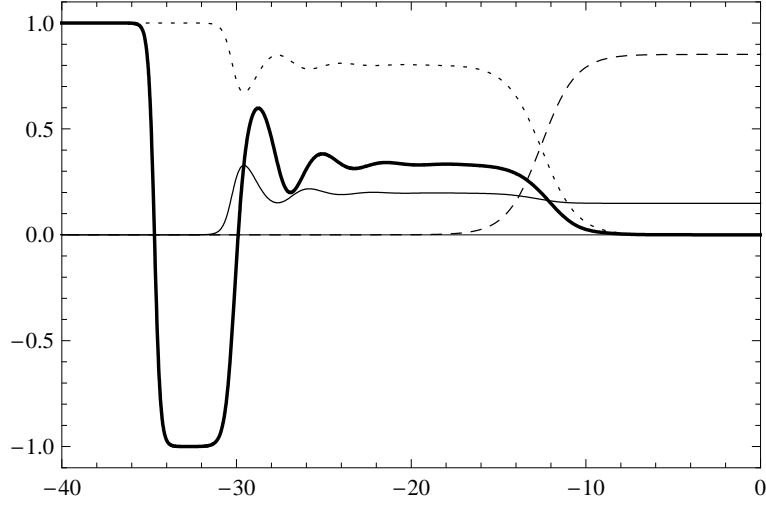
Figure 3.8: For $\lambda = 4.5$ Dashed line: $\Omega_{\text{DM}} + \Omega_{\text{baryons}}$, dotted line: Ω_{RAD}, thin continuous line: Ω_ϕ, thick continuous line: w_ϕ, in terms of the natural logarithm of the scale factor (from $\log a \simeq -40$ to nowadays $\log a_0 = 0$). Here $\Omega_{\text{DM},0} + \Omega_{\text{baryons},0} = 0.852$ and $\Omega_{\phi,0} = 0.148$.

the evolution of the electromagnetic potential:

$$\tilde{A}''_\pm + \left(k^2 \pm g_\phi \sqrt{f\,\rho_{\text{MAT},0}} \frac{\eta_0}{\eta} k \right) \tilde{A}_\pm = 0\,. \tag{3.90}$$

This is a particular differential equation, called Coulomb wave equation[1] defining $q_\pm \equiv \mp g_\phi \sqrt{f\,\rho_{\text{MAT},0}}\,\eta_0/2 = \mp q$ and $x \equiv k\eta$ it becomes:

$$\frac{d^2\tilde{A}_\pm}{dx^2} + \left(1 - \frac{2q_\pm}{x} \right) \tilde{A}_\pm = 0\,. \tag{3.91}$$

The solution of this equation can be written in terms of regular $(F_0(q,x))$

---

[1]The Coulomb wave equation is [110]:

$$\frac{d^2w}{dx^2} - \left[1 - \frac{2q}{x} - \frac{L(L+1)}{x^2} \right] w = 0\,,$$

with $x > 0, -\infty < q < \infty, L$ a non negative integer. Here, in order to solve Eq. (3.91), we are particular interested to the particular case $L = 0$.

and irregular $(G_0(q, x))$ Coulomb wave functions [84, 110]:

$$
\begin{aligned}
\tilde{A}_+ &= f_+ F_0(q_+, x) + g_+ G_0(q_+, x) \\
&= f_+ F_0(-q, x) + g_+ G_0(-q, x) \,, \\
\tilde{A}_- &= f_- F_0(q_-, x) + g_- G_0(q_-, x) \\
&= f_- F_0(q, x) + g_- G_0(q, x) \,,
\end{aligned}
$$

where $f_+, f_-, g_+, g_- \in \mathbb{C}$; in a compact notation:

$$
\tilde{A}_\pm(q, x) = f_\pm F_0(\mp q, x) + g_\pm G_0(\mp q, x) \,. \tag{3.92}
$$

The Stokes parameters contain the derivative respect to conformal time η, so we evaluate:

$$
\tilde{A}'_\pm(q, x) = k \left[f_\pm \frac{\partial F_0(\mp q, x)}{\partial x} + g_\pm \frac{\partial G_0(\mp q, x)}{\partial x} \right] \,. \tag{3.93}
$$

The solution given in Eq. (3.92) verifies the *Wronskian condition* $(\tilde{A}_\pm \tilde{A}'^{*}_\pm - \tilde{A}'_\pm \tilde{A}^{*}_\pm = i)$ if the following relation holds:

$$
f^{*}_\pm g_\pm - f_\pm g^{*}_\pm = \frac{i}{k} \quad \Longrightarrow \quad \Im \left(f^{*}_\pm g_\pm \right) = \frac{1}{2k} \,. \tag{3.94}
$$

3.4.1 Vanishing coupling $(g_\phi = 0)$

If there is no coupling between the electromagnetic tensor and the pseudoscalar field $(g_\phi = 0)$ Eq. (3.30) reduces to:

$$
\tilde{A}''_\pm + k^2 \tilde{A}_\pm = 0 \,. \tag{3.95}
$$

Obviously the solution is:

$$
\tilde{A}_\pm(x) = f_\pm \sin(x) + g_\pm \cos(x) \,, \tag{3.96}
$$

and the derivative respect conformal time η is:

$$
\begin{aligned}
\tilde{A}'_\pm(x) &= k \left[f_\pm \cos(x) - g_\pm \sin(x) \right] \\
&= \frac{k}{2} \left[e^{ix} \left(f_\pm + i g_\pm \right) + e^{-ix} \left(f_\pm - i g_\pm \right) \right] \,. \tag{3.97}
\end{aligned}
$$

The elements of the coherence matrix $\tilde{\mathbf{J}}$ are:

$$\tilde{J}_{\pm\pm} = \frac{k^2}{2a^4} \left\langle |f_\pm|^2 + |g_\pm|^2 + \left(|f_\pm|^2 - |g_\pm|^2\right) \cos 2x \right.$$
$$\left. - \left(f_\pm^* g_\pm + f_\pm g_\pm^*\right) \sin 2x \right\rangle ,$$

$$\tilde{J}_{\pm\mp} = \frac{k^2}{2a^4} \left\langle f_\pm^* f_\mp + g_\pm^* g_\mp + \left(f_\pm^* f_\mp - g_\pm^* g_\mp\right) \cos 2x \right.$$
$$\left. - \left(f_\mp g_\pm^* + f_\pm^* g_\mp\right) \sin 2x \right\rangle .$$

For a pure monochromatic wave ensemble averages can be omitted and the elements oscillate with period $2x$ due to the presence of both forward ($\tilde{A}' \propto e^{-ix}$) and backward ($\tilde{A}' \propto e^{+ix}$) moving waves.

In order to describe the propagation of an electromagnetic wave in a region with no coupling between photons and field ϕ (vacuum) we can use only forward moving waves, therefore setting $f_\pm = -ig_\pm$ in Eq. (3.97) we obtain:

$$\tilde{A}'_\pm(x) = -ikg_\pm e^{-ix} . \tag{3.98}$$

The dependence from $g_\pm$ can be replaced by the value of at $\tilde{A}'_\pm$ at a particular time (e.g. recombination time):

$$\tilde{A}'_\pm(x) = \tilde{A}'_\pm(x_{\text{rec}}) e^{-i(x - x_{\text{rec}})} . \tag{3.99}$$

In this particular situation the elements of the coherence matrix does not depend on x:

$$\tilde{\mathbf{J}} = \frac{1}{a^4} \begin{pmatrix} \left\langle \tilde{A}'^*_+(x) \tilde{A}'_+(x) \right\rangle & \left\langle \tilde{A}'^*_+(x) \tilde{A}'_-(x) \right\rangle \\ \left\langle \tilde{A}'^*_-(x) \tilde{A}'_+(x) \right\rangle & \left\langle \tilde{A}'^*_-(x) \tilde{A}'_-(x) \right\rangle \end{pmatrix}$$
$$= \frac{1}{a^4} \begin{pmatrix} \left\langle \tilde{A}'^*_+(x_{\text{rec}}) \tilde{A}'_+(x_{\text{rec}}) \right\rangle & \left\langle \tilde{A}'^*_+(x_{\text{rec}}) \tilde{A}'_-(x_{\text{rec}}) \right\rangle \\ \left\langle \tilde{A}'^*_-(x_{\text{rec}}) \tilde{A}'_+(x_{\text{rec}}) \right\rangle & \left\langle \tilde{A}'^*_-(x_{\text{rec}}) \tilde{A}'_-(x_{\text{rec}}) \right\rangle \end{pmatrix}$$
$$= \left(\frac{a_{\text{rec}}}{a}\right)^4 \tilde{\mathbf{J}}_{\text{rec}} . \tag{3.100}$$

So the Stokes parameters evolve according to:

$$\tilde{I} = \left(\frac{a_{\text{rec}}}{a}\right)^4 \tilde{I}_{\text{rec}} , \quad \tilde{Q} = \left(\frac{a_{\text{rec}}}{a}\right)^4 \tilde{Q}_{\text{rec}} ,$$
$$\tilde{U} = \left(\frac{a_{\text{rec}}}{a}\right)^4 \tilde{U}_{\text{rec}} , \quad \tilde{V} = \left(\frac{a_{\text{rec}}}{a}\right)^4 \tilde{V}_{\text{rec}} .$$

Obviously the degrees of polarization are constant ($\tilde{\Pi}_L = \tilde{\Pi}_{L,\,\mathrm{rec}}$ and $\tilde{\Pi}_C = \tilde{\Pi}_{C,\,\mathrm{rec}}$) and also the angle of linear polarization does not change with time. If there is no coupling between the pseudoscalar field and photons the electromagnetic wave propagates freely and the polarization does not change.

3.4.2 Non-vanishing coupling ($g_\phi \neq 0$)

In the general case, when the coupling does not vanishes ($g_\phi \neq 0$), we expand the solution (3.92) for large value of x neglecting terms proportional to $\mathcal{O}(x^{-2})$.

The Coulomb functions can be expanded for large values of x [110]:

$$F_0 \;=\; g\cos\theta + f\sin\theta\,, \tag{3.101}$$

$$G_0 \;=\; f\cos\theta - g\sin\theta\,, \tag{3.102}$$

similarly for the first derivative respect to x:

$$F_0' \;=\; g^*\cos\theta + f^*\sin\theta\,, \tag{3.103}$$

$$G_0' \;=\; f^*\cos\theta - g^*\sin\theta\,, \tag{3.104}$$

with $\theta \equiv x - q\log 2x + \arg\Gamma(1+iq)$ and:

$$f = \sum_{k=0}^{\infty} f_k\,, \qquad g = \sum_{k=0}^{\infty} g_k\,,$$

$$f^* = \sum_{k=0}^{\infty} f_k^*\,, \qquad g^* = \sum_{k=0}^{\infty} g_k^*\,,$$

where:

$$f_0 = 1\,, \quad f_{k+1} = a_k f_k - b_k g_k\,; \tag{3.105}$$

$$g_0 = 0\,, \quad g_{k+1} = a_k g_k + b_k f_k\,; \tag{3.106}$$

$$f_0^* = 0\,, \quad f_{k+1}^* = a_k f_k^* - b_k g_k^* - \frac{f_{k+1}}{x}\,; \tag{3.107}$$

$$g_0^* = 1 - \frac{q}{x}\,, \quad g_{k+1}^* = a_k g_k^* + b_k f_k^* - \frac{g_{k+1}}{x}\,; \tag{3.108}$$

$$a_k = \frac{(2k+1)q}{2(k+1)x}\,, \quad b_k = \frac{q^2 - k(k+1)}{2(k+1)x}\,. \tag{3.109}$$

Restricting to the first and second order:

$$f = 1 + \frac{q}{2x} + \frac{5q^2 - q^4}{8x^2} + \mathcal{O}\left(\frac{1}{x^3}\right) , \tag{3.110}$$

$$g = \frac{q^2}{2x} + \frac{2q^3 - q}{4x^2} + \mathcal{O}\left(\frac{1}{x^3}\right) , \tag{3.111}$$

$$f^* = -\frac{q^2}{2x} + \frac{4q^3 - 2q^2 + q}{4x^2} + \mathcal{O}\left(\frac{1}{x^3}\right) , \tag{3.112}$$

$$g^* = 1 - \frac{q}{2x} - \frac{q^4 + 3q^2}{8x^2} + \mathcal{O}\left(\frac{1}{x^3}\right) . \tag{3.113}$$

Summarizing the asymptotic expansion of $F_L(q, x)$ and $F_L(q, x)$ for large values of x is:

$$F_0(q, x) \simeq \frac{q^2}{2x} \cos\theta + \left(1 + \frac{q}{2x}\right) \sin\theta , \tag{3.114}$$

$$G_0(q, x) \simeq \left(1 + \frac{q}{2x}\right) \cos\theta - \frac{q^2}{2x} \sin\theta , \tag{3.115}$$

and for the first derivative:

$$F_0'(q, x) \simeq \left(1 - \frac{q}{2x}\right) \cos\theta - \frac{q^2}{2x} \sin\theta , \tag{3.116}$$

$$G_0'(q, x) \simeq -\frac{q^2}{2x} \cos\theta - \left(1 - \frac{q}{2x}\right) \sin\theta . \tag{3.117}$$

Therefore, expanding Coulomb functions for large value of x and neglecting $\mathcal{O}\left(\frac{1}{x^2}\right)$ terms, Eq. (3.92) becomes:

$$\tilde{A}_\pm(q, x) \simeq f_\pm \left[\frac{q^2}{2x} \cos\left(x \pm \alpha\left(q, x\right)\right) + \left(1 \mp \frac{q}{2x}\right) \sin\left(x \pm \alpha\left(q, x\right)\right)\right]$$
$$+ g_\pm \left[\left(1 \mp \frac{q}{2x}\right) \cos\left(x \pm \alpha\left(q, x\right)\right) - \frac{q^2}{2x} \sin\left(x \pm \alpha\left(q, x\right)\right)\right] , \tag{3.118}$$

where $\alpha\left(q, x\right) \equiv q \log 2x - \arg\Gamma(1 + iq)$. The derivative respect to conformal

time is:

$$
\begin{aligned}
\tilde{A}'_{\pm}(q,x) \;\simeq\; & k\left\{ f_{\pm}\left[\left(1\pm\frac{q}{2x}\right)\cos\left(x\pm\alpha\left(q,x\right)\right)-\frac{q^2}{2x}\sin\left(x\pm\alpha\left(q,x\right)\right)\right]\right. \\
& \left.+g_{\pm}\left[-\frac{q^2}{2x}\cos\left(x\pm\alpha\left(q,x\right)\right)-\left(1\pm\frac{q}{2x}\right)\sin\left(x\pm\alpha\left(q,x\right)\right)\right]\right\} \\
=\; & \frac{k}{2}\left[e^{i(x\pm\alpha(q,x))}\left(1\pm\frac{q}{2x}+i\frac{q^2}{2x}\right)(f_{\pm}+ig_{\pm})\right. \\
& \left. e^{-i(x\pm\alpha(q,x))}\left(1\pm\frac{q}{2x}-i\frac{q^2}{2x}\right)(f_{\pm}-ig_{\pm})\right].
\end{aligned}
\tag{3.119}
$$

In general both forward moving waves ($\tilde{A}_{\pm}\propto e^{-ik\eta}$) and backward moving waves ($\tilde{A}_{\pm}\propto e^{ik\eta}$) must be taken into account for propagation of light in a medium. Chosen a particular value for the constants $f_{\pm}$ and $g_{\pm}$ that verifies the Wronskian relation (3.94) the evolution of polarization is fixed.

If we assume, according with [111, 112], that the photon pseudoscalar conversion is a small effect due to low energy of CMB photons, the production of backward moving waves can be neglected (see [113] for the use of this approximation). The Eq. (3.119) setting $f_{\pm}=-ig_{\pm}$ becomes:

$$
\tilde{A}'_{\pm}(q,x)\simeq -ikg_{\pm}\left(1\pm\frac{q}{2x}-i\frac{q^2}{2x}\right)e^{-i(x\pm\alpha(q,x))},
\tag{3.120}
$$

and in terms of the value at recombination time:

$$
\begin{aligned}
\tilde{A}'_{\pm}(q,x)\simeq\; & \tilde{A}'_{\pm}(q,x_{\mathrm{rec}})\left[1\pm\frac{q}{2}\left(\frac{1}{x}-\frac{1}{x_{\mathrm{rec}}}\right)\right. \\
& \left. -i\frac{q^2}{2}\left(\frac{1}{x}-\frac{1}{x_{\mathrm{rec}}}\right)\right]\exp\left\{-i\left[x-x_{\mathrm{rec}}\pm\Delta\alpha\right]\right\},
\end{aligned}
\tag{3.121}
$$

where we have introduced

$$
\begin{aligned}
\Delta\alpha \;\equiv\; & \alpha(q,x)-\alpha(q,x_{\mathrm{rec}})=q\log\left(\eta/\eta_{\mathrm{rec}}\right) \\
=\; & \frac{q}{2}\log\left(a/a_{\mathrm{rec}}\right).
\end{aligned}
\tag{3.122}
$$

In the usual definition for the Stokes parameters describing linear polarization (see Eqs. (1.30-1.31)) $\tilde{A}(q,x)$ appears in the combination:

$$
\langle\tilde{A}'^{*}_{+}(q,x)\tilde{A}'_{-}(q,x)\rangle\simeq e^{2i\Delta\alpha}\langle\tilde{A}'^{*}_{+}(q,x_{\mathrm{rec}})\tilde{A}'_{-}(q,x_{\mathrm{rec}})\rangle.
\tag{3.123}
$$

The plane of linear polarization is rotated of an angle $\Delta\alpha$ independent on k whose dependence on the difference between the present value of ϕ and the corresponding one at recombination is the same of the adiabatic approximation (see Eq. (3.64)) and of Eq. (1.77).

If we use the Stokes parameter definition given in Eqs. (3.70-3.71) also terms like $k^2 \langle \tilde{A}^*_\pm \tilde{A}_\mp \rangle$ contribute to linear polarization, but the final effect does not change:

$$k^2 \langle \tilde{A}^*_+(q,x)\tilde{A}_-(q,x) \rangle \simeq e^{2i\Delta\alpha} k^2 \langle \tilde{A}^*_+(q,x_{\rm rec})\tilde{A}_-(q,x_{\rm rec}) \rangle \,, \qquad (3.124)$$

and therefore:

$$\langle \tilde{A}'^*_+(q,x)\tilde{A}'_-(q,x) \rangle + k^2 \langle \tilde{A}^*_+(q,x)\tilde{A}_-(q,x) \rangle \simeq$$
$$e^{2i\Delta\alpha} \left[\langle \tilde{A}'^*_+(q,x_{\rm rec})\tilde{A}'_-(q,x_{\rm rec}) \rangle + k^2 \langle \tilde{A}^*_+(q,x_{\rm rec})\tilde{A}_-(q,x_{\rm rec}) \rangle \right] \quad (3.125)$$

linear polarization plane it is always rotated of an angle $\Delta\alpha$.

Concerning circular polarization, using the definition of V given in Eq. (1.32), the degree of circular polarization changes from recombination to nowadays:

$$\tilde{\Pi}_{C,0} \simeq \left| \tilde{\Pi}_{C,\rm rec} + q \left(\frac{1}{x} - \frac{1}{x_{\rm rec}} \right) \left(1 - \tilde{\Pi}^2_{C,\rm rec} \right) \right| \,. \qquad (3.126)$$

Instead V_2, introduced in Eq. (3.72), contains both terms of the form $\langle \tilde{A}'^*_\pm \tilde{A}'_\pm \rangle$ and $k^2 \langle \tilde{A}^*_\pm \tilde{A}_\pm \rangle$. They transform according to:

$$\begin{aligned}
\langle \tilde{A}'^*_\pm(x)\tilde{A}'_\pm(x) \rangle &\simeq \left[1 \pm q \left(\frac{1}{x} - \frac{1}{x_{\rm rec}} \right) \right] \langle \tilde{A}'^*_\pm(x_{\rm rec})\tilde{A}'_\pm(x_{\rm rec}) \rangle \,, \\
k^2 \langle \tilde{A}^*_\pm(x)\tilde{A}_\pm(x) \rangle &\simeq \left[1 \mp q \left(\frac{1}{x} - \frac{1}{x_{\rm rec}} \right) \right] k^2 \langle \tilde{A}^*_\pm(x_{\rm rec})\tilde{A}_\pm(x_{\rm rec}) \rangle \,.
\end{aligned}$$

Note that, in this case, the two contributes delete:

$$\langle \tilde{A}'^*_+(x)\tilde{A}'_+(x) \rangle + k^2 \langle \tilde{A}^*_+(x)\tilde{A}_+(x) \rangle \simeq \langle \tilde{A}'^*_+(x_{\rm rec})\tilde{A}'_+(x_{\rm rec}) \rangle + k^2 \langle \tilde{A}^*_+(x_{\rm rec})\tilde{A}_+(x_{\rm rec}) \rangle \,,$$
$$(3.127)$$

therefore, at first order in x, no circular polarization is generated if we use definition of the Stokes parameter given in Eq. (3.72).
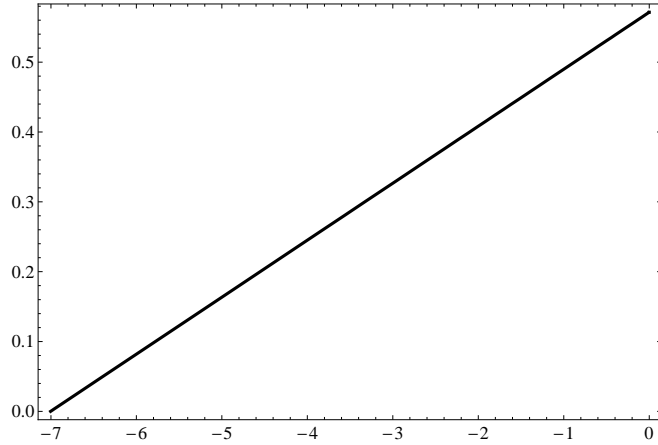
Figure 3.9: Evolution of the linear polarization rotation angle $\theta(\eta)$ in the exponential potential case for $g_\phi = 10^{-28}\,\mathrm{eV}^{-1}$, in terms of the natural logarithm of the scale factor (from $\log a = -7$ to nowadays $\log a_0 = 0$) in a flat CDM model with $\Omega_\phi \simeq 0.148$.

3.4.3   CMBP constraints on the coupling constant g_ϕ

In the particular approximation in which we neglect backward moving waves we can constrain the parameter q using the upper limits on isotropic frequency-independent rotation of the linear polarization plane of CMBP. Current measures and constraints on the polarization pattern of anisotropies produce an upper limit on the linear polarization rotation angle of the order of few degrees (see Tab. 1.1). We now use these constraints and our analytic expression:

$$\begin{aligned} |\theta| &= \frac{|q|}{2}\log(1 + z_{\mathrm{rec}}) \\ &\simeq \frac{1}{4}\sqrt{\frac{3}{2\pi}\Omega_{\phi,0}}\,|g_\phi|\,M_{\mathrm{pl}}\log(1 + z_{\mathrm{rec}})\,, \end{aligned} \qquad (3.128)$$

to obtain an upper bound for q, which can be turned into a upper bound on g_ϕ; if $|\theta| \lesssim 6$ deg, then:

$$|g_\phi| \lesssim 10^{-30}\,\mathrm{eV}^{-1}\,, \qquad (3.129)$$

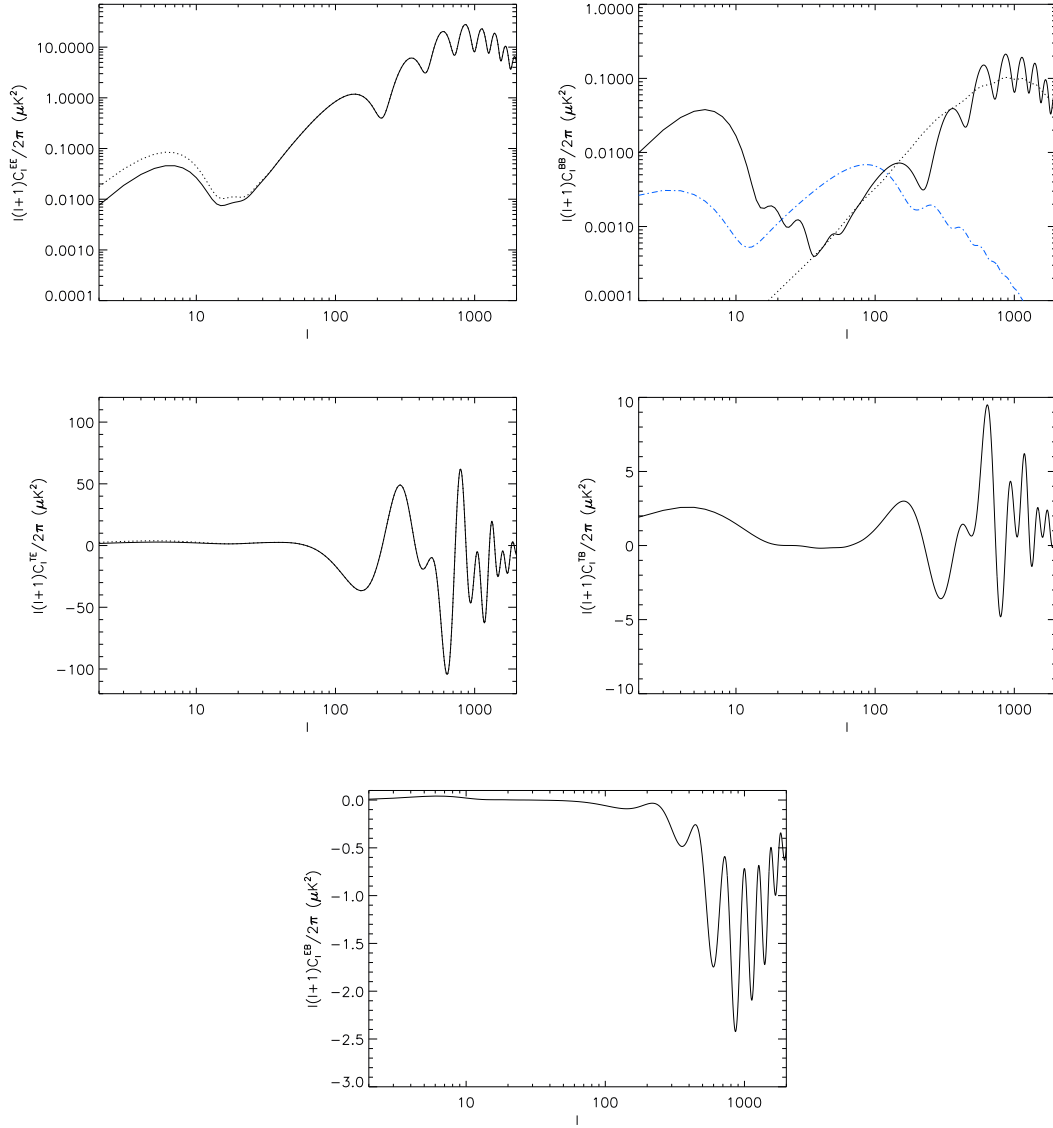where we have assumed: $\Omega_{\phi,0} \simeq 0.148$ and $z_{\mathrm{rec}} \simeq 1100$.

Figure 3.10: Exponential potential case. EE (a), BB (b), TE (c), TB (d) and EB (e) angular power spectra for $g_\phi = 10^{-28}\,\mathrm{eV}^{-1}$ (black solid line); the black dotted line is the standard case in which there is no coupling ($\theta = 0$). For the BB power spectrum (b) we plot for comparison also the polarization signal induced by gravitational lensing (black dotted line), and primordial BB signal if $r = 0.1$ (blue dot-dashed line). The cosmological parameters of the flat CDM model used here are $\Omega_b = 0.0462$, $\Omega_c = 0.9538$ ($\Omega_\phi \simeq 0.148$), $\tau = 0.09$, $n_s = 1$, $A_s = 2.3 \times 10^{-9}$, $H_0 = 72\,\mathrm{km\,s^{-1}\,Mpc^{-1}}$.
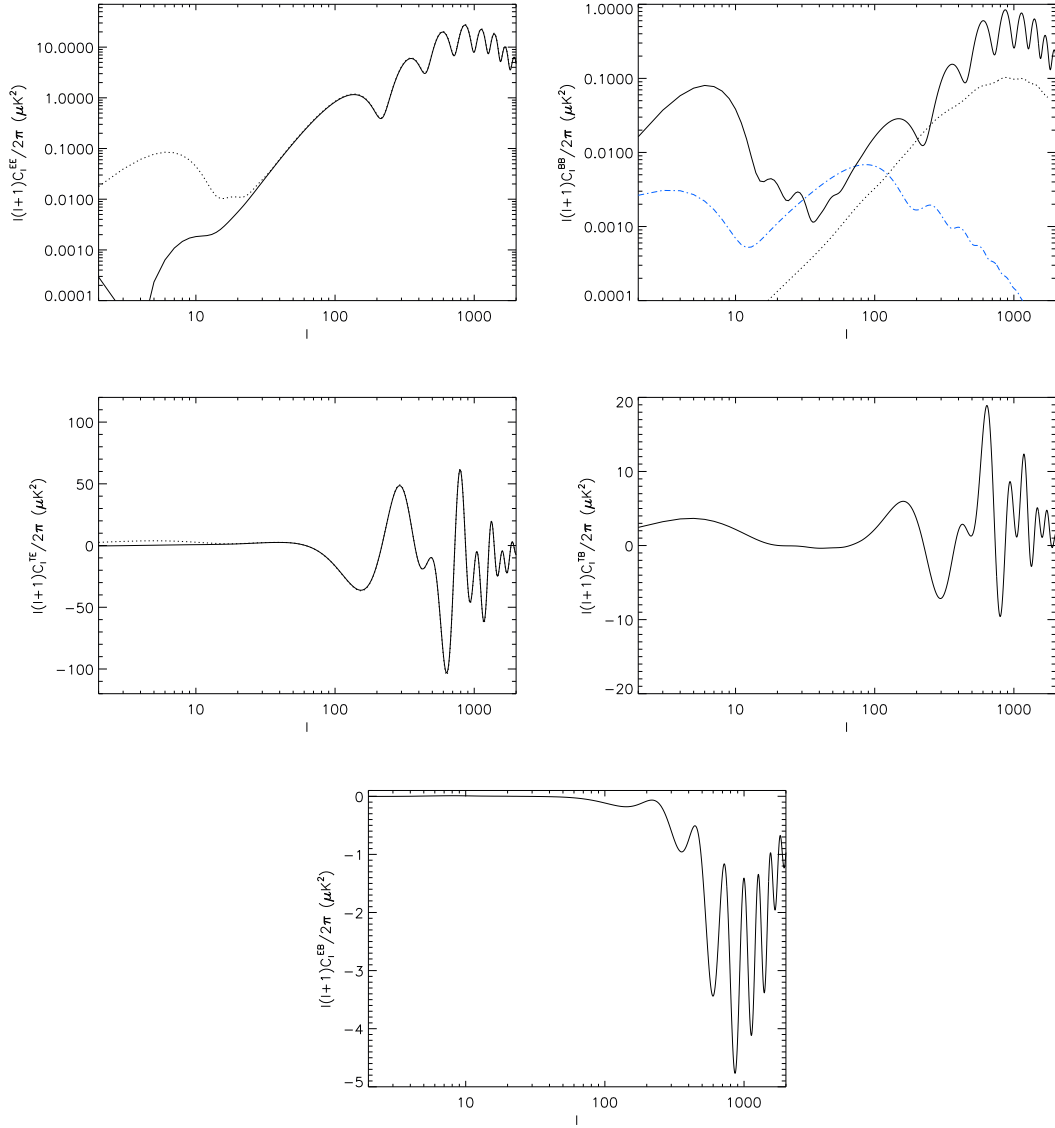
Figure 3.11: Exponential potential case. EE (a), BB (b), TE (c), TB (d) and EB (e) angular power spectra for $g_\phi = 2 \times 10^{-28}\,\mathrm{eV}^{-1}$ (black solid line); the black dotted line is the standard case in which there is no coupling ($\theta = 0$). For the BB power spectrum (b) we plot for comparison also the polarization signal induced by gravitational lensing (black dotted line), and primordial BB signal if $r = 0.1$ (blue dot-dashed line). The cosmological parameters of the flat CDM model used here are $\Omega_b = 0.0462$, $\Omega_c = 0.9538$ ($\Omega_\phi \simeq 0.148$), $\tau = 0.09$, $n_s = 1$, $A_s = 2.3 \times 10^{-9}$, $H_0 = 72\,\mathrm{km\,s^{-1}\,Mpc^{-1}}$.

The angle of linear polarization $\theta(\eta)$ appearing in Eqs. (1.63) and (1.64) can be replaced with:

$$|\theta(\eta)| \simeq \frac{1}{2}\sqrt{\frac{3}{2\pi}\Omega_{\phi,0}}\,|g_\phi|\,M_{\rm pl}\log\left(\frac{\eta}{\eta_{\rm rec}}\right)\,,\qquad(3.130)$$

(see Fig. 3.9 for the temporal evolution of the linear polarization angle) and the polarization power spectra are evaluated using the expression given in section 1.5, see angular power spectra of Figs. 3.10 and 3.11.

3.5 Ultralight pseudo Nambu-Goldstone bosons dark energy

Even before acceleration of the universe was discovered, the cosmological implications of an universe dominated by ultralight Pseudo Nambu-Goldstone were studied in Refs. [7, 90] and [91] (see section 2.3 for further details). This model is still in agreement with observations [92] and can be probed by a future experiment experiment reaching stage 4 of the Dark Energy Task Force (DETF) methodology (which includes Planck CMB measurements, future surveys of SNIa, baryon acoustic oscillations, and weak gravitational lensing). This analysis does not take into account cosmological birefringence of CMB polarization that we discuss here.

We solve numerically this system of equations from radiation dominated epoch to nowadays:

$$\begin{cases} \ddot{\phi} + 3H\dot{\phi} - \frac{M^4}{f}\sin\frac{\phi}{f} = 0 \\ H^2 = \frac{8\pi}{3M_{\rm pl}^2}\left(\rho_{\rm RAD} + \rho_{\rm MAT} + \rho_\phi\right) \end{cases}\qquad(3.131)$$

For $M \sim 10^{-3}$ eV and $f \lesssim M_{\rm pl}/\sqrt{8\pi}$ the pseudoscalar field mimes the cosmological constant contribution.[2] Anyway in the future, when the expansion rate of the universe will become smaller, the field will start to oscillate

---

[2]There are indications form string theory that f cannot be larger than $M_{\rm pl}/\sqrt{8\pi}$ [114, 115].
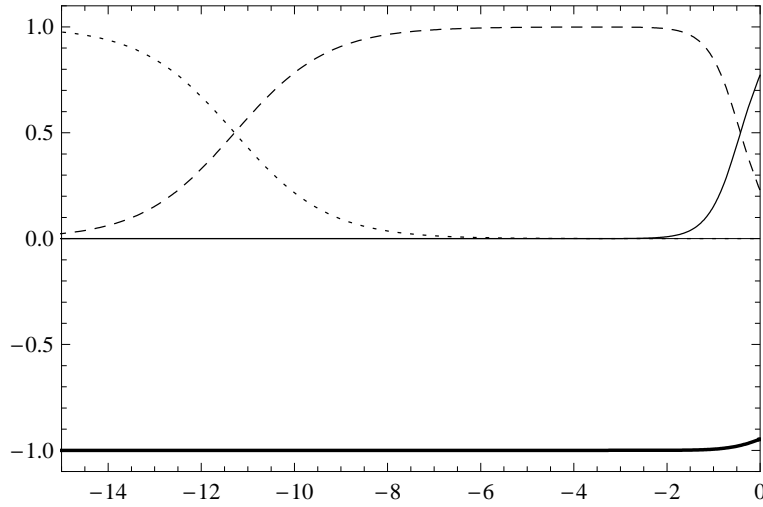
Figure 3.12: Dotted line: Ω_{RAD}, dashed line: Ω_{MAT}, thin continuous line: Ω_ϕ, thick continuous line w_ϕ, in terms of the natural logarithm of the scale factor (from $\log a \simeq -15$ to nowadays $\log a_0 = 0$). Fixed $M = 8.8 \times 10^{-4}$ eV, $f = M_{\mathrm{pl}}/\sqrt{8\pi}$, $\Theta_i = 0.87$ and $\dot{\Theta}_i = 0$.

and the universe will become cold dark matter dominated. Fixed a particular value for f, M, Θ_i and $\dot{\Theta}_i$ in Figs. 3.12 and 3.13 we show the evolution of the different components of the universe energy density and the cosmological evolution of the pseudoscalar field (see Figs. 3.14 and 3.15).

The pseudoscalar field becomes dynamical only recently. In oder to estimate the effects of this quick dynamical evolution of the scalar field on the polarization power spectra we fit the numerical solutions for w_ϕ and Θ with the following functions:

$$w_\phi(\eta) \;\; \simeq \;\; b_1 \exp\left[b_2 \frac{\eta}{\eta_0} \right] + b_3 \,, \tag{3.132}$$

$$\Theta(\eta) \;\; \simeq \;\; c_1 \exp\left[c_2 \frac{\eta}{\eta_0} \right] + c_3 \,. \tag{3.133}$$

The approximate global symmetry $\phi \to \phi + \mathrm{const}$ of this pseudo Nambu-Goldstone model suppresses most of possible interactions with ordinary matter, but it leaves open one possibility: a pseudoscalar electromagnetic inter-
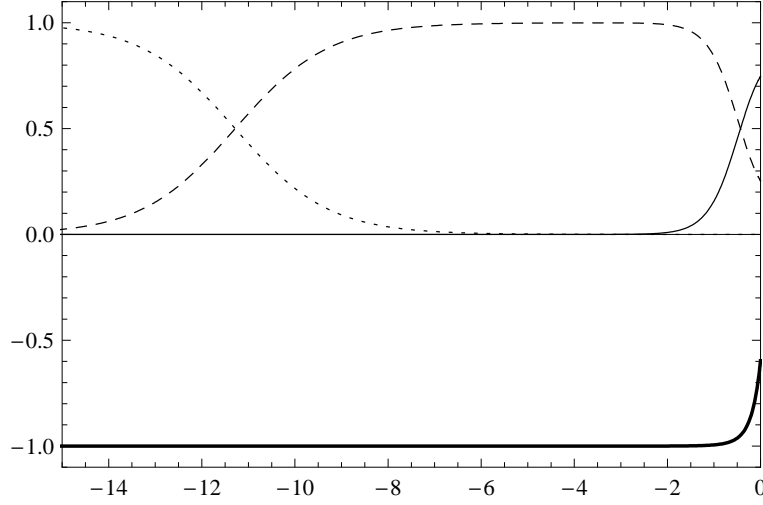
Figure 3.13: Dotted line: Ω_{RAD}, dashed line: Ω_{MAT}, thin continuous line: Ω_ϕ, thick continuous line w_ϕ, in terms of the natural logarithm of the scale factor (from $\log a \simeq -15$ to nowadays $\log a_0 = 0$). Fixed $M = 8.5 \times 10^{-4}$ eV, $f = 0.3 M_{\mathrm{pl}}/\sqrt{8\pi}$, $\Theta_i = 0.25$ and $\dot{\Theta}_i = 0$.

action in which ϕ couples to $\mathbf{E} \cdot \mathbf{B}$ [87]; the coupling constant inverse is of the order of the energy braking scale f:

$$\mathcal{L}_{\phi\gamma} = -\frac{1}{4f}\phi F^{\mu\nu}\tilde{F}_{\mu\nu} \,. \tag{3.134}$$

For a wave propagation from η_1 to η_2 the plane of linear polarization rotates (in the adiabatic approximation) of:

$$
\begin{aligned}
\theta(\eta_1, \eta_2) &= \frac{g_\phi}{2}\left[\phi(\eta_2) - \phi(\eta_1)\right] \\
&= \frac{1}{2f}\left[f\Theta(\eta_2) - f\Theta(\eta_1)\right] \\
&= \frac{1}{2}\left[\Theta(\eta_2) - \Theta(\eta_1)\right] \,.
\end{aligned}
\tag{3.135}
$$

Assumed $\theta(\eta_{\mathrm{rec}}) = 0$ we are interested to the time dependent rotation angle:

$$\theta(\eta) = \frac{1}{2}\left[\Theta(\eta) - \Theta(\eta_{\mathrm{rec}})\right] \,. \tag{3.136}$$
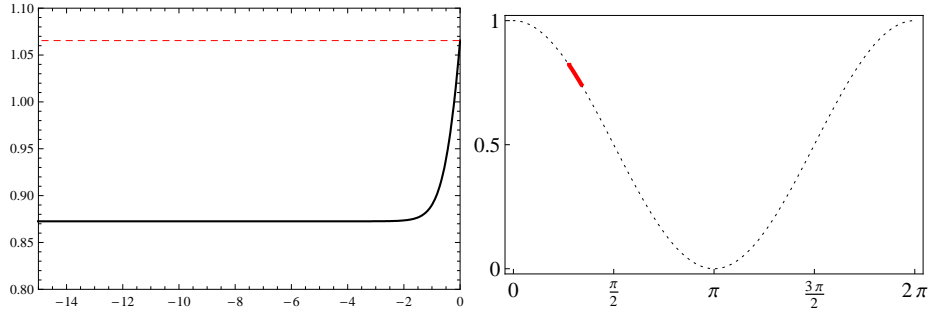
Figure 3.14: *Left side:* evolution of PNGB field ϕ/f in terms of the natural logarithm of the scale factor from $\log a \simeq -15$ to nowadays $\log a_0 = 0$. *Right side:* variation of PNGB field ϕ/f from radiation era to nowadays (see [92]), fixed $M = 8.8 \times 10^{-4}$ eV, $f = M_{\rm pl}/\sqrt{8\pi}$, $\Theta_i = 0.87$ and $\dot{\Theta}_i = 0$.

Fixed $M = 8.8 \times 10^{-4}$ eV, $f = M_{\rm pl}/\sqrt{8\pi}$, $\Theta_i = 0.87$ and $\dot{\Theta}_i = 0$ we use the following fit for the parameter w_ϕ of the equation of state:

$$w_\phi(\eta) = -1 + 5 \times 10^{-5} \exp\left[6.9\frac{\eta}{\eta_0}\right] . \qquad (3.137)$$

The linear polarization rotation angle is described by the function:

$$\theta(\eta) = 7 \times 10^{-5} \exp\left[7.4\frac{\eta}{\eta_0}\right] \text{ rad} . \qquad (3.138)$$

see Fig. 3.16. Using this expression we evaluate the linear polarization angular power spectra $E\,E$ (see Fig. 3.18a), $B\,B$ (see Fig. 3.18b), $T\,E$ (see Fig. 3.18c), $T\,B$ (see Figs. 3.18d), and $E\,B$ (see Figs. 3.18e).

Fixed $M = 8.5 \times 10^{-4}$ eV, $f = 0.3M_{\rm pl}/\sqrt{8\pi}$, $\Theta_i = 0.25$ and $\dot{\Theta}_i = 0$ we use the following fit for the parameter w_ϕ of the equation of state:

$$w_\phi(\eta) = -1 + 6 \times 10^{-8} \exp\left[16\frac{\eta}{\eta_0}\right] . \qquad (3.139)$$

The linear polarization rotation angle is described by the function:

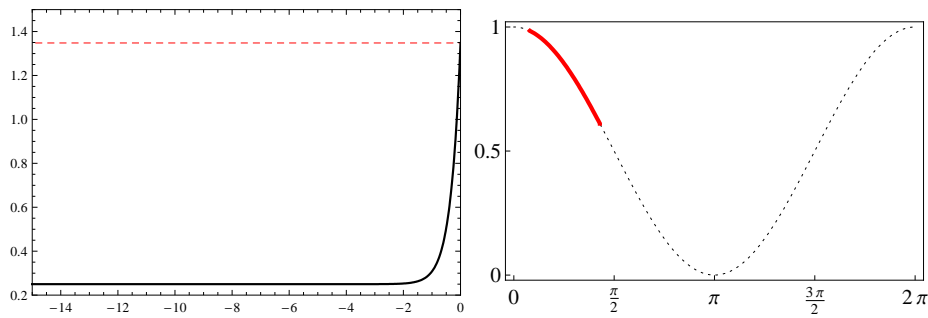$$\theta(\eta) = 2 \times 10^{-4} \exp\left[9.3\frac{\eta}{\eta_0}\right] \text{ rad} . \qquad (3.140)$$

Figure 3.15: *Left side:* evolution of PNGB field ϕ/f in terms of the natural logarithm of the scale factor from $\log a \simeq -15$ to nowadays $\log a_0 = 0$. *Right side:* variation of PNGB field ϕ/f from radiation era to nowadays (see [92]), fixed $M = 8.5 \times 10^{-4}$ eV, $f = 0.3 M_{\mathrm{pl}}/\sqrt{8\pi}$, $\Theta_i = 0.25$ and $\dot{\Theta}_i = 0$.

see Fig. 3.17. Using this expression we evaluate the linear polarization angular power spectra $E\,E$ (see Fig. 3.19a), $B\,B$ (see Fig. 3.19b), $T\,E$ (see Fig. 3.19c), $T\,B$ (see Figs. 3.19d), and $E\,B$ (see Figs. 3.19e).

In this case of a pseudoscalar field acting as dark enrergy ϕ becomes dynamical only very recently, so there is a big difference in considering a dynamical or a constant rotation angle. Power spectra modifications can be easily overestimated if the rotation of linear polarization is simply described by a time independent rotation angle. Howerver, at least in some cases (e.g. $M = 8.5 \times 10^{-4}$ eV, $f = 0.3 M_{\mathrm{pl}}/\sqrt{8\pi}$, $\Theta_i = 0.25$ and $\dot{\Theta}_i = 0$), power spectra modifications are almost of the same order of current constraints (see Fig. 3.20 for $T\,B$ and $E\,B$ power spectra).

Complementary constraints on dark energy models can be obtained looking at behavior of perturbations. Besides the background evolution such dark energy perturbations are therefore a key point to distinguish the cosmological constant Λ from others dark energy models [116]. We define the
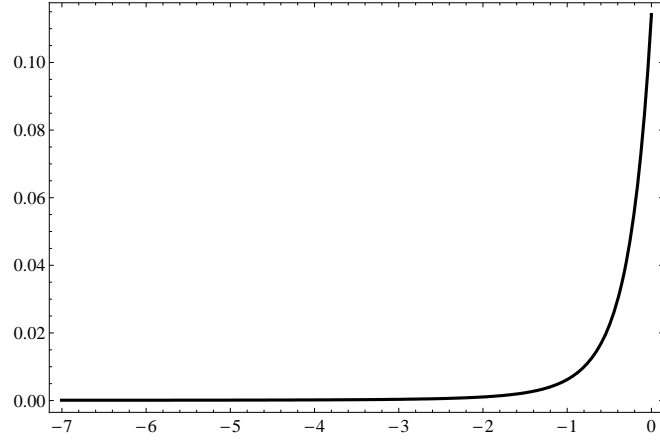
Figure 3.16: Evolution of the linear polarization rotation angle $\theta(\eta)$ for a ultralight pseudo Nambu-Goldstone boson acting as dark energy, in terms of the natural logarithm of the scale factor (from $\log a = -7$ to nowadays $\log a_0 = 0$) in a ΛCDM model with $\Omega_{\mathrm{MAT}} = 0.3$. Fixed $M = 8.8 \times 10^{-4}$ eV, $f = M_{\mathrm{pl}}/\sqrt{8\pi}$, $\Theta_i = 0.87$ and $\dot{\Theta}_i = 0$.
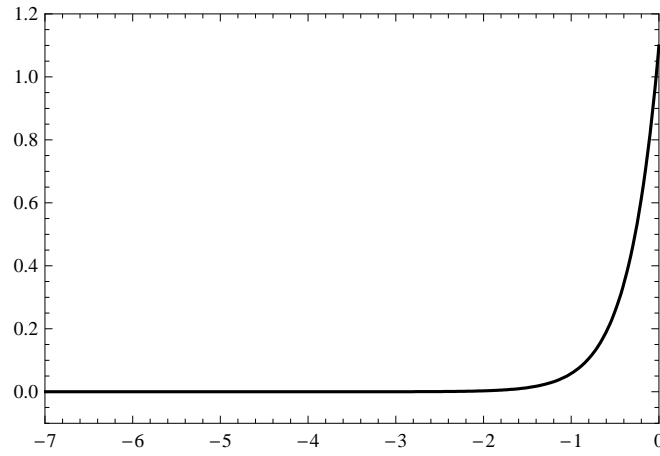

Figure 3.17: Evolution of the linear polarization rotation angle $\theta(\eta)$ for a ultralight pseudo Nambu-Goldstone boson acting as dark energy, in terms of the natural logarithm of the scale factor (from $\log a = -7$ to nowadays $\log a_0 = 0$) in a ΛCDM model with $\Omega_{\mathrm{MAT}} = 0.3$. Fixed $M = 8.5 \times 10^{-4}$ eV, $f = 0.3 M_{\mathrm{pl}}/\sqrt{8\pi}$, $\Theta_i = 0.25$ and $\dot{\Theta}_i = 0$.

pressure/density ratio, the density perturbation and velocity potential as:

$$w_\phi \equiv \frac{p_\phi}{\rho_\phi} = \frac{\frac{\dot{\phi}^2}{2} - V(\phi)}{\frac{\dot{\phi}^2}{2} + V(\phi)}, \tag{3.141}$$

$$\delta_\phi \equiv \frac{\delta\rho_\phi}{\rho_\phi} = \frac{\dot{\phi}\delta\dot{\phi} + V_{,\phi}\delta\phi}{\frac{\dot{\phi}^2}{2} + V(\phi)}, \tag{3.142}$$

$$\theta_\phi \equiv \frac{k^2\delta\phi}{a\dot{\phi}}. \tag{3.143}$$

In order to evolve dark energy perturbations it is necessary to specify also pressure perturbations [117]:

$$\begin{aligned}
\delta p_\phi &= c_\phi^2 \delta\rho_\phi + 3H(1+w_\phi)\frac{\theta_\phi\rho_\phi}{k^2}\left(c_\phi^2 - \frac{\dot{p}_\phi}{\dot{\rho}_\phi}\right) \\
&= c_\phi^2 \delta\rho_\phi + 3H(1+w_\phi)\frac{\theta_\phi\rho_\phi}{k^2}\left[c_\phi^2 - w_\phi + \frac{\dot{w}_\phi}{3H(1+w_\phi)}\right], \tag{3.144}
\end{aligned}$$

where we have used $\dot{\rho}_\phi = -3H\rho_\phi(1+w_\phi)$.

The equations for the evolution of perturbations in the synchronous gauge (see section 1.5) are [25]:

$$\begin{aligned}
\dot{\delta}_\phi &= -\frac{\dot{h}}{2}(1+w_\phi) - \frac{\theta_\phi}{a}(1+w_\phi) - 3H(c_\phi^2 - w)\delta_\phi \\
&\quad -9H^2(1+w_\phi)\frac{\theta_\phi}{k^2}\left[c_\phi^2 - w + \frac{\dot{w}_\phi}{3H(1+w_\phi)}\right], \tag{3.145}
\end{aligned}$$

$$\dot{\theta}_\phi = -H(1-3c_\phi^2)\theta_\phi + \frac{k^2}{1+w_\phi}\frac{c_\phi^2}{a}\delta_\phi. \tag{3.146}$$

used $\frac{\delta p_\phi}{\delta\rho_\phi}\delta_\phi = \frac{\delta p_\phi}{\rho_\phi}$; in terms of derivative respect to conformal time η:

$$\begin{aligned}
\delta'_\phi &= -\frac{h'}{2}(1+w_\phi) - \theta_\phi(1+w_\phi) - 3\mathcal{H}(c_\phi^2 - w)\delta_\phi \\
&\quad -9\mathcal{H}^2(1+w_\phi)\frac{\theta_\phi}{k^2}\left[c_\phi^2 - w_\phi + \frac{w'_\phi}{3\mathcal{H}(1+w_\phi)}\right], \tag{3.147}
\end{aligned}$$

$$\theta'_\phi = -\mathcal{H}(1-3c_\phi^2)\theta_\phi + \frac{k^2}{1+w_\phi}c_\phi^2\delta_\phi. \tag{3.148}$$

In the modified Boltzmann code it is necessary to insert the correct initial conditions for perturbations. In Fig. 3.12 we see that the parameter w_ϕ

departs from -1 (cosmological constant case) at low z, we obtain an over-estimate of the effect of dark energy perturbations considering $w_\phi = w_0$. In this case the equations for evolution of perturbations are:

$$\delta'_\phi = -(1 + w_\phi)\left(\frac{h'}{2} + \theta_\phi\right) - 3\mathcal{H}(c_\phi^2 - w)\delta_\phi$$

$$-9\mathcal{H}^2(1 + w_\phi)\frac{\theta_\phi}{k^2}\left(c_\phi^2 - w_\phi\right) , \tag{3.149}$$

$$\theta'_\phi = -\mathcal{H}(1 - 3c_\phi^2)\theta_\phi + \frac{k^2}{1 + w_\phi}c_\phi^2\delta_\phi . \tag{3.150}$$

Expanding the perturbations in power series of $k\eta$:

$$\delta_\phi = A\,(k\eta)^2 , \tag{3.151}$$

$$\theta_\phi = B\,(k\eta)^3 , \tag{3.152}$$

$$h = C\,(k\eta)^2 , \tag{3.153}$$

and remembering that in radiation dominated universe $\mathcal{H} = \eta^{-1}$, Eq. (3.149) becomes:

$$3Bk^3\eta^2 = -(1 - 3c_\phi^2)Bk^3\eta^2 + \frac{c_\phi^2 k^2}{1 + w_\phi}A\,(k\eta)^2 , \tag{3.154}$$

therefore:

$$B = \frac{Ac_\phi^2 k}{(1 + w_\phi)(4 - 3c_\phi^2)} . \tag{3.155}$$

Inserting these relations in Eq. (3.150) we obtain:

$$A = -\frac{C(1 + w_\phi)(4 - 3c_\phi^2)}{8 + 6c_\phi^2 - 12w_\phi} . \tag{3.156}$$

The initial conditions for dark energy perturbations used in the modified Boltzmann code are:

$$\delta_\phi = -\frac{C(1 + w_\phi)(4 - 3c_\phi^2)}{8 + 6c_\phi^2 - 12w_\phi}C\,(k\eta)^2 , \tag{3.157}$$

$$\theta_\phi = -\frac{c_\phi^2}{8 + 6c_\phi^2 - 12w_\phi}Ck^4\eta^3 , \tag{3.158}$$

where C is related to initial conditions for the synchronous gauge [25].

3.6 Comparison with constant rotation angle approximation

In this section we compare the angular power spectra obtained modifying the public code CAMB [4] considering the correct dynamic of the pseudoscalar field ($\theta = \theta(\eta)$) as described in section 1.5, with the ones obtained in the constant rotation angle approximation ($\theta = $ const) for the three different potential considered in the previous sections:

- oscillating behavior: Figs. 3.21 and 3.22;

- monotonic behavior: Figs. 3.23 and 3.24;

- ultralight pseudo Nambu-Goldstone bosons acting as dark energy: Fig. 3.25 and 3.26.

In section 1.5 we have already shown how the power spectra in the constant rotation angle approximation [Eqs. (1.72)-(1.76)] can be obtained from the general expressions [Eqs. (1.65)-(1.69)].

Power spectrum modifications obtained starting directly form the Boltzmann equations and taking into account the temporal evolution of the pseudoscalar field are usually smaller than effects predicted considering a constant rotation angle equal to the total rotation angle from last scattering to nowadays. If the cosmological pseudoscalar field evolves quickly, then the constant rotation angle approximation clearly leads to an overestimate of the effects.

It is important to stress that the constant rotation angle approximation is clearly an operative approximation. The additional term in the Boltzmann equations concerning a physical mechanism rotating the linear polarization plane is (see Eq. 1.54):

$$\mp i2\theta'(\eta)\Delta_{Q\pm iU}(k,\eta)\,. \tag{3.159}$$

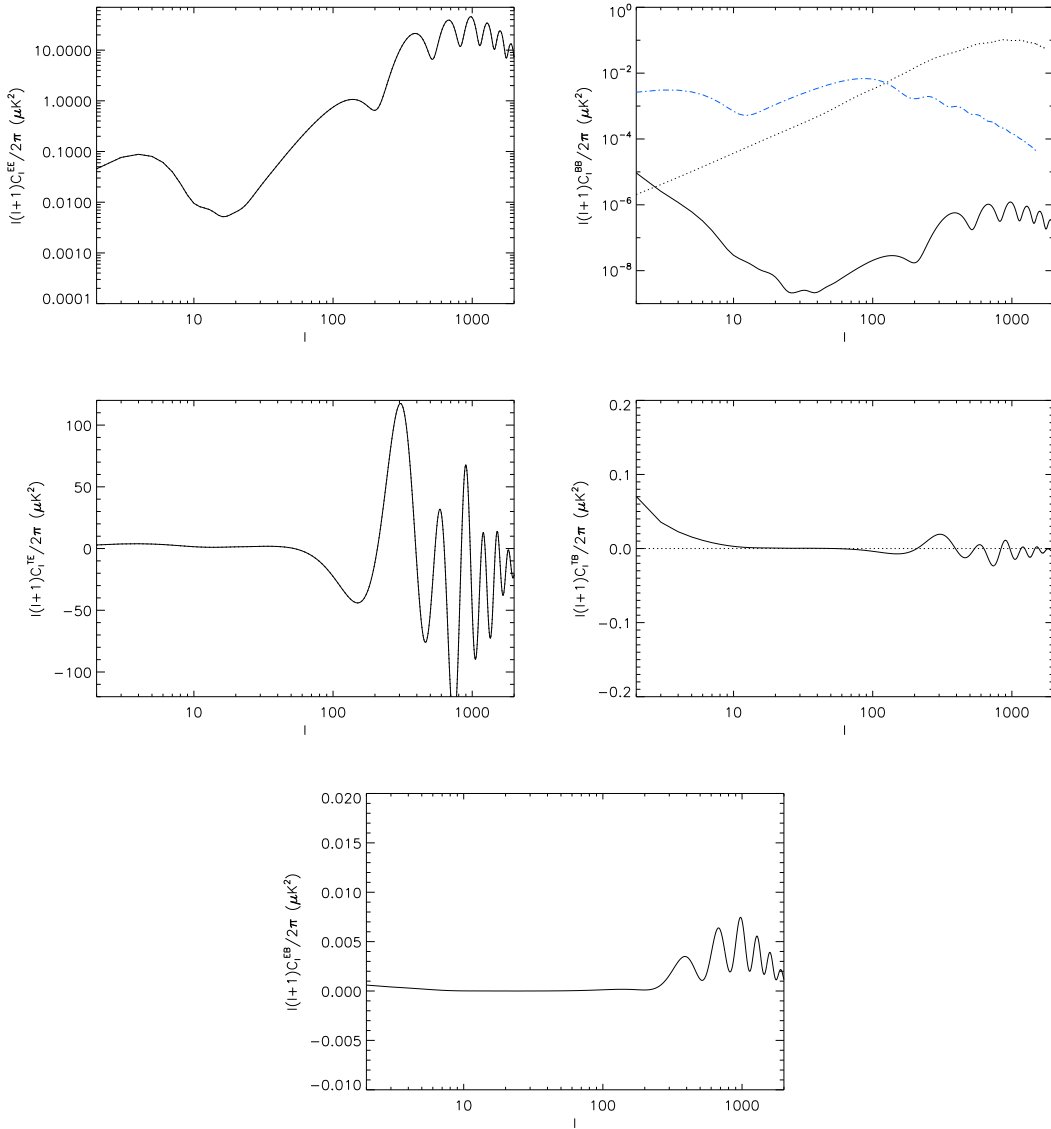therefore for $\theta = $ const the new term vanishes.

Figure 3.18: Ultralight pseudo Nambu-Goldstone bosons case fixed $M = 8.8 \times 10^{-4}$ eV, $f = M_{\mathrm{pl}}/\sqrt{8\pi}$, $\Theta_i = 0.87$ and $\dot{\Theta}_i = 0$. EE (a), BB (b), TE (c), TB (d) and EB (e) angular power spectra (black solid line), approximating the rotation angle with the constant, and for $\theta = 0$ (black dotted line). For the BB power spectrum (b) we plot for comparison also the polarization signal induced by gravitational lensing (black dotted line), and BB signal induced by lensing (black dotted line). The cosmological parameters of the flat ΛCDM model used here are $\Omega_b\,h^2 = 0.022$, $\Omega_c\,h^2 = 0.123$, $\tau = 0.09$, $n_s = 1$, $A_s = 2.3 \times 10^{-9}$, $H_0 = 100\,h\,\mathrm{km\,s^{-1}\,Mpc^{-1}} = 72\,\mathrm{km\,s^{-1}\,Mpc^{-1}}$.
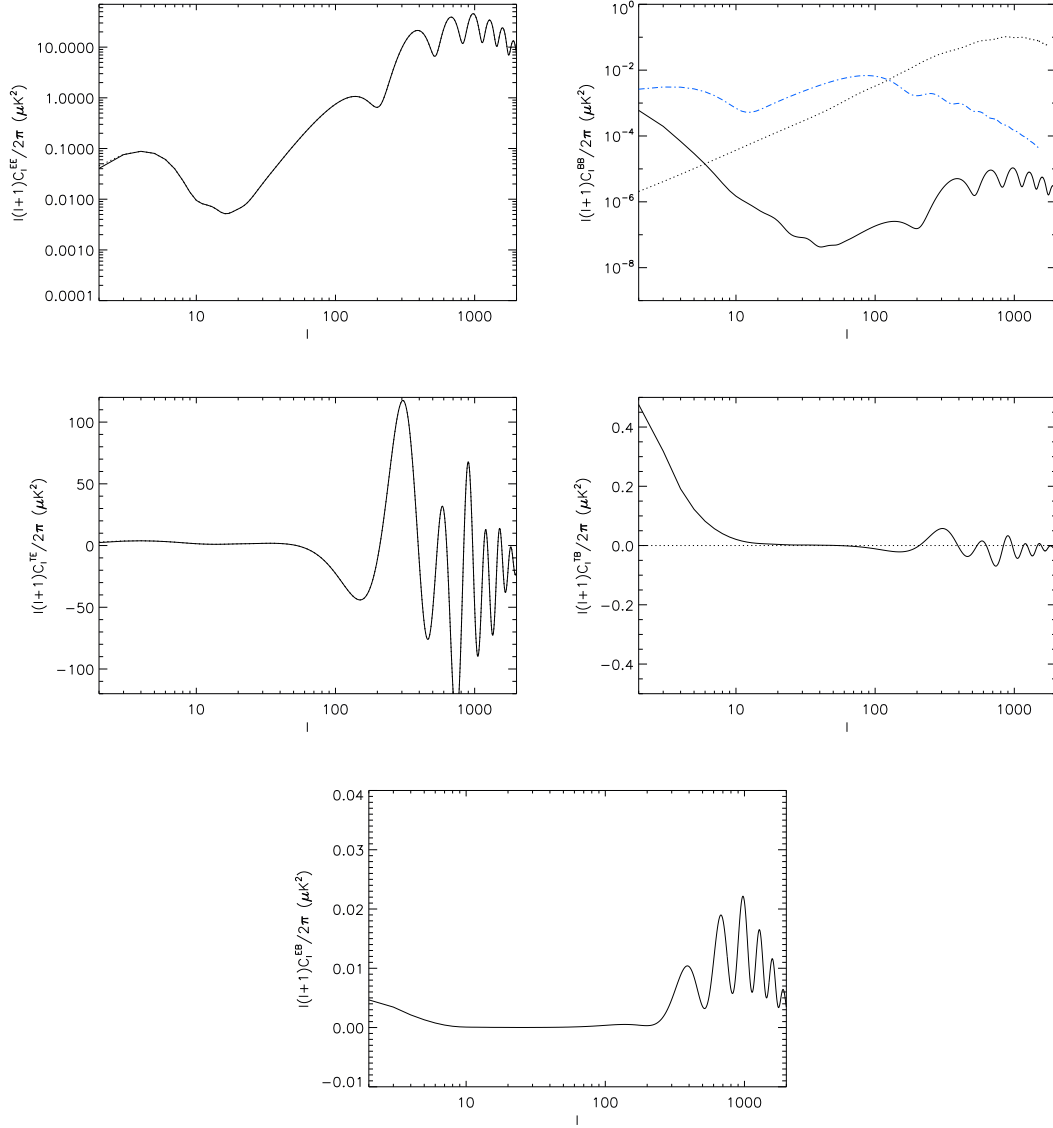
Figure 3.19: Ultralight pseudo Nambu-Goldstone bosons case fixed $M = 8.5 \times 10^{-4}$ eV, $f = 0.3 M_{\mathrm{pl}}/\sqrt{8\pi}$, $\Theta_i = 0.25$ and $\dot{\Theta}_i = 0$. EE (a), BB (b), TE (c), TB (d) and EB (e) angular power spectra (black solid line), approximating the rotation angle with the constant, and for $\theta = 0$ (black dotted line). For the BB power spectrum (b) we plot for comparison also the polarization signal induced by gravitational lensing (black dotted line), and BB signal induced by lensing (black dotted line). The cosmological parameters of the flat ΛCDM model used here are $\Omega_b h^2 = 0.022$, $\Omega_c h^2 = 0.123$, $\tau = 0.09$, $n_s = 1$, $A_s = 2.3 \times 10^{-9}$, $H_0 = 100\,h\,\mathrm{km\,s^{-1}\,Mpc^{-1}} = 72\,\mathrm{km\,s^{-1}\,Mpc^{-1}}$.
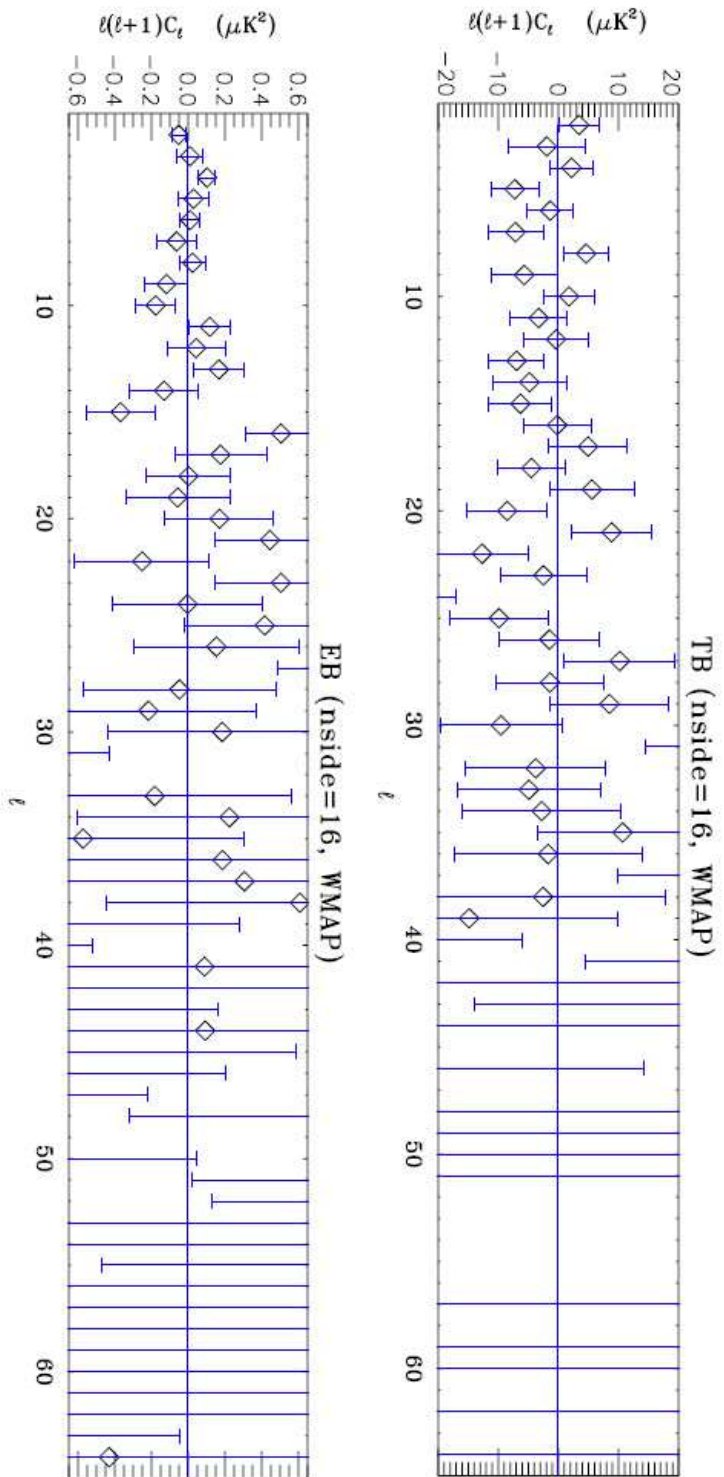
Figure 3.20: Estimates of angular power spectra TB and EB at large scales (low-ℓ) obtained by an optimal estimator (BolPol) using WMAP five years data sets. Private communication by Fabio Finelli and Alessandro Gruppuso.
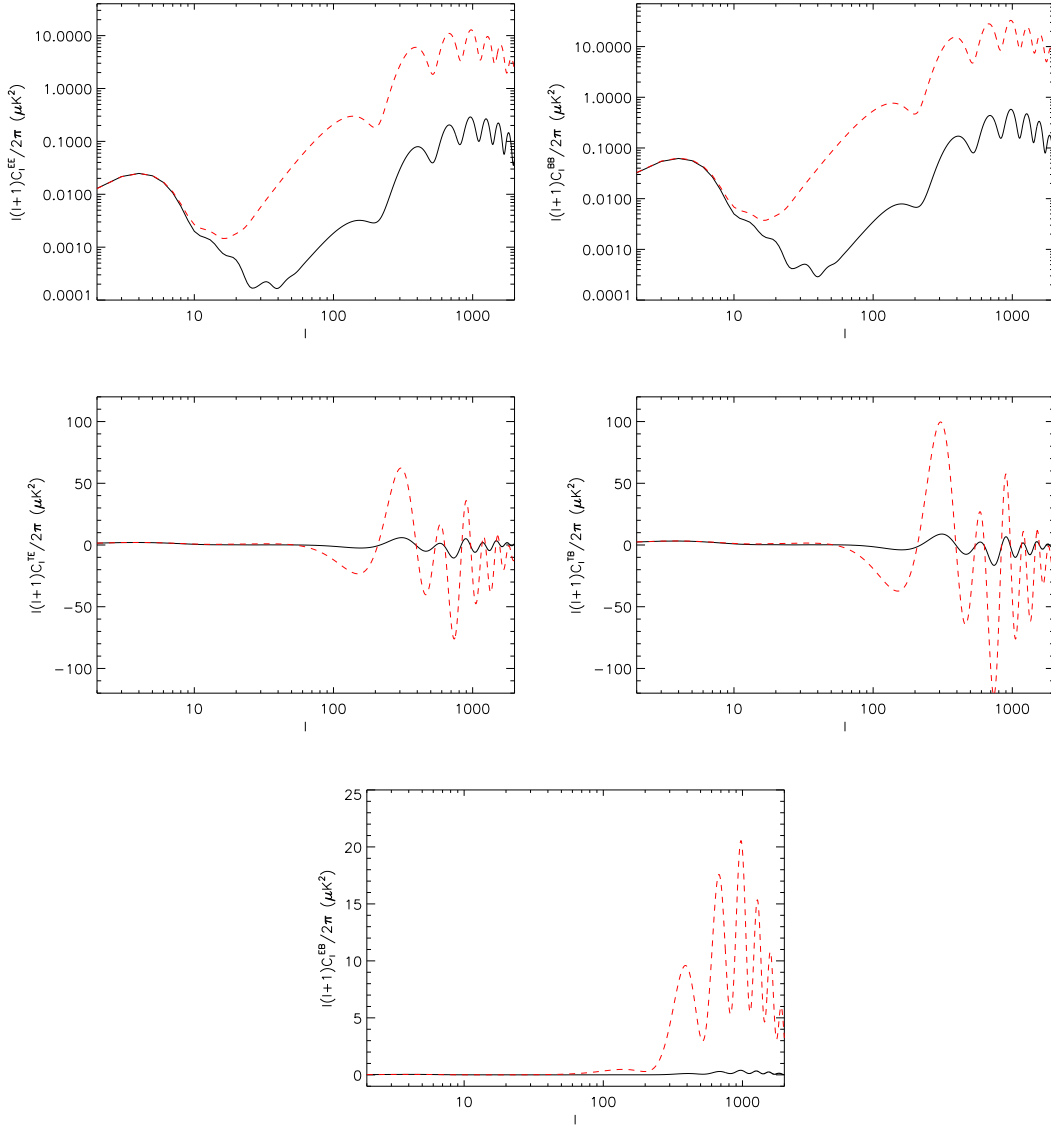
Figure 3.21: Cosine-type potential case. $E\,E$ (a), $B\,B$ (b), $T\,E$ (c), $T\,B$ (d) and $E\,B$ (e) angular power spectra for $m = 10^{-22}$ eV and $g_\phi = 5 \times 10^{-21}$ eV^{-1} (black solid line) and approximating the rotation angle with the constant value $\theta_{\rm rec}$ (red dashed line). The cosmological parameters of the flat ΛCDM model used here are $\Omega_b\, h^2 = 0.022$, $\Omega_c\, h^2 = 0.123$, $\tau = 0.09$, $n_s = 1$, $A_s = 2.3 \times 10^{-9}$, $H_0 = 100\, h\, {\rm km\, s}^{-1}\, {\rm Mpc}^{-1} = 72\, {\rm km\, s}^{-1}\, {\rm Mpc}^{-1}$.
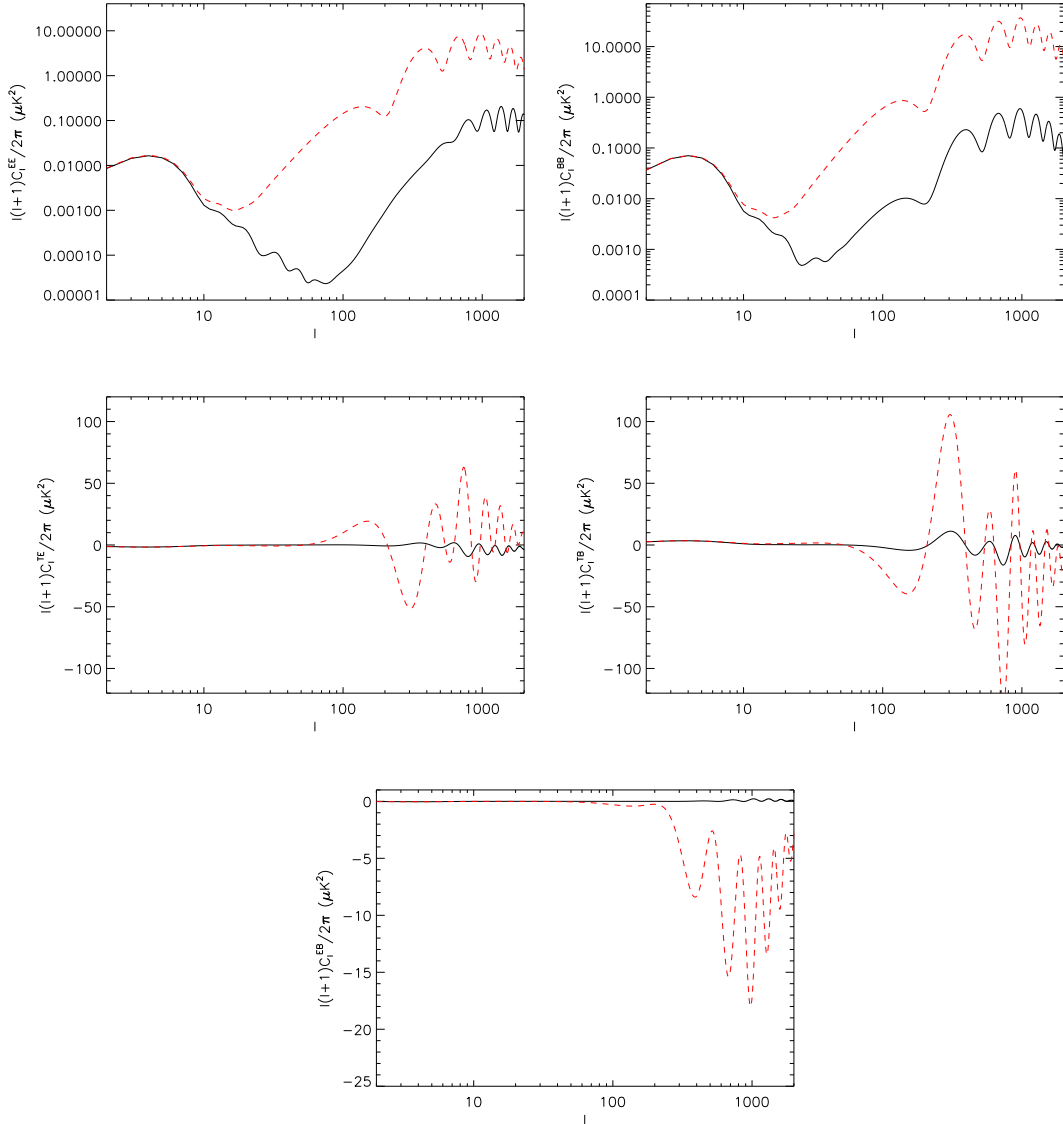
Figure 3.22: Cosine-type potential case. EE (a), BB (b), TE (c), TB (d) and EB (e) angular power spectra for $m = 10^{-22}$ eV and $g_\phi = 1 \times 10^{-20}$ eV^{-1} (black solid line) and approximating the rotation angle with the constant value θ_{rec} (red dashed line). The cosmological parameters of the flat ΛCDM model used here are $\Omega_b h^2 = 0.022$, $\Omega_c h^2 = 0.123$, $\tau = 0.09$, $n_s = 1$, $A_s = 2.3 \times 10^{-9}$, $H_0 = 100 h \, \mathrm{km \, s^{-1} \, Mpc^{-1}} = 72 \, \mathrm{km \, s^{-1} \, Mpc^{-1}}$.

Figure 3.23: Exponential potential case. EE (a), BB (b), TE (c), TB (d) and EB (e) angular power spectra for $g_\phi = 10^{-28}\,\mathrm{eV}^{-1}$ (black solid line) and approximating the rotation angle with the constant value θ_{rec} (red dashed line); the black dotted line is the standard case in which there is no coupling. The cosmological parameters of the flat CDM model used here are $\Omega_b = 0.0462$, $\Omega_c = 0.9538$ ($\Omega_\phi \simeq 0.148$), $\tau = 0.09$, $n_s = 1$, $A_s = 2.3 \times 10^{-9}$, $H_0 = 72\,\mathrm{km\,s^{-1}\,Mpc^{-1}}$.
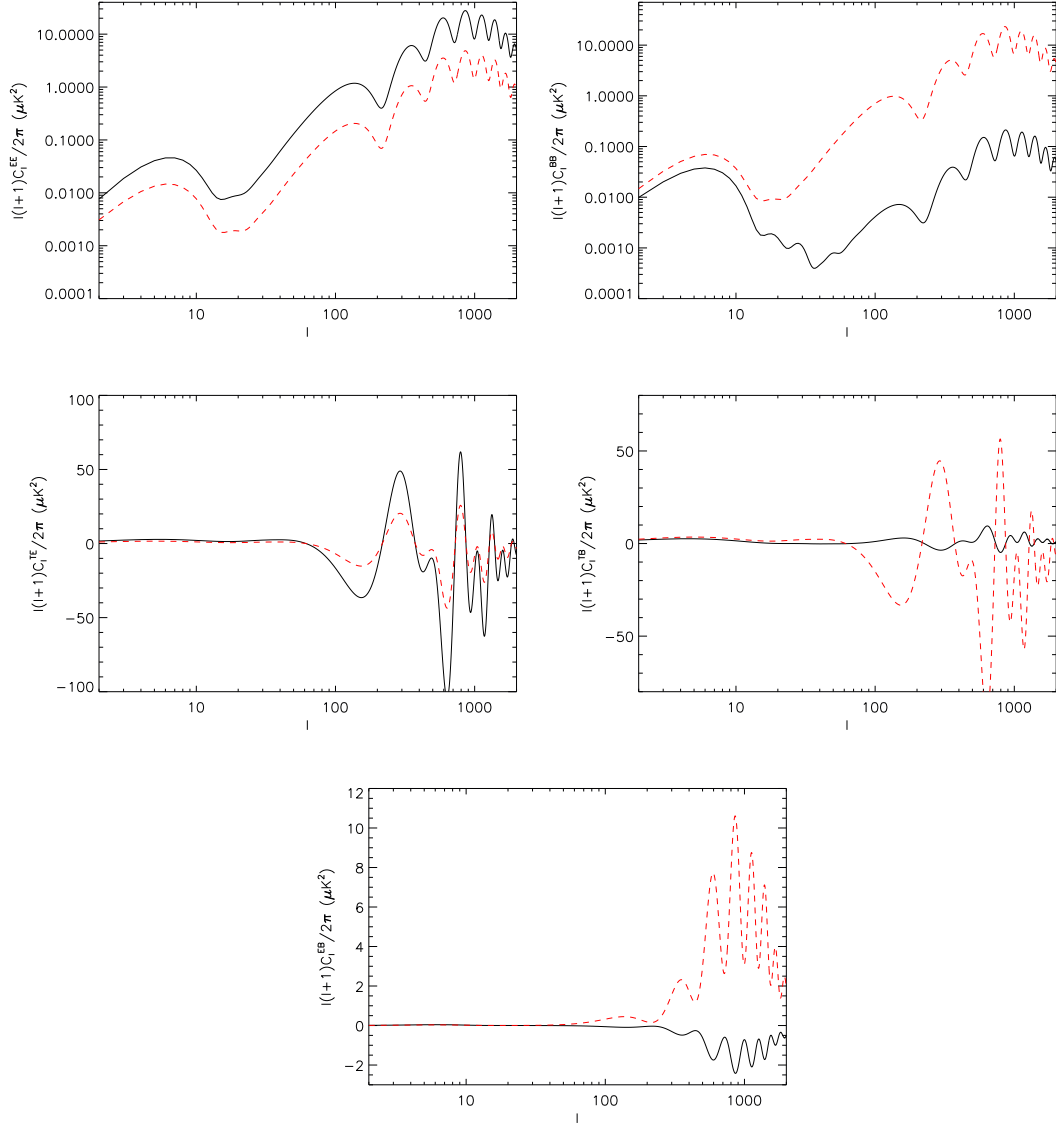
Figure 3.24: Exponential potential case. EE (a), BB (b), TE (c), TB (d) and EB (e) angular power spectra for $g_\phi = 2 \times 10^{-28}\,\text{eV}^{-1}$ (black solid line) and approximating the rotation angle with the constant value θ_{rec} (red dashed line); the black dotted line is the standard case in which there is no coupling. The cosmological parameters of the flat CDM model used here are $\Omega_b = 0.0462$, $\Omega_c = 0.9538$ ($\Omega_\phi \simeq 0.148$), $\tau = 0.09$, $n_s = 1$, $A_s = 2.3 \times 10^{-9}$, $H_0 = 72\,\text{km}\,\text{s}^{-1}\,\text{Mpc}^{-1}$.
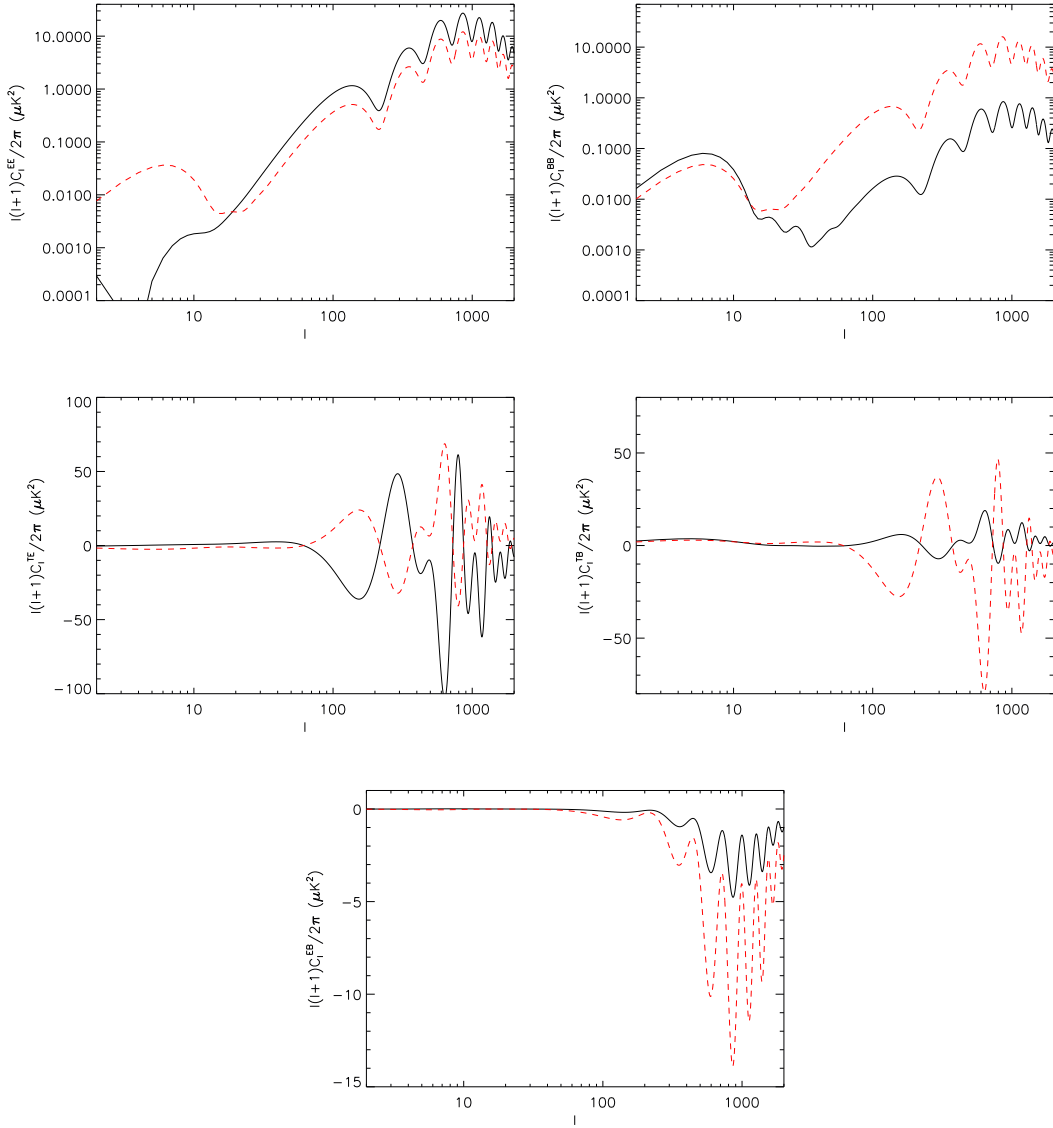
Figure 3.25: Ultralight pseudo Nambu-Goldstone bosons case fixed $M = 8.8 \times 10^{-4}$ eV, $f = M_{\mathrm{pl}}/\sqrt{8\pi}$, $\Theta_i = 0.87$ and $\dot{\Theta}_i = 0$. EE (a), BB (b), TE (c), TB (d) and EB (e) angular power spectra (black solid line), approximating the rotation angle with the constant value θ_{rec} (red dashed line). The cosmological parameters of the flat ΛCDM model used here are $\Omega_b h^2 = 0.022$, $\Omega_c h^2 = 0.123$, $\tau = 0.09$, $n_s = 1$, $A_s = 2.3 \times 10^{-9}$, $H_0 = 100\,h\,\mathrm{km\,s^{-1}\,Mpc^{-1}} = 72\,\mathrm{km\,s^{-1}\,Mpc^{-1}}$.
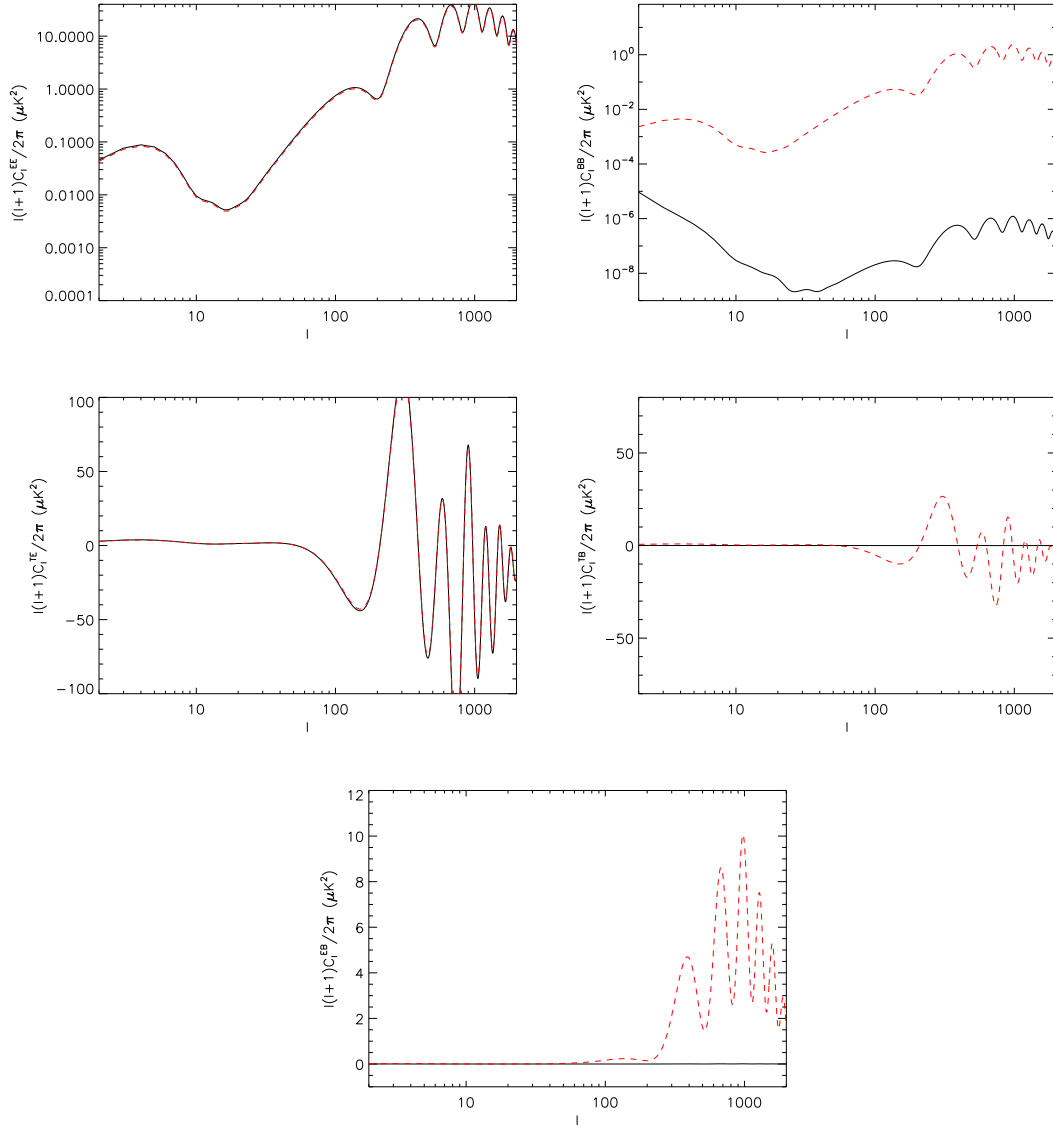
Figure 3.26: Ultralight pseudo Nambu-Goldstone bosons case fixed $M = 8.5 \times 10^{-4}$ eV, $f = 0.3 M_{\mathrm{pl}}/\sqrt{8\pi}$, $\Theta_i = 0.25$ and $\dot{\Theta}_i = 0$. EE (a), BB (b), TE (c), TB (d) and EB (e) angular power spectra (black solid line), approximating the rotation angle with the constant value θ_{rec} (red dashed line). The cosmological parameters of the flat ΛCDM model used here are $\Omega_b h^2 = 0.022$, $\Omega_c h^2 = 0.123$, $\tau = 0.09$, $n_s = 1$, $A_s = 2.3 \times 10^{-9}$, $H_0 = 100 h \, \mathrm{km \, s^{-1} \, Mpc^{-1}} = 72 \, \mathrm{km \, s^{-1} \, Mpc^{-1}}$.

Chapter 4

Ultrahigh-energy cosmic rays

Up to now we mainly focused on Standard Model extensions that can be tested at small energies, in particular photon coupling with pseudoscalar particles. Other extensions predict effects visible mainly at high energy. In this second part of the thesis we consider ultrahigh-energy cosmic rays and quantum gravity inspired modifications of the QED dispersion relations.

4.1 Introduction

Cosmic rays are observed today in an energy range extending over almost twelve decades in energy (from hundreds of MeV to 10^{20} eV) and more than thirty orders of magnitude in flux [118, 119].

At low energies the energy spectrum (Fig. 4.1) changes with variations in solar activity, while it behaves as a power-law at energies above GeV: $\propto E^{-\gamma}$ with $\gamma \sim 2.7$. At energy $E \sim 4 \times 10^{15}$ eV a "knee" is observed in the spectrum, which becomes steeper: the power law index γ increases from 2.7 to 3.0. The slope changes again at the so called "ankle" ($E \sim 5 \times 10^{18}$ eV) where the spectrum flatten again to a power law index $\gamma \sim 2.8$.

Here we are interested in particular in ultrahigh-energy cosmic rays, particles with energy higher than EeV $\equiv 10^{18}$ eV.

In the conventional "bottom-up" scenario all high energy particles are
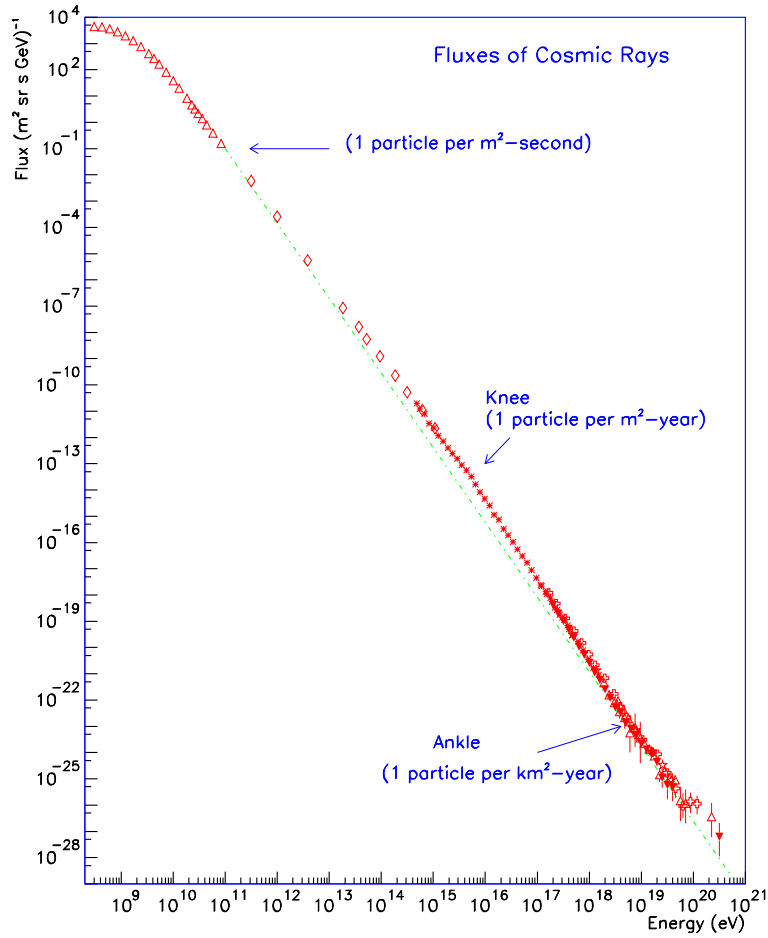
Figure 4.1: Cosmic rays energy spectrum. Figure taken from [119].

accelerated in astrophysical environments, typically in a magnetized astrophysical shock wave. In order to be accelerated particles has to be confined in accelerators, so the maximal attainable energy is given by the requirement that the gyroradius r_g of a particle of energy E, momentum p, and charge eZ is smaller than the size R of the magnetized region:

$$r_g \equiv \frac{p}{ezB} < R\,, \tag{4.1}$$

where B is the component of the magnetic field perpendicular to the motion of the particle. For ultra-relativistic particles $E \simeq p$, so the following upper

limit on attainable energy is obtained [120]:

$$E < 10^{18} \, Z \left(\frac{R}{\text{kpc}} \right) \left(\frac{B}{\mu\text{G}} \right) \text{eV} \,. \tag{4.2}$$

Note that this is only an upper limit since we are neglecting the finite life time of the accelerator and energy loss processes (synchrotron radiation, production of secondary particles, ...).

Anyway at ultrahigh-energies even more powerful acceleration processes than shock acceleration seem to be needed, and the explanation of the production mechanism for these events draws a lot of theoretical interest.

4.2 Propagation and interactions

In this section main concepts concerning cosmic rays propagation are summarized following Ref. [118, 119].

We consider the propagation of a cosmic ray of energy E, momentum $\boldsymbol{p}$, and mass m through a background of particles of energy ε, momentum $\boldsymbol{p_b}$, and mass m_b. The squared center of mass energy is:

$$\begin{aligned} s &= (E + \varepsilon)^2 - (\boldsymbol{p} + \boldsymbol{p_b})^2 \\ &= m^2 + m_b^2 + 2E\epsilon \left(1 - \mu\beta\beta_b \right) \,, \end{aligned} \tag{4.3}$$

where μ is the cosine of the angle between $\boldsymbol{p}$ and $\boldsymbol{p_b}$, $\beta^2 \equiv 1 - m^2/E^2$, and $\beta_b^2 \equiv 1 - m_b^2/\varepsilon^2$.

The energy loss of the cosmic rays can be described through the *interaction length* $l(E)$:

$$\frac{1}{l(E)} \equiv \int d\varepsilon \, n_b(\varepsilon) \int_{-1}^{1} d\mu \frac{1 - \mu\beta\beta_b}{2} \sigma(s) \,, \tag{4.4}$$

or through the *energy attenuation length* $l_E(E)$:

$$\frac{1}{l_E(E)} \equiv \int d\varepsilon \, n_b(\varepsilon) \int_{-1}^{1} d\mu \frac{1 - \mu\beta\beta_b}{2} \sigma(s)\eta(s) \,, \tag{4.5}$$

where $n_b(\varepsilon)$ is the number density of background particles per unit energy at energy ε, $\sigma(s)$ is the cross section of the particular interaction considered

between cosmic ray and background particle, and $\eta(s)$ is the fraction of the cosmic ray energy transfered to the recoiling final state particle of interest (inelasticity):

$$\eta(E) = 1 - \frac{1}{\sigma(s)} \int dE' E' \frac{d\sigma}{dE'}(E', s) \,, \tag{4.6}$$

E' is the energy of the recoiling particle in units of the incoming cosmic ray energy E.

If deflections from linear propagation are negligible (small deflection angles) the evolution of the number densities for a set of species $n_i(E)$, for an isotropic background distribution, are given by one dimensional Boltzmann equations (*transport equation*):

$$
\begin{aligned}
\frac{\partial n_i(E)}{\partial t} = {}& \Phi_i(E) \\
& - n_i(E) \int d\varepsilon\, n_{\rm b}(\varepsilon) \int_{-1}^{1} d\mu \frac{1 - \mu\beta_{\rm b}\beta}{2} \sum_j \sigma_{i \to j}\left(s = E\varepsilon(1 - \mu\beta_{\rm b}\beta_i)\right) \\
& + \int dE' \int d\varepsilon\, n_{\rm b}(\varepsilon) \int_{-1}^{1} d\mu \sum_j \frac{1 - \mu\beta_{\rm b}\beta_j}{2} n_j(E') \frac{d\sigma_{j \to i}}{dE}\left(s = E\varepsilon(1 - \mu\beta_{\rm b}\beta_j), E\right) \,,
\end{aligned}
\tag{4.7}
$$

where $\Phi_i(E)$ is the injection spectrum.

Assuming a continuous energy loss rate $b(E) \equiv \frac{dE}{dt} = \frac{E}{l_E(E)}$ the density of the leading particle is given by the *diffusion equation*:

$$\frac{\partial n(E)}{\partial t} = \phi(E) - \frac{\partial}{\partial E}\left[b(E)n(E)\right] \,. \tag{4.8}$$

The differential flux today at energy E is:

$$j(E) = \frac{1}{4\pi} \int_0^{t_0} dt' \frac{1}{(1+z)^3} \frac{dE_i(E, z)}{dE} \Phi\left(E_i\left(E, z\right), z\right) \,, \tag{4.9}$$

where $E_i\left(E, z\right)$ is the particle energy at injection redshift z in the continuous energy loss approximation when it reaches us with energy E:

$$E_i(E, z) = E + \int_{t_0}^{t_i} b(E) dt \,. \tag{4.10}$$

In terms of redshift z the Hubble parameter is defined as $H = (z+1)^{-1}\frac{dz}{dt}$, so:

$$dt = \frac{dz}{(1+z)H(z)} = \frac{dz}{(1+z)H_0 \left[\Omega_{\text{MAT}}(1+z)^3 + \Omega_{\text{RAD}}(1+z)^4 + \Omega_\Lambda\right]^{1/2}}, \tag{4.11}$$

where we have used the Friedmann equation for a spatially flat universe with matter energy density parameter Ω_{MAT}, radiation energy density parameter Ω_{RAD} and cosmological constant energy density parameter Ω_Λ. So, using the relation between cosmic time and redshift given in Eq. (4.11), the expressions for the differential flux and for the energy at injection redshift become:

$$j(E) = \frac{1}{4\pi}\int_0^\infty dz \frac{1}{(1+z)^4 H}\frac{dE_i(E,z)}{dE}\Phi\left(E_i\left(E,z\right),z\right), \tag{4.12}$$

$$E_i\left(E,z\right) - E = \int_0^z |b(E)|\frac{dt}{dz}dz. \tag{4.13}$$

If $l_E(E)$ is much smaller than the horizon size, then the redshift and evolution effects can be ignored, for an homogeneous production spectrum $\Phi(E)$, the differential flux is:

$$j(E) \simeq \Phi(E)l_E(E). \tag{4.14}$$

4.2.1 Nucleons and nuclei

The energy loss of ultrahigh energy nucleons and nuclei during propagation is mainly due to collision with photons of background radiation.

In 1966, soon after the discovery of the Cosmic Microwave Background, K. Greisen [121], G. T. Zatsepin V. A. Kuzmin [122] studied the effect of this low energy photon background on propagation of UHECR. When a nucleons with energy E, momentum $\boldsymbol{p}$ and mass m propagates though a background of low energy photons with energy ε and momentum $\boldsymbol{\omega}$ photo-pion production ($N\,\gamma_{\text{b}} \to N'\,\pi$) is kinematically possible if:

$$
\begin{aligned}
s &\geq (m_{\text{N}'} + m_\pi)^2 \\
(E+\varepsilon)^2 - (\boldsymbol{p}+\boldsymbol{\omega})^2 &\geq (m_{\text{N}'} + m_\pi)^2 \\
m_{\text{N}}^2 + 2E\varepsilon\left(1-\mu\right) &\geq (m_{\text{N}'} + m_\pi)^2.
\end{aligned}
$$

For an head on collision of the initial particles $\mu = \cos \pi = -1$, the threshold energy for the reaction $N \gamma_{\mathrm{b}} \to N \pi_0$ is:

$$E \simeq \frac{2 m_{\mathrm{N}} m_\pi + m_\pi^2}{4 \varepsilon} \simeq 7 \times 10^{19} \left(\frac{10^{-3}\,\mathrm{eV}}{\varepsilon} \right) \mathrm{eV} \,. \qquad (4.15)$$

Above this energy the nucleons interaction length quickly drops below 10 Mpc decreasing of more than two orders in magnitude compared to lower energies (Greisen-Zatsepin-Kuzmin cutoff). Assuming a photo-pion production cross section of the order $\sigma_{N\gamma} \sim 100\,\mu\mathrm{b}$ and $n_{\mathrm{CMB}} \sim 410\,\mathrm{cm}^{-3}$ for the the density of CMB photons, a rough estimate of the interaction length is: $l_{\mathrm{GZK}} \sim (\sigma_{N\gamma} n_{\mathrm{CMB}})^{-1} \sim 2 \times 10^{25}\,\mathrm{cm} = 8\,\mathrm{Mpc}\,.$

The decay of neutral pions into photons is the main sources of UHE photons in more conventional cosmic rays models. Other more exotic non-acceleration models predict a certain flux of UHE photons due for example to annihilation of primordial relics or super heavy dark matter. Instead charged pions decay contributes to the neutrino's flux.

At lower energies the main energy loss process is pair production by protons ($p \gamma_{\mathrm{b}} \to p\, e^+ e^-$) with a kinematic threshold of:

$$E \simeq \frac{m_{\mathrm{e}}(m_{\mathrm{p}} + m_{\mathrm{e}})}{\varepsilon} \simeq 5 \times 10^{17} \left(\frac{10^{-3}\,\mathrm{eV}}{\varepsilon} \right) \mathrm{eV} \,. \qquad (4.16)$$

Propagation of neutrons below 10^{20} eV is strongly limited by $\beta-$decay ($n \to p\, e^- \bar{\nu}_e$); the neutron range of propagation R_n is of the order of:

$$R_n = \frac{\tau_n E}{m_n} \simeq 0.9 \left(\frac{E}{10^{20}\,\mathrm{eV}} \right) \mathrm{Mpc} \,. \qquad (4.17)$$

The main energy losses processes for ultrahigh energy nucleons are photo-disintegration in the interaction with low energy photons with a interaction length of the orders of 10 Mpc ($A + \gamma_{\mathrm{b}} \to A' A''$) and the same energy loss process of nucleons, e.g. electron-positron pair production ($Z + \gamma_{\mathrm{b}} \to Z\, e^+ e^-$).

4.2.2 Photons and electrons

Also in the electromagnetic sector the main energy loss mechanism is due to interaction with low energy background photons, the leading processes are:

1. pair production ($\gamma \, \gamma_{\rm b} \rightarrow e^+ \, e^-$);

2. inverse Compton scattering ($e^\pm \, \gamma_{\rm b} \rightarrow e^\pm \, \gamma$);

3. synchrotron radiation.

The kinematic threshold for **pair production** is:

$$
\begin{aligned}
s &\geq (2m_{\rm e})^2 \\
2E\varepsilon(1-\mu) &\geq 4m_{\rm e}^2 \, ,
\end{aligned}
\tag{4.18}
$$

so, for an head on collision ($\mu = -1$):

$$
E \geq \frac{m_{\rm e}^2}{\varepsilon} \simeq 2.6 \times 10^{14} \left(\frac{10^{-3}\,{\rm eV}}{\varepsilon} \right) \, {\rm eV} \, .
\tag{4.19}
$$

The total cross section evaluated from QED is well known and is given by (e.g. see [123]):

$$
\sigma_{\rm PP} = \frac{3}{16}\sigma_T \left(1 - \beta^2\right) \left[\left(3 - \beta^4\right) \ln \frac{1+\beta}{1-\beta} - 2\beta \left(2 - \beta^2\right) \right] \, ,
\tag{4.20}
$$

where $\sigma_{\rm T}$ is the Thomson cross section and β the velocity of the outgoing $e^+ \, e^-$ pair in the center of mass frame:

$$
\sigma_{\rm T} = \frac{e^4}{6\pi m_{\rm e}^2} \sim 0.6\,{\rm b} \quad {\rm and} \quad \beta = \sqrt{1 - \frac{4m_{\rm e}^2}{s}} \, .
$$

The total cross section peaks near the threshold, and in fact right at the threshold for $\beta \rightarrow 0$ (Thomson regime):

$$
\sigma_{\rm PP}(\beta \rightarrow 0) \simeq \frac{3}{8}\sigma_T \beta \, .
\tag{4.21}
$$

The most effective targets for photons of energy E are background photons of energy $\varepsilon \simeq m_{\rm e}^2/E$. So, for ultrahigh-energy photons the the universal radio

background is very important, unfortunately it is difficult to distinguish the galactic and extragalactic components and this give rise to some uncertainties on the predicted interaction lengths.

In the extreme Klein-Nishina limit ($\beta \to 1$ or $s \gg m_e^2$) $\beta \simeq 1 - 2m_e^2/s$, so:

$$\sigma_{\mathrm{PP}}(\beta \to 1) \simeq \frac{3}{4}\sigma_{\mathrm{T}}\frac{m_e^2}{s}\left(2\ln\frac{s}{m_e^2} - 2\right) \propto \frac{1}{s}\ln s \propto \frac{1}{E}. \qquad (4.22)$$

Note that if the energy E of the incoming photon increases, then also the mean free path increases (Klein-Nishina suppression). In this limit either e^+ or e^- carries most of the initial energy.

Inverse Compton scattering has no threshold and the total cross section is given by (e.g. see [123]):

$$\sigma_{\mathrm{ICS}} = \frac{3}{8}\sigma_{\mathrm{T}}\frac{m_e^2}{s\beta}\left[\frac{2}{\beta(1+\beta)}\left(2 + 2\beta - \beta^2 - 2\beta^3\right) - \frac{1}{\beta^2}\left(2 - 3\beta^2 - \beta^3\right)\ln\frac{1+\beta}{1-\beta}\right], \qquad (4.23)$$

here β is the velocity of the outgoing $e^\pm$: $\beta = (s - m_e^2)/(s + m_e^2)$. Most of the energy range of interest is in the extreme Klein-Nishina limit since $\sigma_{\mathrm{ICS}}(\beta \to 0) \simeq 0$, instead:

$$\sigma_{\mathrm{ICS}}(\beta \to 1) \simeq \frac{3}{8}\sigma_{\mathrm{T}}\frac{m_e^2}{s}\left(1 + 2\ln\frac{2}{1-\beta}\right) \propto \frac{1}{s}\ln s \propto \frac{1}{E}. \qquad (4.24)$$

In this limit most of the electron energy goes to the photon; the power transfered from $e^\pm$ to γ for interaction is:

$$P_{\mathrm{ICS}} = -\frac{dE}{dt} = -\frac{2}{9\pi}u_\gamma\left(\frac{e}{m_e}\right)^4 p^2, \qquad (4.25)$$

where p is the electron momentum and u_γ is the energy density of low energy photons.

In the extreme Klein-Nishina limit when ultrahigh-energy photons interact on background photons an electron positron pair is created where either e^+ or e^- carries most of the initial energy. The leading particle then undergoes inverse Compton scattering loosing almost all its energy, since inelasticity for inverse Compton scattering is larger than 90%, and the scattered

background photon carries out almost all the energy of the initial UHE photon. This two steps process is called *(electromagnetic cascade)* and plays an important role on the propagation of ultrahigh-energy photons and electrons. The effective penetration length of the cascade is larger than just the mean free path of the single interactions, so the ultrahigh-energy flux can be considerably larger than the flux predicted considering only the absorption due to pair production.

Long range extragalactic magnetic fields affect the propagation of UHECR via **synchrotron radiation**; the expression of the total power emitted is very similar to Eq. (4.25) for inverse Compton scattering:

$$P_{\mathrm{SYN}} = -\frac{dE}{dt} = -\frac{2}{9\pi}u_B\left(\frac{e}{m_{\mathrm{e}}}\right)^4 p^2\,, \qquad (4.26)$$

where $u_B = B^2/8\pi$ is the energy density of the magnetic field B. Sufficiently strong extragalactic magnetic fields can inhibit the development of the electromagnetic cascade if the synchrotron cooling time scale is smaller than the time scale of inverse Compton scattering.

Higher order processes with more than two final particles become important at higher energies. Double pair production ($\gamma\,\gamma_{\mathrm{b}} \to e^+\,e^-\,e^+\,e^-$) begins to dominate on pair production above 10^{22} eV; for electrons the contribution of triplet pair production ($e\,\gamma_{\mathrm{b}} \to e\,e^+\,e^-$) is negligible up to 10^{22} eV.

4.3 Observational data

UHECRs cannot be detected directly because their flux is too low (less than one particle per km^2 per year), and even if one of them crossed a detector it would be very difficult do determine its energy or composition. Since the pioneering works of Pierre Victor Auger in the thirties UHECR have been detected using their interactions with the Earth's atmosphere.

Primary UHECRs interact with the upper layers of the atmosphere and generate extensive air-showers, cascades of secondary particles, partly absorbed in the atmosphere and partly reaching the ground. These air-showers

can be detected through *surface detectors* sampling a small amount of the billions of particles of the shower reaching the ground, or through *fluorescence telescopes* measuring the energy deposited in the atmosphere by shower's particles (nitrogen atoms excited by charged particles of the shower emit a spectrum of ultra-violet fluorescence light while returning to ground state). Experiments combining both detection techniques are called *hybrid detectors*: the surface detectors observe the time development of a transverse section of the shower, while fluorescence telescopes observe the air-shower longitudinally.

All the informations collected by these detectors must be analysed in order to reconstruct the properties of the primary particle which originated the shower.

- The *energy* of the primary particle.
  UHECR energy spectrum should dramatically steepen above $E_{\mathrm{GZK}} \sim 5 \times 10^{19}$ eV for any distribution of protons and nuclei sources, but the HiRes (High Resolution Fly's Eye detector) and the AGASA (Akeno Giant Air-Shower Array) experiments gave conflict results on the existence of the GZK cutoff. A cutoff is consistent with the few events above 10^{20} eV seen by HiRes [124, 125], but there is a tension with the 11 events above 10^{20} eV detected by AGASA [126, 127]. The first data releases of the Pierre Auger Observatory seem to to support the existence of a cutoff [128].

- The *direction* of the primary particle.
  Before 2007 arrival directions appeared approximately isotropic, but now there are some claims of correlation with large scale structures [129].

- The *nature* (chemical composition) of the primary particle.
  The chemical composition of the primary particles is mainly reconstructed looking at the number of muons detected in ground arrays (heavier is the primary nucleus more muons are produced $N_\mu \propto A$)

and observing the atmospheric depth of the shower maximum (X_{max}) in fluoressence telescopes.

In particular showers initiated by UHE photons develop differently from showers induced by nuclear primaries. Since the the number of particles produced in electromagnetic interactions is lower compared to hadronic ones, the air showers generated by photons reach shower maximum X_{max} at much greater depth than their nuclear counterpart. Particularly it is already possible to put upper limits on the fraction of photons on the 10% level at energies above 10^{19} eV using Auger hybrid observations [9], AGASA [130, 131, 132] and Yakutsk [132, 133] data. Above 10^{20} eV, the current upper limit is $\sim 40\%$ [132]. In fact, the latest upper limits from the surface detector data of the Pierre Auger observatory are already at the level of $\sim 2\%$ above 10^{19} eV [134, 135]. In the next few year these constraints will improve with statistics: The Pierre Auger experiment can reach a sensitivity of $\sim 0.3\%$ within a few years and $\sim 0.03\%$ within 20 years around 10^{19} eV, and a sensitivity at the 10% level around 10^{20} eV within 20 years [136].

Chapter 5

Lorentz invariance violation - an introduction

We present in this chapter a very brief and highly incomplete introduction to violation of Lorentz invariance; for extensive review see Refs. [137, 138, 139, 140] and references therein.

5.1 Introduction

One of the most important problems in theoretical physics concerns the lack of a unified theory for interactions and in particular the quest for a quantum gravity theory.

Direct observations of quantum gravity effects are difficult to obtain because of the big difference between terrestrial energies and the natural quantum gravity scale ($M_{\text{pl}} \simeq 1.22 \times 10^{28}$ eV). However in the last years there was an effort not only in developing new theoretical models for quantum gravity, but also an effort in studying observational phenomena where quantum gravity phenomena could play a role (quantum gravity phenomenology). A partial list of such "windows on quantum gravity" is [141]:

- deviations from Newton's law at very short distances;

- Planck-scale fuzziness of spacetime;

- possible production in TeV-scale quantum gravity scenarios of mini black holes at colliders or in cosmic rays;

- quantum gravity induced violations of discrete symmetries of the Standard Model, as well as spacetime symmetries.

Here we will focus in particular on quantum gravity induced violations of the Lorentz symmetry [137]:

- cumulative effects: long baseline dispersion and vacuum birefringence (signals from γ-ray bursts, active galactic nuclei, pulsars, galaxies . . .);

- new threshold reactions (photon decay, vacuum Čerenkov effect, . . .);

- shifted existing threshold reactions (GZK cutoff, . . .);

- Lorentz violation induced decays not characterized by a threshold (photon splitting, . . .);

- maximal velocity (synchrotron peak from supernova remnants, . . .).

Different quantum gravity models suggest that Lorentz violation is not exact, but there is no firm calculated prediction from any model for the size of the violation [142].

The most common systematic approach for studying Lorentz violation is to construct a Lagrangian that contains the Lorentz violating operators of interest. In the early nineties S. M. Carroll, G. B. Field and R. Jackiw studied the Chern-Simons lagrangian in $3 + 1$ dimensions [102]:

$$\mathcal{L}_{\text{CS}} \propto k_\mu A_\nu \tilde{F}^{\mu\nu} \,, \tag{5.1}$$

the new term is gauge invariant but not Lorentz invariant and produces a frequency independent rotation of the plane of linear polarization [33] (see section 3.2.2). Almost ten years later D. Colladay and V. A. Kostelecky [143] proposed a systematic extension of the Standard Model of particle physics incorporating all possible Lorentz violations in the renormalizable sector.

That model provided a framework for computing in effective field theory the observable consequences for many experiments/observations. The minimal Standard Model extension (mSME) proposed in [143] consists of the Standard Model of particle physics plus all Lorentz violating operators (with mass dimension ≤ 4) that can be written without changing the field content or violating the gauge symmetry. The leading terms in the QED sector are the:

- dimension 3 terms:

$$-b_a\bar{\psi}\gamma_5\gamma^a\psi - \frac{1}{2}H_{ab}\bar{\psi}\sigma^{ab}\psi \,, \tag{5.2}$$

- dimension 4 terms:

$$-\frac{1}{4}k^{abcd}F_{ab}F_{cd} + \frac{i}{2}\bar{\psi}\left(c_{ab} + d_{ab}\gamma_5\right)\gamma^a\overleftrightarrow{D}^b\psi \,, \tag{5.3}$$

the dimension one coefficients b_a, H_{ab} and the dimensionless k^{abcd}, c_{ab}, d_{ab} are constant tensors characterizing the Lorentz violation. If rotation invariance is preserved they are all constructed from a given unit timelike vector u^a and the Minkowski metric η_{ab} ($b_a \propto u_a$, $H_{ab} = 0$, $k^{abcd} \propto u^{[a}\eta^{b][c}u^{d]}$, $c_{ab} \propto u_a u_b$, $d_{ab} \propto u_a u_b$).

R. C. Myers and M. Pospelov [144] started the study of Lorentz violation effective field theory in higher mass dimension sector (see also Ref. [142] for further developments). They considered in particular dimension five operators where Lorentz violation is described by a background four-vector u^a ($u \cdot u = 1$). The constructed operators satisfy six generic criteria [144]:

1. quadratic in the same field;

2. one more derivative than the usual kinetic term;

3. gauge invariant;

4. Lorentz invariant except for the appearance of u^a;

5. not reducible to lower dimension operators by the equation of motion;

6. not reducible to a total derivative.

Conditions (2) and (5) ensure that these operators lead to $\mathcal{O}(E^3)$ modifications (rather than $\mathcal{O}(E^2 m)$ and $\mathcal{O}(E m^2)$ - m is the particle mass).We also assume that these operators are suppressed by a factor $1/M_{\rm pl}$ and that $m\,,E \ll M_{\rm pl}$.

For *vector particles* we consider the $U(1)$ gauge field, the leading kinetic term is: $\mathcal{L}_0 = \frac{1}{4}F_{\mu\nu}F^{\mu\nu}$, the equations of motion are Maxwell equations ($\partial_a F^{ab} = 0$), fixed the gauge $\partial \cdot A = 0$: $\Box A_a = 0$ (or $k^2 A_a(k) = 0$ in momentum space). Remembering Maxwell equations and Bianchi identities ($\partial_{[a} F_{bc]} = 0$) one finds that there is only one term producing a nontrivial modification of the dispersion relation:

- dimension 5 terms (photons):

$$-\frac{\xi}{2M_{\rm pl}}u^m F_{ma}\left(u \cdot \partial\right)\left(u_n \tilde{F}^{na}\right).$$ (5.4)

The equation of motion becomes:

$$\Box A_a = \frac{\xi}{2M_{\rm pl}}\epsilon_{abcd}u^b\left(u \cdot \partial\right)^2 F^{cd}.$$ (5.5)

For a photons moving along the z axis with $k^a = (E, 0, 0, p)$, the equation for transverse polarization along the x and y axis in the Lorentz frame where $u^a = (1, 0, 0, 0)$ is:

$$\left(E^2 - p^2 \mp \frac{\xi}{M_{\rm pl}p^3}\right)(\epsilon_x \pm i\epsilon_y) = 0\,,$$ (5.6)

so, we have the following Lorentz invariance violating dispersion relation for photons:

$$E_\pm^2 = p^2 \pm \frac{\xi}{M_{\rm pl}}p^3\,.$$ (5.7)

Photons of different polarization have opposite Lorentz violating term.

For *fermions* we work with Dirac spinor, the leading kinetic term is $\mathcal{L}_0 = \bar{\psi}\left(i\,\slashed{\partial}\,-m\right)\psi$. There are only two terms with the desired form:

- dimension 5 terms (electrons):

$$-\frac{1}{2M_{\text{pl}}} u^m \bar{\psi} \gamma_m \left(\zeta_1 + \zeta_2 \gamma_5 \right) \left(u \cdot \partial \right)^2 \psi \,. \tag{5.8}$$

The modified dispersion relations are:

$$E_\pm^2 = p^2 + m^2 + \frac{2\left(\zeta_1 \pm \zeta_2 \right)}{M_{\text{pl}}} p^3 \,, \tag{5.9}$$

where $\pm$ refer to the electron helicity. If we write $\eta_\pm = 2\left(\zeta_1 \pm \zeta_2 \right)$ for electron Lorentz violation parameters, those for positrons are:

$$\eta_\pm^{\text{positron}} = -\eta_\mp^{\text{electron}} \,, \tag{5.10}$$

since a positron of energy, momentum, and spin angular momentum $(E, \mathbf{p}, \mathbf{J})$ correspond to the absence of an electron with $(-E, -\mathbf{p}, -\mathbf{J})$.

All this dimension five terms violate CPT symmetry as well as Lorentz invariance, they would be forbidden if CPT were preserved.

A simpler approach to a phenomenological description of Lorentz violation is via deformation of the dispersion relations. Two mass scales are introduced: $M \sim M_{\text{pl}}$ the scale of quantum gravity and μ_i a particle physics mass scale (possibly the mass of the particle). If rotation invariance is preserved the dispersion relation for the particle i can be written as:

$$E_i^2 = m_i^2 + p_i^2 + p_i^2 f_i \left(E_i, p_i; \mu_i, M \right) \,, \tag{5.11}$$

where E_i and p_i are the energy and the momentum of the particle. Lorentz violation parameters depend on the particle type and indeed it turns out that they must sometimes be different but related in certain ways for particles with opposite helicity/polarization and for particles and antiparticles. A dispersion relation that is not boost invariant can hold only in one frame; we assume that this frame coincides with that of the cosmic microwave background.

5.2   Astrophysical constraints on QED Lorentz violation

Today dimension three and four operators are already tightly constrained: $\mathcal{O}(10^{-46})$, $\mathcal{O}(10^{-27})$ while we would expect them of $\mathcal{O}(1)$ (for a compilation see, e. g., Ref. [145]). E.g. see Ref. [146] for CMB polarization birefringence constraints on Lorentz invariance violating terms for photons. This is why much attention was focused on dimension 5 and higher non-renormalizable operators (which are already Planck suppressed). In this section we will focus mainly on dimension five Lorentz violation operators.

Time of flight. Photon time of flight constraints limit differences in the arrival time at Earth for photons originating in a distant event. The arrival time difference for wavevectors k_1 and k_2 is:

$$\Delta t = \xi_1 \frac{k_2 - k_1}{M_{\text{pl}}} d \,.$$

(5.12)

It increases with the distance of the source d and with the energy difference. A possible problem is that it is not known if photons of different energies are produced simultaneously; however, since time of flight is a propagation effect, a survey at different redshifts can separate Lorentz violation effect from intrinsic source effect. Constraints of the order $|\xi_1| < \mathcal{O}(10^2)$ were obtained using the high energy radiation emitted by some γ-ray bursts and active galaxies [147].

Birefringence. Birefringence constraints arise from the fact that Lorentz violation parameters for right and left circular polarized photons are opposite for dimension five Lorentz violation operators. Dispersion relation for photons introduced in Eq. (5.7) leads to a rotation of the linear polarization plane through the frequency dependent angle:

$$\theta(k, d) = \frac{\omega_+(k) - \omega_-(k)}{2} \simeq \xi_1 \frac{k^2}{2M_{\text{pl}}} d \,.$$

(5.13)

Since detectors have a finite bandwidth ($k_1 \le E \le k_2$) an order of magnitude constraint can be obtained from the fact that if the angle of polarization

rotation were different more than $\pi/2$ over the detector energy range, then the instantaneous polarization at the detector would fluctuate sufficiently for the net polarization of signal to be suppressed well below the observable value [148]:

$$\xi_1 \lesssim \frac{\pi M_{\text{pl}}}{(k_2^2 - k_1^2)\, d}\,. \tag{5.14}$$

A more refined limit can be obtained by calculating the maximum observable polarization angle. In Ref. [149] recent polarimetric observations of the Crab Nebula in the hard X-ray band by INTEGRAL [150] showing the absence of vacuum birefringence effects were used to constrain Lorentz violation for photons $|\xi_1| < 9 \times 10^{-10}$ at 3σ confidence level. The same considerations applied to optical or UV photons of the afterglow from distant γ-ray bursts lead to the constraint $|\xi_1| < 2 \times 10^{-7}$ [152]. A former, more stringent constraint, $|\xi_1| < 2 \times 10^{-15}$ [148], was based on polarization of MeV γ-rays which could not be confirmed [141].

Vacuum Čerenkov effect. The spontaneous emission of photons by charged particles in vacuum ($e \rightarrow e\,\gamma$) is forbidden in Lorentz invariant physics, but it can be allowed if electron dispersion relation is sufficiently modified. If $\xi_1 \simeq 0$ the threshold energy for this process is [138]:

$$p \simeq \left(\frac{m_e^2 M_{\text{pl}}}{2\eta}\right)^{1/3} \simeq 11\,\text{TeV}\,\eta^{-1/3}\,. \tag{5.15}$$

The inverse Compton Čerenkov constraint uses the electrons of energy up to 50 TeV, inferred via the observation of 50 TeV γ rays from the Crab nebula which are explained by inverse Compton scattering. This leads to the bound $\eta \lesssim 10^{-2}$ for at least one of the fermion parameters.

Synchrotron emission. For negative values of η the electron has a maximal group velocity less than the speed of light, hence there is a maximal synchrotron frequency that can be produced. This yield to the constraint [138]:

$$\eta \lesssim -\frac{M_{\text{pl}}}{m_e} \left(\frac{0.34\, eB}{n_e \omega_{\text{obs}}}\right)^{3/2}\,. \tag{5.16}$$

The Crab synchrotron emission has been observed to extend at least up to energies of about 100 MeV, the magnetic field in the emission region has been estimated on a value between 0.15 and 0.6 mG. Then we infer that at least one of the two parameters η_+ or η_- must be grater of -7×10^{-8}.

In Ref. [151] the information provided by multiwavelength observation were compared with a full and self consistent computation of the broad band spectrum of the Crab nebula. η_+ and η_- have been both constrained to have a magnitude smaller than 10^{-5} at 95% confidence level.

Constraints based on **modified reaction threshold** (e.g. pair production) were so far obtained from observations of multi-TeV γ rays from blazars at distances ≥ 100 Mpc, resulting constraints are of the order $|\xi_1| \lesssim 1$ [153]; see next section for stronger constraints based on propagation of ultrahigh energy cosmic rays.

In Fig. 5.1 are summarized different constraints for $\mathcal{O}(E/M_{\mathrm{pl}})$ modifications of electron and photon dispersion relations.

CPT symmetry alone could exclude dimension five operators, moreover the constraints on $\mathcal{O}(E/M_{\mathrm{pl}})$ modifications of the dispersion relation are becoming quite strong. Therefore the interest in dimension six operators is increasing and it is already possible to constrain $\mathcal{O}(E^2/M_{\mathrm{pl}}^2)$ modifications of the dispersion relations (see next chapter).
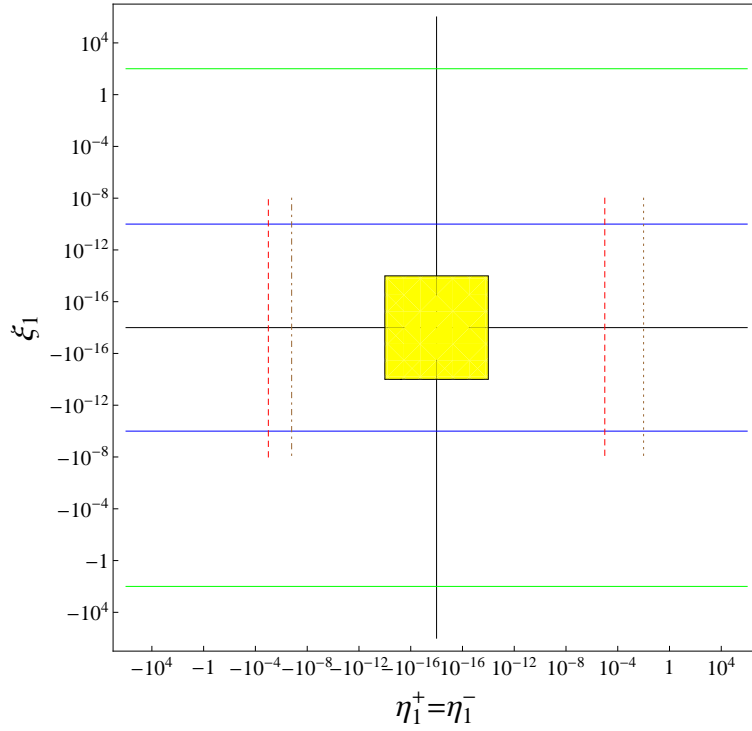
Figure 5.1: Astrophysical constraints on $\mathcal{O}(E/M_{\mathrm{pl}})$ QED Lorentz violation: time of flight constraints $|\xi_1| < \mathcal{O}(10^2)$ (green lines), birefringence constraints $|\xi_1| < 9 \times 10^{-10}$ (blue lines), Crab nebula constraints $|\eta_\pm| < 10^{-5}$ (red dotted lines), vacuum Čerenkov constraints $\eta \lesssim 10^{-2}$ for at least one of the fermion parameters (brown dotted line), synchrotron emission constraints $\eta \gtrsim -7 \times 10^{-8}$ for at least one of the fermion parameters (brown dot-dashed line). The order of magnitude of the region allowed by propagation of ultrahigh energy photons is marked in yellow (see next chapter).

Chapter 6

Lorentz violation and ultrahigh-energy photons

6.1 Introduction

Many modern extensions of the Standard Model of particle physics, including string theory and various other approaches aiming at unification of quantum mechanics with general relativity, suggest that the Lorentz symmetry may be broken or modified at energy and length scales approaching the Planck scale. While such effects necessarily have to be tiny at energies up to the electroweak scale in order to satisfy laboratory constraints [145], they can be magnified at higher energies as they can occur in astrophysics. The observation of standard radiation processes as they are predicted in the absence of Lorentz invariance violation then often allows to derive strong constraints on Lorentz invariance violating (LIV) effects [137, 140].

LIV effects could, for example, change the propagation and thus spectra and composition of the highest energy particles observed in Nature [8, 154]. This was shown in case of ultrahigh-energy cosmic rays producing pions by the Greisen-Zatsepin-Kuzmin (GZK) effect [155] above the threshold at $\sim 7 \times 10^{19}$ eV and in case of pair production of high energy photons with the diffuse low energy photon background [154].

While the thresholds of electron-positron pair production by high energy $\gamma-$rays on low energy background photons have not yet been experimentally confirmed beyond doubt, constraints on LI breaking for photons have been established based on the very existence of TeV $\gamma-$rays from astrophysical objects [156].

Here we exploit the fact that if pair production of high energy $\gamma-$rays on the cosmic microwave background (CMB) would be inhibited above $\sim 10^{19}\,\mathrm{eV}$, one would expect a large fraction of $\gamma-$rays in the cosmic ray flux at these energies, independent on where the real pair production threshold is located. Based on the fact that no significant $\gamma-$ray fraction is observed, we derive limits on LI violating parameters for photons and electrons that are more stringent than former limits. Moreover, we also show how the excluded parameter ranges would be extended if ultrahigh energy photons were detected in the future.

For the coefficients of LIV terms linearly suppressed with the Planck scale values larger than $\sim 10^{-5}$ for electrons and positrons are currently ruled out by the observation of synchrotron radiation from the Crab Nebula [151]. We find that the observation of photons above $\simeq 10^{19}\,\mathrm{eV}$ would rule out that any one of the three LIV coefficients for electrons, positrons and photons has absolute value $\gtrsim 10^{-14}$. This is in agreement with Ref. [157] which considers a two dimensional subset of the general three-dimensional parameter range.

In contrast, we will find that for LIV terms quadratically suppressed with the Planck scale, arbitrarily large values of one of the LIV terms for electrons and positrons can not be ruled out by UHE photon observations if the coefficients of the two other LIV terms have absolute value $\lesssim 10^{-6}$.

6.2   Fraction of UHE photons

Neutral pions created by the GZK effect decay into ultrahigh energy photons. They subsequently interact with low-energy background photons of the CMB and the universal radio background (URB) through pair production,
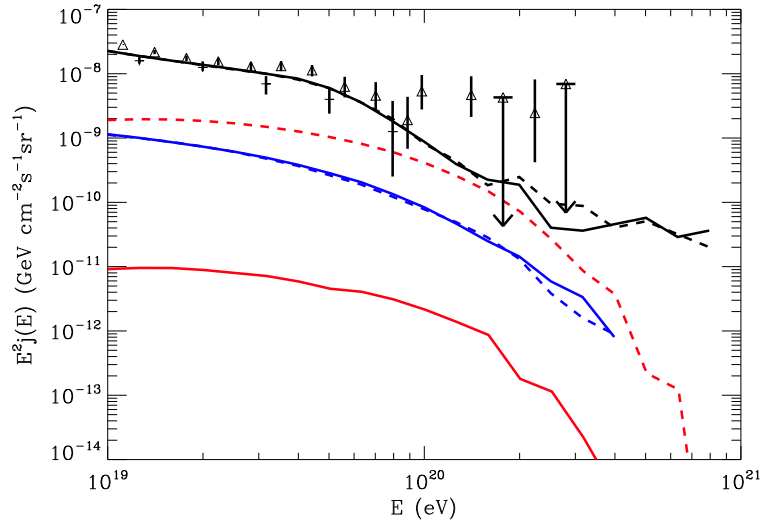
Figure 6.1: Fluxes for uniform $E^{-2.6}$ proton injection between 10^{19} and 10^{21} eV up to redshift 3. AGASA data [162] are shown as triangles, HiRes data [124] as crosses. Solid lines: with CMB and the minimal version of the universal radio background, based on observations [163]; from top to bottom: protons, neutrinos per flavor, and photons. Dashed lines: without any pair production by photons above 10^{19} eV; from top to bottom: protons, photons, and neutrinos per flavor.

$\gamma\,\gamma \to e^+\,e^-$. This leads to the development of an electromagnetic cascade and suppresses the photon flux above the pair production threshold on the CMB of $\sim 10^{15}$ eV. Above $\sim 10^{19}$ eV the interaction length for photons is smaller than a few Mpc, whereas for nucleons above the GZK threshold at $\sim 7 \times 10^{19}$ eV it is of the order of 20 Mpc. As a result, the photon fraction theoretically expected is smaller than $\sim 1\%$ around 10^{19} eV, and smaller than $\sim 10\%$ around 10^{20} eV [158, 159], in agreement with experimental upper limits (see section 4.3).

The breaking of Lorentz invariance, by modifying the dispersion relations for photons and/or electrons, would affect the energy threshold for pair production. If the changes in the dispersion relations are sufficiently large, pair
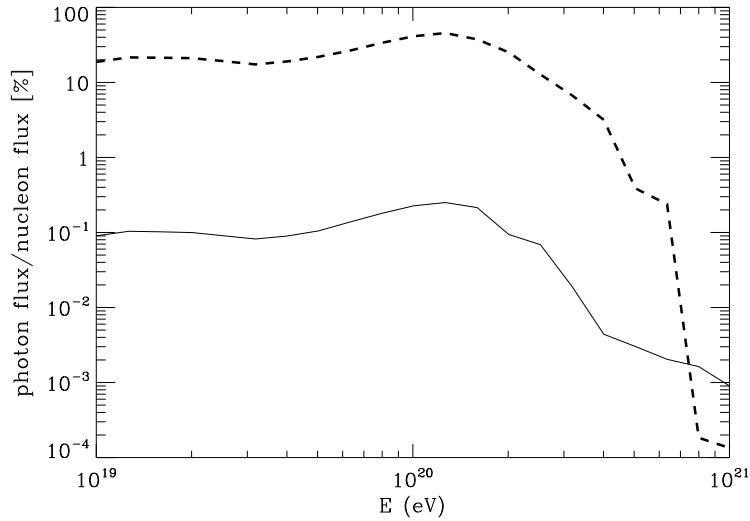
Figure 6.2: The ratio of the integral photon to primary cosmic ray flux above a given energy as a function of that energy for the two scenarios shown in Fig. 6.1.

production can become kinematically forbidden at ultrahigh energies and such photons could reach us from cosmological distances. As a consequence, at least if ultrahigh energy cosmic rays consist of mostly protons, one would expect a significant photon fraction in cosmic rays above 10^{19} eV, in conflict with experimental upper limits. Figs. 6.1 and 6.2, which were obtained with the CRPropa code [160, 161], show that the ratio of the integral photon to primary cosmic ray flux above 10^{19} eV would be $\simeq 20\%$, and thus higher than the above mentioned experimental upper limits. In this scenario, we have used a relatively steep proton injection spectrum $\propto E^{-2.6}$. Harder injection spectra also give acceptable fits above $\sim 10^{19}$ eV, as well as higher photon fractions due to increased pion production [159]. Whereas for pair production without LI breaking, the predicted photon fraction always stays below experimental upper limits, harder injection spectra and larger maximal energies in the absence of pair production would overshoot the experimental limits even more than in Figs. 6.1 and 6.2.

Therefore, LI violating parameters for photons and electrons can be constrained by the requirement that pair production be allowed between low energy background photons and photons of energies between 10^{19} eV and 10^{20} eV. We will assume that pion production itself is not significantly modified and that the modifications of the dispersion relations of electrons and positrons are significantly smaller than for photons (this only in section 6.5). This is consistent since the photon content of other particles is on the percent level [164].

6.3   Modified dispersion relations

We indicate the 4-momenta for ultrahigh-energy photons with $(\omega, \boldsymbol{k})$, for low-energy background photons with $(\omega_{\mathrm{b}}, \boldsymbol{k}_{\mathrm{b}})$, for electrons with $(E_{\mathrm{e}}, \mathbf{p}_{\mathrm{e}})$, and for positrons with $(E_{\mathrm{p}}, \mathbf{p}_{\mathrm{p}})$.

The following modifications to the Lorentz invariant dispersion relations are considered:

$$\omega_{\pm}^2 = k^2 + \xi_n^{\pm} k^2 \left(\frac{k}{M_{\mathrm{pl}}}\right)^n, \tag{6.1}$$

$$\omega_{\mathrm{b}}^2 = k_{\mathrm{b}}^2, \tag{6.2}$$

$$E_{\mathrm{e},\pm}^2 = p_{\mathrm{e}}^2 + m_{\mathrm{e}}^2 + \eta_n^{\mathrm{e},\pm} p_{\mathrm{e}}^2 \left(\frac{p_{\mathrm{e}}}{M_{\mathrm{pl}}}\right)^n, \tag{6.3}$$

where $n \geq 1$, $M_{\mathrm{pl}} \simeq 10^{19}$ GeV is the Planck mass, $m_{\mathrm{e}} \simeq 0.5$ MeV is the electron mass, and the $+(-)$ sign in Eq. (6.1) for photons indicates right (left) polarization, while in Eq. (6.3) for electrons denotes positive (negative) helicity.

The LIV parameters $\xi_n^{\pm}$ for the two photon polarizations are not independent; they are related by effective field theory considerations [144, 142] as $\xi_n^+ = (-1)^n \xi_n^-$ for $n = 1, 2$. Because of this relation, the photon dispersion relation can be expressed in terms of the single parameter ξ_n^+ which we denote as ξ_n in the following.

Effective field theory predicts the relation $\eta_n^{\mathrm{p},\pm} = (-1)^n \eta_n^{\mathrm{e},\mp}$ between the LIV parameters for fermions and anti-fermions for $n = 1$ and $n = 2$ [148, 142].

It is, therefore, not necessary to introduce new parameters in the modified dispersion relation for positrons which can thus be written as

$$E_{p,\pm}^2 = p_p^2 + m_e^2 + (-1)^n \eta_n^{e,\mp} p_p^2 \left(\frac{p_p}{M_{pl}}\right)^n . \tag{6.4}$$

Thus, for the remainder of this chapter we can restrict ourselves to the parameters $\eta_n^{e,\pm}$, for which we simply write $\eta_n^\pm$.

As a result, LIV modifications in the QED sector are described by three parameters at a given suppression by the power $n = 1, 2$ of the Planck scale, namely by one for photons (ξ_n) and two for electron and positron (η_n^+ and η_n^-). Note, however, that in some particular cases, kinematics is governed by just one parameter for the pair: If the final state of a certain process consists of an electron-positron pair with opposite helicity, due to the relation $\eta_n^{p,\pm} = (-1)^n \eta_n^{e,\mp}$, only either η_n^+ or η_n^- appears.

6.4   Threshold equations

If Lorentz invariance is preserved, the main process influencing the propagation of UHE photons is pair production: Photons with energy higher than m_e^2/k_b produce an electron-positron pair interacting with low-energy background photons of energy k_b. For interaction with CMB photons ($k_b \simeq 6 \times 10^{-4}$ eV) the lower threshold is $\sim 4 \times 10^{14}$ eV, and the UHE photon flux is highly suppressed due to this interaction.

If the dispersion relations for photons and fermions are modified by LIV terms, then the lower threshold for this process can be modified and pair production can also become forbidden above a certain upper threshold. Moreover, other processes, usually forbidden if Lorentz invariance is preserved, can become allowed. In particular, photon decay ($\gamma \to e^- e^+$) and photon splitting ($\gamma \to N\gamma$) can play an important role in the propagation of UHE photons. Note that if pair production is forbidden above a certain upper threshold, than photon decay must also be forbidden: If the production of an electron positron pair is kinematically forbidden for two photons (pair pro-

duction), then it will be forbidden also for a single photon (photon decay), otherwise pair production on an infinitely soft background photon would be allowed [157].

The characteristic timescale of these processes is relevant for their relative importance: In particular, for UHE photons the photon splitting timescale is usually larger than the propagation timescale [157, 156], therefore, in the following we will focus mainly on pair production and photon decay processes.

Which and how many LIV parameters are involved in pair production or in photon decay processes depends on the polarization of incoming photon(s) and on the helicity of the outgoing electron and positron, see Tab. 6.1. Although right at the threshold, where the electron positron pair is produced without angular momentum, only the s-wave contributes to the process and certain helicity combinations are forbidden, above the threshold also higher partial waves contribute and all possible channels (all partial waves) must be considered.

Note that the kinematics of pion decay $\pi^0 \to \gamma\,\gamma$ is not significant modified. Using the exact relation for energy-momentum conservation, the kinematic relation for the decay of a neutral pion of mass m_π into two $\gamma-$rays of energy-momentum $(\omega_1, \mathbf{k}_1)$ and $(\omega_1, \mathbf{k}_2)$, respectively, and equal helicity is $2\omega_1\omega_2 - 2\mathbf{k}_1 \cdot \mathbf{k}_2 + \xi_n(k_1^{n+2} + k_2^{n+2})/M_{\mathrm{Pl}}^n = m_\pi^2$. For $|\xi_n| \lesssim 1$, the absolute values of the LI violating terms are always much smaller than the ones of $\omega_1\omega_2$ and $\mathbf{k}_1 \cdot \mathbf{k}_2$, which themselves are much larger than m_π^2 in most of the phase space.

6.4.1 Pair production $(\gamma\,\gamma_{\mathrm{b}} \to e^-\,e^+)$

Exact energy momentum conservation implies that

$$(\omega_\pm + \omega_{\mathrm{b}})^2 - (\mathbf{k} + \mathbf{k}_b)^2 = (E_{\mathrm{e},\pm} + E_{\mathrm{p},\pm})^2 - (\mathbf{p}_e + \mathbf{p}_p)^2 \,. \qquad (6.5)$$

The left-hand side is maximized for a head-on collision of the two photons, while the right-hand side is minimized for parallel final momenta of the pair [156, 165]. Expanding in terms of the LIV parameters, and writing

	UHE γ	e^-	e^+	(ξ, η_e, η_p)	number of LIV param.	s-wave allowed for PP	s-wave allowed for PD
1	+	+	+	$(\xi_n, \eta_n^+, (-1)^n\eta_n^-)$	3	No	Yes
2	+	+	−	$(\xi_n, \eta_n^-, (-1)^n\eta_n^+)$	2	Yes	No
3	+	−	+	$(\xi_n, \eta_n^-, (-1)^n\eta_n^-)$	2	Yes	No
4	+	−	−	$(\xi_n, \eta_n^-, (-1)^n\eta_n^+)$	3	No	Yes
5	−	+	+	$((-1)^n\xi_n, \eta_n^+, (-1)^n\eta_n^-)$	3	No	Yes
6	−	+	−	$((-1)^n\xi_n, \eta_n^+, (-1)^n\eta_n^+)$	2	Yes	No
7	−	−	+	$((-1)^n\xi_n, \eta_n^-, (-1)^n\eta_n^-)$	2	Yes	No
8	−	−	−	$((-1)^n\xi_n, \eta_n^-, (-1)^n\eta_n^+)$	3	No	Yes

Table 6.1: Photon, electron and positron LIV parameters (ξ, η_e, η_p) appearing in the combination $\xi - \eta_p y^{n+1} - \eta_e(1-y)^{n+1}$ in the kinematic equations (6.6) and (6.20) for pair production and photon decay, respectively, for both polarizations of the UHE photon and for all helicity configurations of the electron-positron pair. Recall that for electrons, the sign index $\pm$ in $\eta_n^\pm$ refers to the helicity, whereas for positrons it refers to the inverse helicity. For each combination we show the number of LIV parameters contributing to the kinematics, and whether conservation of total angular momentum allows the s-wave channel for pair production (PP), or for photon decay (PD) at threshold.

$p_{\mathrm{e}} = (1-y)k$ and $p_{\mathrm{p}} = yk$ as functions of the asymmetry y in the final momenta, for right polarized photons we obtain the equation:

$$\left[\xi_n - (-1)^n \eta_n^{\mp} y^{n+1} - \eta_n^{\pm} (1-y)^{n+1}\right] k^2 \left(\frac{k}{M_{\mathrm{pl}}}\right)^n$$

$$+4kk_{\mathrm{b}} - \frac{m_{\mathrm{e}}^2}{y(1-y)} = 0\,, \tag{6.6}$$

where all four combinations of $\eta_n^{\mp}$ and $\eta_n^{\pm}$ can occur in the square bracket. Note that due to the relation $\eta_n^{\mathrm{p},\pm} = (-1)^n \eta_n^{\mathrm{e},\mp}$, for electrons, the sign index $\pm$ in $\eta_n^{\pm}$ refers to the helicity, whereas for positrons it refers to the inverse helicity. As a consequence, equal sign indices in the two terms correspond to opposite helicities for electron and positron, whereas opposite sign indices correspond to equal helicities. For left polarized UHE photons ξ_n must be replaced with $(-1)^n \xi_n$. The second term inside square brackets refers to positrons and the third one to electrons. By definition, in the third term η_n^+ refers to electrons of positive helicity, and η_n^- to electrons of negative helicity. In contrast, in the second term η_n^+ refers to positrons of negative helicity, whereas η_n^- refers to positrons of positive helicity. Therefore, Eq. (6.6) reduces to Eq. (3) of Ref. [157] in the channel where electrons and positrons have opposite helicities, where kinematics depends only on either η_n^+ or η_n^-. Alternatively, one also obtains this equation in the channel where electrons and positrons have the same helicities, if one assumes the relation $\eta_n^+ = \eta_n^-$ between electron LIV parameters with opposite helicity.

When all LIV parameters vanish, we find the usual Lorentz invariant lower threshold $(k_{\mathrm{LI}} = m_{\mathrm{e}}^2/k_{\mathrm{b}})$ for a symmetric final configuration $y = 1/2$, .

For given values for LIV parameters we determine numerically the lower and upper thresholds of this process using Eq. (6.6) and its derivative with respect to k and y [156].

Defining $x \equiv 4y(1-y)k/k_{\mathrm{LI}}$, Eq. (6.6) can be rewritten as

$$\alpha_n x^{n+2} + x - 1 = 0\,, \tag{6.7}$$

where, for right polarized photons,

$$\alpha_n \equiv \frac{\xi_n - (-1)^n \eta_n^{\mp} y^{n+1} - \eta_n^{\pm} (1-y)^{n+1}}{2^{2(n+2)} y^{n+1} (1-y)^{n+1}} \frac{m_{\rm e}^{2(n+1)}}{k_{\rm b}^{n+2} M_{\rm pl}^n}, \tag{6.8}$$

and for left polarized photons ξ_n must be replaced by $(-1)^n \xi_n$.

If $n \geq 1$, Eq. (6.7) has at most two positive solutions, corresponding to a lower or an upper threshold. If there were more than two positive solutions, there would be two or more stationary points for $x > 0$, but the derivative of Eq. (6.7) vanishes for

$$(n + 2) \alpha_n x^{n+1} + 1 = 0, \tag{6.9}$$

and the solutions of this equation are

$$x_s = [(n + 2) \alpha_n]^{-\frac{1}{n+1}} \exp \left[i \frac{\pi + 2\pi s}{n + 1} \right] \ (\text{if } \alpha_n > 0), \tag{6.10}$$

$$x_s = [(n + 2) |\alpha_n|]^{-\frac{1}{n+1}} \exp \left[i \frac{2\pi s}{n + 1} \right] \ (\text{if } \alpha_n < 0), \tag{6.11}$$

where $s = 0, \ldots, n$. These expressions are real and positive only for $s = 0$, therefore there cannot be more than one stationary point. This excludes the possibility that there could be more than two thresholds for pair production.

We will argue that current upper limits on the photon fraction of UHE cosmic rays in the energy range between $\simeq 10^{19}$ eV and $\simeq 10^{20}$ eV require that pair production has to be kinematically allowed for both UHE photon polarizations shown in Tab. 6.1, otherwise at least one channel would be unabsorbed and one would expect $\gtrsim 10\%$ photons. This will rule out certain ranges in the parameter space of the three LIV parameters ξ_n and $\eta_n^{\pm}$. However, in order to be conservative, we will rule out only parameter combinations for which the photon is stable. This is because for unstable photons, the absence of photons in the observed ultra-high energy cosmic ray flux could be due to photon decay, $\gamma \to e^- e^+$, at least as long as any electron-positron pairs in the decay products cannot recreate a significant photon flux by inverse Compton scattering on the CMB. On the other hand, the observation of a UHE photon would rule out photon decay because this

process would occur on microscopic time scales once it is allowed. We will, therefore, also consider photon decay in the following.

We follow the procedure described in Ref. [156] in order to determine numerically the lower and upper thresholds of this process using Eq. (6.6) and its derivative with respect to k and y.

In particular for $n = 1$ the equation for energy-momentum conservation is (see Eq. 6.6):

$$F(x,y) = \left[\xi_1 + \eta_1^{\mp} y^2 - \eta_1^{\pm} (1-y)^2\right] \frac{m_{\rm e}^4}{k_{\rm b}^3 M_{\rm pl}} x^3 + x - \frac{1}{y(1-y)} = 0\,, \quad (6.12)$$

This equation can be solved for $x = x(y)$; so lower threshold corresponds to a global minimum of $x(y)$:

$$\left.\frac{dx(y)}{dy}\right|_T = 0 \quad \text{and} \quad \left.\frac{d^2x(y)}{dy^2}\right|_T > 0\,. \quad (6.13)$$

Threshold is by definition a solution for the kinematic equation, $F(x,y)$ is identically zero, hence its total derivative respect to y vanishes:

$$\left.\frac{dF(x,y)}{dy}\right|_T = \left.\frac{\partial F(k,y)}{\partial x(y)}\frac{dx(y)}{dy}\right|_T + \left.\frac{\partial F(x,y)}{\partial y}\right|_T = 0$$

$$\Longrightarrow \left.\frac{\partial F(x,y)}{\partial t}\right|_T = 0\,,$$

$$\left.\frac{d^2F(x,y)}{dy^2}\right|_T = \left.\frac{\partial^2 F(x,y)}{\partial x^2(y)}\frac{dx(y)}{dy}\right|_T + \left.\frac{\partial F(x,y)}{\partial x(y)}\frac{d^2x(y)}{dy^2}\right|_T + \left.\frac{\partial^2 F(x,y)}{\partial y^2}\right|_T = 0$$

$$\Longrightarrow -\left.\left(\frac{\partial^2 F(x,y)}{\partial y^2}\right)\middle/\left(\frac{\partial F(x,y)}{\partial x(y)}\right)\right|_T > 0\,.$$

Besides $\partial F(x,y)/\partial x(y) > 0$ for lower threshold (e.g. see Fig. 6.8).

Similarly for upper threshold, global maximum of $x(y)$:

$$\left.\frac{dx(y)}{dy}\right|_T = 0 \quad \text{and} \quad \left.\frac{d^2x(y)}{dy^2}\right|_T < 0\,, \quad (6.14)$$

also upper threshold is by definition a solution for the kinematic equation,

$F(x, y)$ is identically zero, hence its total derivative respect to y vanishes:

$$\frac{dF(x, y)}{dy}\bigg|_T = \frac{\partial F(k, y)}{\partial x(y)}\frac{dx(y)}{dy}\bigg|_T + \frac{\partial F(x, y)}{\partial y}\bigg|_T = 0$$

$$\implies \frac{\partial F(x, y)}{\partial t}\bigg|_T = 0\,,$$

$$\frac{d^2 F(x, y)}{dy^2}\bigg|_T = \frac{\partial^2 F(x, y)}{\partial x^2(y)}\frac{dx(y)}{dy}\bigg|_T + \frac{\partial F(x, y)}{\partial x(y)}\frac{d^2 x(y)}{dy^2}\bigg|_T + \frac{\partial^2 F(x, y)}{\partial y^2}\bigg|_T = 0$$

$$\implies -\left(\frac{\partial^2 F(x, y)}{\partial y^2}\right) \Big/ \left(\frac{\partial F(x, y)}{\partial x(y)}\right)\bigg|_T < 0\,.$$

Besides $\partial F(x, y)/\partial x(y) < 0$ for upper threshold (e.g. see Fig. 6.8).

Summarising possible candidates for the thresholds (both lower and upper) are the solutions of the system:

$$\begin{cases} F(k, y) = 0 \\ \frac{\partial F(k,y)}{\partial y} = 0 \\ \frac{\partial^2 F(x,y)}{\partial y^2} < 0 \end{cases} \tag{6.15}$$

it is possible to distinguish lower thresholds from upper ones considering $\partial F(x, y)/\partial x(y)$.

In this $n = 1$ case it is worthwhile not to consider directly $F(x, y)$, but $G(x, y) \equiv y(1 - y)F(x, y)$. Figs. 6.3 and 6.4 show graphically the solution of the system (6.15) in the (x,y) plane fixed two particular sets of values for

the LIV parameters.

$$
\begin{aligned}
G(x,y) &= y(1-y)\left[\xi_1 + \eta_1^{\mp} y^2 - \eta_1^{\pm}(1-y)^2\right]\frac{m_e^4}{k_b^3 M_{\rm pl}}x^3 \\
&\quad + 4y(1-y)x - 1 = 0\,, \tag{6.16}\\
\frac{\partial G(x,y)}{\partial y} &= \frac{4m_e^4(\eta_1^{\pm}-\eta_1^{\mp})}{k_b^3 M_{\rm pl}}x^3 y^3 - \frac{3m_e^4(3\eta_1^{\pm}-\eta_1^{\pm})}{k_b^3 M_{\rm pl}}x^3 y^2 \\
&\quad - 2\frac{4M_{\rm pl}k_b^3 + m_e^4 x^2(\xi_1 - 3\eta_1^{\pm})}{k_b^3 M_{\rm pl}}xy \\
&\quad + \frac{4k_b^3 M_{\rm pl}x + (\xi_1 - \eta_1^{\pm})m_e^4 x^3}{k_b^3 M_{\rm pl}} = 0\,, \tag{6.17}\\
\frac{\partial^2 G(x,y)}{\partial y^2} &= \frac{12m_e^4(\eta_1^{\pm}-\eta_1^{\mp})}{k_b^3 M_{\rm pl}}x^3 y^2 - \frac{6m_e^4(3\eta_1^{\pm}-\eta_1^{\mp})}{k_b^3 M_{\rm pl}}x^3 y \\
&\quad - 2\frac{4M_{\rm pl}k_b^3 + m_e^4 x^2(\xi_1 - 3\eta_1^{\pm})}{k_b^3 M_{\rm pl}}x < 0\,. \tag{6.18}
\end{aligned}
$$

6.4.2 Photon decay $(\gamma \to e^- e^+)$

For the reaction $\gamma \to e^- e^+$ 4-momentum conservation implies:

$$
\omega_\pm^2 - k^2 = \left(E_{\rm e,\pm} + E_{\rm p,\pm}\right)^2 - \left(\mathbf{p}_e + \mathbf{p}_p\right)^2\,, \tag{6.19}
$$

and proceeding as for pair production we obtain for right polarized UHE photons:

$$
\left[\xi_n - (-1)^n \eta_n^{\mp} y^{n+1} - \eta_n^{\pm}(1-y)^{n+1}\right]k^2\left(\frac{k}{M_{\rm pl}}\right)^n
$$
$$
-\frac{m_e^2}{y(1-y)} = 0\,. \tag{6.20}
$$

The corresponding equation for left polarized photons is obtained by substituting ξ_n with $(-1)^n\xi_n$.

Note that Eq. (6.6) for pair production reduces to Eq. (6.20) for photon decay when the energy of the background photon $k_{\rm b}$ vanishes.

Photon decay is kinematically forbidden in the Lorentz invariant case, but it can become allowed, above a certain energy threshold, for certain values
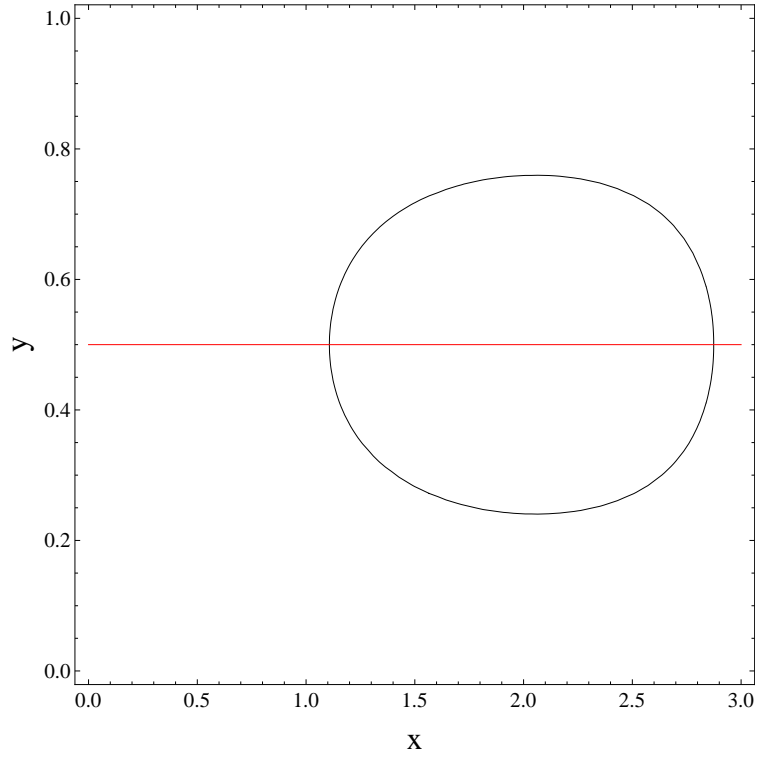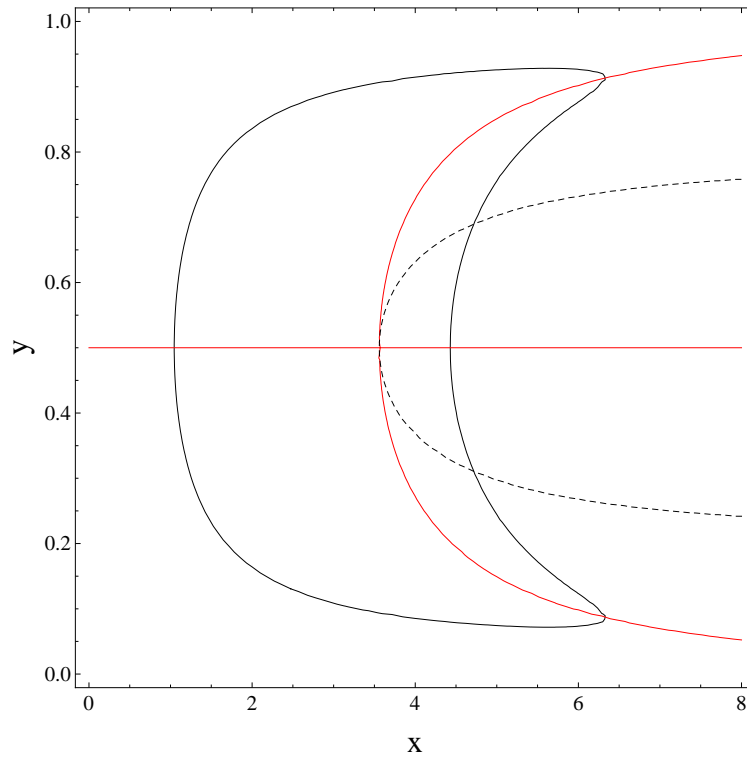
Figure 6.3: Determination of upper and lower threshold for pair production fixed $(\xi, \eta_1^{\mp}, \eta_1^{\pm}) = (-10^{-5}, 0, 0)$. In the (x, y) plane, where $x \equiv 4y(1 - y)k/k_{\mathrm{LI}}$ gives the new threshold in terms of the Lorentz invariant one and $y \equiv p_{\mathrm{p}}/k$ is the asymmetry between electron and positron final momenta, we solve graphically the system (6.15) plotting in black $G(x, y) = 0$ and in red red $\partial G(x, y)/\partial y = 0$. Lower threshold is $(1.1, 0.5)$ and upper threshold is $(2.9, 0.5)$.

Figure 6.4: Determination of upper and lower threshold for pair production fixed $(\xi, \eta_1^{\mp}, \eta_1^{\pm}) = (-10^{-5}, 10^{-5}, -10^{-5})$. In the (x, y) plane we solve graphically the system (6.15) plotting in black $G(x, y) = 0$, in red red $\partial G(x, y)/\partial y = 0$, and with a dashed line $\partial^2 G(x, y)/\partial y^2 = 0$. Lower threshold is $(1.05, 0.5)$ and asymmetric upper thresholds are $(6.3, 0.08)$ and $(6.3, 0.92)$.

of the LIV parameters. We again search numerically for this threshold by employing Eq. (6.20) and its derivatives with respect to k and y.

If a photon of a certain energy is detected, at least one photon polarization must be stable, i.e. cannot decay into any helicity configuration of the final pair.

Eq. (6.20) can be rewritten as:

$$\alpha_n x^{n+2} - 1 = 0 \,, \tag{6.21}$$

and its solutions are of the form

$$x_s \;=\; \alpha_n^{-\frac{1}{n+2}} \exp\left[i \frac{2\pi s}{n+2} \right] \quad (\text{if } \alpha_n > 0) \,, \tag{6.22}$$

$$x_s \;=\; |\alpha_n|^{-\frac{1}{n+2}} \exp\left[i \frac{\pi + 2\pi s}{n+2} \right] \quad (\text{if } \alpha_n < 0) \,, \tag{6.23}$$

where $s = 0, \ldots, n+1$. Note that these expressions give at most one positive solution x_s, therefore, there cannot be more than one threshold for photon decay.

6.5   Lorentz violation for photons and ultrahigh-energy photons

As first step we consider how photon propagation is modified when the LIV parameters for electrons and positrons are negligible ($\eta_n^\pm \ll \xi_n$).

The kinematic condition for pair production, according to Eq. (6.7), is:

$$F_0(x; \alpha_n^0) \equiv \alpha_n^0 x^{n+2} + x - 1 = 0 \,, \tag{6.24}$$

defined:

$$\alpha_n^0 \equiv \frac{\xi_n}{2^{n(n+2)} y^{n+1}(1-y)^{n+1}} \frac{m_{\mathrm{e}}^{2(n+1)}}{k_{\mathrm{b}}^{n+2} M_{\mathrm{pl}}^n} \,. \tag{6.25}$$

If $\alpha_n^0 \geq 0$, Eq. (6.24) admits one real positive solution $x_n^l(\alpha_n^0) < 1$ for each value of $\alpha_n^0 > 0$. Therefore, for photons with a *positive* LI violating term in
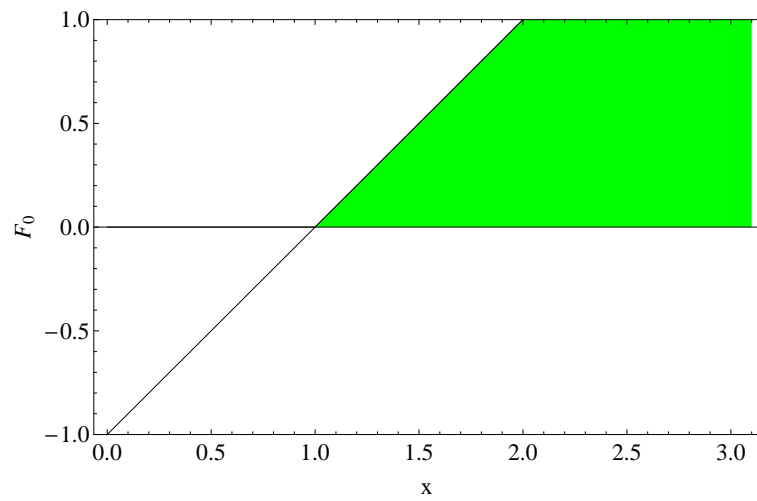
Figure 6.5: Regions where pair production is kinematically allowed ($F_0(x; \alpha_1^0) \geq 0$) for $\alpha_1^0 = 0$ (Lorentz invariant case).
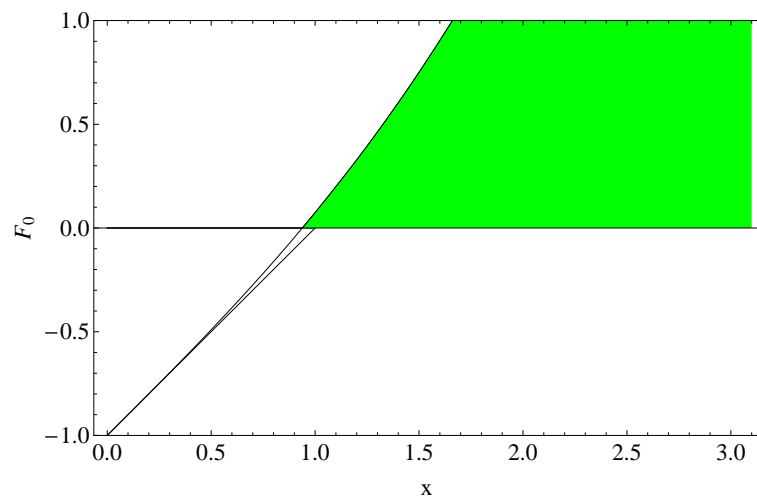

Figure 6.6: Regions where pair production is kinematically allowed ($F_0(x; \alpha_1^0) \geq 0$) for $\alpha_1^0 > 0$.
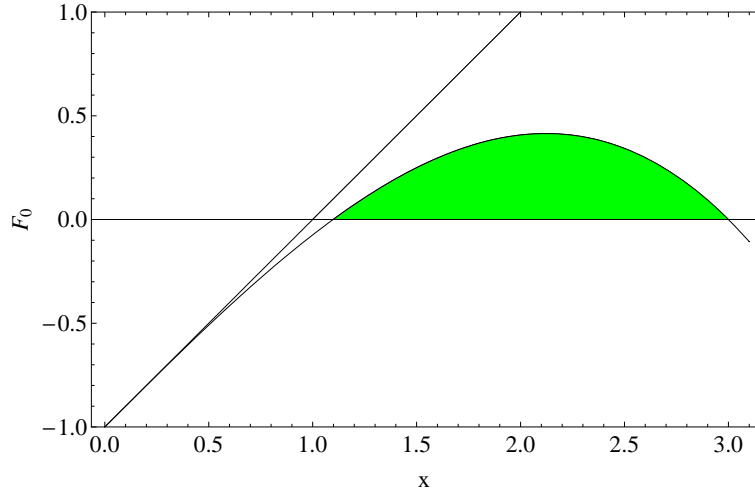
Figure 6.7: Regions where pair production is kinematically allowed $(F_0(x; \alpha_1^0) \geq 0)$ for $\alpha_1^0 < 0$.

the modified dispersion relation Eq. (6.1), pair production is kinematically allowed above a threshold $k_{\mathrm{LI}} x_n^l(\alpha_n^0) < k_{\mathrm{LI}}$, see Figs. 6.5 and 6.6.

Otherwise, if the coefficient of x^{n+2} in Eq. (6.24) is negative, this equation has real solutions only if $|\alpha_n^0| \leq \alpha_n^{0,cr} \equiv (n+1)^{n+1} / (n+2)^{n+2}$. In particular, if $|\alpha_n^0| = \alpha_n^{0,cr}$ there is only one real solution and pair production is kinematically allowed only for a particular value of the momentum of the ultra-high-energy photon. If $|\alpha_n^0| < \alpha_n^{0,cr}$, there are two real solutions, $0 < x_n^l(\alpha_n^0) < x_n^u(\alpha_n^0)$, and thus pair production is only allowed in the range of energies $k_{\mathrm{LI}} x_n^l(\alpha_n^0) \leq \omega \leq k_{\mathrm{LI}} x_n^u(\alpha_n^0)$ (see Fig 6.7). These different cases are summarized in Fig. 6.8.

Requiring pair production to be allowed, we obtain constraints only from photons with a negative sign in the modified dispersion relation, because for photons with a positive LI breaking term, pair production is allowed for any value of α_n^0 above $k_{\mathrm{LI}} x_n^l(\alpha_n^0) < k_{\mathrm{LI}}$. We also stress that photons with negative LI breaking term are stable against *photon decay* $(\gamma \to e^+ e^-)$ and *photon splitting* $(\gamma \to N\gamma)$.

Requiring the interaction of ultra-high-energy photons, $10^{19}\,\mathrm{eV} \lesssim k \lesssim$
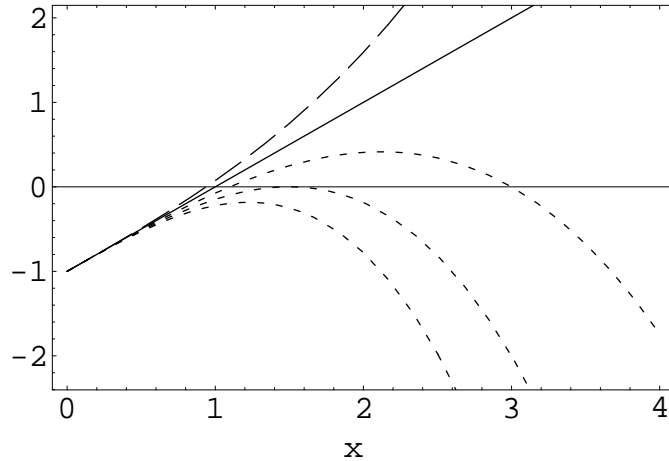
Figure 6.8: Plot of $F_0(x; \alpha_1^0)$ fixed different values of α_1^0. Dashed line: photons with a positive LI breaking term $\alpha_1^0 = 2/27$; continuous line: photons with unbroken LI, $\alpha_1^0 = 0$; dotted line: photons with a negative LI breaking term, with $\alpha_1^0 = -6/27$, $-4/27$, $-2/27$, in ascending order. Pair production is kinematically allowed for values of x for which the curves are positive.

10^{20} eV, with CMB photons of energy $\omega_b \simeq 6 \times 10^{-4}$ eV corresponds to requiring that pair production is kinematically allowed for $2.3 \times 10^4 \lesssim x \lesssim 2.3 \times 10^5$. Since photons with a negative LI breaking term in the dispersion relation have both a lower and an upper energy threshold for pair production, denoted by $x_n^l(\alpha_n^0)$ and $x_n^u(\alpha_n^0)$, respectively, we have the two conditions $x_n^l(\alpha_n^0) \lesssim 2.3 \times 10^4$ and $2.3 \times 10^5 \lesssim x_n^u(\alpha_n^0)$. These will lead to constraints on α_n^0 and thus ξ_n.

Constraints on Lorentz invariance breaking to first order in the Planck mass. In this case $n = 1$ and the first condition, $x_1^l(\alpha_1^0) \lesssim 2.3 \times 10^4$ is always true if the lower threshold exists, $\alpha_1^0 > -\alpha_1^{0,cr} = -4/27$. The second condition $2.3 \times 10^5 \lesssim x_1^u(\alpha_1^0)$ is fulfilled if $\alpha_1^0 \gtrsim -1.9 \times 10^{-11}$. These two necessary conditions can be translated into a constraint for ξ_1 using the definition for α_n^0, Eq. (6.25), and $k_{\text{LI}} \simeq 4.4 \times 10^{14}$ eV :

$$\alpha_1^0 \equiv \xi_1 \frac{k_{\mathrm{LI}}}{4\omega_b} \left(\frac{k_{\mathrm{LI}}}{M_{\mathrm{pl}}} \right) \gtrsim -1.9 \times 10^{-11} \,; \quad \xi_1 \gtrsim -2.4 \times 10^{-15} \,. \qquad (6.26)$$

In this case effective field theory requires LI violating terms in the dispersion relation with opposite sign for left and right polarized photons [144]. Therefore, in order to avoid photon fractions in cosmic rays $\gtrsim 5$ times higher than observed above $\sim 10^{19} \,\mathrm{eV}$, pair production has to be allowed for both polarizations, and thus for both signs in the dispersion relation. Thus the constraint obtained for $\xi_1 < 0$ is valid also for positive LI violating terms: $|\xi_1| \lesssim 2.4 \times 10^{-15}$.

Constraints on Lorentz invariance breaking to second order in the Planck mass. In this case $n = 2$ and the first condition, $x_2^l (\alpha_2^0) \lesssim 2.3 \times 10^4$ is always true if the lower threshold exists, $\alpha_2^0 > -\alpha_2^{0,cr} = -27/256$. The second condition $2.3 \times 10^5 \lesssim x_2^u (\alpha_2^0)$ is fulfilled if $\alpha_2^0 \gtrsim -8.2 \times 10^{-17}$. These two necessary conditions then lead to the following constraint for ξ_2

$$\alpha_2^0 \equiv \xi_2 \frac{k_{\mathrm{LI}}}{4\omega_b} \left(\frac{k_{\mathrm{LI}}}{M_{\mathrm{pl}}} \right)^2 \gtrsim -8.2 \times 10^{-17} \,; \quad \xi_2 \gtrsim -2.4 \times 10^{-7} \,. \qquad (6.27)$$

For interactions with the URB, $k_{\mathrm{LI}} \simeq 6 \times 10^{19} \,\mathrm{eV}$, we obtain the constraint assuming the existence of at least one solution with $x_n^l(\alpha_n^0) \lesssim 2$. This eventually leads to the conditions $|\xi_1| \lesssim 7.2 \times 10^{-21}$ at first order, and $-\xi_2 \lesssim 8.5 \times 10^{-13}$ at second order. These are several orders of magnitudes more restrictive than the constraints Eqs. (6.26) and (6.27) obtained in the CMB case. Therefore, if the constraints from interactions with the CMB are violated, there would also be no interaction with the URB and so no pair production on any relevant background. Thus the constraint from pair production with the CMB is not modified by the presence of the URB.

6.6 Lorentz violation in QED and ultrahigh-energy photons

Current upper limits on the photon fraction in the energy range between $\simeq 10^{19}\,\text{eV}$ and $\simeq 10^{20}\,\text{eV}$ already establish strong constraints on the LIV parameters in the cases $n = 1$ and $n = 2$ (see previous section, and Ref. [157]).

If photon decay is forbidden, pair production must be kinematically allowed for both high energy photon polarizations, otherwise the predicted photon flux would be too high. According to the current non-detection of UHE photons [136] this leads to the condition that the lower threshold for pair production must be below $\simeq 10^{19}\,\text{eV}$ and the upper threshold for pair production must be above $\simeq 10^{20}\,\text{eV}$. At the threshold the pair can be produced only in s-waves, whereas higher partial waves are forbidden. Above the lower threshold and below the upper threshold the pairs can also be produced in higher partial waves which, therefore, also have to be considered. In fact, at energies that are factors of a few away from the thresholds, say at $\simeq 3 \times 10^{19}\,\text{eV}$, the pair is produced with relative velocities not much smaller than the speed of light and, without doing a detailed calculation, higher partial waves are thus not expected to be significantly suppressed. Therefore, according to Tab. 6.1, all three LIV parameters enter the problem. The experimental upper limits on the UHE photon flux require that a given combination $(\xi_n, \eta_n^+, \eta_n^-)$ of LIV parameters is ruled out if at least one photon polarization state is stable against decay and does not pair produce for any helicity configurations of the final pair. Taking into account higher partial waves for pair production then leads to conservative constraints because only these parameter combinations are ruled out that do not lead to pair production into any of the final state configurations shown in Tab. 6.1.

If a UHE photon were detected and its polarization were not measured, then there should be at least one polarization state that is stable over macroscopic time scales. Then the LIV parameter region where photon decay is kinematically allowed for at least one helicity configuration of the final state

electron-positron pair, for both photon polarizations, would be ruled out.

Note that at the threshold for pair production, where only the s-wave channel is allowed, according to Tab. 6.1, only opposite helicities for electron and positron contribute and the kinematics depends on only one fermionic LIV parameter, either η_n^+ or η_n^-. In contrast, at the threshold for photon decay, where the photon, electron and positron momenta are all parallel, only equal helicities for electron and positron contribute and the kinematics depends on all two fermionic LIV parameters, since total angular momentum cannot be conserved if electron and positron have opposite helicity. For photon decay, therefore, even at the threshold only the assumption of an additional relation between the electron LIV parameters for different helicities, e.g. $\eta_n^+ = \eta_n^-$, leads to a reduction of the kinematics to only one fermionic LIV parameter.

6.6.1 Case $n = 1 - \mathcal{O}(p/M_{\mathrm{pl}})$ modifications of the dispersion relations

For first order suppression in the Planck scale, the excluded LIV parameters resulting from the current non-detection of a photon component of cosmic rays in the energy range between 10^{19} eV and 10^{20} eV are shown in Fig. 6.9. The excluded parameter region is symmetric with respect to a sign change of the photon LIV parameter ξ_1 because pair production must be allowed for both photon polarizations which correspond to opposite signs of ξ_1 for $n = 1$. Note that if the absolute values of the LIV parameters η_1^+ and η_1^- for electrons and positrons are smaller than the one for the LIV parameter for photons, parameters of size $|\xi_1| \gtrsim 10^{-14}$ are ruled out.

For the parameter range shown in Fig. 6.10 photons of energy $E \sim 10^{19}$ eV and of both polarizations would be unstable. Thus, if a $\sim 10^{19}$ eV photon were detected without determining its polarization, this parameter range would be excluded. The allowed parameter range has the structure of a double-cone and is symmetric with respect to a sign change of the photon LIV parameter ξ_1 because opposite photon polarizations correspond to op-
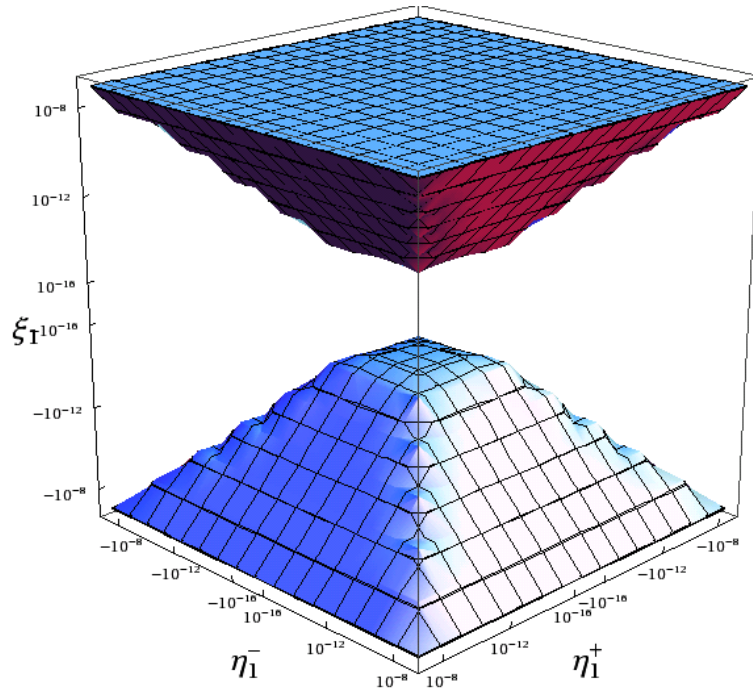
Figure 6.9: Case $n = 1$. Region excluded by present upper limits on the UHE photon flux ($10^{19}\,\mathrm{eV} \lesssim \omega \lesssim 10^{20}\,\mathrm{eV}$).

posite signs of ξ_1 and within our conservative treatment only one photon polarization needs to be stable. As a result, the region that would be excluded by a $\sim 10^{19}$ eV photon detection is also symmetric with respect to a sign change of ξ_1. The resulting constraints would be very strong: If, for example, $|\xi_1| \ll |\eta_1^\pm|$, then $|\eta_1^\pm| \gtrsim 10^{-16}$ would be excluded.

The sign and parameter combinations entering the kinematics in Tab. 6.1 lead to additional symmetries of parameter ranges excluded and allowed by pair production and/or photon decay under sign changes of η_1^+ or η_1^- and under exchange of η_1^+ and η_1^-.

As Figs. 6.9 and 6.10 show, combining both constraints from UHE photon flux limits and detection of an UHE photon it would be possible to rule out all LIV parameters of absolute value larger than 10^{-14}.

Fig. 6.11 shows, for the same range of LIV parameters studied in Figs. 6.9
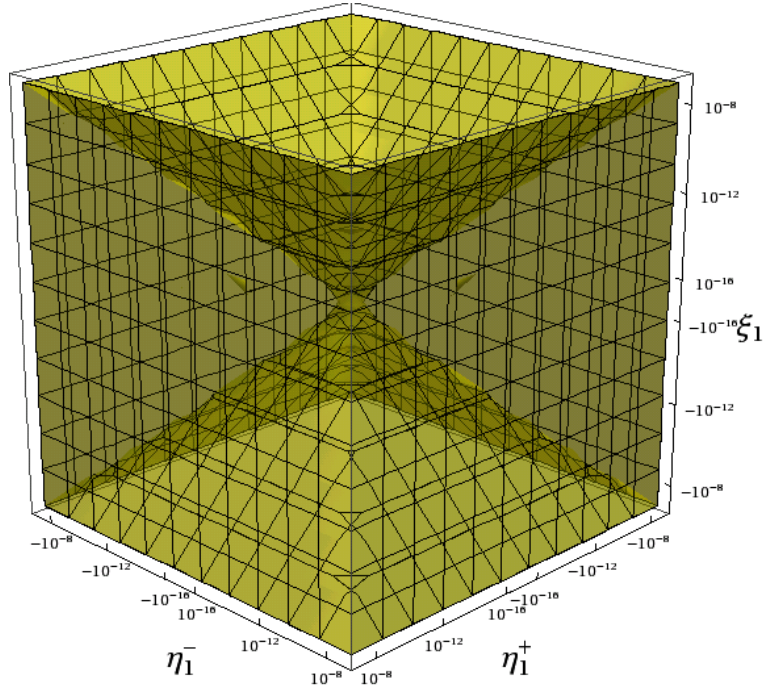
Figure 6.10: Case $n = 1$. Region excluded if a 10^{19} eV photon were detected (shaded). The allowed region has the shape of a double-cone centered at the origin and opening towards the positive and negative ξ_1-directions.

and 6.10, a typical two dimensional section, $\eta_1^+ = \eta_1^-$, of the excluded regions. This section is relevant if only one leptonic LIV parameter enters the kinematics Eqs. (6.6) and (6.20). According to Tab. 6.1 this occurs very close to the threshold where only s-waves contribute to pair production and electrons and positrons thus have opposite helicity [157]. Alternatively, the section $\eta_1^+ = \eta_1^-$ is relevant also away from the threshold if the general (restrictive) assumption is made that the LIV parameter for a positive helicity electron is equal to the LIV parameter for a negative helicity electron ($\eta_1^+ = \eta_1^-$). Note, however, at least in the $n = 1$ case considered, that the order of magnitude of the largest LIV parameters allowed does not depend on any particular relation assumed between η_1^+ and η_1^-: Parameters of absolute value larger than 10^{-14} are always ruled out.
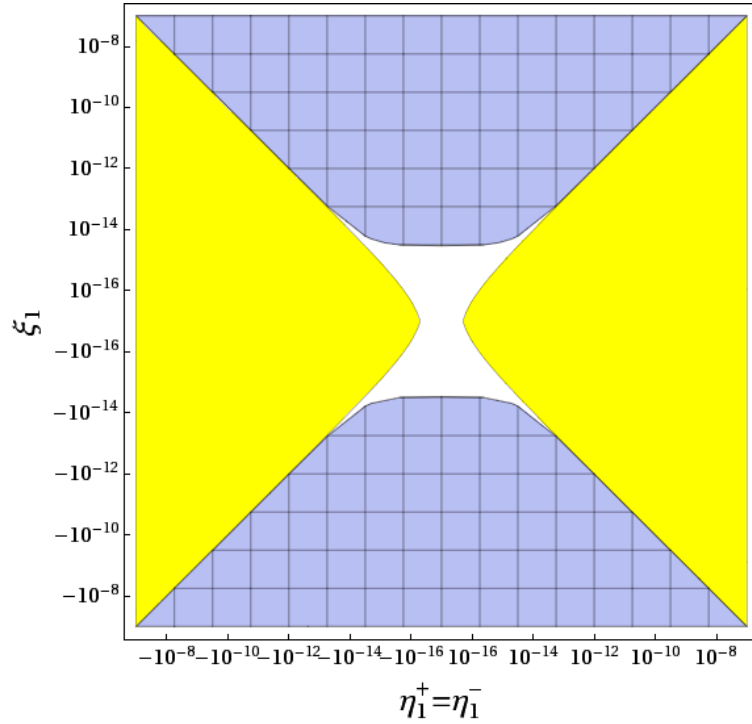
Figure 6.11: Case $n = 1$, $\eta_1^+ = \eta_1^-$. Combined constraint using both the current upper limits on the photon fraction in the energy range between 10^{19} eV and 10^{20} eV (blue shaded, checkered region), and assuming that a 10^{19} eV photon were detected (yellow shaded region).

Fig. 6.12 shows, for the case $\eta_1^+ = \eta_1^-$, how the uncertainties in the photon fraction limits influence the constraints on LIV parameters. Lowering the maximum energy, up to which we consider the bounds on the photon flux meaningful, from 10^{20} eV to 5×10^{19} eV, the excluded region is slightly reduced.

6.6.2 Case $n = 2 - \mathcal{O}(p^2/M_{\mathrm{pl}}^2)$ modifications of the dispersion relations

The relations between the LIV parameters of photons with opposite polarization ($\xi_2^+ = \xi_2^-$), and between the LIV parameters of electrons and positrons
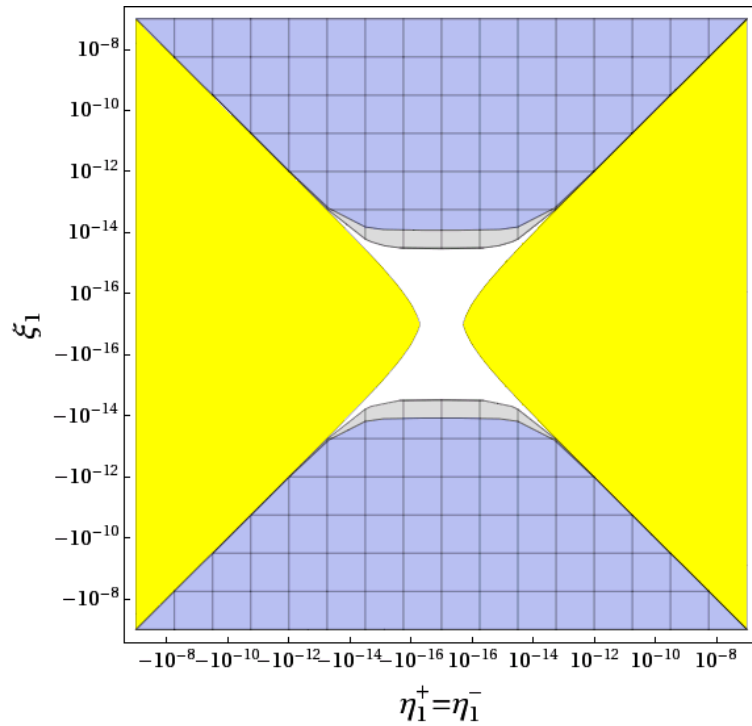
Figure 6.12: Case $n = 1$, $\eta_1^+ = \eta_1^-$. Combined constraint using the current upper limits on the photon fraction in the energy range between 10^{19} eV and 10^{20} eV (gray plus blue shaded, checkered regions), in the energy range between 10^{19} eV and 5×10^{19} eV (blue region), and assuming that a 10^{19} eV photon were detected (yellow shaded region).
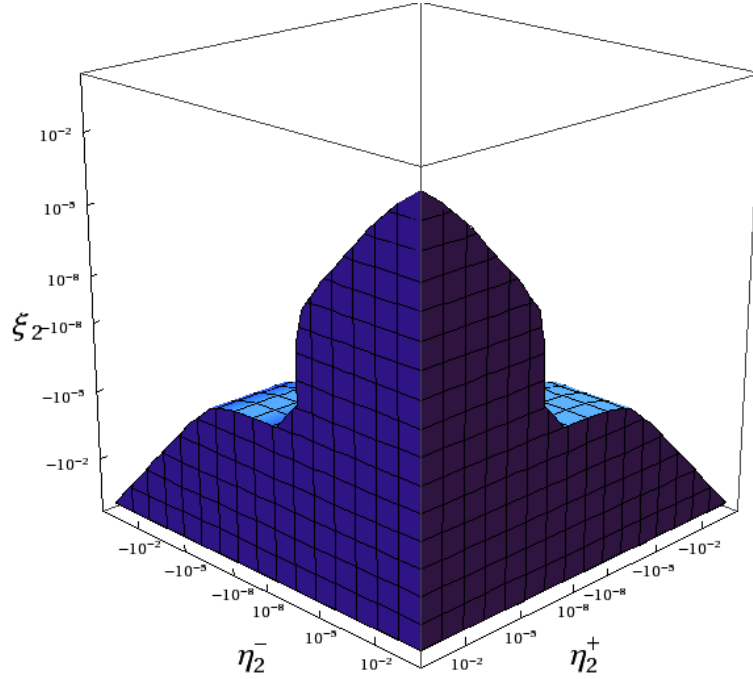
Figure 6.13: Case $n = 2$. Region excluded by present upper limits on the UHE photon flux ($10^{19}\,\mathrm{eV} \lesssim \omega \lesssim 10^{20}\,\mathrm{eV}$).

($\eta_2^{\mathrm{p};\pm} = \eta_2^{\mathrm{e};\mp}$) have opposite sign with respect to the $n = 1$ case, because second order Planck scale suppressed modifications of the dispersion relations correspond to CPT-even LIV operators. Therefore, for given polarizations of the incoming photon and given helicities of the final electron positron pair, the signs of the parameters appearing in the kinematic equations for pair production and for photon decay are different from the case $n = 1$, see Tab. 6.1. As a result, the region of the LIV parameter space ruled out for $n = 2$ is not only smaller than the one for $n = 1$, but also has a different shape. In particular, it does not exhibit the symmetry under sign changes of either one of the three LIV parameters ξ_2, η_2^+ or η_2^-.

The current non-detection of UHE photons require that photons in the energy range between 10^{19} eV and 10^{20} eV are subject to pair production, and the resulting excluded range of $n = 2$ LIV parameters is shown in Fig. 6.13.
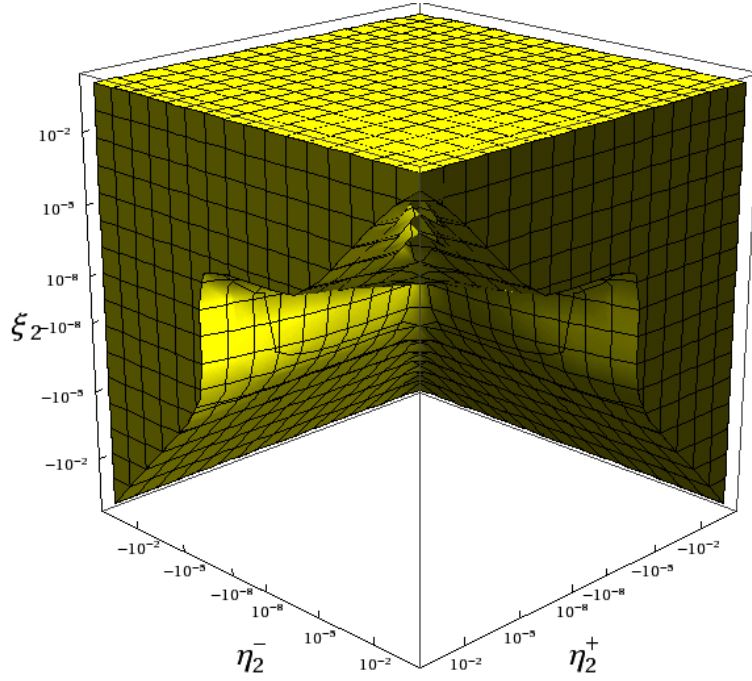
Figure 6.14: Case $n = 2$. Region excluded if a 10^{19} eV photon were detected.

Note that if $\left|\eta_2^+\right|$ and $\left|\eta_2^-\right|$ for electrons and positrons are smaller than $|\xi_2|$, then $\xi_2 \lesssim -10^{-6}$ is ruled out.

Fig. 6.14 shows the excluded region if a 10^{19} eV photon were detected in the future, and Fig. 6.15 represents the combination of the two regions that would then be excluded.

Differently from the $n = 1$ case the excluded region does not surround the origin in all directions, therefore these two conditions do not rule out all LIV parameters larger than a certain value. The shape of the excluded region now strongly depends on the particular relation between the electron LIV parameters. We consider here, for the same range of LIV parameters, three different two dimensional sections of the excluded region of Fig. 6.15, namely $\eta_2^+ = \eta_2^-$, $\eta_2^+ = -\eta_2^-$, and $\eta_2^- = 0$.

The first one, shown in Fig. 6.16, corresponds to the particular case where the LIV parameters for electrons do not depend on helicity ($\eta_2^+ = \eta_2^-$),
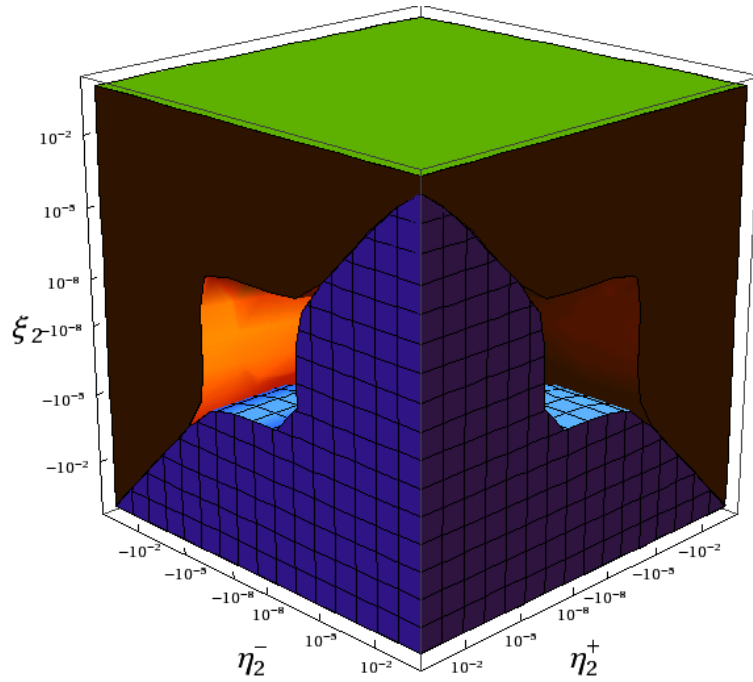
Figure 6.15: Case $n = 2$. Combined constraint using both the current upper limits on the photon fraction in the energy range between 10^{19} eV and 10^{20} eV (blue shaded, checkered region), and assuming that a 10^{19} eV photon were detected (uncheckered region).

such that only one leptonic LIV parameter enters the kinematics Eqs. (6.6) and (6.20). As for the case $n = 1$, Tab. 6.1 shows that this section is relevant very close to the threshold where electron and positron have opposite helicity since only s-waves contribute to pair production [157]. In this case all LIV parameters of absolute value larger than $\sim 10^{-6}$ are ruled out in agreement with Ref. [157]. Away from the threshold, the section $\eta_2^+ = \eta_2^-$ is relevant only under the restrictive assumption that the electron LIV parameters are equal for both polarizations. For this particular section we also estimate in Fig. 6.17 how uncertainties on the energy range of the upper limits on the flux of UHE photons modify the constrained region.

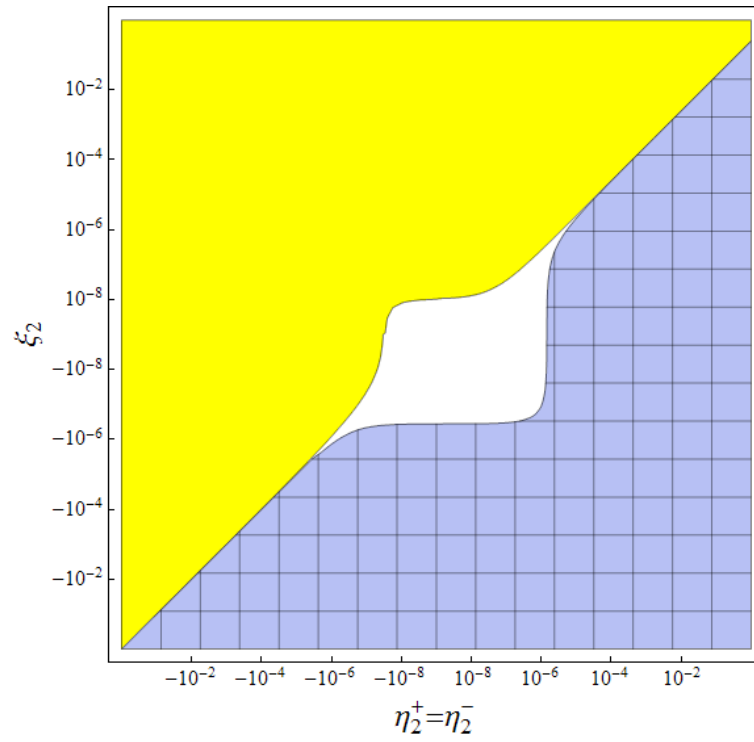An orthogonal cut corresponds to the case where the LIV parameter

Figure 6.16: Case $n = 2$, $\eta_2^+ = \eta_2^-$. Combined constraint using both the current upper limits on the photon fraction in the energy range between 10^{19} eV and 10^{20} eV (blue shaded, checkered region), and assuming that a 10^{19} eV photon were detected (yellow shaded region).
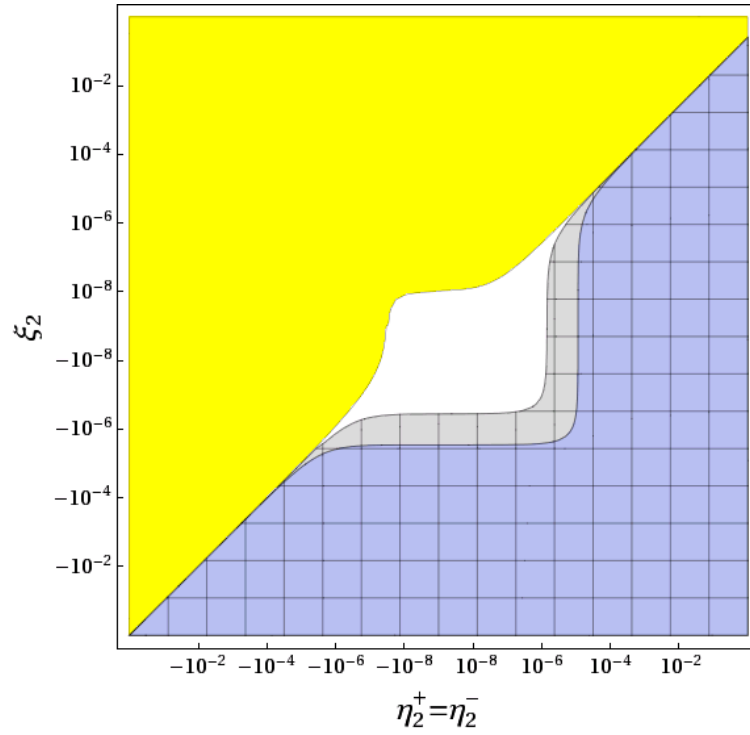
Figure 6.17: Case $n = 2$, $\eta_2^+ = \eta_2^-$. Combined constraint using the current upper limits on the photon fraction in the energy range between 10^{19} eV and 10^{20} eV (gray plus blue regions), in the energy range between 10^{19} eV and 5×10^{19} eV (blue shaded, checkered region), and assuming that a 10^{19} eV photon were detected (yellow shaded region).
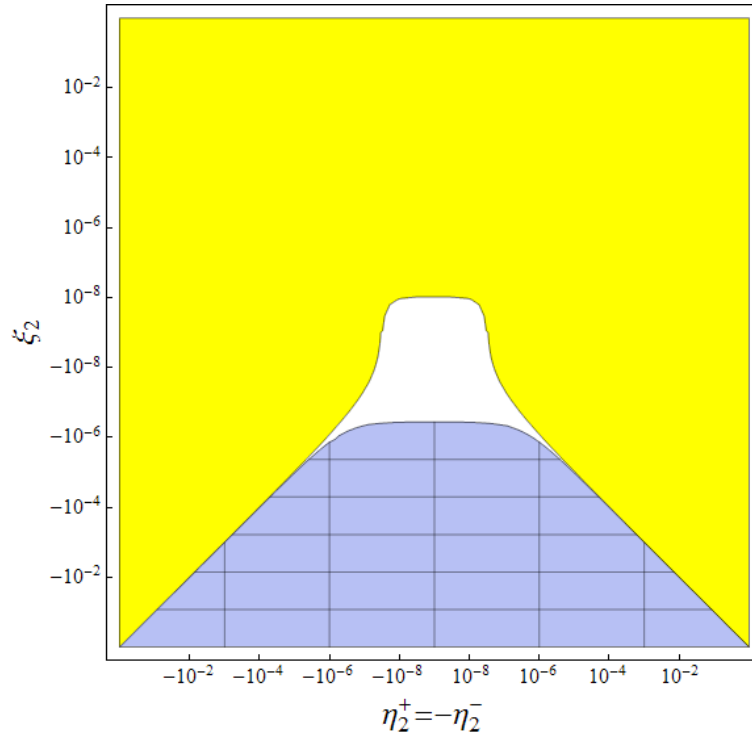
Figure 6.18: Case $n = 2$, $\eta_2^+ = -\eta_2^-$. Combined constraint using both the current upper limits on the photon fraction in the energy range between 10^{19} eV and 10^{20} eV (blue shaded, checkered region), and assuming that a 10^{19} eV photon were detected (yellow shaded region).
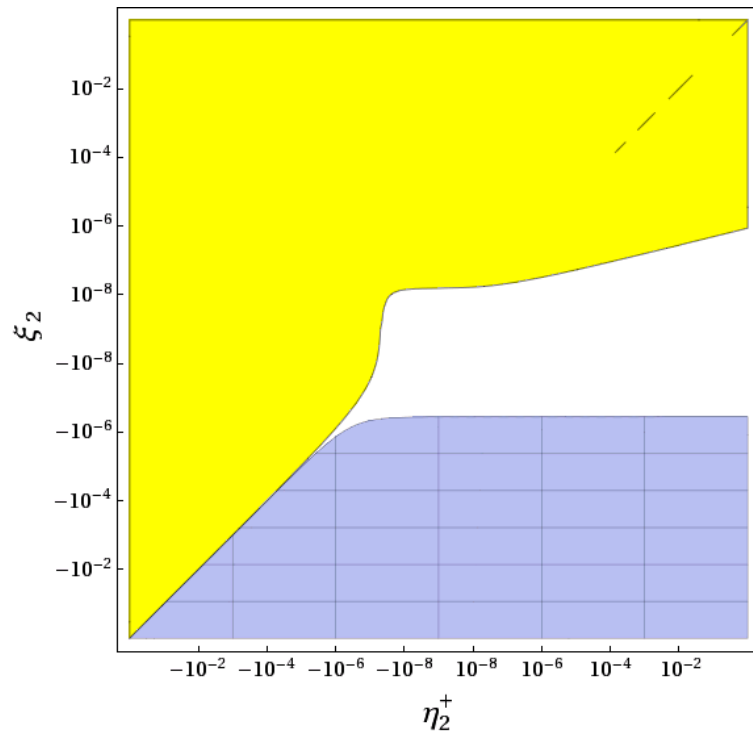
Figure 6.19: Case $n = 2$, $\eta_2^- = 0$. Combined constraint using both the current upper limits on the photon fraction in the energy range between 10^{19} eV and 10^{20} eV (blue shaded, checkered region), and assuming that a 10^{19} eV photon were detected (yellow shaded region).

for positive helicity electrons is opposite equal to the LIV parameter for negative helicity electrons, $\eta_2^+ = -\eta_2^-$, see Fig. 6.18. The shapes of the two excluded regions are modified with respect to Fig. 6.16: The region of the LIV parameter space ruled out by the detection of a 10^{19} photon increases, while the region excluded by the current upper limits on the flux of UHE photon decreases. However, also in this case, all LIV parameters of absolute value larger than $\sim 10^{-6}$ can be ruled out.

Fig. 6.19 represents the excluded region in the $\eta_2^- = 0$ plane: The shapes of the two excluded regions change, moreover, it is no more possible to rule out all LIV parameters of absolute value larger than $\sim 10^{-6}$. If $|\xi_2| \lesssim 10^{-6}$, arbitrarily large $\left|\eta_2^+\right|$ are currently not excluded, and even if a $\sim 10^{19}\,\text{eV}$ photon were detected in the future, arbitrarily large positive η_2^+ could still not be excluded.

Note that this is true not only in the $\eta_2^- = 0$ plane, but whenever the absolute values of the LIV parameters of both the photon (ξ_2) and of one of the lepton sector (η_2^+ or η_2^-) are smaller than $\sim 10^{-6}$, see Fig. 6.15: It is then no more possible to exclude all LIV parameters with modulus larger than a certain threshold.

As an application, the current constraints based on the non-detection of UHE photons rule out any possible interpretation of flares of the active galaxy Markarian 501 in terms of quantum gravity effects [166] within the effective field theory approach with exact energy-momentum conservation assumed in the present work. Such an interpretation would be based on an energy dependent index of refraction in vacuum such that the speed of light is modified to $v(\omega) = 1 + \xi_1(\omega/M_{\text{pl}}) + \xi_2(\omega/M_{\text{Pl}})^2$ and would require $\xi_1 \lesssim -25$ or $\xi_2 \lesssim -3 \times 10^{16}$, clearly ruled out by our constraints. Note, however, that the constraints obtained here do not apply to particular scenarios, such as quantum-gravitational foam models, in which energy fluctuates due to non-trivial particle recoil off excitations in the string/D-particle foam [167, 168].

6.7 Conclusions

In this chapter we derived general constraints on LIV dispersion relations in the QED sector from the propagation of UHE photons. The kinematics of pair production and photon decay is discussed in terms of all three LIV parameters ξ_n, η_n^+ and η_n^- both for linear ($n = 1$) and for second order ($n = 2$) suppression with the Planck scale.

The upper limits on the flux of UHE photons require that combinations of the LIV parameters for which the UHE photons are stable and cannot pair produce on low-energy (e.g. CMB) photons are excluded. Similarly, the detection of photons of $\sim 10^{19}$ eV would exclude those combinations of the LIV parameters for which both photon polarizations are unstable.

For terms in the dispersion relation linearly suppressed by the Planck scale the resulting constraints are very strong: Using the non-detection of an UHE photon flux and anticipating the detection of a $\sim 10^{19}$ eV photon, it will be possible to exclude all LIV parameters with absolute value $\gtrsim 10^{-14}$.

In contrast, in the $n = 2$ case, the LIV parameter region excluded using these arguments based on UHE photon propagation does not completely surround the origin. If UHE photons are eventually detected, the maximum absolute value allowed for LIV parameters in the photon sector will be $\sim 10^{-6}$, whereas currently only values smaller than $\sim -10^{-6}$ are ruled out. However, even if UHE photons were detected, constraints on the electron parameters can be evaded for some particular combinations: If, for example, the modulus of one of the two parameters η_2^+ or η_2^- is smaller than $\sim 10^{-6}$, then the modulus of the other parameter is constrained neither by the upper limit on the UHE photon flux nor by a putative future detection of a $\sim 10^{19}$ eV photon. However, the case where the moduli of both η_2^+ and η_2^- are $\gtrsim 10^{-6}$ can still be excluded once UHE photons are detected.

Conclusions

In this thesis we have shown how light propagation can be used in order to constrain particle physics models beyond the Standard Model. We have studied in particular the effects of non standard physics on the polarization of cosmic microwave background radiation and on the flux of ultrahigh energy γ-rays.

In the first part we have discussed the consequences of coupling between cosmological pseudoscalar fields and photons. In particular we have paid attention to the rotation of linear polarization plane from last scattering surface to nowadays. This rotation, induced by the photon-pseudoscalar interaction, modifies the gradient and curl of the polarization pattern (E and B following [22]), creating B modes from E modes. The parity violating nature of the interaction generates also non-zero parity-odd correlators (TB and EB) which would be otherwise vanishing in the standard Gaussian cosmological case [16, 23]. In particular the TB power spectrum may be very useful to constrain the coupling constant g_ϕ between photons and pseudoscalars, since it is larger than the auto and cross power spectra in polarization; these non-standard correlators are already constrained by present data sets [6, 33, 34]. We have modified the public code CAMB [4] in order to take into account the rotation of linear polarization plane by a cosmological pseudoscalar field coupled with photons. We have studied in detail two representative examples for the dynamics of a pseudo Nambu-Goldstone field behaving as dark matter (cosine type and exponential potential) and one behaving as dark energy (ultralight pseudoscalar field). In these three cases the polarization

power spectra generated by the modified version of CAMB for cosmological birefringence have been compared with the ones obtained in the widely used approximation in which the linear polarization rotation angle is assumed constant in time. The cosine type potential leads to an oscillating behaviour of the pseudoscalar field (e.g. axion), in this case we have shown how CMB cosmological birefringence constraints, based on current data sets, can become important for small masses. In the exponential potential case the pseudoscalar field monotonically decreases; present CMB observations constrain the coupling constant g_ϕ to small values as $\mathcal{O}\left(10^{-30}\right)$ eV, if backward moving waves can be neglected. For ultralight pseudo Nambu-Goldstone bosons acting as dark energy effects are smaller and further detailed investigation is needed.

We are planning to extend these considerations to scalar fields predicted by particle physics models (e.g. dark energy chameleons, ...) in order to study how theoretical predictions change with respect to those based on pseudoscalar fields.

In the second part of this thesis we have used the current upper limits on the flux of ultrahigh-energy photons in order to constrain Lorentz violating terms in the dispersion relations of photons, electrons and positrons. Many Quantum Gravity theories suggest indeed the breaking of Lorentz invariance with the strength of the effects increasing with energy. The most promising experimental tests of such theories, therefore, exploit the highest energies at our disposal which are usually achieved in violent astrophysical processes: the propagation of photons, electrons and positrons at ultrahigh energies (above $\sim 10^{19}$ eV) can be considerably changed if the dispersion relations of these particles are slightly modified. First we have pointed out that the current non-observation of photons in the ultrahigh energy cosmic ray flux at such energies can put strong constraints on such modified dispersion relations. Written the photon dispersion relation in the form $\omega^2 = k^2 + \xi_n k^2 (k/M_{\text{Pl}})^n$, with new terms suppressed by a power n of the Planck mass M_{Pl}, we have shown that first and second order terms of size $|\xi_1| \gtrsim 10^{-14}$ and $\xi_2 \lesssim -10^{-6}$,

respectively, would lead to a photon component in cosmic rays above 10^{19} eV that should already have been detected. Subsequently we have generalized these constraints to all three Lorentz invariance breaking parameters that can occur in the dispersion relations for photons, electrons and positrons at first and second order suppression with the Planck scale. We have also shown how the excluded regions in these three-dimensional parameter space would be extended if ultrahigh energy photons were detected in the future.

In principle, Lorentz violation for other elementary particles can be constrained by using similar arguments. We are planning to estimate the effects of modified dispersion relation for neutrinos, in this case, ultrahigh-energy neutrino telescopes data can be used in order to improve bounds on possible Lorentz violation terms for these particles.

Appendix A

Systematics of CMBP

We present here a summary of conventions and some results of Refs. [169, 170, 171] following the presentation given in Ref. [13].

Polarization effects are divided into two categories:

1. those which are associated with transfer between polarization states of the incoming radiation, mainly induced by *the detector system* (see section A.1);

2. those which are associated with the anisotropy of CMB polarization and temperature, mainly induced by *the finite resolution or beam of the telescope* (see section A.2).

A.1   Detector system

In this section we describe the action of detector on the polarization of the radiation passing through it. We refer mainly to three papers:

1. "Benchmark parameters for CMB polarization experiments," W. Hu, M. M. Hedman and M. Zaldarriaga [169];

2. "Systematic errors in cosmic microwave background polarization measurements," D. O'Dea, A. Challinor and B. R. Johnson [170];

3. "A study of CMB differencing polarimetry with particular reference to Planck," J. P. Hamaker, J. P. Leahy [171].

Polarization transfer: an introduction to Jones matrices [169]

The polarization state of the radiation is described by the **intensity (or coherency) matrix** $\langle E_i E_j^* \rangle$ where $\mathbf{E}$ is the electric field vector and the brackets denote time averaging. As a hermitian matrix, it can be decomposed into the Pauli basis:

$$\begin{aligned} \mathbf{P} &= C \langle \mathbf{E}\mathbf{E}^\dagger \rangle \\ &= C \left(I\mathbf{I} + Q\sigma_3 + U\sigma_1 + V\sigma_2 \right) \\ &= C \begin{pmatrix} I+Q & U-iV \\ U+iV & I-Q \end{pmatrix} . \end{aligned} \qquad (A.1)$$

The instrumental response to the radiation modifies the incoming state before detection and is generally described by a **transfer or Jones matrix**:

$$\mathbf{E}_{\text{out}} = \mathbf{J}\,\mathbf{E}_{\text{in}} . \qquad (A.2)$$

Schematics and matrix operators for selected radiometer components are listed in Fig. A.1.

The polarization matrix is then transformed as:

$$\mathbf{P}_{\text{out}} = \mathbf{J}\mathbf{P}_{\text{in}}\mathbf{J}^\dagger . \qquad (A.3)$$

With an estimate of the transfer matrix of the instrumental response $\hat{\mathbf{J}}$, the incoming radiation can be recovered as:

$$\begin{aligned} \hat{\mathbf{P}}_{\text{in}} &= \hat{\mathbf{J}}^{-1}\mathbf{P}_{\text{out}}(\hat{\mathbf{J}}^\dagger)^{-1} \\ &= (\hat{\mathbf{J}}^{-1}\mathbf{J})\mathbf{P}_{\text{in}}(\hat{\mathbf{J}}^{-1}\mathbf{J})^\dagger . \end{aligned} \qquad (A.4)$$

The errors in the transfer matrix determination will then mix the determined Stokes parameters .

Ideally the transfer matrix of the components that split and couple the radiation into the detector is proportional to the identity matrix: $\hat{\mathbf{J}} \propto \mathbf{I}$. In
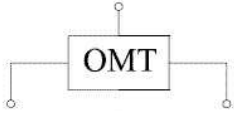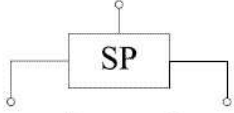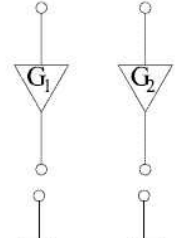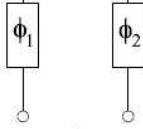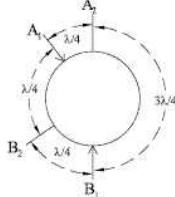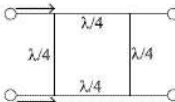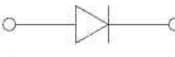
Component Name	Schematic/Symbol	Operator Equivalent
Orthomode Transducer	OMT	$\begin{bmatrix} 1 & 0 \\ 0 & 1 \end{bmatrix}$
Septum Polarizer (Circular Hybrid Polarizer)	SP	$\frac{1}{\sqrt{2}} \begin{bmatrix} 1 & i \\ i & 1 \end{bmatrix}$
Amplifiers	G_1 G_2	$\begin{bmatrix} G_1 & 0 \\ 0 & G_2 \end{bmatrix}$
Phase Shifters	ϕ_1 ϕ_2	$\begin{bmatrix} e^{i\phi_1} & 0 \\ 0 & e^{i\phi_2} \end{bmatrix}$
Magic Tee (180° Hybrid)		$\frac{1}{\sqrt{2}} \begin{bmatrix} 1 & 1 \\ 1 & -1 \end{bmatrix}$
Short-Slot Hybrid Coupler (90° Hybrid)		$\frac{1}{\sqrt{2}} \begin{bmatrix} 1 & i \\ i & 1 \end{bmatrix}$
Quarter-Wave Plate at Angle θ	N/A	$\frac{1}{\sqrt{2}} \begin{bmatrix} -\cos 2\theta - i & \sin 2\theta \\ \sin 2\theta & \cos 2\theta - i \end{bmatrix}$
Detection Devices		
Diode		$\begin{bmatrix} 1 & 0 \\ 0 & 0 \end{bmatrix}$ or $\begin{bmatrix} 0 & 0 \\ 0 & 1 \end{bmatrix}$
Multiplier		$\begin{bmatrix} 0 & 1 \\ 1 & 0 \end{bmatrix} = U$

Figure A.1: Schematics and matrix operators for selected radiometer components. Adopted from [172].
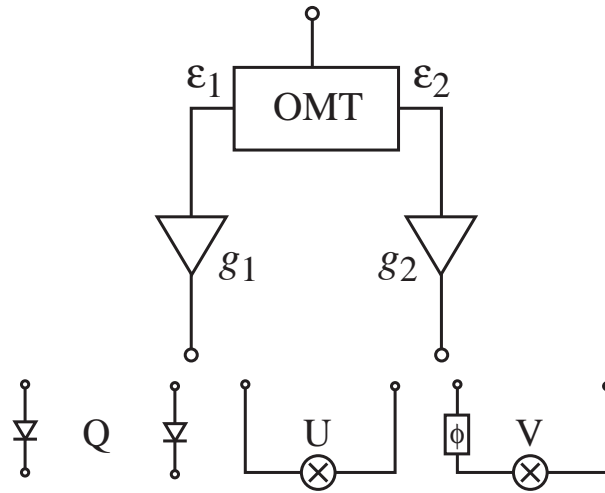
Figure A.2: Block diagram for simple polarimeters. The orthomode transducer (OMT) separates two orthogonal linear polarization states with a leakage (polconversion) between the two characterized by (ϵ_1, ϵ_2). After amplification with gain fluctuations (g_1, g_2) the polarization state is detected by one or more of the following techniques: *differencing the lines* to produce Q, *correlating the lines* to produce U, *correlating the lines with a phase shift* $\phi = \pi/2$ to produce V. The roles of Q and V may be interchanged by placing a quarter-wave plate at the front end. Figure taken from [169].

reality it contains systematic errors so that $\hat{\mathbf{J}}^{-1}\mathbf{J} \propto \mathbf{J}$. Let us parameterize these errors as [173]:

$$\hat{\mathbf{J}}^{-1}\mathbf{J} = \begin{pmatrix} 1 + g_1 & \epsilon_1 e^{i\phi_1} \\ \epsilon_2 e^{-i\phi_2} & (1 + g_2)e^{i\alpha} \end{pmatrix}, \qquad (A.5)$$

where:

- $g_{1,2}$ are fluctuations in the gains of the two lines;

- α is the phase difference between the lines;

- $\epsilon_{1,2}$ express the non-orthogonality or cross-coupling between the lines;

- $\phi_{1,2}$ are the phases of these couplings.

First consider the simple **differencing** of the time averaged intensity in the two lines under the assumption that $g_{1,2}$, $\epsilon_{1,2}$, $\alpha \ll 1$,

$$\begin{aligned} \delta Q &= \delta\left[\langle E_1 E_1^* \rangle - \langle E_2 E_2^* \rangle\right] \\ &= (g_1 + g_2)Q - (\epsilon_2 \cos\phi_2 - \epsilon_1 \cos\phi_1)U + (g_1 - g_2)I, \qquad (A.6) \end{aligned}$$

so:

- common-mode gain fluctuations act as a *normalization error* $a = (g_1 + g_2)$;

- the cross-couplings act as a *rotation* $\omega = (\epsilon_2 \cos\phi_2 - \epsilon_1 \cos\phi_1)/2$;

- differential gain fluctuations *leak temperature into polarization* $\gamma_1 = (g_1 - g_2)$.

For a **simple correlation polarimeter** the errors in the determination becomes:

$$\begin{aligned} \delta U &= \delta\left[\langle E_1 E_2^* \rangle + \langle E_2 E_1^* \rangle\right] \\ &= (g_1 + g_2)U + (\epsilon_2 \cos\phi_2 - \epsilon_1 \cos\phi_1)Q \\ &\quad + (\epsilon_1 \cos\phi_1 + \epsilon_2 \cos\phi_2)I, \qquad (A.7) \end{aligned}$$

so again:

- $a = (g_1 + g_2)$;

- $\omega = (\epsilon_2 \cos \phi_2 - \epsilon_1 \cos \phi_1)/2$;

but:

- the leakage from I into U is $\gamma_2 = (\epsilon_1 \cos \phi_1 + \epsilon_2 \cos \phi_2)$.

Instead of differential gain fluctuations, the cross-coupling between the lines is responsible for the monopole leakage in a correlation system. Notice that under the assumption:

- $\alpha \ll 1$;

- vanishing intrinsic circular polarization ($V = 0$);

the *phase error* α does not appear to first order.

When $\alpha = \pi/2$ the correlation polarimeter actually measures V not U. In general, the phase error α rotates U into V. A **complex correlation polarimeter** actually takes advantage of the (U,V) rotation to measure (Q,U) simultaneously:

1. circular polarization states are coupled into the lines using, for example a *quarter wave plate before the OMT* (this effectively converts Q into V in the instrument basis). The Jones matrix of the quarter wave plate is:

$$\mathbf{J}_{1/4}(\theta) = \frac{1}{\sqrt{2}} \begin{pmatrix} -\cos 2\theta - i & \sin 2\theta \\ \sin 2\theta & \cos 2\theta - i \end{pmatrix}, \qquad (A.8)$$

   where θ gives the orientation of the plate with respect to the OMT (ideally $\theta = \pi/4$).

2. After amplification, the signal can be coupled into *two different correlators*, which include different phase shifts between the lines.

3. These *additional phase shifts* can be represented with the transfer function:

$$\mathbf{J}_{\text{phase}}(\phi) = \begin{pmatrix} 1 & 0 \\ 0 & e^{i\phi} \end{pmatrix}. \qquad (A.9)$$

For one correlator ϕ is set to zero, yielding an estimate of U, while the other correlator has $\phi = \pi/2$, providing an estimate of Q.

Considering the effect of certain *imperfections*:

- the *actual transfer matrices* of the two correlations are:

$$
\begin{aligned}
\mathbf{J}_U &= \mathbf{J}_{\text{line}}(g_1, g_2, \epsilon_1, \epsilon_2)\mathbf{J}_{1/4}(\pi/4 + \beta)\,, \\
\mathbf{J}_Q &= \mathbf{J}_{\text{phase}}(\pi/2 + \psi)\mathbf{J}_{\text{line}}(g_1, g_2, \epsilon_1, \epsilon_2)\mathbf{J}_{1/4}(\pi/4 + \beta)\,,
\end{aligned}
$$

- the *assumed transfer matrices* are:

$$
\begin{aligned}
\hat{\mathbf{J}}_U &= \mathbf{J}_{1/4}(\pi/4)\,, \\
\hat{\mathbf{J}}_Q &= \mathbf{J}_{\text{phase}}(\pi/2)\mathbf{J}_{1/4}(\pi/4)\,,
\end{aligned}
$$

Then the errors become:

$$
\delta(Q \pm iU) = [(g_1 + g_2) \pm 2i\beta](Q \pm iU) + \psi U + (\epsilon_1 + \epsilon_2)\Theta\,. \qquad \text{(A.10)}
$$

there is an asymmetry between Q and U which is first order in the phase error ψ. More generally, a technique that simultaneously measures Q and U may have separate transfer properties (calibration, rotation, etc.) that appear as a coupling of opposite spin states $Q + iU$ and $Q - iU$. We will call such effects spin flip terms.

Receiver Müller matrices [170]

The Müller matrices describe the propagation of the Stokes parameters through the receiver element of a given observing system. Gathering the Stokes parameters in a Stokes vector $\mathbf{s} \equiv (I, Q, U, V)^T$, we have for the observed Stokes vector:

$$
\mathbf{s}_{\text{obs}} = \begin{pmatrix} M_{II} & M_{IQ} & M_{IU} & M_{IV} \\ M_{QI} & M_{QQ} & M_{QU} & M_{QV} \\ M_{UI} & M_{UQ} & M_{UU} & M_{UV} \\ M_{VI} & M_{VQ} & M_{VU} & M_{VV} \end{pmatrix} \mathbf{s}. \qquad \text{(A.11)}
$$

We adopt the convention here that Müller matrices are always expressed in the instrument basis. It is convenient to work with the **complex Müller matrix** whose elements have definite spin, i.e.

$$
\mathbf{p}_{\text{obs}} \;=\; \begin{pmatrix} M_{II} & M_{IP} & M_{IP^*} & M_{IV} \\ M_{PI} & M_{PP} & M_{PP^*} & M_{PV} \\ M_{P^*I} & M_{P^*P} & M_{P^*P^*} & M_{P^*V} \\ M_{VI} & M_{VP} & M_{VP^*} & M_{VV} \end{pmatrix} \mathbf{p} = \mathbf{M}\mathbf{p}\,, \qquad (A.12)
$$

where we have defined the **complex Stokes vector**:

$$
\mathbf{p} \;=\; \begin{pmatrix} I \\ Q + iU \\ Q - iU \\ V \end{pmatrix} = \begin{pmatrix} I \\ P \\ P^* \\ V \end{pmatrix}. \qquad (A.13)
$$

The components of this matrix are related to those in equation (A.11) as follows:

- for the total intensity I

$$
M_{IP} = \tfrac{1}{2}(M_{IQ} - iM_{IU}), \quad M_{IP^*} = \tfrac{1}{2}(M_{IQ} + iM_{IU}),
$$

- for the polarization P

$$
\begin{aligned}
M_{PI} &= M_{QI} + iM_{UI}, \quad M_{PV} = M_{QV} + iM_{UV}, \\
M_{PP} &= \tfrac{1}{2}(M_{QQ} + M_{UU}) + \tfrac{1}{2}i(M_{UQ} - M_{QU}), \\
M_{PP^*} &= \tfrac{1}{2}(M_{QQ} - M_{UU}) + \tfrac{1}{2}i(M_{UQ} + M_{QU});
\end{aligned}
$$

- for the polarization P^*

$$
\begin{aligned}
M_{P^*I} &= M_{PI}^*, & M_{P^*V} &= M_{PV}^*, \\
M_{P^*P} &= M_{PP^*}^*, & M_{P^*P^*} &= M_{PP}^*;
\end{aligned}
$$

- for the polarization V

$$
M_{VP} = \tfrac{1}{2}(M_{VQ} - iM_{VU}), \quad M_{VP^*} = \tfrac{1}{2}(M_{VQ} + iM_{VU}).
$$

Transformation properties of the Müller matrix under rotations of the instrument: 1. rotate the instrument by ψ; 2. simultaneously back-rotate the observed polarization; so we are describing the measured polarization in the original sky basis);

1. in its basis (rotated basis), the instrument sees incoming radiation with complex Stokes vector:

$$
\begin{pmatrix}
1 & 0 & 0 & 0 \\
0 & e^{-2i\psi} & 0 & 0 \\
0 & 0 & e^{2i\psi} & 0 \\
0 & 0 & 0 & 1
\end{pmatrix}
\begin{pmatrix}
I \\
P \\
P^* \\
V
\end{pmatrix}
= \mathbf{\Lambda}(\psi)\mathbf{p}\,,
\tag{A.14}
$$

2. the observed polarization in the sky (non rotated) basis is:

$$
\mathbf{p}_{\text{obs}}(\psi) = \mathbf{\Lambda}^\dagger(\psi)\mathbf{M}\mathbf{\Lambda}(\psi)\mathbf{p}\,.
\tag{A.15}
$$

Only the diagonal elements of $\mathbf{M}$ are invariant under $\mathbf{M} \mapsto \mathbf{\Lambda}^\dagger(\psi)\mathbf{M}\mathbf{\Lambda}(\psi)$. In the case of an *ideal instrument*, $\mathbf{M}$ is equal to the identity matrix and any systematic errors that affect the Stokes parameters will lead to small perturbations from this:

$$
\mathbf{p}_{\text{obs}} = \mathbf{M}\mathbf{p} =
\begin{pmatrix}
M_{II} & M_{IP} & M_{IP^*} & M_{IV} \\
\gamma_1 + i\gamma_2 & 1 + a + 2i\omega & f_1 + if_2 & w_1 + iw_2 \\
\gamma_1 - i\gamma_2 & f_1 - if_2 & 1 + a - 2i\omega & w_1 - iw_2 \\
M_{VI} & M_{VP} & M_{VP^*} & M_{VV}
\end{pmatrix}
\begin{pmatrix}
I \\
P \\
P^* \\
V
\end{pmatrix}
\tag{A.16}
$$

So:

$$
\begin{aligned}
\delta(Q + iU) &= \delta P_{\text{obs}} \\
&= P_{\text{obs}} - P \\
&= (\gamma_1 + i\gamma_2)I + (a + 2i\omega)P + (f_1 + if_2)P^* + (w_1 + iw_2)V\,,
\end{aligned}
$$

in general:

$$
\delta(Q \pm iU) = (a \pm 2i\omega)(Q \pm iU) + (f_1 \pm if_2)(Q \mp iU) + (\gamma_1 \pm i\gamma_2)I + (w_1 \pm iw_2)V\,.
\tag{A.17}
$$

- a: miscalibration of the polarization amplitude;

- ω: a rotation of the polarization orientation;

- f_1 and f_2: transformations between the two polarization spin states;

- γ_1 and γ_2: leakage from total intensity to Q and to U;

- w_1 and w_2: leakage from circular polarization.

Under a *rotation of the instrument* as described above:

$$
\begin{aligned}
\mathbf{p}_{\text{obs}} &= \mathbf{\Lambda}^\dagger(\psi)\mathbf{M}\mathbf{\Lambda}(\psi)\mathbf{p} \\
&= \begin{pmatrix}
M_{II}I & M_{IP}P & M_{IP^*}P^* & M_{IV}V \\
e^{2i\psi}(\gamma_1 + i\gamma_2)I & (1 + a + 2i\omega)P & e^{4i\psi}(f_1 + if_2)P^* & e^{2i\psi}(w_1 + iw_2)V \\
e^{-2i\psi}(\gamma_1 - i\gamma_2)I & e^{-4i\psi}(f_1 - if_2)P & (1 + a - 2i\omega)P^* & e^{-2i\psi}(w_1 - iw_2)V \\
M_{VI}I & M_{VP}P & M_{VP^*}P^* & M_{VV}V
\end{pmatrix}
\end{aligned}
$$

we find:

$$
\begin{aligned}
\delta(Q + iU) &= \delta P_{\text{obs}} \\
&= e^{2i\psi}(\gamma_1 + i\gamma_2)I + (a + 2i\omega)P + e^{4i\psi}(f_1 + if_2)P^* + e^{2i\psi}(w_1 + iw_2)V
\end{aligned}
$$

in general:

$$
\begin{aligned}
\delta(Q \pm iU) &= (a \pm 2i\omega)(Q \pm iU) + (f_1 \pm if_2)(Q \mp iU)e^{\pm 4i\psi} + (\gamma_1 \pm i\gamma_2)Ie^{\pm 2i\psi} \\
&+ (w_1 \pm iw_2)Ve^{\pm 2i\psi}. \tag{A.18}
\end{aligned}
$$

This suggests that the f, γ and w errors can be controlled with instrument rotation as these terms have different spin properties to the fields they are perturbing.

Receiver errors

Polarization Müller matrix elements for two common polarimeters that have particular relevance to CMB polarimetry:
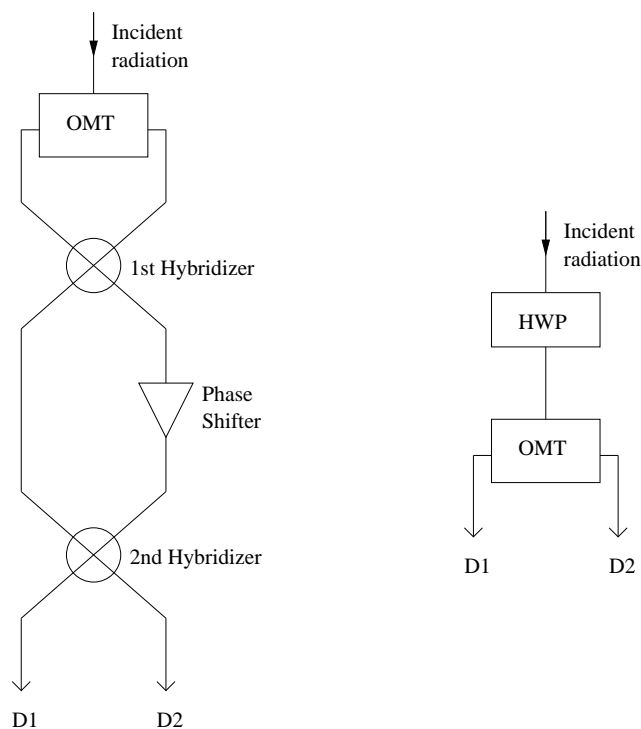
Figure A.3: Block diagrams for a pseudo-correlation receiver (left) and a rotating half-wave-plate receiver (right). For the **pseudo-correlation receiver**, the incident radiation is split into two orthogonal components by the ortho-mode transducer (OMT), and then propagates through a 90° hybridizer. A time dependent phase shift is introduced along one arm, and the radiation passes through a second 90° hybridizer before being detected. For the **rotating half-wave-plate receiver**, the incident radiation simply passes through a rotating half-wave-plate before being split by the OMT and detected. Figure taken from [170].

- the pseudo-correlation receiver;

- the rotating half-wave-plate receiver.

The propagation of radiation through a receiver can be described by a **Jones matrix**, $\mathbf{J}$, such that the electric field after passing through the receiver, $\mathbf{E}_{\mathrm{rec}}$, is

$$\mathbf{E}_{\mathrm{rec}} = \mathbf{JE}, \tag{A.19}$$

where $\mathbf{E}$ is the incident electric field. (In this section only, the elements of $\mathbf{E}$ are the complex amplitudes of the two linear polarizations, A and B, which, for an ideal optical system, couple in the far-field to the x and $-y$ components of the electric field of the incident radiation.) The **Müller matrix** for the receiver can be found from the relations:

$$\begin{pmatrix} I \\ Q \\ U \\ V \end{pmatrix}_{\mathrm{obs}} = \mathbf{M} \begin{pmatrix} I \\ Q \\ U \\ V \end{pmatrix}, \tag{A.20}$$

$$\begin{pmatrix} I+Q & U+iV \\ U-iV & I-Q \end{pmatrix}_{\mathrm{obs}} = \mathbf{J} \begin{pmatrix} I+Q & U+iV \\ U-iV & I-Q \end{pmatrix} \mathbf{J}^{\dagger}. \tag{A.21}$$

For a receiver with several components, the Jones matrix of the receiver is the product of the matrices for each component (provided that reflections can be ignored).

For the **pseudo-correlation receiver**, the ideal Jones matrix is

$$\begin{aligned} \mathbf{J}_{\mathrm{pc}} &= \mathbf{J}_{\mathrm{hybrid,2}} \mathbf{J}_{\mathrm{phase}} \mathbf{J}_{\mathrm{hybrid,1}} \mathbf{J}_{\mathrm{omt}} \\ &= \frac{1}{\sqrt{2}} \begin{pmatrix} 1 & i \\ i & 1 \end{pmatrix} \begin{pmatrix} 1 & 0 \\ 0 & e^{i\varphi t} \end{pmatrix} \frac{1}{\sqrt{2}} \begin{pmatrix} 1 & i \\ i & 1 \end{pmatrix} \begin{pmatrix} 1 & 0 \\ 0 & 1 \end{pmatrix} \\ &= \frac{1}{2} \begin{pmatrix} 1-e^{i\varphi t} & i(1+e^{i\varphi t}) \\ i(1+e^{i\varphi t}) & -1+e^{i\varphi t} \end{pmatrix}, \end{aligned} \tag{A.22}$$

where φt is the time-dependent phase shift, assumed to be continuous here. After passing through the receiver:

$$E_{\text{rec,A}} = \frac{1}{2}\left[(1 - e^{i\varphi t})E_{\text{x}} + i(1 + e^{i\varphi t})E_{\text{y}}\right],$$

$$E_{\text{rec,B}} = \frac{1}{2}\left[(-1 + e^{i\varphi t})E_{\text{y}} + i(1 + e^{i\varphi t})E_{\text{x}}\right],$$

where E_{x} and E_{y} are components of the incident electric field. The power in the two components, in the ideal, noiseless case, for a particular pointing is:

$$
\begin{aligned}
D_1 &\equiv \langle|E_{\text{rec,A}}|^2\rangle \\
&= \tfrac{1}{2}\left[(E_{\text{x}}E_{\text{x}}^* + E_{\text{y}}E_{\text{y}}^*) - (E_{\text{x}}E_{\text{x}}^* - E_{\text{y}}E_{\text{y}}^*)\cos\varphi t - (E_{\text{x}}E_{\text{y}}^* - E_{\text{x}}^*E_{\text{y}})\sin\varphi t\right] \\
&= \tfrac{1}{2}(I - Q\cos\varphi t - U\sin\varphi t), \\
D_2 &\equiv \langle|E_{\text{rec,B}}|^2\rangle = \tfrac{1}{2}(I + Q\cos\varphi t + U\sin\varphi t).
\end{aligned}
$$

The output of the pseudo-correlation receiver does not depend on Stokes parameter V (circular polarization), in the ideal noiseless case.

We can now follow systematic errors introduced in the Jones matrices through to the observed Stokes parameters. We parametrize the systematic errors in the various receiver components as follows:

$$
\begin{aligned}
\mathbf{J}_{\text{omt}} &= \begin{pmatrix} 1 + g_1 & \epsilon_1 e^{i\theta_1} \\ \epsilon_2 e^{i\theta_2} & (1 + g_2)e^{i\alpha} \end{pmatrix}, \\
\mathbf{J}_{\text{phase}} &= \begin{pmatrix} 1 & 0 \\ 0 & e^{i(\varphi t + \delta\phi)} \end{pmatrix}, \\
\mathbf{J}_{\text{hybrid,j}} &= \frac{1}{\sqrt{2}} \begin{pmatrix} (1 + A_j)e^{ia_j} & i(1 + B_j)e^{ib_j} \\ i(1 + C_j)e^{ic_j} & (1 + D_j)e^{id_j} \end{pmatrix},
\end{aligned}
\tag{A.23}
$$

where $j = 1, 2$ labels the two hybridizers. Each parameter corresponds to a potential, physical systematic error (g_1 and g_2 represent gain errors in the two arms of the OMT, ...). Following the same process as in the ideal case, we find the effect of these errors on the observed Stokes parameters. Assuming that the systematic errors do not vary significantly over the time of the observation, and expanding to linear order, the errors are related to

the parameters introduced in equation (A.17) by:

$$
\begin{aligned}
a &= \tfrac{1}{2}(A_1 + B_1 + C_1 + D_1 + A_2 + B_2 + C_2 + D_2) \\
&\quad + g_1 + g_2 \,; \\
2\omega &= \tfrac{1}{2}(a_1 + b_1 - c_1 - d_1 + a_2 + c_2 - b_2 - d_2) \\
&\quad + \epsilon_2 \cos\theta_2 - \epsilon_1 \cos\theta_1 - \delta\phi \,; \\
\gamma_1 &= g_1 - g_2 + \tfrac{1}{2}(A_1 + C_1 - B_1 - D_1) \,; \\
\gamma_2 &= \epsilon_1 \cos\theta_1 + \epsilon_2 \cos\theta_2 + \tfrac{1}{2}(a_1 + d_1 - b_1 - c_1) \,; \\
f_1 &= 0 \,; \\
f_2 &= 0 \,; \\
w_1 &= \tfrac{1}{2}(B_1 + C_1 - A_1 - D_1) + \epsilon_1 \sin\theta_1 + \epsilon_2 \sin\theta_2 \,; \\
w_2 &= \tfrac{1}{2}(b_1 + d_1 - a_1 - c_1 + 2\alpha) \,.
\end{aligned}
\tag{A.24}
$$

As expected, we see that differential gain errors $g_1 - g_2$ lead to instrumental Q polarization (γ_1). 'Spin-flip' errors, coupling P to P^*, are absent at first order but appear at second order in the perturbation and higher. It should be noted that the validity of the perturbative expansion depends in part on the relative amplitudes of the polarization and total-intensity fields. For example, we are implicitly assuming that any parameter that contributes to a at first order and to γ_1 at only second order is sufficiently small to suppress the total-intensity leakage caused to well below the level of the polarization leakage.

For the **half-wave-plate receiver**, with the plate rotating at an angular velocity φ, the ideal Jones matrix is:

$$
\begin{aligned}
\mathbf{J}_{\mathrm{rhwp}} &= \mathbf{J}_{\mathrm{omt}} \mathbf{J}_{\mathrm{rot}}^{\mathrm{I}} \mathbf{J}_{\mathrm{hwp}} \mathbf{J}_{\mathrm{rot}} \\
&= \begin{pmatrix} 1 & 0 \\ 0 & 1 \end{pmatrix} \begin{pmatrix} \cos\varphi t & -\sin\varphi t \\ \sin\varphi t & \cos\varphi t \end{pmatrix} \\
&\quad \times \begin{pmatrix} 1 & 0 \\ 0 & -1 \end{pmatrix} \begin{pmatrix} \cos\varphi t & \sin\varphi t \\ -\sin\varphi t & \cos\varphi t \end{pmatrix} \\
&= \begin{pmatrix} \cos 2\varphi t & \sin 2\varphi t \\ \sin 2\varphi t & -\cos 2\varphi t \end{pmatrix} .
\end{aligned}
\tag{A.25}
$$

This leads to similar ideal detector outputs as the pseudo-correlator, but with Q and U modulated at a frequency of 4φ:

$$
\begin{aligned}
D_1 &= \tfrac{1}{2}(I + Q\cos 4\varphi t + U\sin 4\varphi t)\,, \\
D_2 &= \tfrac{1}{2}(I - Q\cos 4\varphi t - U\sin 4\varphi t)\,.
\end{aligned}
$$

Systematic errors in the OMT are parametrized as in Eq. (A.23), and for the other components,

$$
\begin{aligned}
\mathbf{J}_{\mathrm{hwp}} &= \begin{pmatrix} 1 + h_1 & \zeta_1 e^{i\chi_1} \\ \zeta_2 e^{i\chi_2} & -(1+h_2)e^{i\beta} \end{pmatrix}, \\
\mathbf{J}_{\mathrm{rot}} &= \begin{pmatrix} \cos(\varphi t + \delta\phi) & \sin(\varphi t + \delta\phi) \\ -\sin(\varphi t + \delta\phi) & \cos(\varphi t + \delta\phi) \end{pmatrix}.
\end{aligned}
\tag{A.26}
$$

Propagating these errors through to the observed Stokes parameters, we find the only non-zero polarization couplings are:

$$
\begin{aligned}
a &= g_1 + g_2 + h_1 + h_2\,, \\
2\omega &= \epsilon_1 \cos\theta_1 - \epsilon_2 \cos\theta_2 - 4\delta\phi\,, \\
&\quad - \zeta_1 \cos\chi_1 - \zeta_2 \cos\chi_2\,.
\end{aligned}
\tag{A.27}
$$

The observation that P couples only to P actually holds exactly for this receiver, and not just to first order. By comparing equations (A.24) and (A.27) we can begin to draw some useful conclusions as to the relative suitability of these receivers for CMB polarimetry. The half-wave-plate receiver has the considerable advantage of having no total intensity leakage, given the assumptions made. The large difference in the amplitude of the temperature and polarization signals means that such leakage is potentially very damaging, and hence any systematic errors that contribute to γ_1 and γ_2 will have very strict tolerance limits.

Planck polarimetry [171]

Description of a single receptor

In the domain of (quasi-)monochromatic time-varying electromagnetic and

electrical signals a single receptor is described by the equation:

$$v = \mathbf{r}^\dagger \mathbf{E}, \tag{A.28}$$

where $\mathbf{r}$ is the receptor vector, it consists of 2 complex numbers definable by 4 real parameters:

- δ_R characterises the orientation of the dipole;

- ϵ_R characterises the ellipticity of the dipole;

- g characterises the complex gain of the amplifier;

$$\mathbf{r} = g\mathbf{R}(\delta_R) \begin{pmatrix} \cos\epsilon_R \\ -i\sin\epsilon_R \end{pmatrix} = g \begin{pmatrix} \cos\delta_R\cos\epsilon_R + i\sin\delta_R\sin\epsilon_R \\ \sin\delta_R\cos\epsilon_R - i\cos\delta_R\sin\epsilon_R \end{pmatrix}. \tag{A.29}$$

In the Stokes domain the output power is:

$$
\begin{aligned}
P_R &= \langle v^* v \rangle = \mathbf{r}^\dagger P r \\
&= G_R \left[I + (Q\cos 2\delta_R + U\sin 2\delta_R)\cos 2\epsilon_R - V\sin 2\epsilon_R \right] \\
&= \mathbf{w} \begin{pmatrix} I \\ Q \\ U \\ V \end{pmatrix},
\end{aligned} \tag{A.30}
$$

where:

- $G_R \equiv \|g\|^2$ is the receptor's intensity gain;

- $\Lambda_R \equiv \cos 2\epsilon_R$ is polarimetric efficiency for linear polarization;

- δ_R is misorientation.

Müller matrix describing a two receptor horn

In the output we measure only the powers in the 'a' and 'b' channels, i.e. the diagonal elements of the coherency matrix, which equal the output $I \pm Q$; these outputs are combined in data reduction to obtain estimates of I and

Q. So we are interested only in the upper part of the Müller matrix for a *Planck* horn channel:

$$\begin{pmatrix} I \\ Q \end{pmatrix}_{\text{obs}} = G_H \begin{pmatrix} 1 & M_{IQ} & M_{IU} & M_{IV} \\ M_{QI} & M_{QQ} & M_{QU} & M_{QV} \end{pmatrix} \begin{pmatrix} I \\ Q \\ U \\ V \end{pmatrix}, \qquad \text{(A.31)}$$

where G_H is the horn's intensity gain. The Müller Matrix is a combination of the **w** vectors for 'a' and 'b' receptors:

$$\mathbf{M} = \frac{1}{2} \begin{pmatrix} \mathbf{w}_a + \mathbf{w}_b \\ \mathbf{w}_a - \mathbf{w}_b \end{pmatrix}$$

$$= \begin{pmatrix} G_a + G_b & G_a \cos 2\delta_a \cos 2\epsilon_a - G_b \cos 2\delta_b \cos 2\epsilon_b & \cdots \\ G_a - G_b & G_a \cos 2\delta_a \cos 2\epsilon_a + G_b \cos 2\delta_b \cos 2\epsilon_b & \cdots \end{pmatrix}$$

$$\begin{pmatrix} \cdots & G_a \sin 2\delta_a \cos 2\epsilon_a - G_b \sin 2\delta_b \cos 2\epsilon_b & -G_a \sin 2\epsilon_a + G_b \sin 2\epsilon_b \\ \cdots & G_a \sin 2\delta_a \cos 2\epsilon_a + G_b \sin 2\delta_b \cos 2\epsilon_b & -G_a \sin 2\epsilon_a - G_b \sin 2\epsilon_b \end{pmatrix}.$$

$$\text{(A.32)}$$

A.2 Local contamination

An experiment necessarily has *finite resolution* and thus there is an additional class of contamination associated with the resolution or beam of the experiment [169]. Radiation from the sky is then coupled into one line of the detector through a *perfectly polarized beam*:

$$B(\hat{\mathbf{n}}; \mathbf{b}, e) = \frac{1}{2\pi\sigma^2(1 - e^2)} \exp\left[-\frac{1}{2\sigma^2}\left(\frac{(n_1 - b_1)^2}{(1 + e)^2} + \frac{(n_2 - b_2)^2}{(1 - e)^2} \right) \right], \quad \text{(A.33)}$$

where:

- **b** is the offset between the beam center and the desired direction on the sky;

- σ is the mean beamwidth;

- e is the ellipticity.

These parameters are different for the different polarizations, and the difference in the beams enters into the Q measurement:

$$B(\hat{\mathbf{n}}; \mathbf{b}_a, e_a) - B(\hat{\mathbf{n}}; \mathbf{b}_b, e_b) \,. \tag{A.34}$$

To first order in the sums and differences of the ellipticities and pointing errors:

$$
\begin{aligned}
\sigma\mathbf{p} &= (\mathbf{b}_a + \mathbf{b}_b)/2 \,, \\
\sigma\mathbf{b}_d &= (\mathbf{b}_a - \mathbf{b}_b)/2 \,, \\
e_s &= (e_a + e_b)/2 \,, \\
q &= (e_a - e_b)/2 \,,
\end{aligned}
\tag{A.35}
$$

we obtain:

$$\hat{Q}(\hat{\mathbf{n}}; \sigma) \approx Q(\hat{\mathbf{n}}; \sigma) + \sigma\mathbf{p} \cdot \nabla Q(\hat{\mathbf{n}}; \sigma) + \sigma\mathbf{b}_d \cdot \nabla I(\hat{\mathbf{n}}; \sigma) + \sigma^2 q[\partial_1^2 - \partial_2^2]I(\hat{\mathbf{n}}; \sigma) \,, \tag{A.36}$$

where the average beam $B(\hat{\mathbf{n}}) = B(\hat{\mathbf{n}}; 0, 0)$ and we drop second derivative terms in Q.

In theory, the only Müller matrix that one should deal with is that for a complete horn channel. It is a function of pointing coordinates $\boldsymbol{\Theta}$, an orientation angle ψ between sky and Planck coordinates and signal frequency or spectrum β. In practice subsystem Müller matrices are useful for evaluative modeling. We shall distinguish two types:

Circuit matrices that describe subsystems with single dual-polarization input and output.

Beam matrices that describe a collector stage or a complete horn with the entire polarized sky as input.

A.3 B-mode contamination

Implications of polarization transfer and local contamination on the B-modes of the polarization [169].

The polarization and contamination fields may in general be decomposed into harmonics appropriate to their properties under rotation or spin.

$$[S_1 \pm iS_2](\hat{\mathbf{n}}) = (\mp 1)^s \int \frac{d^2 l}{(2\pi)^2} [S_a \pm iS_b](\mathbf{l}) e^{\pm is\phi_l} , \qquad (A.37)$$

where $\cos \phi_l = l_x / l$.

- $Q \pm iU$ is a spin ± 2 field and we will follow the conventional nomenclature that its harmonics are named $E \pm iB$;

- the calibration a, rotation ω, and quadrupole leakage to be spin-0 fields;

- the pointing $p_1 \pm ip_2$ and dipole leakage $d_1 \pm id_2$ to be ± 1 fields;

- the monopole leakage $\gamma_1 \pm i\gamma_2$ to be ± 2 fields;

- the spin-flip $f_1 \pm if_2$ to be ± 4 fields.

Under the assumption of statistical isotropy of the fields, their two point correlations are defined by their *(cross) power spectra*:

$$\langle S(\mathbf{l})^* S'(\mathbf{l}') \rangle = (2\pi)^2 \delta(\mathbf{l} - \mathbf{l}') C_l^{SS'} , \qquad (A.38)$$

where S, S' are any of the fields.

We will calculate the contamination to the B-mode polarization power spectrum *assuming no intrinsic B-modes* and generally will plot:

$$\Delta B \equiv \left(\frac{l(l+1)}{2\pi} C_l^{BB} \right)^{1/2} , \qquad (A.39)$$

in units of μK.

The changes to the B-mode harmonics due to the *calibration, rotation, spin-flip and pointing* take the form:

$$\delta B(\mathbf{l}) = \int \frac{d^2 l_1}{(2\pi)^2} S(\mathbf{l}_1) E(\mathbf{l}_2) W_S(\mathbf{l}_1, \mathbf{l}_2) , \qquad (A.40)$$

with $\mathbf{l}_2 = \mathbf{l} - \mathbf{l}_1$ and:

- calibration $W_a = \sin[2(\phi_{l_2} - \phi_l)]$,

- rotation $_\omega = 2\cos[2(\phi_{l_2} - \phi_l)]$,

- pointing $W_{p_a} = \sigma(\mathbf{l}_2 \times \hat{\mathbf{l}}_1) \cdot \hat{\mathbf{z}} \sin[2(\phi_{l_2} - \phi_l)] \; W_{p_b} = \sigma(\mathbf{l}_2 \cdot \hat{\mathbf{l}}_1) \sin[2(\phi_{l_2} - \phi_l)]$,

- spin-flip $W_{f_a} = \sin[2(2\phi_{l_1} - \phi_{l_2} - \phi_l) \; W_{f_b} = \cos[2(2\phi_{l_1} - \phi_{l_2} - \phi_l)]$.

Here $\mathbf{l}_1 = l_1 \hat{\mathbf{l}}_1$.

These relations imply contamination to the BB power spectrum of:

$$\delta C_l^{BB} = \sum_{SS'} \int \frac{d^2 l_1}{(2\pi)^2} C_{l_1}^{SS'} C_{l_2}^{EE}(\sigma) W_S^* W_{S'} , \qquad (A.41)$$

where:

$$C_l^{EE}(\sigma) = C_l^{EE} \exp(-l(l+1)\sigma) , \qquad (A.42)$$

is the EE power spectrum smoothed over the average beam.

Similarly the change due to *temperature leakage* can be described by:

$$\delta B(\mathbf{l}) = \int \frac{d^2 l_1}{(2\pi)^2} S(\mathbf{l}_1) I(\mathbf{l}_2) W_S(\mathbf{l}_1, \mathbf{l}_2) , \qquad (A.43)$$

with:

- monopole leakage $W_{\gamma_a} = \sin[2(\phi_{l_1} - \phi_l)] \; W_{\gamma_b} = \cos[2(\phi_{l_1} - \phi_l)]$;

- dipole leakage $W_{d_a} = -(l_2\sigma)\cos[\phi_{l_1} + \phi_{l_2} - 2\phi_l] \; W_{d_b} = (l_2\sigma)\sin[\phi_{l_1} + \phi_{l_2} - 2\phi_l]$;

- quadrupole leakage $W_q = -(l_2\sigma)^2 \sin[2(\phi_{l_2} - \phi_l)]$;

leading to:

$$\delta C_l^{BB} = \sum_{SS'} \int \frac{d^2 l_1}{(2\pi)^2} C_{l_1}^{SS'} C_{l_2}^{II}(\sigma) W_S^* W_{S'} , \qquad (A.44)$$

for the power spectrum contamination.

A.4   Scientific impact

For definiteness, let us take as a *fiducial model*: a baryon density of $\Omega_b h^2 = 0.02$, cold dark matter density of $\Omega_c h^2 = 0.128$, a cosmological constant of $\Omega_\Lambda = 0.65$, reionization optical depth $\tau = 0.05$, an initial amplitude of comoving curvature fluctuations of $\delta_\zeta = 4.79 \times 10^{-5}$ ($\sigma_8 = 0.92$), and a scalar spectral index of $n = 1$ in a spatially flat universe.
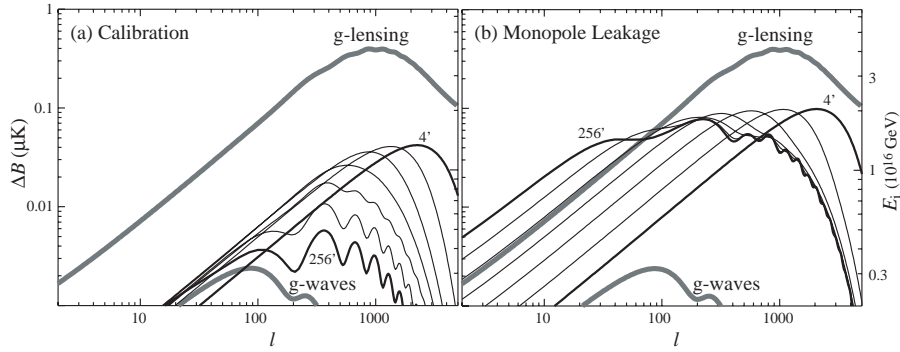

Figure A.4: Coherence dependence of B-mode contamination (a) for *calibration a* with rms $A_a = 10^{-2}$ (b) for *monopole-leakage* γ_a, γ_b with $A_{\gamma_a} = A_{\gamma_b} = 10^{-3}$ added in quadrature. The beam scale is Full Width at Half Minimum (FWHM) $= (8\ln 2)^{1/2}\sigma = 1'$ to remove beam effects and the FWHM coherence $(8\ln 2)^{1/2}\alpha$ is stepped from $256'$ to $4'$ in factors of 2. Other effects follow the trend of calibration errors not monopole leakage. For a coherence large compared with the CMB acoustic peaks, B contamination picks up their underlying structure. Here and in the following figures, the *gravitational lensing* and *minimum detectable gravitational wave* ($E_i = 3.2 \times 10^{15}$GeV) B-modes are shown for reference (thick shaded lines). The scaling with E_i of the peak in the B-mode spectrum is shown on the right hand axis. Figure taken from [169].
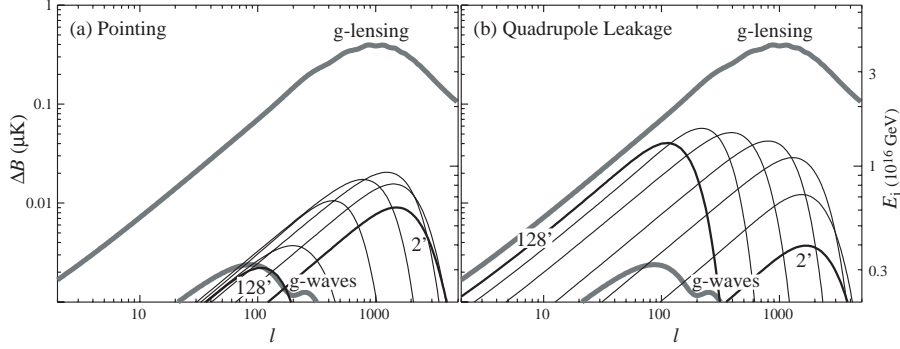
Figure A.5: Beam dependence of B-mode contamination for (a) *pointing* with an rms $A_{p_a} = A_{p_b} = 10^{-2}$ (in units of the Gaussian beam width) added in quadrature (b) *quadrupole leakage* with an rms $A_q = 0.002$ (in units of differential beam ellipticity). The coherence α is set to $\max(\sigma, 10'/(8\ln 2)^{1/2})$ and the beam is stepped from $128'$ to $2'$ in factors of 2. Figure taken from [169].
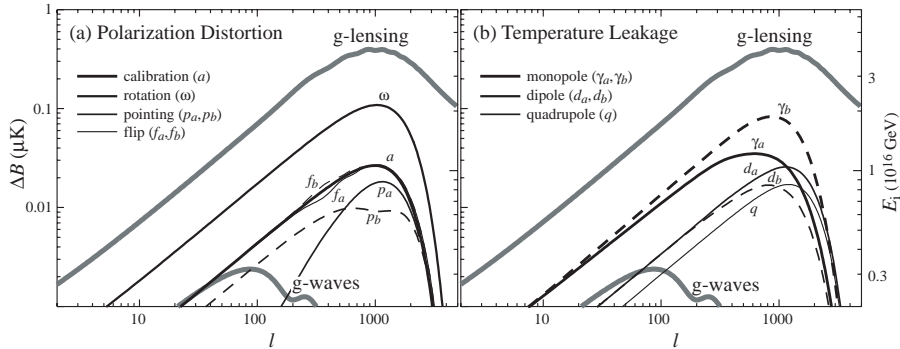
Figure A.6: All effects for a beam and coherence of FWHM = $(8\ln 2)^{1/2}\sigma = 10'$. (a) *Polarization distortion* for an rms of $A = 10^{-2}$ from calibration a, rotation ω ($0.6°$ rms), pointing (p_a, p_b) ($2.5''$ rms) , and spin flip (f_a, f_b). (b) *Temperature leakage* for an rms of $A = 10^{-3}$ from monopole (γ_a, γ_b), dipole (d_a, d_b) and quadrupole (q) terms. The "b" component of each effect is shown with dashed lines. Figure taken from [169].

Bibliography

[1] E. W. Kolb and M. S. Turner, *"The Early universe,"* Front. Phys. **69** (1990) 1.

[2] G. G. Raffelt, *"Stars As Laboratories For Fundamental Physics: The Astrophysics Of Neutrinos, Axions, And Other Weakly Interacting Particles,"*, 1996 Chicago, USA: Univ. Pr.

[3] F. Finelli and M. Galaverni, "Rotation of Linear Polarization Plane and Circular Polarization from Cosmological Pseudoscalar Fields," arXiv:0802.4210 [astro-ph], *submitted.*

[4] A. Lewis, A. Challinor and A. Lasenby, "Efficient Computation of CMB anisotropies in closed FRW models," Astrophys. J. **538**, 473 (2000) [arXiv:astro-ph/9911177].

[5] A. Lue, L. M. Wang and M. Kamionkowski, "Cosmological signature of new parity-violating interactions," Phys. Rev. Lett. **83** (1999) 1506 [arXiv:astro-ph/9812088].

[6] E. Komatsu *et al.* [WMAP Collaboration], "Five-Year Wilkinson Microwave Anisotropy Probe WMAP Observations:Cosmological Interpretation," arXiv:0803.0547 [astro-ph].

[7] J. A. Frieman, C. T. Hill, A. Stebbins and I. Waga, "Cosmology with ultralight pseudo Nambu-Goldstone bosons," Phys. Rev. Lett. **75**, 2077 (1995) [arXiv:astro-ph/9505060].

[8] S. R. Coleman and S. L. Glashow, "High-energy tests of Lorentz invariance," Phys. Rev. D **59**, 116008 (1999) [arXiv:hep-ph/9812418].

[9] J. Abraham *et al.* [Pierre Auger Collaboration], "An upper limit to the photon fraction in cosmic rays above 10**19-eV from the Pierre Auger observatory," Astropart. Phys. **27**, 155 (2007) [arXiv:astro-ph/0606619].

[10] M. Galaverni and G. Sigl, "Lorentz Violation in the Photon Sector and Ultrahigh Energy Cosmic Rays," Phys. Rev. Lett. **100**, 021102 (2008) [arXiv:0708.1737 [astro-ph]].

[11] M. Galaverni and G. Sigl, "Lorentz Violation and Ultrahigh-Energy Photons," Phys. Rev. D **78**, 063003 (2008) [arXiv:0807.1210 [astro-ph]].

[12] see http://www.fe.infn.it/idapp/.

[13] M. Galaverni, F. Finelli, "Systematics of Cosmic Microwave Background Polarization," Internal Report IASF-BO 454/2007.

[14] M. J. Rees, "Polarization and Spectrum of the Primeval Radiation in an Anisotropic Universe," Ap. J. **153** (1968) L1

[15] S. Chandrasekhar, *"Radiative transfer,"* 1960 Dover, New York.

[16] W. Hu and M. J. White, "A CMB Polarization Primer," New Astron. **2**, 323 (1997) [arXiv:astro-ph/9706147].

[17] J. Kovac, E. M. Leitch, C. Pryke, J. E. Carlstrom, N. W. Halverson and W. L. Holzapfel, "Detection of polarization in the cosmic microwave background using DASI," Nature **420**, 772 (2002) [arXiv:astro-ph/0209478].

[18] L. Page *et al.* [WMAP Collaboration], "Three year Wilkinson Microwave Anisotropy Probe (WMAP) observations: Polarization analysis," Astrophys. J. Suppl. **170**, 335 (2007) [arXiv:astro-ph/0603450].

[19] M. Born, E. Wolf, *"Principles of Optics,"* 1980 Pergamon Press.

[20] L. Mandel, E. Wolf, *"Optical Coherence and Quantum Optics,"* 1995 Cambridge University Press.

[21] A. Kosowsky, "Cosmic microwave background polarization," Annals Phys. **246** (1996) 49 [arXiv:astro-ph/9501045].

[22] M. Zaldarriaga and U. Seljak, "An All-Sky Analysis of Polarization in the Microwave Background," Phys. Rev. D **55** (1997) 1830 [arXiv:astro-ph/9609170].

[23] M. Zaldarriaga, "Fluctuations in the cosmic microwave background," arXiv:astro-ph/9806122.

[24] A. Cooray, A. Melchiorri and J. Silk, "Is the Cosmic Microwave Background Circularly Polarized?," Phys. Lett. B **554** (2003) 1 [arXiv:astro-ph/0205214].

[25] C. P. Ma and E. Bertschinger, "Cosmological perturbation theory in the synchronous and conformal Newtonian gauges," Astrophys. J. **455**, 7 (1995) [arXiv:astro-ph/9506072].

[26] J. R. Bond and G. Efstathiou, "The statistics of cosmic background radiation fluctuations," Mon. Not. Roy. Astron. Soc. **226**, 655 (1987).

[27] A. Kosowsky and A. Loeb, "Faraday Rotation of Microwave Background Polarization by a Primordial Magnetic Field," Astrophys. J. **469**, 1 (1996) [arXiv:astro-ph/9601055].

[28] D. D. Harari, J. D. Hayward and M. Zaldarriaga, "Depolarization of the cosmic microwave background by a primordial magnetic field and its effect upon temperature anisotropy," Phys. Rev. D **55**, 1841 (1997) [arXiv:astro-ph/9608098].

[29] E. S. Scannapieco and P. G. Ferreira, "Polarization - temperature correlation from primordial magnetic field," Phys. Rev. D **56**, 7493 (1997) [arXiv:astro-ph/9707115].

[30] C. Scoccola, D. Harari and S. Mollerach, "B polarization of the CMB from Faraday rotation," Phys. Rev. D **70**, 063003 (2004) [arXiv:astro-ph/0405396].

[31] G. C. Liu, S. Lee and K. W. Ng, "Effect on cosmic microwave background polarization of coupling of quintessence to pseudoscalar formed from the electromagnetic field and its dual," Phys. Rev. Lett. **97**, 161303 (2006) [arXiv:astro-ph/0606248].

[32] G. C. Liu, N. Sugiyama, A. J. Benson, C. G. Lacey and A. Nusser, "Polarization of the Cosmic Microwave Background from Non-Uniform Astrophys. J. **561**, 504 (2001) [arXiv:astro-ph/0101368].

[33] B. Feng, M. Li, J. Q. Xia, X. Chen and X. Zhang, "Searching for CPT violation with WMAP and BOOMERANG," Phys. Rev. Lett. **96** (2006) 221302 [arXiv:astro-ph/0601095].

[34] P. Cabella, P. Natoli and J. Silk, "Constraints on CPT violation from WMAP three year polarization data: A wavelet analysis," Phys. Rev. D **76**, 123014 (2007) [arXiv:0705.0810 [astro-ph]].

[35] E. Y. Wu *et al.* [QUaD Collaboration], "Parity violation constraints using 2006-2007 QUaD CMB polarization spectra," arXiv:0811.0618 [astro-ph].

[36] G. B. Rybicki and A. P. Lightman, *"Radiative Processes in Astrophysics,"* 1979 New York: Wiley-Interscience

[37] T. Beckert and H. Falcke, "Circular Polarization of Radio Emission from Relativistic Jets," arXiv:astro-ph/0112398.

[38] P. Lubin, P. Melese and G. Smoot, "Linear and circular polarization of the cosmic background radiation," Astrophys. J. **273**, L51 (1983)

[39] S. Hanany and P. Rosenkranz, "Polarization of the Atmosphere as a Foreground for Cosmic Microwave Background Polarization Experiments," New Astron. Rev. **47** (2003) 1159

[40] J. H. P. Wu *et al.*, "AMiBA Observations, Data Analysis and Results for Sunyaev-Zel'dovich Effects," arXiv:0810.1015 [astro-ph].

[41] C. Amsler *et al.* [Particle Data Group], "Review of particle physics," Phys. Lett. B **667**, 1 (2008).

[42] J. E. Kim, "Light Pseudoscalars, Particle Physics and Cosmology," Phys. Rept. **150** (1987) 1.

[43] G. G. Raffelt, "Astrophysical methods to constrain axions and other novel particle phenomena," Phys. Rept. **198** (1990) 1.

[44] G. G. Raffelt, "Particle physics from stars," Ann. Rev. Nucl. Part. Sci. **49**, 163 (1999) [arXiv:hep-ph/9903472].

[45] S. J. Asztalos, L. J. Rosenberg, K. van Bibber, P. Sikivie and K. Zioutas, "Searches for astrophysical and cosmological axions," Ann. Rev. Nucl. Part. Sci. **56** (2006) 293.

[46] R. D. Peccei, "The strong CP problem and axions," Lect. Notes Phys. **741**, 3 (2008) [arXiv:hep-ph/0607268].

[47] P. Sikivie, "Axion cosmology," Lect. Notes Phys. **741**, 19 (2008) [arXiv:astro-ph/0610440].

[48] G. G. Raffelt, "Astrophysical axion bounds," Lect. Notes Phys. **741**, 51 (2008) [arXiv:hep-ph/0611350].

[49] R. Battesti *et al.*, "Axion searches in the past, at present, and in the near future," Lect. Notes Phys. **741**, 199 (2008) [arXiv:0705.0615 [hep-ex]].

[50] P. Sikivie, "The pool-table analogy with axion physics," Phys. Today **49N12**, 22 (1996) [arXiv:hep-ph/9506229].

[51] C. A. Baker *et al.*, "An improved experimental limit on the electric dipole moment of the neutron," Phys. Rev. Lett. **97**, 131801 (2006) [arXiv:hep-ex/0602020].

[52] R. D. Peccei and H. R. Quinn, "CP Conservation In The Presence Of Instantons," Phys. Rev. Lett. **38** (1977) 1440.

[53] S. Weinberg, "A New Light Boson?," Phys. Rev. Lett. **40**, 223 (1978).

[54] F. Wilczek, "Problem Of Strong P And T Invariance In The Presence Of Instantons," Phys. Rev. Lett. **40**, 279 (1978).

[55] J. E. Kim, "Weak Interaction Singlet And Strong CP Invariance," Phys. Rev. Lett. **43**, 103 (1979).

[56] M. A. Shifman, A. I. Vainshtein and V. I. Zakharov, "Can Confinement Ensure Natural CP Invariance Of Strong Interactions?," Nucl. Phys. B **166**, 493 (1980).

[57] A. R. Zhitnitsky, "On Possible Suppression Of The Axion Hadron Interactions. (In Russian)," Sov. J. Nucl. Phys. **31**, 260 (1980) [Yad. Fiz. **31**, 497 (1980)].

[58] M. Dine, W. Fischler and M. Srednicki, "A Simple Solution To The Strong CP Problem With A Harmless Axion," Phys. Lett. B **104**, 199 (1981).

[59] S. Andriamonje *et al.* [CAST Collaboration], "An improved limit on the axion-photon coupling from the CAST experiment," JCAP **0704**, 010 (2007) [arXiv:hep-ex/0702006].

[60] E. A. Paschos and K. Zioutas, "A Proposal For Solar Axion Detection Via Bragg Scattering," Phys. Lett. B **323**, 367 (1994).

[61] S. Cebrian *et al.*, "Prospects of solar axion searches with crystal detectors," Astropart. Phys. **10**, 397 (1999) [arXiv:astro-ph/9811359].

[62] R. Bernabei *et al.*, "Investigating pseudoscalar and scalar dark matter," Int. J. Mod. Phys. A **21**, 1445 (2006) [arXiv:astro-ph/0511262].

[63] P. Gondolo and G. Raffelt, "Solar neutrino limit on the axion-like interpretation of the DAMA signal," arXiv:0807.2926 [astro-ph].

[64] S. J. Asztalos *et al.*, "An improved RF cavity search for halo axions," Phys. Rev. D **69**, 011101 (2004) [arXiv:astro-ph/0310042].

[65] L. Maiani, R. Petronzio and E. Zavattini, "Effects Of Nearly Massless, Spin Zero Particles On Light Propagation In A Magnetic Field," Phys. Lett. B **175**, 359 (1986).

[66] W. Heisenberg and H. Euler, "Consequences of Dirac's theory of positrons," Z. Phys. **98** (1936) 714 [arXiv:physics/0605038].

[67] J. S. Schwinger, "On gauge invariance and vacuum polarization," Phys. Rev. **82**, 664 (1951).

[68] E. Zavattini *et al.* [PVLAS Collaboration], "Experimental observation of optical rotation generated in vacuum by a magnetic field," Phys. Rev. Lett. **96**, 110406 (2006) [Erratum-ibid. **99**, 129901 (2007)] [arXiv:hep-ex/0507107].

[69] E. Zavattini *et al.* [PVLAS Collaboration], "New PVLAS results and limits on magnetically induced optical rotation and ellipticity in vacuum," Phys. Rev. D **77**, 032006 (2008) [arXiv:0706.3419 [hep-ex]].

[70] D. J. Gross, R. D. Pisarski and L. G. Yaffe, "QCD And Instantons At Finite Temperature," Rev. Mod. Phys. **53**, 43 (1981).

[71] M. Dine and W. Fischler, "The not-so-harmless axion," Phys. Lett. B **120**, 137 (1983).

[72] L. F. Abbott and P. Sikivie, "A cosmological bound on the invisible axion," Phys. Lett. B **120**, 133 (1983).

[73] J. Preskill, M. B. Wise and F. Wilczek, "Cosmology of the invisible axion," Phys. Lett. B **120**, 127 (1983).

[74] S. Y. Pi, "Inflation Without Tears," Phys. Rev. Lett. **52**, 1725 (1984).

[75] A. D. Linde, "Inflation And Axion Cosmology," Phys. Lett. B **201**, 437 (1988).

[76] M. Tegmark, A. Aguirre, M. Rees and F. Wilczek, "Dimensionless constants, cosmology and other dark matters," Phys. Rev. D **73**, 023505 (2006) [arXiv:astro-ph/0511774].

[77] M. P. Hertzberg, M. Tegmark and F. Wilczek, "Axion Cosmology and the Energy Scale of Inflation," Phys. Rev. D **78**, 083507 (2008) [arXiv:0807.1726 [astro-ph]].

[78] M. Beltran, J. Garcia-Bellido and J. Lesgourgues, "Isocurvature bounds on axions revisited," Phys. Rev. D **75** (2007) 103507 [arXiv:hep-ph/0606107].

[79] F. Wilczek, "Axions And Family Symmetry Breaking," Phys. Rev. Lett. **49**, 1549 (1982).

[80] Y. Chikashige, R. N. Mohapatra and R. D. Peccei, "Are There Real Goldstone Bosons Associated With Broken Lepton Number?," Phys. Lett. B **98**, 265 (1981).

[81] C. Coriano', N. Irges and E. Kiritsis, "On the effective theory of low scale orientifold string vacua," Nucl. Phys. B **746**, 77 (2006) [arXiv:hep-ph/0510332].

[82] J. E. Kim and H. P. Nilles, "A quintessential axion," Phys. Lett. B **553**, 1 (2003) [arXiv:hep-ph/0210402].

[83] N. Kaloper and L. Sorbo, "Of pNGB QuiNtessence," JCAP **0604**, 007 (2006) [arXiv:astro-ph/0511543].

[84] M. M. Anber and L. Sorbo, "N-flationary magnetic fields," JCAP **0610**, 018 (2006) [arXiv:astro-ph/0606534].

[85] K. Dutta and L. Sorbo, "Confronting pNGB quintessence with data," Phys. Rev. D **75**, 063514 (2007) [arXiv:astro-ph/0612457].

[86] S. M. Carroll, "The cosmological constant," Living Rev. Rel. **4**, 1 (2001) [arXiv:astro-ph/0004075].

[87] S. M. Carroll, "Why is the universe accelerating?," eConf **C0307282**, TTH09 (2003) [AIP Conf. Proc. **743**, 16 (2005)] [arXiv:astro-ph/0310342].

[88] E. J. Copeland, M. Sami and S. Tsujikawa, "Dynamics of dark energy," Int. J. Mod. Phys. D **15**, 1753 (2006) [arXiv:hep-th/0603057].

[89] L. Amendola and R. Barbieri, "Dark matter from an ultra-light pseudo-Goldsone-boson," Phys. Lett. B **642**, 192 (2006) [arXiv:hep-ph/0509257].

[90] J. A. Frieman, C. T. Hill and R. Watkins, "Late time cosmological phase transitions: Particle physics models and cosmic evolution," Phys. Rev. D **46**, 1226 (1992).

[91] M. Fukugita and T. Yanagida, "Model for the cosmological constant," Yukawa Institute preprint YITP-K-1098, February 1994.

[92] A. Abrahamse, A. Albrecht, M. Barnard and B. Bozek, "Exploring Parameter Constraints on Quintessential Dark Energy: the Pseudo-Nambu Goldstone Boson Model," Phys. Rev. D **77**, 103503 (2008) [arXiv:0712.2879 [astro-ph]].

[93] S. M. Carroll, "Quintessence and the rest of the world," Phys. Rev. Lett. **81**, 3067 (1998) [arXiv:astro-ph/9806099].

[94] D. Harari and P. Sikivie, "Effects of a Nambu-Goldstone boson on the polarization of radio galaxies and the cosmic microwave background," Phys. Lett. B **289**, 67 (1992).

[95] S. M. Carroll and G. B. Field, "The Einstein equivalence principle and the polarization of radio galaxies," Phys. Rev. D **43** (1991) 3789.

[96] S. M. Carroll and G. B. Field, "Is there evidence for cosmic anisotropy in the polarization of distant radio sources?," Phys. Rev. Lett. **79**, 2394 (1997) [arXiv:astro-ph/9704263].

[97] D. Boyanovsky, H. J. de Vega, R. Holman and S. Prem Kumar, "Non-equilibrium production of photons via $\pi_0 \to 2\gamma$ in DCCs," Phys. Rev. D **56**, 3929 (1997) [arXiv:hep-ph/9703422].

[98] D. S. Lee and K. W. Ng, "Photon production of axionic cold dark matter," Phys. Rev. D **61**, 085003 (2000) [arXiv:hep-ph/9909282].

[99] K. R. S. Balaji, R. H. Brandenberger and D. A. Easson, "Spectral dependence of CMB polarization and parity," JCAP **0312**, 008 (2003) [arXiv:hep-ph/0310368].

[100] W. D. Garretson, G. B. Field and S. M. Carroll, "Primordial magnetic fields from pseudoGoldstone bosons," Phys. Rev. D **46** (1992) 5346 [arXiv:hep-ph/9209238].

[101] F. Finelli and A. Gruppuso, "Resonant amplification of gauge fields in expanding universe," Phys. Lett. B **502**, 216 (2001) [arXiv:hep-ph/0001231].

[102] S. M. Carroll, G. B. Field and R. Jackiw, "Limits on a Lorentz and Parity Violating Modification of Electrodynamics," Phys. Rev. D **41**, 1231 (1990).

[103] C. W. Misner, K. S. Thorne and J. A. Wheeler, *"Gravitation,"* 1973 San Francisco

[104] S. Alexander, J. Ochoa and A. Kosowsky, "Generation of Circular Polarization of the Cosmic Microwave Background," arXiv:0810.2355 [astro-ph].

[105] F. de Felice and C. J. S. Clarke, "Relativity on curved manifolds," *Cambridge University Press, Cambridge, England, 1990*

[106] N. D. Birrell and P. C. W. Davies, "Quantum Fields In Curved Space," *Cambridge, Uk: Univ. Pr. (1982) 340p*

[107] M. S. Turner, "Coherent Scalar Field Oscillations In An Expanding Universe," Phys. Rev. D **28**, 1243 (1983).

[108] A. Gruppuso and F. Finelli, "Analytic results for a flat universe dominated by dust and dark energy," Phys. Rev. D **73**, 023512 (2006) [arXiv:astro-ph/0512641].

[109] E. J. Copeland, A. R. Liddle and D. Wands, "Exponential potentials and cosmological scaling solutions," Phys. Rev. D **57**, 4686 (1998) [arXiv:gr-qc/9711068].

[110] M. Abramowitz and I. A. Stegun, *"Handbook of Mathematical Functions with Formulas, Graphs, and Mathematical Tables,"* 1964 New York, USA

[111] P. Jain, S. Panda and S. Sarala, "Electromagnetic polarization effects due to axion photon mixing," Phys. Rev. D **66** (2002) 085007 [arXiv:hep-ph/0206046].

[112] A. Mirizzi, G. G. Raffelt and P. D. Serpico, "Photon axion conversion in intergalactic magnetic fields and cosmological consequences," Lect. Notes Phys. **741**, 115 (2008) [arXiv:astro-ph/0607415].

[113] S. Das, P. Jain, J. P. Ralston and R. Saha, "Probing dark energy with light: Propagation and spontaneous polarization," JCAP **0506** (2005) 002 [arXiv:hep-ph/0408198].

[114] M. Dine, "Dark matter and dark energy: A physicist's perspective," arXiv:hep-th/0107259.

[115] T. Banks, M. Dine, P. J. Fox and E. Gorbatov, "On the possibility of large axion decay constants," JCAP **0306**, 001 (2003) [arXiv:hep-th/0303252].

[116] R. R. Caldwell, R. Dave and P. J. Steinhardt, "Cosmological Imprint of an Energy Component with General Equation-of-State," Phys. Rev. Lett. **80**, 1582 (1998) [arXiv:astro-ph/9708069].

[117] L. R. Abramo, F. Finelli and T. S. Pereira, "Constraining Born-Infeld models of dark energy with CMB anisotropies," Phys. Rev. D **70**, 063517 (2004) [arXiv:astro-ph/0405041].

[118] V. L. Ginzburg, V. A. Dogiel, V. S. Berezinsky, S. V. Bulanov and V. S. Ptuskin, "Astrophysics of cosmic rays," *Amsterdam, Netherlands: North-Holland (1990) 534 p*

[119] P. Bhattacharjee and G. Sigl, "Origin and propagation of extremely high energy cosmic rays," Phys. Rept. **327**, 109 (2000) [arXiv:astro-ph/9811011].

[120] G. Sigl, "Ultrahigh-energy cosmic rays: A Probe of physics and astrophysics at Science **291**, 73 (2001) [arXiv:astro-ph/0104291].

[121] K. Greisen, "End To The Cosmic Ray Spectrum?," Phys. Rev. Lett. **16**, 748 (1966);

[122] G. T. Zatsepin and V. A. Kuzmin, "Upper Limit Of The Spectrum Of Cosmic Rays," JETP Lett. **4**, 78 (1966) [Pisma Zh. Eksp. Teor. Fiz. **4**, 114 (1966)].

[123] S. Lee, "On The Propagation Of Extragalactic High-Energy Cosmic And Gamma-Rays," Phys. Rev. D **58**, 043004 (1998) [arXiv:astro-ph/9604098].

[124] R. U. Abbasi *et al.* [High Resolution Fly's Eye Collaboration], "Measurement of the flux of ultrahigh energy cosmic rays from monocular observations by the High Resolution Fly's Eye experiment," Phys. Rev. Lett. **92**, 151101 (2004) [arXiv:astro-ph/0208243].

[125] R. Abbasi *et al.* [HiRes Collaboration], "Observation of the GZK cutoff by the HiRes experiment," Phys. Rev. Lett. **100**, 101101 (2008) [arXiv:astro-ph/0703099].

[126] N. Hayashida *et al.*, "Observation of a very energetic cosmic ray well beyond the predicted 2.7-K cutoff in the primary energy spectrum," Phys. Rev. Lett. **73**, 3491 (1994).

[127] M. Takeda *et al.*, "Extension of the cosmic-ray energy spectrum beyond the predicted Greisen-Zatsepin-Kuzmin cutoff," Phys. Rev. Lett. **81**, 1163 (1998) [arXiv:astro-ph/9807193].

[128] J. Abraham *et al.* [Pierre Auger Collaboration], "Observation of the suppression of the flux of cosmic rays above 4×10^{19} eV," Phys. Rev. Lett. **101**, 061101 (2008) [arXiv:0806.4302 [astro-ph]].

[129] J. Abraham *et al.* [Pierre Auger Collaboration], "Correlation of the highest energy cosmic rays with nearby extragalactic objects," Science **318**, 938 (2007) [arXiv:0711.2256 [astro-ph]].

[130] K. Shinozaki *et al.*, "Upper limit on gamma-ray flux above 10**19-eV estimated by the Akeno Giant Air Shower Array experiment," Astrophys. J. **571**, L117 (2002).

[131] M. Risse *et al.*, "Upper limit on the photon fraction in highest-energy cosmic rays from AGASA data," Phys. Rev. Lett. **95**, 171102 (2005) [arXiv:astro-ph/0502418].

[132] G. I. Rubtsov *et al.*, "Upper limit on the ultra-high-energy photon flux from AGASA and Yakutsk data," Phys. Rev. D **73**, 063009 (2006) [arXiv:astro-ph/0601449].

[133] A. V. Glushkov, D. S. Gorbunov, I. T. Makarov, M. I. Pravdin, G. I. Rubtsov, I. E. Sleptsov and S. V. Troitsky, "Constraining the fraction of primary gamma rays at ultra-high energies from the muon data of the Yakutsk extensive-air-shower array," JETP Lett. **85**, 131 (2007) [arXiv:astro-ph/0701245].

[134] M. D. Healy for the Pierre Auger Collaboration, "Search for Ultra-High Energy Photons with the Pierre Auger Observatory," arXiv:0710.0025 [astro-ph].

[135] J. Abraham *et al.* [Pierre Auger Collaboration], "Upper limit on the cosmic-ray photon flux above 10^{19} eV using the surface detector of the Pierre Auger Observatory," Astropart. Phys. **29**, 243 (2008) [arXiv:0712.1147 [astro-ph]].

[136] M. Risse and P. Homola, "Search for ultra-high energy photons using air showers," Mod. Phys. Lett. A **22**, 749 (2007) [arXiv:astro-ph/0702632].

[137] T. Jacobson, S. Liberati and D. Mattingly, "Lorentz violation at high energy: Concepts, phenomena and astrophysical constraints," Annals Phys. **321**, 150 (2006) [arXiv:astro-ph/0505267].

[138] T. Jacobson, S. Liberati and D. Mattingly, "Astrophysical bounds on Planck suppressed Lorentz violation," Lect. Notes Phys. **669** (2005) 101 [arXiv:hep-ph/0407370].

[139] D. Mattingly, "Modern tests of Lorentz invariance," Living Rev. Rel. **8**, 5 (2005) [arXiv:gr-qc/0502097].

[140] W. Bietenholz, "Cosmic Rays and the Search for a Lorentz Invariance Violation," arXiv:0806.3713 [hep-ph].

[141] S. Liberati, "Quantum gravity phenomenology via Lorentz violations," PoS **P2GC**, 018 (2007) [arXiv:0706.0142 [gr-qc]].

[142] D. Mattingly, "Have we tested Lorentz invariance enough?," PoS **QG-PH**, 026 (2007) [arXiv:0802.1561 [gr-qc]].

[143] D. Colladay and V. A. Kostelecky, "Lorentz-violating extension of the standard model," Phys. Rev. D **58**, 116002 (1998) [arXiv:hep-ph/9809521].

[144] R. C. Myers and M. Pospelov, "Ultraviolet Modifications of Dispersion Relations in Effective Field Theory," Phys. Rev. Lett. **90** (2003) 211601 [arXiv:hep-ph/0301124].

[145] V. A. Kostelecky and N. Russell, "Data Tables for Lorentz and CPT Violation," arXiv:0801.0287 [hep-ph].

[146] T. Kahniashvili, R. Durrer and Y. Maravin, "Testing Lorentz Invariance Violation with WMAP Five Year Data," Phys. Rev. D **78**, 123009 (2008) [arXiv:0807.2593 [astro-ph]].

[147] S. D. Biller *et al.*, "Limits to quantum gravity effects from observations of TeV flares in active galaxies," Phys. Rev. Lett. **83**, 2108 (1999) [arXiv:gr-qc/9810044].

[148] T. A. Jacobson, S. Liberati, D. Mattingly and F. W. Stecker, "New limits on Planck scale Lorentz violation in QED," Phys. Rev. Lett. **93**, 021101 (2004) [arXiv:astro-ph/0309681].

[149] L. Maccione, S. Liberati, A. Celotti, J. G. Kirk and P. Ubertini, "Gamma-ray polarization constraints on Planck scale violations of special relativity," Phys. Rev. D **78**, 103003 (2008) [arXiv:0809.0220 [astro-ph]].

[150] A. J. Dean *et al.* , "Polarized Gamma-Ray Emission from the Crab," Science **321**, 1183 (2008).

[151] L. Maccione, S. Liberati, A. Celotti and J. G. Kirk, "New constraints on Planck-scale Lorentz Violation in QED from the Crab Nebula," JCAP **0710**, 013 (2007) [arXiv:0707.2673 [astro-ph]].

[152] Y. Z. Fan, D. M. Wei and D. Xu, "Gamma-ray Burst UV/optical afterglow polarimetry as a probe of Quantum Gravity," Mon. Not. Roy. Astron. Soc. **376**, 1857 (2007) [arXiv:astro-ph/0702006].

[153] F. W. Stecker, "Constraints on Lorentz invariance violating quantum gravity and large extra dimensions models using high energy gamma ray observations," Astropart. Phys. **20**, 85 (2003) [arXiv:astro-ph/0308214].

[154] R. Aloisio, P. Blasi, P. L. Ghia and A. F. Grillo, "Probing the structure of space-time with cosmic rays," Phys. Rev. D **62**, 053010 (2000) [arXiv:astro-ph/0001258].

[155] K. Greisen, "End To The Cosmic Ray Spectrum?," Phys. Rev. Lett. **16**, 748 (1966); G. T. Zatsepin and V. A. Kuzmin, "Upper Limit Of The Spectrum Of Cosmic Rays," JETP Lett. **4**, 78 (1966) [Pisma Zh. Eksp. Teor. Fiz. **4**, 114 (1966)].

[156] T. Jacobson, S. Liberati and D. Mattingly, "Threshold effects and Planck scale Lorentz violation: Combined constraints from high energy astrophysics," Phys. Rev. D **67**, 124011 (2003) [arXiv:hep-ph/0209264].

[157] L. Maccione and S. Liberati, "GZK photon constraints on Planck scale Lorentz violation in QED," JCAP **0808**, 027 (2008) [arXiv:0805.2548 [astro-ph]].

[158] G. Sigl, "Non-Universal Spectra of Ultrahigh Energy Cosmic Ray Primaries and Secondaries in a Structured Universe," Phys. Rev. D **75**, 103001 (2007) [arXiv:astro-ph/0703403].

[159] G. B. Gelmini, O. Kalashev and D. V. Semikoz, "GZK Photons Above 10 EeV," JCAP **0711**, 002 (2007) [arXiv:0706.2181 [astro-ph]].

[160] see http://apcauger.in2p3.fr//CRPropa.

[161] E. Armengaud, G. Sigl, T. Beau and F. Miniati, "CRPropa: A numerical tool for the propagation of UHE cosmic rays, gamma-rays and neutrinos," Astropart. Phys. **28**, 463 (2007) [arXiv:astro-ph/0603675].

[162] K. Shinozaki [AGASA Collaboration], "AGASA results," Nucl. Phys. Proc. Suppl. **151**, 3 (2006); see also http ://www-akeno.icrr.u-tokyo.ac.jp/AGASA/.

[163] T. A. Clark, L. W. Brown, J. K. Alexander, Nature **228**, 847 (1970).

[164] O. Gagnon and G. D. Moore, "Limits on Lorentz violation from the highest energy cosmic rays," Phys. Rev. D **70**, 065002 (2004) [arXiv:hep-ph/0404196].

[165] D. Mattingly, T. Jacobson and S. Liberati, "Threshold configurations in the presence of Lorentz violating dispersion relations," Phys. Rev. D **67**, 124012 (2003) [arXiv:hep-ph/0211466].

[166] J. Albert *et al.* [MAGIC Collaboration and Other Contributors Collaboration], "Probing quantum gravity using photons from a flare of the active galactic nucleus Markarian 501 observed by the MAGIC telescope," Phys. Lett. B **668**, 253 (2008) [arXiv:0708.2889 [astro-ph]].

[167] J. R. Ellis, N. E. Mavromatos and D. V. Nanopoulos, "Space-time foam effects on particle interactions and the GZK cutoff," Phys. Rev. D **63**, 124025 (2001) [arXiv:hep-th/0012216].

[168] J. Ellis, N. E. Mavromatos and D. V. Nanopoulos, "Derivation of a Vacuum Refractive Index in a Stringy Space-Time Foam Model," Phys. Lett. B **665**, 412 (2008) [arXiv:0804.3566 [hep-th]].

[169] W. Hu, M. M. Hedman and M. Zaldarriaga, "Benchmark parameters for CMB polarization experiments," Phys. Rev. D **67** (2003) 043004 [arXiv:astro-ph/0210096].

[170] D. O'Dea, A. Challinor and B. R. Johnson, "Systematic errors in cosmic microwave background polarization measurements," Mon. Not. Roy. Astron. Soc. **376**, 1767 (2007) [arXiv:astro-ph/0610361].

[171] J. P. Hamaker, J. P. Leahy, "A study of CMB differencing polarimetry with particular reference to Planck," ESA Report SCI-A/2003.312/JT.

[172] C. O'Dell, "A New Upper Limit on the Polarization of the Cosmic Microwave Background Radiation," arXiv:astro-ph/0201224.

[173] C. Heiles *et al.*, "Müller Matrix Parameters for Radio Telescopes and their Observational Determination," arXiv:astro-ph/0107352.

Abstract of the thesis

Photon Propagation as a Probe
for Fundamental Physics.

In this thesis we show how light propagation can be used in order to constrain particle physics models beyond the Standard Model. We study in particular the effects of non standard physics on the polarization of cosmic microwave background radiation and on the flux of ultrahigh energy γ-rays ($E_\gamma > 10^{19}$ eV).

In the first part we discuss the effects on cosmic microwave background polarization of coupling between photons and pseudoscalar fields acting as dark matter (e.g. axions) or as dark energy (e.g. ultralight pseudo Nambu-Goldstone bosons). In particular we describe how the public code CAMB can be modified in order to take into account the rotation of the linear polarization plane from last scattering surface to nowadays, produced by photon propagation in a cosmological background of pseudoscalar particles. Polarization power spectra are compared with the ones obtained in the widely used approximation in which the rotation angle is assumed constant in time. We show how polarization-polarization and temperature-polarization angular power spectra can be very useful to constrain the coupling constant g_ϕ between photons and pseudoscalars.

In the second part of this thesis we use the current upper limits on the flux of ultrahigh-energy photons in order to constrain Lorentz invariance violating terms in the dispersion relations for elementary particles. Theories trying to unify quantum mechanics with general relativity and many supersymmetry models predict indeed that Lorentz symmetry has to be modified at energies of the order of the Planck scale (10^{28} eV). If standard dispersion relations of elementary particles are modified, then the propagation and therefore also the energy spectrum of ultrahigh-energy cosmic rays can be considerably changed. We study in particular how it is possible to constrain Lorentz invariance violating terms for photons and electrons (suppressed both at first and second order of the Planck mass) improving current constraints by several orders of magnitude.

The main results are summarized in the following papers:

- F. Finelli and M. Galaverni, "Rotation of Linear Polarization Plane and Circular Polarization from Cosmological Pseudoscalar Fields," arXiv:0802.4210 [astro-ph], *submitted*.

- M. Galaverni, F. Finelli, "Systematics of Cosmic Microwave Background Polarization," Internal Report IASF-BO 454/2007.

- M. Galaverni and G. Sigl, "Lorentz Violation in the Photon Sector and Ultra-High Energy Cosmic Rays," Phys. Rev. Lett. **100**, 021102 (2008) [arXiv:0708.1737 [astro-ph]].

- M. Galaverni and G. Sigl, "Lorentz Violation and Ultrahigh-Energy Photons," Phys. Rev. D **78**, 063003 (2008) [arXiv:0807.1210 [astro-ph]].

Resumé de la thesè

PROPAGATION DES PHOTONS COMME UNE SONDE
POUR LA PHYSIQUE FONDAMENTALE.

Dans cette thèse, nous montrons comment la propagation de la lumière peut être utilisée en vue de contraindre les modèles de physique des particules au-delà du modèle standard. Nous étudions en particulier les effets de la physique non standard sur la polarisation du rayonnement du fond diffus cosmologique et sur le flux de photons d'ultra-haute énergie ($E_\gamma > 10^{19}$ eV).

Dans la première partie nous discutons les effets sur la polarisation du fond diffus cosmologique du couplage entre les photons et les champs pseudoscalaires, qui agissent en tant que matière noire (par exemple les axions) ou en tant que énergie noire (par exemple les pseudobosons ultra-légers de Nambu-Goldstone). En particulier, nous décrivons comment le code public CAMB peut être modifié afin de prendre en compte la rotation du plan de polarisation linéaire à partir de la surface de dernière diffusion jusqu'à maintenant, produite par la propagation des photons dans un fond cosmologique de particules pseudoscalaires. Les spectres de puissance de polarisation sont comparés avec ceux obtenus dans l'approximation largement utilisée, dans laquelle l'angle de rotation est supposé constant dans le temps. Nous montrons comment les spectres de puissance polarisation-polarisation

193

et température-polarisation peuvent être très utiles pour contraindre la constante de couplage g_ϕ entre photons et pseudoscalaires.

Dans la deuxième partie de cette thèse, nous utilisons la limite supérieure experimentelle actuelle sur le flux de photons d'ultra-haute énergie afin de contraindre les termes qui violent l'invariance de Lorentz dans les relations de dispersion pour les particules élémentaires. Les théories qui tentent d'unifier la mécanique quantique avec la relativité générale et nombreux modèles de supersymétrie prédisent en effet que la symétrie de Lorentz doit être modifié à des énergies de l'ordre de l'échelle de Planck (10^{28} eV). Si les relations de dispersion standard des particules élémentaires sont modifiées, alors la propagation et donc aussi le spectre d'énergie des rayons cosmiques d'ultra-haute énergie peuvent être considérablement changés. Nous étudions en particulier comment il est possible de contraindre les conditions qui violent l'invariance de Lorentz pour les photons et les électrons (supprimées à la fois au premier et deuxième ordre de la masse de Planck) en améliorant les contraintes actuelles de plusieurs ordres de grandeur.

Les principaux résultats sont résumés dans les articles suivants:

- F. Finelli and M. Galaverni, "Rotation of Linear Polarization Plane and Circular Polarization from Cosmological Pseudoscalar Fields," arXiv:0802.4210 [astro-ph], *submitted.*

- M. Galaverni, F. Finelli, "Systematics of Cosmic Microwave Background Polarization," Internal Report IASF-BO 454/2007.

- M. Galaverni and G. Sigl, "Lorentz Violation in the Photon Sector and Ultra-High Energy Cosmic Rays," Phys. Rev. Lett. **100**, 021102 (2008) [arXiv:0708.1737 [astro-ph]].

- M. Galaverni and G. Sigl, "Lorentz Violation and Ultrahigh-Energy Photons," Phys. Rev. D **78**, 063003 (2008) [arXiv:0807.1210 [astro-ph]].

Riassunto della tesi

La Propagazione dei Fotoni come Sonda
per la Fisica Fondamntale.

In questa tesi mostriamo come la propagazione dei fotoni possa essere utilizzata per vincolare possibili estensioni del Modello Standard della fisica delle particelle. Studiamo in particolare gli effetti di questa fisica non standard sulla polarizzazione della radiazione cosmica di fondo a microonde e sul flusso di fotoni ad altissime energie ($E_\gamma > 10^{19}$ eV).

Nella prima parte analizziamo le modifiche alla polarizzazione della radiazione cosmica di fondo dovute all'interazione tra fotoni e campi pseudoscalari, che agiscono o come materia oscura (es. assioni) o come energia oscura (es. ultralight pseudo Nambu-Goldstone bosons). Mostriamo come il codice pubblico CAMB possa essere modificato per tenere conto di una rotazione del piano di polarizzazione lineare prodotta dalla propagazione dei fotoni in un background cosmologico di particelle pseudoscalari che varia nel tempo dalla superficie di ricombinazione a oggi. Gli spettri di potenza angolare della polarizzazione della radiazione cosmica così ottenuti sono quindi confrontati con quelli ricavati nell'approssimazione di angolo di rotazione costante nel tempo. Mostriamo inoltre come gli spettri temperatura-polarizzazione e polarizzazione-polarizzazione possano rivelarsi molto utili per vinco-

lare la costante di accoppiamento g_ϕ tra i fotoni e le particelle pseudoscalari.

Nella seconda parte della tesi si utilizzano gli attuali limiti sul flusso di fotoni ad altissime energie per vincolare termini che violano la simmetria di Lorentz nella relazione energia impulso per particelle elementari. Infatti diverse teorie che cercano di unificare la meccanica quantistica con la relatività generale e molti modelli di supersimmetria prevedono che, per energie dell'ordine della scala di Planck (10^{28} eV), la simmetria di Lorentz debba essere modificata. Se le relazioni di dispersione standard sono alterate, allora anche la propagazione e di conseguenza lo spettro dei raggi cosmici ad altissima energia può essere modificato notevolmente. In questa tesi mostriamo come sia possibile costringere notevolmente l'ampiezza di termini che non soddisfano l'invarianza di Lorentz, benché soppressi al primo o al second'ordine nella scala di Planck; si considerano nello specifico modifiche alla relazione di dispersione dei fotoni e degli elettroni.

I principali risultati sono riassunti nei seguenti articoli:

- F. Finelli and M. Galaverni, "Rotation of Linear Polarization Plane and Circular Polarization from Cosmological Pseudoscalar Fields," arXiv:0802.4210 [astro-ph], *submitted*.

- M. Galaverni, F. Finelli, "Systematics of Cosmic Microwave Background Polarization," Internal Report IASF-BO 454/2007.

- M. Galaverni and G. Sigl, "Lorentz Violation in the Photon Sector and Ultra-High Energy Cosmic Rays," Phys. Rev. Lett. **100**, 021102 (2008) [arXiv:0708.1737 [astro-ph]].

- M. Galaverni and G. Sigl, "Lorentz Violation and Ultrahigh-Energy Photons," Phys. Rev. D **78**, 063003 (2008) [arXiv:0807.1210 [astro-ph]].